ARID1a Is An Inhibitor Of Wnt Signalling In *Xenopus* and Human

Alexander Thomas Watson

This thesis is submitted for the degree of Doctor of Philosophy

University College London

Supervisor: Jim Smith
Systems Biology,
National Institute for Medical Research

I declare that the work in this thesis is my own. For the mass spectrometry experiments I collaborated with Lina Herhaus and Gopal Sapkota at the MRC Protein Phosphorylation Unit, University of Dundee.

Acknowledgements

Abstract

Wnt signalling regulates a wide range of events throughout embryonic development, adult homeostasis and the onset of disease. Within the frog *Xenopus laevis* activation of the Wnt pathway results in one of the first major events during embryogenesis: the establishment of the dorsal-ventral axis. At the molecular level the Wnt pathway in *Xenopus* embryos is similar to that in many other organisms – including humans – therefore what is learned about protein functions from studies in *Xenopus* can be extrapolated to other species.

My PhD has focussed on the role of *ARID1a* in the regulation of the Wnt pathway. ARID1a is the largest subunit of the chromatin remodelling BAF complex, which is the vertebrate homologue of the yeast SWI/SNF complex. The BAF complex functions by repositioning nucleosomes within chromatin, and plays a role in a variety of cellular functions such as the regulation of transcription, RNA splicing and DNA damage repair.

 ARID1a was originally identified in the fruit fly *Drosophila,* where it was implicated as a repressor of Wg. My studies verify and expand upon this work, investigating the role of *ARID1a* as a repressor of the Wnt pathway in *Xenopus* and in Human Embryonic Kidney 293 (HEK293) cells. I carried out a mass spectrometry screen in HEK293 cells and identified two interacting proteins for further study: BCL7a and DDX5. I demonstrate that these two proteins are also able to inhibit Wnt signalling in *Xenopus*, and suggest mechanisms by which this repression may occur.

Table of Contents

List of Figures and Tables

Chapter 1

Chapter 2

Chapter 3

Chapter 4

Chapter 5

Chapter 6

Chapter 7

List Of Abbreviations

AFM	Atomic force microscopy
APC	Adenomatous polyposis coli protein
ARID	AT-rich interacting domain
ARID1a	AT-rich interacting domain containing protein 1a
ARID1a_CO	ARID1a mismatch morpholino
ARID1a_TB	ARID1a translation blocking morpholino
ARID1a_SC	ARID1a mismatch morpholino
ARID1a_SB	ARID1a splice blocking morpholino
ARP	Actin related protein
BAF	Brg1/Brm associated factor
esBAF	Embryonic stem cell specific BAF complex
nBAF	Neural specific BAF complex
npBAF	Neural progenitor specific BAF complex
BCL7a	B-cell CLL/lymphoma protein 7a
β-TrCP	β-Transducin repeat containing protein
Brg1	Brahma related gene 1
Brm	Brahma
CBP	CREP-binding protein
CK1	Casein kinase 1
CRAPome	Contaminant repository for affinity purification database
CRD	Cysteine rich domain
CtBP	C-terminal binding protein
DDX5	DEAD box containing protein 5
DDX5_CO	DDX5 mismatch morpholino
DDX5_TB	DDX5 translation blocking morpholino
Dkk	Dickkopf
Dox	Doxycycline
Dsh/Dvl	Dishevelled
EM	Electron microscopy
FGF	Fibroblast growth factor
Fz/Fzd/Dfz	Frizzled
GFP	Green fluorescent protein
Grg	Groucho-related gene
GSK3	Glycogen synthase kinase 3
HA	Haemagglutinin
HDAC	Histone deacetylase
HEK	Human embryonic kidney
ISWI	Imitation Switch
LCM	L-cell conditioned media
LEF	Lymphoid enhancer factor
LRP	Low density lipoprotein receptor like protein
MALDI-TOF	Matrix assisted laser desorption/ionisation – time of flight

PBAF	Polybromo-containing BAF complex
PCR	Polymerase chain reaction
qPCR	Quantitative PCR
RSC	Remodels the structure of chromatin
Sia	Siamois
SNF	Sucrose non-fermenting
TCF	T-cell factor
TGFβ	Transforming growth factor β
TLE	Transducin-like enhancer of split
TUNEL	Terminal deoxynucleotidyl transferase dUTP nick end labeling
UTR	Untranslated region
WCM	Wnt-conditioned media
WIF1	Wnt-inhibitory factor 1
WRE	Wnt recognition element
Xnr3	Xenopus Nodal related 3

Chapter 1: Introduction

My project focuses on the role of *ARID1a* in the regulation of the Wnt pathway in *Xenopus* embryos and in Human Embryonic Kidney 293 (HEK293) cells. I first describe ARID1a and the complex to which it belongs. I then give an overview of the Wnt pathway.

1.1 ARID1a and the BAF Complex

ARID1a is the largest subunit of the Brg/Brm-Associated Factor (BAF) complex, which is the vertebrate orthologue of the yeast SWI-SNF complex. The BAF is part of the chromatin remodelling complex (CRC) family that repositions nucleosomes to affect a range of cellular processes. I shall first describe what is known about the BAF complex, followed by the specific functions of ARID1a.

1.1.1 Composition of the SWI-SNF/BAF and RSC/PBAF Complexes

1.1.1.1 Yeast

The SWI-SNF complex was first identified in *Saccharomyces cerevisiae* from two independent mutational screens. *Sucrose Non-Fermenting 2 (SNF2)* was identified as a gene that regulated the expression of Suc2, an enzyme required for sucrose fermentation (Neigeborn and Carlson, 1984), while mutations in SWI2 prevented mating type switching (Egel et al., 1984). Later, it was discovered that SWI2 and SNF2 are encoded by the same gene (Laurent and Carlson, 1992), and that it forms a complex with other proteins identified in the original mutational screens (Cairns et al., 1994; Laurent et al., 1991). Subsequently, the SWI-SNF complex has been shown to comprise 12 core subunits and to have access to at least 18 accessory subunits as determined by mass spectrometry experiments (van Vugt et al., 2007), see Table 1.1 for species comparison). Stoichiometric analysis revealed that six of the subunits exist as a single copy (SWI1, SWI2, SNF5, ARP7, ARP9, SWP73), four are present as two copies (SWI3, SNF6, SNF11, SWP82) and one (SWP29) as three copies (Smith et al., 2003).

Table 1.1 The SWI-SNF and BAF Complexes

	Yeast	Worm	Fly	Frog	Mouse	Human
Conserved subunits	Swi2/Snf2	SWSN-4/psa-4	BRM	BRG1/SMARCA4 (BRM/SMARCA2)*	BRG1/SMARCA4 BRM/SMARCA2	BRG1/SMARCA4 hBRM/SMARCA2
		Swsn-8/LET-526	OSA/eyelid	ARID1a/ARID1a BAF250b/ARID1b	ARID1a/ARID1a BAF250b/ARID1b	ARID1a/ARID1a BAF250b/ARID1b
	Swi3	SWSN-1/psa-1	MOR/BAP155	(SMARCC1)* BAF170/SMARCC2	BAF155/SMARCC1 BAF170/SMARCC2	BAF155/SMARCC1 BAF170/SMARCC2
	Swp73	SWSN-2.2 + SWSN-2.1/HAM-3	BAP60	BAF60a/SMARCD1 BAF60b/SMARCD2 BAF60c/SMARCD3	BAF60a/SMARCD1 BAF60b/SMARCD2 BAF60c/SMARCD3	BAF60a/SMARCD1 BAF60b/SMARCD2 BAF60c/SMARCD3
	Rsc11/Arp7 Rsc12/Arp9	SWSN-6	BAP55 BAP47	BAF53a/ACTL6a (BAF53b/ACTL6b)*	BAF53a BAF53b	BAF53a BAF53b
	Snf5	SNFC-5	SNR1/BAP45	SMARCB1	BAF47/SNF5/SMARCB1	BAF47/SNF5/SMARCB1/INI1
		PHF-10 DPFF-1	E(y)3/SAYP TTH + D4	(PHF10)* DPF1/BAF45b DPF3/BAF45c DPF2/BAF45d	PHF10/BAF45a DPF1/BAF45b DPF3/BAF45c DPF2/BAF45d	PHF10/BAF45a DPF1/BAF45b DPF3/BAF45c DPF2/BAF45d
		SWSN-3	BAP111/dalao	BAF57/SMARCE1	BAF57/SMARCE1	BAF57/SMARCE1
			β-actin	β-actin	β-actin	β-actin
Unique Subunits	Swi1/Adr6, Swp82, Taf14, Snf6, Snf11					Brd9

Table 1.2 The RSC and PBAF Complexes

	Yeast	Worm	Fly	Frog	Mouse	Human
Conserved Subunits	Rsc1, 2, 4	Swsn-7	BAP170	ARID2/BAF200	ARID2/BAF200	ARID2/BAF200
	Rsc9	Pbrm-1	Polybromo	BAF180	BAF180	BAF180
		Swsn-9		BRD7	BRD7	BRD7
	Sth1	SWSN-4/psa-4	BRM	BRG1/SMARCA4	BRG1/SMARCA4	BRG1/SMARCA4
		SWSN-1/psa-1				
	Rsc6	SWSN-2.2 + SWSN-2.1/HAM-3	BAP60	BAF60a/SMARCD1	BAF60a/SMARCD1	BAF60a/SMARCD1
	Rsc11/Arp7 Rsc12/Arp9	SWSN-6	BAP55	BAF53a	BAF53a	BAF53a
		SNFC-5	SNR1/BAP45	BAF47/SNF5/SMARCB1	BAF47/SNF5/SMARCB1	BAF47/SNF5/SMARCB1
		SWSN-3	BAP111/dalao	ARID2/BAF200		
			β-actin	β-actin	β-actin	β-actin
Unique Subunits	Rsc3, 5, 7, 9, 10, 30, Htl1, Lbd7, Rtt102					

Table 1.1 The SWI-SNF and BAF Complexes

Species comparison of SWI-SNF and BAF complex subunits across *S. cerevisiae, C. elegans, X. laevis, M. musculus* and *H. sapiens.* Orthologous subunits are arranged in rows, and proteins with multiple names are denoted by "/". *X. laevis* genes marked by ()* are non-curated, machine annotated entries in Xenbase. Due to the strong conservation of subunits across large evolutionary distances, it is likely that these predicted genes are real and encode subunits of the BAF complex. Table is adapted from Hargreaves and Crabtree (2011).

Table 1.2 The RSC and PBAF Complexes

Same as for Table 1.1. The entries for *X. laevis* are predicted based on homology with mammalian PBAF complexes. No direct evidence for a *Xenopus* PBAF complex yet exists.

In addition to the SWI-SNF complex, yeast also possess a highly homologous chromatin remodelling complex named R̲emodels the S̲tructure of C̲hromatin (RSC). Discovered in 1996, this has 17 subunits, 3 of which (ARP9, ARP7 and RSC8) are shared with the SWI-SNF complex (Cairns et al., 1996; van Vugt et al., 2007). Functionally RSC acts via a similar mechanism to SWI/SNF, however it targets different genes in a non-redundant manner (Damelin et al., 2002; Hargreaves and Crabtree, 2011).

1.1.1.2 C. elegans

The *C. elegans* SWI-SNF complex subunits have been found through a series of mutational screens. *swsn-1* and *swsn-4* (homologues of SWI3/BAF170 and SWI2/BRG1-BRM respectively) were the first components to be identified (Sawa et al., 2000). Two orthologues of vertebrate BAF60, *swsn-2.1* and *2.2,* exist in *C. elegans,* and the duplication of the *swsn-2* gene appears to be independent of that which occurred for BAF60 in vertebrates (Weinberg et al., 2013). A recent paper (Large and Mathies, 2014) has identified the remaining *C. elegans* SWI-SNF components by *in silico* comparison of the genome with data from the literature. This work demonstrated that *C. elegans* possesses at least one protein for each subunit of the BAF complex. However, few experiments have been carried out on the *C. elegans* SWI-SNF complex, and it lacks the biochemical characterisation that has been carried out in other species.

The animal homologue of the yeast RSC complex is the PBAF complex – so named because it contains the protein *Polybromo* (Mohrmann et al., 2004). The *C. elegans* PBAF complex contains the same core components as the BAF complex with the exception of *swsn-8 (ARID1),* and it additionally contains *swsn-7* (*BAF200*)*, pbrm-1* (*BAF180*) and *swsn-9* (*BRD7*; (Kuzmanov et al., 2014)*. These findings, along with the extensive work carried out on vertebrate BAF complexes, indicate that the SWI-SNF and BAF complexes are highly conserved throughout evolution.

1.1.1.3 Drosophila

The *Drosophila* orthologue of SWI2/SNF2, Brahma (Brm), was discovered as a suppressor of both *Polycomb* and *Antennapedia* mutations (Kennison and Tamkun, 1988), and has sequence similarity to SWI2/SNF2 (Elfring et al., 1994; Tamkun et al., 1992). Brm is the core component of the <u>B</u>rahma <u>a</u>ssociated <u>p</u>rotein (BAP) complex in *Drosophila*, which has orthologous functions and composition to the yeast SWI-SNF and vertebrate BAF complexes (Mohrmann and Verrijzer, 2005). The BAP complex is formed of eight core subunits (see Table 1.1) plus β-actin, all of which are homologous to the vertebrate BAF complex. Unlike other animals studied, *Drosophila* only has one protein homologous to BAF60 – BAP 60.

The *Drosophila* PBAP complex was discovered in 2004 (Mohrmann et al., 2004). Biochemical characterisation shows that PBAP shares most of its subunits with the BAP complex with the noticeable exception of Osa. In addition, the PBAP complex also contained two proteins that were not present in the BAP complex: Polybromo and BAP170.

1.1.1.4 Mouse and Human

Unlike the SWI-SNF/BAF complexes discussed so far, the vertebrate BAF complex is highly pleomorphic. Of the ten core subunits in the human BAF complex, six have multiple proteins encoded by different genes capable of occupying the same functional space within the complex, and they do so in a mutually exclusive manner (see Table 1.1, Fig. 1.1). Vertebrates have two core ATPases that are orthologous to SWI2/SNF2 – Brahma (Brm) and <u>B</u>rahma-<u>r</u>elated <u>g</u>ene 1 (Brg1; (Khavari et al., 1993; Muchardt and Yaniv, 1993).

Brm and Brg1 are mutually exclusive within the BAF complex (Wang et al., 1996), though both proteins are often present within the same cell. Other subunits with alternative proteins are selectively incorporated into BAF complexes. ChIP–reChIP experiments in HeLa cells demonstrated that ARID1a and Brg1 are both present on DNA at the CSF1 promoter, whereas ARID1b and Brm are not (Ryme et al., 2009). In contrast, ARID1b, Brg1 and Brm (but not ARID1a) bind to the ECM1 promoter. These experiments show that distinct BAF complexes exist at different promoters within the same cell, and hint at the importance of different combinations of subunits for BAF complex functionality.

As an additional level of complexity, some BAF components are only expressed in certain cell types, leading to cell-type specific complexes. For example, neural stem/progenitor cells in the developing mouse nervous system have a specific BAF composition, called the npBAF complex. This comprises the core components (ARID1a, Brg1, BAF170 or BAF155, BAF60a, BAF57 and β-actin) and the npBAF specific factors BAF45a and BAF53a (Lessard et al., 2007). As these neuronal stem cells differentiate, there is a switch in expression from BAF45a and BAF53a to BAF45b, c and d, and BAF53b. This switch has a functional significance, because depletion of BAF45a or BAF53a impairs proliferation of neural stem cells, indicating that npBAF complexes positively regulate the cell cycle.

Similar cell-type specificity is seen in BAF complexes in mouse embryonic stem cells (esBAF). esBAF complexes contain a restricted set of subunits including Brg1, ARID1a, BAF155 and BAF45d, and this specific combination of subunits is required for the maintenance of pluripotency (Ho et al., 2009).

There are 3 BAF60 proteins in vertebrates: BAF60a, b and c. BAF60c is predominantly expressed in cardiac and skeletal muscle progenitors, and knock-down of BAF60c using siRNAs causes embryonic lethality by E11 (Lickert et al., 2004). However, unlike the esBAF and n/npBAF complexes, BAF60b was able to rescue deletion of BAF60c, indicating that these two proteins are able to act redundantly. This experiment highlights that while there may be significant functional relevance in each particular composition of the BAF complex, there is still redundancy within the complex.
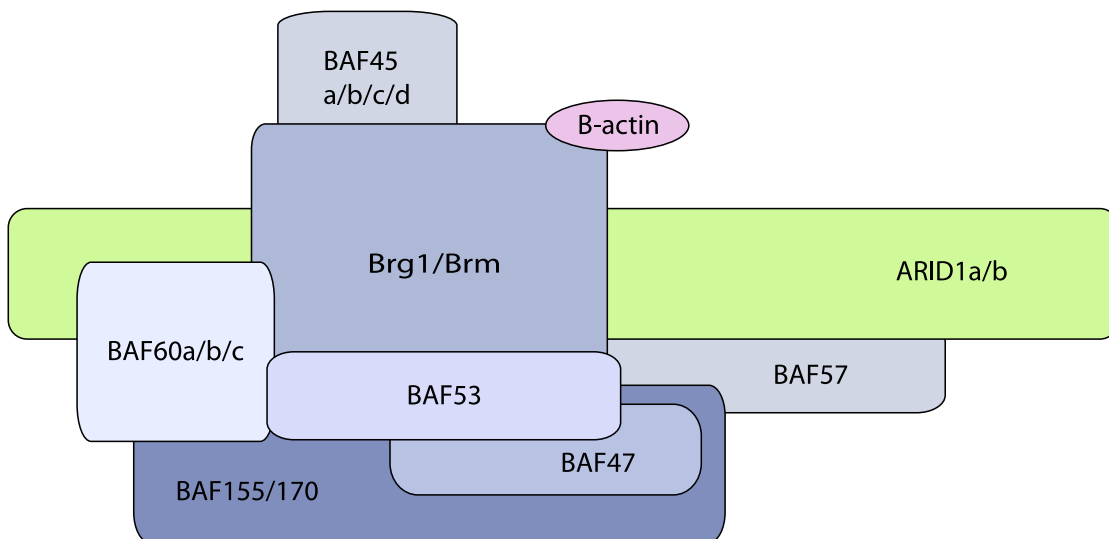
Fig. 1.1 Diagram of the BAF Complex Subunits

The diagram shows the relative size of the major BAF subunits. Proteins that intersect on the diagram have been shown to interact physically by immunoprecipitation or mass spectrometry.

Several mutually exclusive subunits are represented simultaneously: however only one of these proteins will be present in any one BAF complex, and not all subunits are present in all BAF complexes.

Human Polybromo/BAF180 was identified in 2000, and is one of the defining members of the PBAF complex (Xue et al., 2000). It is similar to the yeast RSC proteins Rsc1, 2 and 4, and is orthologous to *Drosophila* Polybromo. Furthermore, vertebrate BAF and PBAF are more similar to one another than are their yeast counterparts SWI-SNF and RSC, and unlike the RSC the range of subunits found in the PBAF complex is more restricted than those in the BAF complex.

1.1.1.5 Xenopus

The vast majority of research carried out on the BAF and PBAF complexes in vertebrates has used mice or human cells. Such biochemical characterisation has not been carried out in other species, but due to the highly conserved nature of the complex it is likely that the BAF and PBAF complexes in other model vertebrates are assembled in a similar manner.

To date, the only BAF subunits to be studied in *Xenopus* are Brg1 and BAF57 (Domingos et al., 2002; Seo et al., 2005). However, orthologues for all of the human and mouse BAF and PBAF complex subunits can be found in the *Xenopus* genome (see Table 1.1, Xenbase). Based on the homology and presence of these factors, it is likely that the *Xenopus* BAF and PBAF complexes are assembled in a similar manner to their mammalian counterparts.

1.1.2 Molecular Mechanism of BAF Functions

Each eukaryotic cell contains about 2 m of DNA packaged into a nucleus with a diameter of only 6 μm. This dense packaging is achieved by wrapping 146 base pairs of DNA around histone octamers to form nucleosomes, with linker regions of~ 38 bp between them (Luger et al., 1997). However, the existence of nucleosomes hinders the ability of *trans*-acting factors to bind to DNA, thus the repositioning of nucleosomes is a key part of processes such as transcription and DNA replication. Chromatin remodelling complexes such as the BAF complex act to reposition nucleosomes — either by sliding them in *cis* along the DNA, or by ejection or insertion of histone octamers.

1.1.2.1 The BAF Complex Repositions Nucleosomes

In vitro, SWI-SNF and BAF complexes are capable of altering the position of nucleosomes on synthetic chromatin in an ATP-dependent manner (summarised in Fig. 1.2). The presence of double stranded DNA is sufficient to induce the ATPase activity of SWI2/SNF2, and ATP is crucial for the remodelling of nucleosomes *in vitro* (Laurent et al., 1993). All chromatin remodelling complexes contain a core ATPase, in the case of the BAF complex these are SWI2/SNF2 in yeast, and either Brg1 or Brm in vertebrates (Clapier and Cairns, 2009).

Much of the evidence from work *in vitro* suggests that the BAF complex acts to slide nucleosomes along DNA. Early experiments used restriction enzyme digest assays, as movement of nucleosomes exposed restriction sites and changed the pattern of DNA cleavage (Kwon et al., 1994). This repositioning of nucleosomes was shown to be a permanent effect, because removal of ATP from the reaction did not cause a reversion back to the original DNaseI cleavage pattern (Imbalzano et al., 1996). In 2001, Lieber and colleagues directly visualised nucleosome remodelling using atomic force microscopy (AFM, (Schnitzler et al., 2001). They demonstrated that the BAF complex reorganised polynucleosomes from evenly spaced "beads on a string" to a clump of nucleosomes at one end with a free DNA tail.

Due to the large size of the BAF complex, no crystal structure is yet available for the entire complex. Imaging by electron microscopy (EM) and AFM have both revealed that the BAF complex adopts a multi-lobed conformation with a nucleotide binding pocket and multiple DNA-binding interfaces (Schnitzler et al., 2001; Smith et al., 2003). More recent work demonstrated that the yeast SWI-SNF complex contains a pocket that can contain an entire nucleosome and approximately 50 bp of flanking DNA (Dechassa et al., 2008). The authors showed that the SNF5 and SWI2 subunits both bind to the histone core of the nucleosome close to the dyad axis. The structural information gained from these studies has been important for developing mechanistic models for the BAF complex.
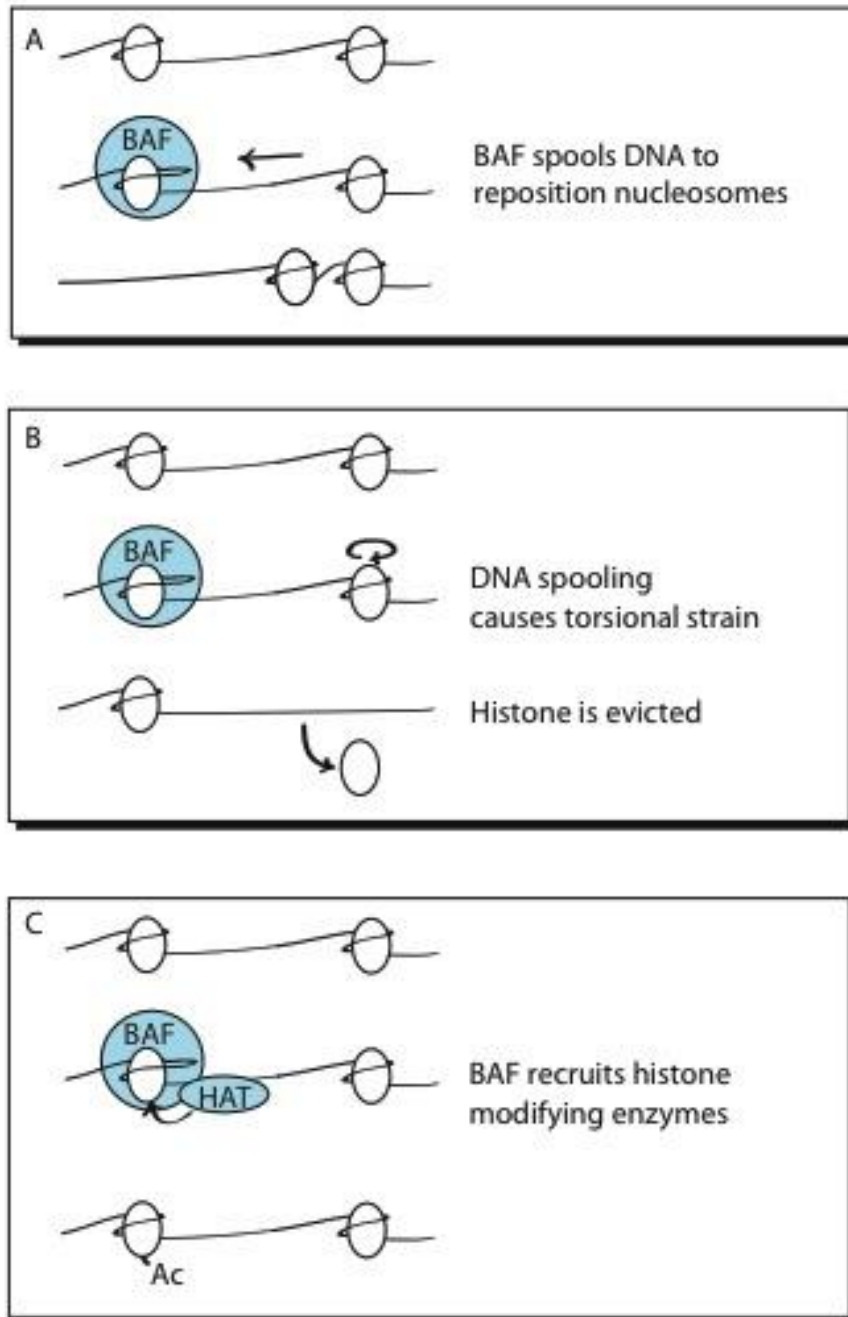
Fig. 1.2 BAF Complex Modification of Nucleosomes
Schematic representations of the BAF complex acting on nucleosomes.
A: The BAF complex binds to a nucleosome and repositions it closer to its neighbour. The BAF complex spools DNA around the nucleosome, creating a loop that the nucleosome can then be slid along to alter its position.
B: BAF complex-mediated eviction of a histone (modified from Dechassa et. Al, 2010). The BAF complex binds to a nucleosome and begins spooling DNA. This creates torsional strain on the distal nucleosome, eventually resulting in the physical displacement of the octamer from DNA.
C: The BAF complex can recruit various histone modifying enzymes to nucleosomes. Additionally, the BAF complex itself binds modified histones, the interplay between the BAF complex and histone modifying enzymes is complex and not well understood. HAT: Histone acetyltransferase. Ac: acetyl residue on histone tail.

1.1.2.2 Two Models For BAF Complex Action

There are currently two models describing how the BAF complex repositions nucleosomes: the twist-diffusion mechanism and the loop-recapture model (Whitehouse et al., 2000). The twist-diffusion model describes a loosening of a base pair that is then propagated around the histone octamer, acting to shift it along the DNA one base pair at a time (Fig. 1.3 A). However significant steric obstacles such as Holliday Junctions and DNA branches failed to affect the ability of the BAF complex to remodel nucleosomes, arguing against a simple twist-diffusion model (Aoyagi and Hayes, 2002; Whitehouse et al., 1999).

Instead, a loop-recapture model was proposed based on the observation that binding of the BAF complex to chromatin resulted in DNA loops (Bazett-Jones et al., 1999). In this model, the nucleosome is anchored by the BAF complex and a DNA loop is spooled around the histone octamer. This loop is then passed around the octamer, shifting the nucleosome by the length of the loop (Fig. 1.3 B). The actual size of these loops is unclear: Bazett-Jones and colleagues visualised loops of over 1 kb using EM, whereas other groups have reported much smaller loops with an average size of 100 bp using AFM and optical tweezers (Schnitzler et al., 2001; Zhang et al., 2006).

An added complication to developing models for BAF complex activity is that nucleosomes are not static entities. Even without chromatin remodelling complexes, DNA spontaneously unwraps and rewraps around histone octamers (Polach and Widom, 1995). FRET measurements revealed that DNA associates with the histones much more rapidly than it unwraps, and this step may affect the ability of proteins such as PolII and the BAF complex to bind to DNA (Li et al., 2004). The authors hypothesise that chromatin remodelling complexes may act as ratchets to harness this spontaneous unwrapping and rewrapping, however the kinetic analysis to test this model has not yet been carried out.

Recently the twist-diffusion mechanism has come back into favour (Mueller-Planitz et al., 2013). High resolution FRET experiments demonstrated that DNA leaves chromatin remodelling complexes one base pair at a time, and that the formation of DNA loops is unlikely (Deindl et al., 2013). It is worth noting that these experiments were carried out with the ISWI complex (imitation switch,

another chromatin remodelling complex), and the BAF complex may act by a different mechanism. Indeed the BAF complex is much larger than the ISWI complex, and may use loops in conjunction with base pair twisting to effect the remodelling of nucleosomes. More experiments using high resolution imaging and kinetic analysis are required to determine which of these two models is correct, or whether the BAF complex acts by a combination of the above.

1.1.2.3 The BAF Complex Can Disassemble Nucleosomes

In addition to sliding nucleosomes, BAF complexes are able to evict and insert histones from chromatin. This was first demonstrated using the yeast RSC complex, where free radiolabelled DNA was incorporated into nucleosomes (Lorch et al., 1999). Subsequently the RSC and SWI-SNF, but not ISWI complexes were shown to catalyse the exchange of H2A/B dimers between nucleosomes (Bruno et al., 2003). Convincing evidence from studies at the yeast *PHO5* locus demonstrated that nucleosomes are lost from closed chromatin loops by disassembly and not by sliding (Boeger et al., 2004). In 2010, Dechassa and colleagues proposed a model where the BAF complex evicts histone octamers by acting simultaneously on two nucleosomes (Dechassa et al., 2010). The proximal nucleosome is bound within the BAF pocket and an intranucleotide loop of DNA is created, similar to the loop-recapture mode. This loop places torsional strain on the distal nucleosome resulting in loss of an H2A/B dimer. Then, as more DNA is wound into the BAF complex, the remaining histones are lost and the distal nucleosome is displaced. This mechanism is supported by recent work suggesting that the predominant method of nucleosome remodelling by the BAF complex *in vivo* is likely to be the eviction or insertion of nucleosomes, rather than the translational shifting observed *in vitro* (Tolstorukov et al., 2013)*.*
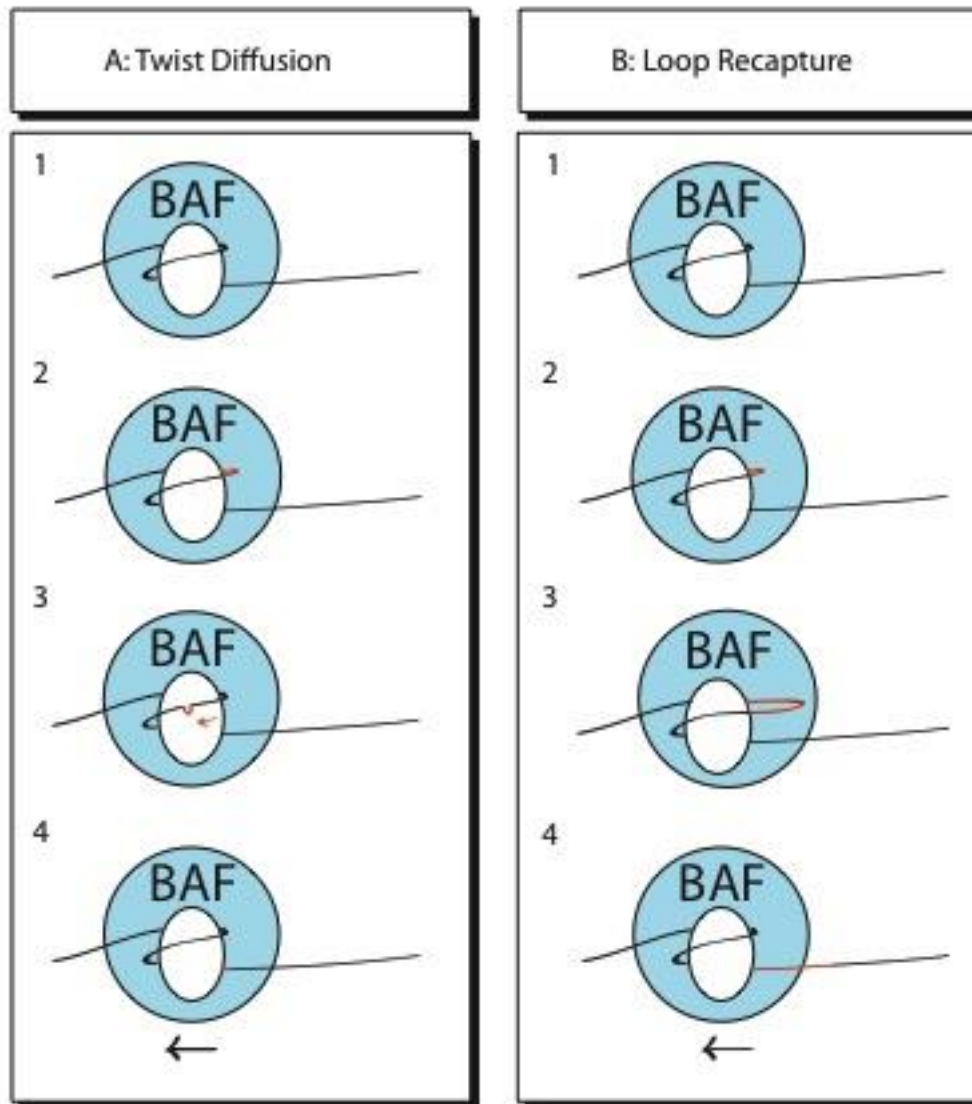
Fig. 1.3 Two Models For BAF Complex Action.
Diagrams detailing two models for how the BAF complex repositions nucleosomes.
A: the twist diffusion model. A single base pair is passed around the nucleosome at a time. 1. The BAF complex binds to the nucleosome. 2. A single base pair is freed from the histone proteins, creating a small hairpin. 3. The hair pin is propagated around the nucleosome. 4. The nucleosome has been moved one base pair to the left.
B: the loop recapture model. A loop of DNA is spooled from the nucleosome and then passed around the nucleosome in a single motion. 1. The BAF complex binds to the nucleosome. 2. A single base pair is freed from the histone proteins, creating a small hairpin. 3. More base pairs are freed from the histones, creating an intranucleosomal DNA loop. 4. The loop is passed around the nucleosome in one movement, shifting the nucleosome to the left by the length of the loop (100-1000 bp).

1.1.2.4 The BAF Complex As A Regulator Of Transcription

Early work with the yeast SWI-SNF complex suggested it was a general promoter of transcription (Peterson and Herskowitz, 1992). *In vitro,* movement of nucleosomes promoted transcription of an artificial viral fragment (Imbalzano et al., 1994), and once remodelling had occurred SWI-SNF was no longer required on the chromatin to promote transcription (Côté et al., 1998). *In vivo* the SWI-SNF complex is essential for nucleosome eviction at the SUC2 promoter, and may act to remove nucleosomes within genes bodies (Schwabish and Struhl, 2007). Similarly in *Drosophila,* Brm acts as a generic activator of transcription (Armstrong et al., 2002)*.* SAYP, the *Drosophila* orthologue of BAF45a, recruits Brg1 and TFIID to promoters, and is required for the presence of PolII at these promoters (Vorobyeva et al., 2009).

In addition to activating transcription, the BAF complex also inhibits gene expression (Sudarsanam et al., 2000). Indeed, recent profiling of Brg1 binding sites shows it is present at a high percentage of total genes, and actually has a slight preference for repressed loci (Tolstorukov et al., 2013). These genome wide studies of BAF complexes failed to find any binding motifs for the complex, indicating that it may be predominantly recruited to DNA by other factors.

A classic example of BAF complex recruitment is the binding of c-myc to SNF5, which was required to activate transcription of a luciferase reporter gene (Cheng et al., 1999). Brg1 is also recruited to promoters by heat shock factor 1 (HSF1), monoubiquitinated histone H2B and zinc finger transcription factors such as the GATA family (Corey et al., 2003; Kadam and Emerson, 2003; Shema-Yaacoby et al., 2013). It is noteworthy that Brm cannot bind to GATA family members and instead binds to the Notch intracellular domain (ICD), further supporting the model that these two highly similar complexes have distinct roles in the regulation of transcription.

Two possible models by which the BAF complex regulates gene expression is by the assembly and disassembly of nucleosome barriers, and by the recruitment of histone modifying complexes (Fig. 1.4 and below). Nucleosome barriers are regions of tightly clustered nucleosomes that interfere with PolII elongation and lead to reduced gene expression (Subtil-Rodríguez and Reyes, 2010).

Such barriers can be removed by the BAF complex to allow transcription to take place (Schwabish and Struhl, 2007). In *Drosophila* the BAP complex actively lays down nucleosome barriers within the *ftz-f1* gene and represses transcription (Vorobyeva et al., 2012). Thus the assembly and disassembly of nucleosome boundaries are a way in which the BAF complex can regulate transcription.

1.1.2.5 The BAF Complex and Histone Modifying Complexes

The BAF complex is able to modify histones as well as reposition them. This was first noticed as a shift in the tail position of the H2A/B dimer (Lee et al., 1999), and compaction of nucleosomes following remodelling (Kassabov et al., 2003). *In vivo,* the BAF complex binds to the Sin3a/HDAC complex (Sif et al., 2001) and to Prmt5 to promote transcription of myogenic genes (Dacwag et al., 2009). Indeed it has been shown that Prmt5 methylates histones that have been deacetylated by Sin3a/HDAC, and this activity requires a functional BAF complex (Pal et al., 2003). *Drosophila* PBAP complexes bind lysine specific demethylase 1 (LSD1) to regulate wing vein patterning (Curtis et al., 2011), and during *in vitro* cardiogenesis ARID1a recruits the Nucleosome Remodelling and Histone Deacetylase (NURD) complex to repress cardiac genes (Singh and Archer, 2014).

An added complexity is that Brg1, Brm and Polybromo all possess bromo domains which facilitate binding to acetylated histones (Mohrmann et al., 2004; Tamkun et al., 1992). This raises the question as to whether the histone marks observed in the above experiments recruit the BAF complex to particular sites, or if the BAF complex directs other histone modifying complexes to the DNA. Due to the highly dynamic nature of chromatin it is likely that both are true, though careful time course experiments are required to determine the precise nature of these interactions.
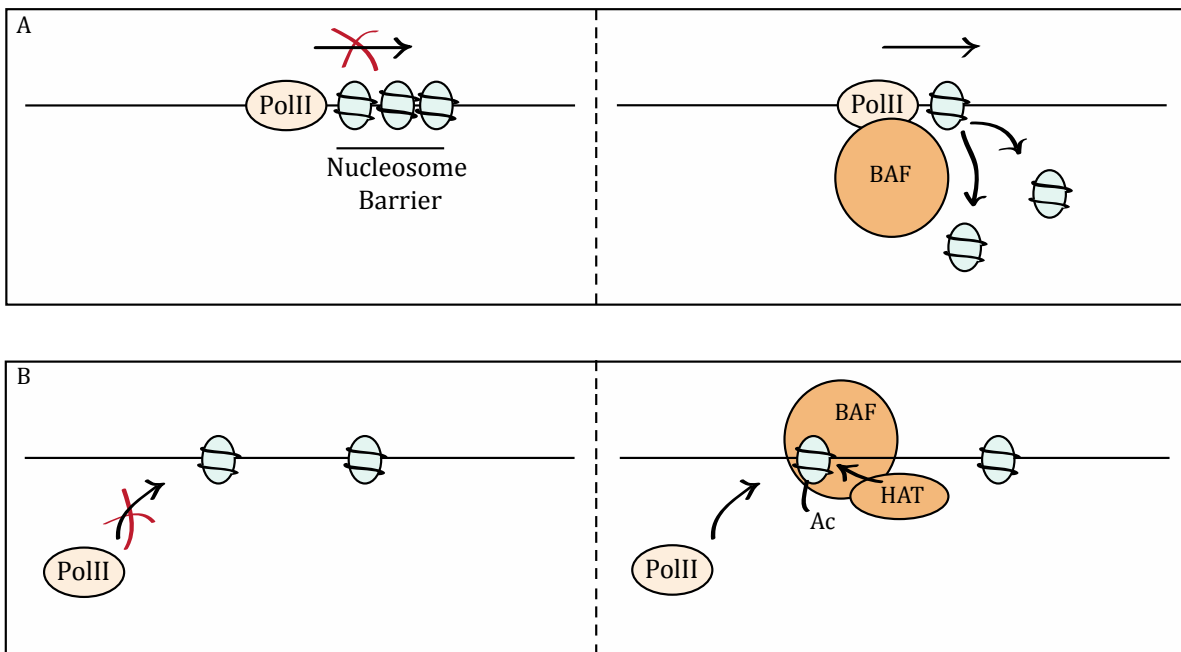
Fig. 1.4 Mechanisms of Gene Regulation By the BAF Complex
A: Nucleosome barriers (regions of tightly clustered nucleosomes) sterically hinder the elongation of PolII and therefore inhibit gene expression. The BAF complex can assemble and disassemble these barriers to allow or repress gene expression respectively.
B: The BAF complex recruits histone modifying enzymes to alter the accessibility of the chromatin state. In the example shown the BAF complex recruits a histone acetyltransferase (HAT), which acetylates histone tails which results in a loose chromatin state where PolII and associated basal transcription factors can bind. The BAF complex can also recruit other families of histone modifiers which negatively regulate the binding of PolII to DNA.

1.1.2.6 Actin Binding Proteins and the Regulation of Transcription

β-actin and the actin-related proteins (ARP) BAF53a and BAF53b are subunits of the BAF complex. Despite the abundance of β-actin and the fact that it is a common contaminant in immunoprecipitation studies, a series of convincing experiments demonstrated that β-actin is a *bona fide* member of the BAF complex (Zhao et al., 1998). In conjunction with Brg1, β-actin and BAF53 allows the BAF complex to bind filamentous (F)-actin (Rando et al., 2002). Expression of Brg1 in SW13 cells (that are deficient for Brg1) causes bundling of actin into stress fibres by inducing expression of the Rho-kinase ROCK1 (Asp et al., 2002).

The importance of actin in the regulation of transcription was first noted in 1999 (Sotiropoulos et al., 1999), where polymerisation of actin filaments was shown to be required for activation of serum response factor (SRF) target genes. Since then it has emerged that actin plays a diverse role in the regulation of chromatin (Miyamoto and Gurdon, 2012). Indeed, PolII transcription is dependent on actin polymerisation mediated by the ARP2/3 complex (Yoo et al., 2006). Monomeric actin binds to and sequesters transcription factors such as PREP2 (Haller et al., 2004). This offers an interesting possibility for actin polymerisation to act as an activator for transcription.

Recent structural work has shown that the BAF53 dimer adopts an unusual front-to-back arrangement within the BAF complex (Schubert et al., 2013). Indeed, the functions of ARPs in the BAF complex may be the regulation of ATPase activity rather than any coupling to actin dynamics (Szerlong et al., 2008).

1.1.3 Functions Of BAF Complex

The BAF complex repositions nucleosomes to regulate many processes throughout embryonic development and adult homeostasis.

1.1.3.1 Embryonic viability

An intact BAF complex is required for embryogenesis in many species. Mutation of *Brm* in *Drosophila* and *swsn-4* in *C. elegans* causes embryonic lethality (Elfring et al., 1998; Sawa et al., 2000), and in mice a null mutation in *Brg1* causes embryonic death at pre-implantation stages (Bultman et al., 2000). In contrast, *Brm$^{-/-}$* mice develop as healthy adults, although they are somewhat larger than normal (Reyes et al., 1998). This difference in requirement between Brg1 and Brm for embryogenesis can be explained by their expression patterns: Brm is expressed at 20-30 fold lower levels than Brg1 in embryonic tissues, and is thought to play a minimal role in development. Unlike studies in other animals, knock down of Brg1 in *Xenopus* using morpholinos did not cause embryonic lethality (Seo et al., 2005). However, Brg1 may only be partially depleted due to the dose of the morpholino used, or by the presence of maternally deposited Brg1 protein.

Similarly, BAF47 (Roberts et al., 2000), ARID1a/Osa (Gao et al., 2008; Treisman et al., 1997), and BAF155 (Han et al., 2008) are all required for embryonic survival across several species indicating that the BAF complex is crucial for the development of metazoans.

1.1.3.2 Embryonic Stem (ES) Cells

The requirement for the BAF complex – indeed specific subunits – to complete embryogenesis may come from the ability of the BAF complex to maintain pluripotency and regulate differentiation. As described in section 1.1.1.4, embryonic stem cells have a particular BAF complex composition called esBAF (Ho et al., 2009; Yan et al., 2008) and mutation of esBAF subunits has profound effects on ES cell biology. Deletion of either Brg1, ARID1a, ARID1b, BAF155 or BAF57 causes loss of self-renewal, pluripotency and reduces the capability of ES cells to differentiate (Gao et al., 2008; Schaniel et al., 2009; Singhal et al., 2014; Yan et al., 2008). Oct4 has been shown to bind to Brg1 and recruit the BAF

complex to DNA, so deletion of esBAF members could impair Oct4-mediated transcription (Singhal et al., 2014). As Oct4 is a master regulator of pluripotency (Jerabek et al., 2014), loss of Oct4 function could explain the observed phenotypes. Additionally, Brg1 has also been shown to antagonise the Polycomb repressive complex 2 (PRC2) and prevent the accumulation of repressive H3K27me3 marks (Ho et al., 2011). Finally, it was observed that the loss of pluripotency following esBAF disruption took place over several cell cycles, indicating that esBAF may regulate DNA replication (Takebayashi et al., 2013).

A final piece of evidence in support of a role for the esBAF complex in pluripotency is that addition of Brg1 and BAF155 to the four 'Yamanaka factors' (Oct4, Sox2, Klf4, and c-myc) significantly enhances the reprogramming of somatic cells into iPS cells (Singhal et al., 2010; Takahashi and Yamanaka, 2006). The mechanism behind BAF action appears to be enhanced de-methylation of pluripotency genes. These studies demonstrate that the BAF complex plays multiple roles within ES cells, which all contribute to the regulation of pluripotency.

1.1.3.3 Neuronal Development

Recent work has identified a key role for the BAF complex during neuronal differentiation. In the mammalian developing nervous system neural progenitor cells divide asymmetrically to give rise to a self-renewed progenitor cell and a differentiated daughter cell (Götz and Huttner, 2005). As progenitor cells differentiate there is a switch in BAF complex composition from npBAF to nBAF (see section 1.1.1.4). npBAF specific subunits are essential for the maintenance of progenitor cells. For example, loss of either BAF45a or BAF53a impairs proliferation of progenitors, whereas overexpression of BAF45a causes excess cell divisions (Lessard et al., 2007). Similarly, the npBAF component SS18 is required for neural progenitor maintenance (Staahl et al., 2013). As neuronal progenitors differentiate, SS18 is replaced by CREST, which is essential for correct outgrowth of dendrites in the daughter cells. Thus the switching of subunits is a key mechanism by which BAF complex function is controlled during differentiation.

Brg1 plays a complex role during neuronal development. In mouse embryos, Brg1 is required to maintain gliogenic neural progenitors, and to ensure the correct differentiation of astrocytes (Matsumoto et al., 2006). Conversely, in adult mice Brg1 controls the differentiation of neurons in conjunction with the transcription factor Pax6, and loss of either Brg1 or Pax6 causes stem cells to differentiate into glia (Ninkovic et al., 2013). Thus the BAF complex controls differentiation into both glia and neurons, although at different developmental times. Finally, there is evidence that the BAF complex plays a role in organ growth. Brm, BAF170, Pax6 and REST form a complex that acts to regulate neurogenesis and control the size of the cortex (Tuoc et al., 2013). Thus the BAF complex has roles in many levels of neuronal development, regulating self - renewal, differentiation and growth of neurons.

1.1.3.4 Other developmental roles

In addition to neurogenesis, the BAF complex is involved in many more processes during embryonic development. BAF60c has a critical role for heart morphogenesis, as mutant mice develop abnormal hearts and die around E10 (Lickert et al., 2004). During the reprogramming of mesoderm to cardiac tissue, BAF60c containing BAF complexes are required to decondense chromatin to allow binding of the transcription factors GATA4 and Tbx6 (Takeuchi and Bruneau, 2009). Interestingly, during somite differentiation in chick BAF60a and b are actively repressed by micro-RNAs (Goljanek-Whysall et al., 2014). Inhibition of these micro-RNAs or overexpression of BAF60a or b causes a delay in myogenesis, demonstrating how tight regulation of BAF complex subunits is important for correct timing and patterning during embryogenesis.

In *Drosophila,* BAF complexes control the differentiation of intestinal stem cells (Zeng et al., 2013), and in *C. elegans* an intact SWI-SNF complex is required for gonadogenesis (Large and Mathies, 2014). Finally the BAF complex is required for both skeletal and smooth muscle myogenesis (Puri and Mercola, 2012; Zhou et al., 2009). These examples show that the BAF complex is used widely throughout development, often using different subunits in a tissue-specific manner.

1.1.3.5 Cancer and the Cell Cycle

There is overwhelming evidence showing that the BAF complex is a critical tumour suppressor and negative regulator of the cell cycle. This was first discovered in 1998, when it was observed that a large proportion of childhood rhabdoid tumours have a mutation in SNF5 (Versteege et al., 1998). Loss of SNF5 in mice gives rise to similar tumours, confirming that SNF5 is a potent tumour suppressor (Roberts et al., 2000). Since then many high throughput sequencing experiments have demonstrated that BAF complex subunits are frequently mutated in ovarian and breast cancers (Yaniv, 2014). An in-depth analysis of BAF complex mutations across the scientific literature found that the BAF complex is frequently mutated over a wide range of cancers, suggesting that the complex plays a general tumour suppressive role rather than a tissue-specific one (Kadoch et al., 2013). Two other observations deserve mention: firstly, mutations in the BAF complex are often mutually exclusive with mutations in p53, indicating that loss of the BAF complex is able to drive tumourigenesis to a similar degree as loss of p53; and secondly BAF complexes often exhibit compound heterozygosity, meaning that rather than a complete knock out of a single subunit, several subunits are partially deleted simultaneously, highlighting the co-dependency of BAF subunits for the complex to function.

At the mechanistic level, cell cycle proteins bind to BAF complex members. In *Drosophila,* Osa binds to Cyclin E (Baig et al., 2010). Brg1, BAF60a and SNF5 bind to p53, are recruited to p53 regulated loci, and are required for activation of transcription of p53 target genes (Lee et al., 2002; Oh et al., 2008).

In addition to the regulation of proliferative genes, the BAF complex plays a role in the repair of DNA damage. Knock down of Brg1 causes an increase in the DNA damage marker H2AX (Alessio et al., 2010). BAF complexes are recruited to double strand break sites and bind to H2AX, and are required for its phosphorylation (Park et al., 2006). In addition to double strand break repair, the BAF and RSC complexes mediate base excision repair and nucleotide excision repair (Czaja et al., 2014; Lans et al., 2012). The tumour suppressive role of the BAF complex is therefore a combination of two effects: the transcriptional inhibition of pro-cycling genes and efficient DNA repair in response to damage.

1.1.3.6 Signalling pathways

The BAF complex positively and negatively regulates several signalling pathways (Simone, 2006). During left/right patterning in zebrafish BAF60c and Brg1 are essential for Notch signalling (Takeuchi et al., 2007). Conversely, Brm negatively regulates the Notch pathway during mouse retinal development (Das et al., 2007). It is likely that the presence of Brg1 or Brm within the complex plays a functional role in regulating responses to signalling cascades. For example Brg1 is required for steroid hormone (Fryer and Archer, 1998; King et al., 2012) and MAPK signalling (Simone et al., 2004), whereas Brm promotes non-canonical NFκB (Tando et al., 2010) and Hippo pathway activation (Skibinski et al., 2014)

Direct antagonism between Brg1 and Brm has been observed in Jurkat cells (Zhang et al., 2010). Under resting conditions, Brm-containing BAF complexes are present on IFNγ activated sequences (GAS) and the associated genes are not expressed. Upon IFNγ stimulation Brm is replaced by Brg1, resulting in relaxing of chromatin and expression of target genes. Hence in this situation the switch between Brm and Brg1 represents a switch between a repressed and an active state. However more studies are required to determine whether this is a general paradigm for the activity of the BAF complex with respect to signalling pathways.

There is also growing literature linking the BAF complex with the Wnt signalling pathway. Brg1 has been shown to bind to β-catenin and is required for transcription of Wnt target genes (Barker et al., 2001). In the developing mouse heart, Brg1 positively regulates Wnt signalling by promoting transcription of Fzd receptors (Griffin et al., 2011). Furthermore, Brg1 enhances Wnt signalling in response to the HDAC inhibitor butyrate, possibly by mediating an opening of TCF-target chromatin (Bordonaro et al., 2008). However, some evidence suggests that, as in other pathways, the BAF complex acts to both positively and negatively regulate Wnt signalling. Mutation of SNF5 causes a loss of TCF4 binding to DNA, and subsequent upregulation of Wnt target genes *myc*, *axin2* and *msx1* (Mora-Blanco et al., 2014). The BAF60c-containing BAF complex upregulates the non-canonical Wnt pathway and reduces nuclear β-catenin levels (Jordan et al., 2013). Thus the role of the BAF complex in Wnt pathway regulation is not straightforward, and requires further investigation.

1.1.4 ARID1a

ARID1a encodes the largest subunit of the BAF complex, sometimes referred to as BAF250a. For clarity, I will refer to the gene as *ARID1a* and the protein product as ARID1a.

ARID1a was first described in *Drosophila* as a suppressor of a mutation affecting eye formation (Treisman et al., 1997). It was named *Eyelid,* but is more commonly known as *Osa* in flies. Osa was then shown to bind Brm as part of the BAP complex (Collins et al., 1999). Shortly after, several groups cloned the mouse and human homologues and demonstrated that ARID1a is incorporated into the vertebrate BAF complex (Dallas et al., 2000; Hurlstone et al., 2002; Kozmik et al., 2001). ARID1a is a 250 kDa protein that only has 2 conserved domains: the AT-rich interacting domain (ARID), and the Eyelid-homology domain (EHD), which has similarities to Armadillo repeats (Fig. 1.1). The ARID region is misleadingly named, as *in vitro* studies have demonstrated that ARID1a possesses no preference for AT-rich sequences (Patsialou et al., 2005; Wilsker et al., 2004). A point mutation in the ARID region was shown to abrogate binding to DNA and caused de-repression of a reporter construct, demonstrating that the ARID region is crucial for the function of ARID1a (Chandler et al., 2012). Despite being an integral subunit of the BAF complex, ARID1a has been shown to shuttle between the nucleus and cytoplasm (Guan et al., 2012). The authors also demonstrated that the major site of ARID1a degradation was the nucleus.
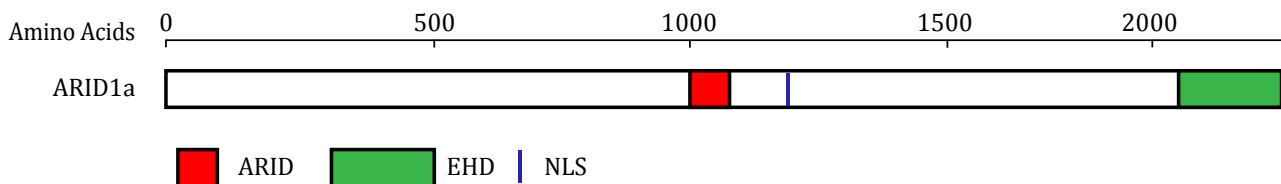
Fig. 1.5 Diagram of the Human ARID1a Protein

ARID1a is a 250 kDa protein with 2 domains. The AT-Rich Interacting Domain (ARID) spans residues 1,000-1,222. The Eyelid Homology Domain (EHD) is positioned at the C-terminus between residues 2,213 and 2,283. There is a putative Nuclear Localisation Sequence (NLS) centred around residue 1376. All three of these features are conserved between vertebrates.

It was later discovered that while *Drosophila* only has a single *Osa* gene, vertebrates have 2 genes that encode the largest subunit of the BAF complex: *ARID1a* and *ARID1b*. These are mutually exclusive members of the complex, and have some shared and some different functions (Wang et al., 2004b). For example, both *ARID1a* and *ARID1b* are required for embryonic viability and maintenance of stem cells (Gao et al., 2008; Yan et al., 2008), and both positively regulate hormone signalling (Inoue et al., 2002). In contrast, ARID1a acts as a negative regulator of the cell cycle, whereas ARID1b promotes proliferation (Nagl et al., 2007). Within the cell, ARID1a is more abundant that ARID1b in most cases studied (Singh and Archer, 2014; Wang et al., 2004a; Yan et al., 2008).

ChIP experiments have shown that ARID1a is most frequently associated with repressed genes, such as c-myc in senescent cells (Nagl et al., 2006). During *in vitro* cardiogenesis ARID1a inhibits cardiac differentiation by repressing expression of *Gata4*, *Myl3* and *cTnT* (Singh and Archer, 2014). However the role of *ARID1a* during cardiogenesis is uncertain, as a previous report showed that ARID1a promoted an open chromatin state at the promoters of key myogenic genes in the secondary heart field (Lei et al., 2012). These seemingly opposite effects may be due to differences in experimental conditions or lineage specific contributions. Regardless, at present the role of *ARID1a* in cardiomyocyte differentiation remains unclear.

In 2010, exonic sequencing revealed that *ARID1a* is mutated in over half of all ovarian clear cell carcinomas (Jones et al., 2010). Since then a large number of studies have identified ARID1a as a prevalent mutant in various forms of cancer (Mao and Shih, 2013). Mutations in *ARID1a* are associated with poor prognosis, and it has been proposed that *ARID1a* could be a useful biomarker for malignancy (Samartzis et al., 2012). Mechanistically it has been shown that ARID1a binds directly to p53, which could explain why ARID1a is such a potent tumour suppressor (Guan et al., 2011).

ARID1a regulates several signalling pathways, including FGF and steroid hormones (Collins and Treisman, 2000; Inoue et al., 2002; Terriente-Félix and de Celis, 2009). *Osa* mutant clones in the *Drosophila* wing disc display ectopic wing margin bristles, a phenotype consistent with enhanced Wg signalling (Treisman

et al., 1997). Subsequent work showed that overexpression of *Osa* was able to repress the Wg target gene *Nubbin* downstream of Armadillo (Collins and Treisman, 2000). However whether this is a direct effect of Osa on the Wg pathway is not clear, and molecular mechanism for the repression remains unknown. In order to investigate this further, I have used *Xenopus* as a model organism to ask whether, and if so how, *ARID1a* represses Wnt signalling in vertebrates.

1.2 The Wnt Pathway

1.2.1 Introduction

The Wnt signalling pathway regulates many events throughout embryogenesis, adult homeostasis and the progression of disease (Clevers, 2006). During early *Xenopus* development, the first role of Wnt/β-catenin signalling (also known as canonical Wnt signalling) is to specify the dorsal side of the embryo. This occurs after fertilisation and cortical rotation, Wnt pathway components activate transcription of *Siamois (Sia)* and *Xenopus Nodal related 3* (*Xnr3*), two key genes that establish the dorsal-ventral axis (see Section 1.2.6 for more detail).

In the absence of Wnt ligand free β-catenin is phosphorylated and then degraded by the destruction complex, a cytoplasmic complex formed of Axin, APC, CK1 and GSK3β (see Section 1.2.4). When Wnt ligands bind their receptors, however, the destruction complex is disrupted and β-catenin is able to accumulate in the cytoplasm. Free β-catenin then enters the nucleus, binds to TCF/LEF family members, and activates transcription (Fig. 1.2 A).

Here I discuss the proteins involved in canonical Wnt signalling and the proposed mechanism by which the pathway is regulated. I then describe the roles of Wnt signalling during early *Xenopus* development and some of the consequences when this pathway is dysregulated in humans.
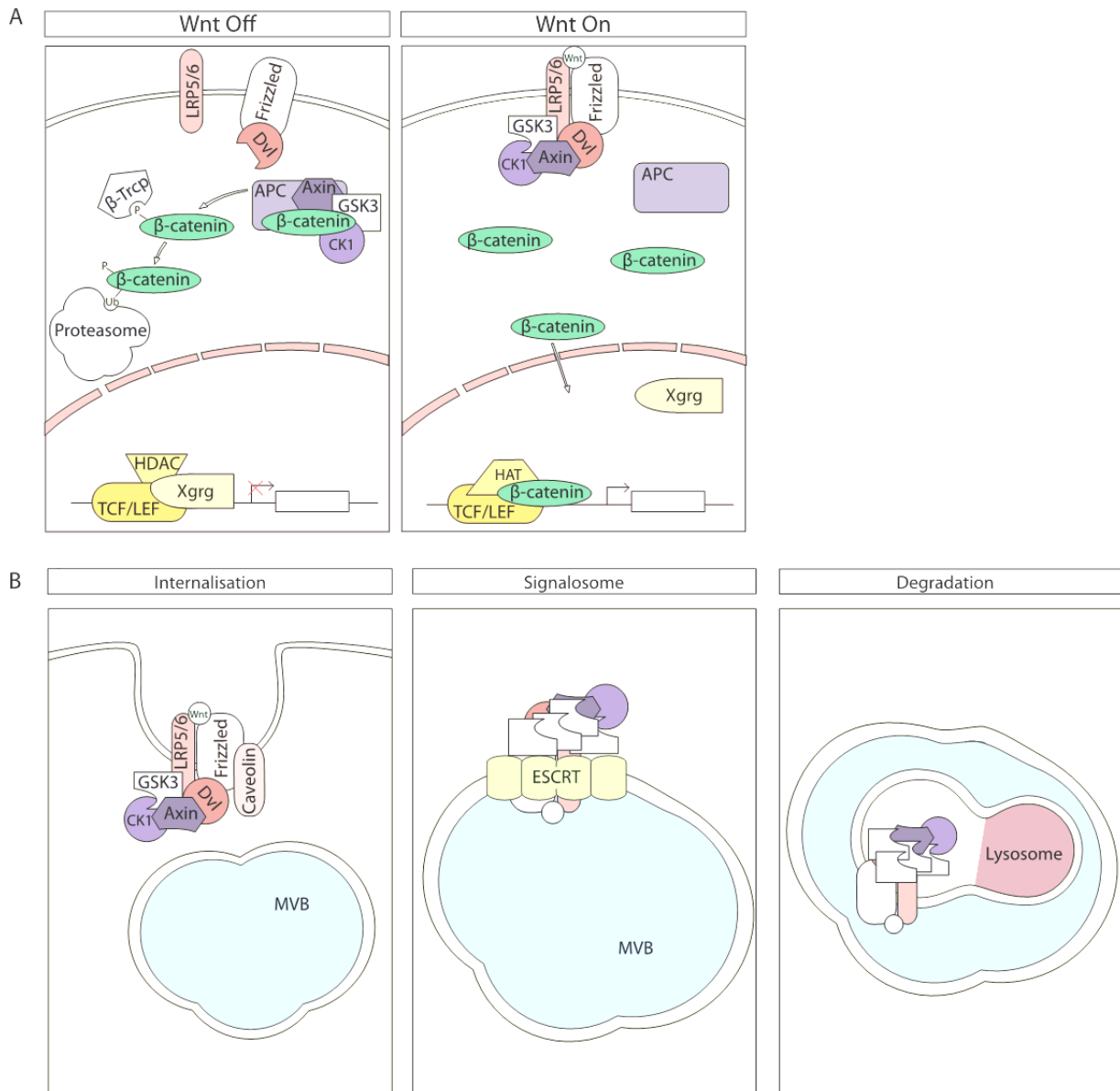
Fig. 1.6 The Wnt Signalling Pathway

A: overview of the Wnt signalling pathway. In the absence of ligand (left panel) β-catenin is phosphorylated, ubiquitinated and degraded by the proteasome. TLE/Groucho proteins bind to TCF/LEF proteins at Wnt Recognition Elements (WRE) and repress transcription. Wnt ligand binding disrupts the destruction complex (right panel) and β-catenin accumulates in the cell. Free β-catenin then displaces TLE/Groucho from TCF/LEF, binds to WREs and induces transcription.

B: Signalosome formation. Over extended periods of time, FZD receptor complexes are internalised in a Caveolin-dependent manner (left panel). Once internalised these receptor complexes form signalosomes, recruiting more GSK3β to multi-vesicular bodies (MVBs, middle panel). Signalosomes are internalised by the ESCRT machinery. Once within MVBs these endosomes fuse with lysosomes and the FZD complex is degraded (right panel). This causes a reduction in cellular GSK3β and subsequent activation of the Wnt pathway.

1.2.2 Wnt Ligands

1.2.2.1 Post-Translational Modification Of Wnt Ligands

Wnt ligands are highly conserved, cysteine-rich proteins consisting of ~250 amino acids. While individual Wnt proteins are conserved, the number of Wnt ligands varies between species: for example humans have 19 Wnt proteins, whereas there are only 16 in *Xenopus*. Following synthesis, Wnts undergo a series of post-translational modifications that are essential for their correct trafficking, secretion and biological activity (Baarsma et al., 2013). With the exception of Wnt8/WntD, all Wnt ligands are N-glycosylated (Herr and Basler, 2012). This modification requires Porcupine (Tanaka, 2002), and loss of Prc phenocopies loss of Wnt signalling in *Drosophila* (Perrimon et al., 1989). However, in tissue culture there seems to be no requirement for N-glysosylation for canonical Wnt activity, while *in vivo* N-glycosylation reduces the potency of Wnt ligands (Doubravska et al., 2011), raising the question as to what is the function of this modification.

Wnt ligands are palmitoylated at serine209 and its orthologous positions (Takada et al., 2006; Willert et al., 2003). Mutation of this serine in *Drosophila* severely reduces the ability of Wnt ligands to activate signalling (Franch-Marro et al., 2008). This palmitoylation of Wnt3a is mediated by Porcupine, and is independent of N-glycosylation (Gao and Hannoush, 2013).

It has been proposed that palmitoylation is required for Wnts to interact with Wntless (Wls)/Evi; (Herr and Basler, 2012), which transports Wnt proteins through the trans-Golgi network to the plasma membrane (Bartscherer et al., 2006; Bänziger et al., 2006; Goodman et al., 2006). While Wls/Evi is the major mechanism by which Wnt ligands are secreted, there is evidence for an alternative secretory pathway. Wnt3a palmitoyl-deficient mutants are secreted in the absence of Wls/Evi, although their activity is much reduced (Neumann et al., 2009). Additionally Wnt8, which is not post-translationally palmitoylated, is secreted via a Wls/Evi independent, Rab1-dependent pathway (Ching et al., 2008).

1.2.2.2 Heparan-Sulphate Proteoglycans and Wnt Ligands

Once secreted, a large proportion of Wnt ligand is retained at the cell surface. This is thought to be mediated by heparan-sulphate proteoglycans (HSPGs) which are located on the outer surface of the plasma membrane. HSPGs are comprised of a central protein modified with HS and glycosaminoglycans (GAGs; (Lin, 2004). Binding of Wnt ligands to HSPGs is crucial for normal signalling, as enzymatic removal of surface proteoglycans or chemical inhibition of sulphases significantly impairs Wnt signalling (Reichsman et al., 1996).

There are currently two models for how HSPGs act to potentiate Wnt signalling: 1) they increase the local concentration of ligand by limiting diffusion to two dimensions (i.e. the plasma membrane); or 2) they act as part of the FZD/LRP5/6 receptor complex (Lin, 2004). In support of the first model, immunostaining of Wnt ligands shows they are retained at the plasma membrane of secreting cells (Pfeiffer et al., 2002). Disruption of HSPGs causes a loss of this localisation, and in *Drosophila* HSPG mutants can be rescued by overexpressing Wg. These observations indicate that HSPGs act to increase the concentration of Wnt ligands (Häcker et al., 1997). Consistent with this model healthy, viable adult *Drosophila* can be obtained when Wg is replaced by a membrane tethered, non-diffusible form of Wg, indicating that Wnt ligands probably have a very limited range of diffusion (Alexandre et al., 2014).

Evidence for the second hypothesis comes from recent work investigating other GAG-containing proteins that bind to extracellular Wnt ligands. For example, biglycan binds to both Wnt3a and LRP6, and is required in calvarial cells for retention of Wnt ligand and full activation of the Wnt pathway (Berendsen et al., 2011). Similarly, in neuroblastoma cells and primary rat hippocampal neurones addition of heparin causes activation of the Wnt pathway by enhancing the activity of Wnt ligands (Colombres et al., 2008). Thus it is possible that GAG-containing proteins act both by trapping Wnt ligands at the cell surface, and by enhancing formation of ligand-receptor complexes.

1.2.2.3 Extracellular Regulators Of Wnt Ligands

Wnt ligands are subject to extracellular regulation by several different secreted proteins: the secreted frizzled related proteins (sFRPs) 1-5, Cerberus, and Wnt inhibitory factor 1 (WIF1; (Baarsma et al., 2013).

sFRPs consist of an N-terminal cysteine-rich domain (CRD) that is 30-50% similar to those of Fzd receptors, including 10 highly conserved cysteine residues, and a C-terminal domain that shares weak homology with netrin (Bafico et al., 1999; Finch et al., 1997). Experiments in tissue culture showed that sFRP1 accumulates at the cell surface and binds to Wnt ligands, sequestering them and preventing activation of the signalling pathway (Bafico et al., 1999; Galli et al., 2006). Somewhat unexpectedly, this ability of sFRP1 to bind Wnt ligands does not require the CRD (Uren et al., 2000).

While sFRPs were originally characterised by their ability to inhibit Wnt signalling, this may not be their normal function *in vivo.* In fact, sFRPs may actively promote Wnt signalling. Work in *Xenopus* showed that sFRP3 (also known as Frzb) and Crescent (Cresc) bind to Wnt ligands and enhance their diffusion (Mii and Taira, 2009). In this case sFRPs act as chaperones to establish a gradient of Wnt ligands across the prospective mesoderm in *Xenopus*.

In agreement with this model, sFRPs have two binding sites for Wnt ligands: a high affinity site that enhances Wnt signalling, and a lower affinity site that inhibits Wnt signalling (Uren et al., 2000).

Several other secreted proteins interact with Wnt ligands in the extracellular space. Cerberus (Cer) and Wif1 bind to Wnt ligands and are able to repress pathway activation (Bouwmeester et al., 1996; Hsieh et al., 1999), although Cer does not affect Wnt signalling in mice (Belo et al., 2000). However the ability of Cer or Wif1 to act as chaperones and enhance the diffusion of Wnt ligands has not been tested, so whether this action of sFRPs is a general property of secreted Wnt interacting proteins is yet to be determined.

1.2.3 Wnt Receptors

1.2.3.1 Frizzled and LRP5/6

In 1996, two groups demonstrated that the transmembrane protein Frizzled is a receptor for Wnt ligands (Bhanot et al., 1996; Yang-Snyder et al., 1996). The Frizzled (FZD) family of receptors consists of ten proteins in mammals (FZD$_{1-10}$), while only four exist in *Drosophila* (Fz, Dfz2-4; (Schulte, 2010). FZD receptors have an extracellular cysteine-rich domain (CRD), seven membrane spanning domains reminiscent of G-protein coupled receptors (GCPRs), and an intracellular domain (Vinson et al., 1989). Crystal structure of the CRD showed that it dimerises to bind Wnt ligands (Dann et al., 2001). This was confirmed in *Xenopus,* where FZD$_3$ forms dimers in response to Wnt signalling. Indeed, forcing the dimerisation of FZD$_3$ or FZD$_7$ is sufficient to induce expression of *Siamois* (*Sia;* (Carron et al., 2003).

There are 19 Wnt ligands and 10 FZD receptors in humans, and it remains very poorly understood how different branches of the Wnt signalling cascade are activated in a controlled manner. The ligands and receptors are promiscuous, and specificity is not simply defined by particular ligands binding to particular receptors. However the large diversity of Wnt and FZD proteins suggests some functional relevance to ligand-receptor pairing. For example Wnt5a is most commonly thought of as an activator of non-canonical signalling (see section 1.2.7). However, when it is paired with FZD$_4$, Wnt5a causes stabilisation of β-catenin and activation of TCF reporters (Mikels and Nusse, 2006). While systematic analysis of Wnt-FZD affinities has yet to be carried out, the K$_D$ values for some components in *Drosophila* have been measured. By titrating soluble alkaline phosphatase-conjugated Fz CRDs against membrane bound Wnt molecules, the Nusse group determined the binding affinity for several different ligand-receptor pairs (Rulifson et al., 2000; Wu and Nusse, 2002). Wg and Wnt2 bound Fz, Dfz2 and Dfz3, whereas Dwnt8 only bound to Dfz4. Strangely, Dwnt3 did not bind to any of the *Drosophila* Fz proteins, but has been shown to bind RYK/Derailed receptors to potentiate non-canonical signalling (Lahaye et al., 2012) see below).

As well as FZDs, low-density lipoprotein receptor like proteins 5 and 6 (LRP5/6) are absolutely required for Wnt signalling. This was discovered when mutations in the *Drosophila Arrow* gene (a homologue of LRP6) blocked Wg signalling upstream of Dishevelled (Dsh in flies, Dvl in vertebrates; (Wehrli et al., 2000), while in *Xenopus* overexpression of LRP6 synergises with Wnt5a to induce secondary axes (Tamai et al., 2000). The extracellular portion of LRP6 consists of three LDLR repeats and four β-propeller domains (He et al., 2004), which bind to Wnt ligands (Liu et al., 2009). Indeed Wnt3a and Wnt9 bind to different β-propeller domains simultaneously, indicating that multiple ligands might act together to stimulate the same receptor complex (Bourhis et al., 2010).

Wnt ligands cause LRP5/6 and FZD to form heterodimers to propagate signals across the membrane (He et al., 2004). Indeed, artificial dimerisation of FZD and LRP6 causes phosphorylation of a PPPSP motif on the C-terminal tail of LRP6, which is sufficient to activate the Wnt pathway (Tamai et al., 2004; Zeng et al., 2008). LRP6 is sequentially phosphorylated, first by GSK3β and then by membrane-tethered CK1γ (Davidson et al., 2005; Zeng et al., 2005). Phospho-LRP6/FZD complexes then recruit Axin and GSK3β to the membrane, disrupting the destruction complex (see section 1.2.4.1;(Cong et al., 2004; Yang-Snyder et al., 1996). Dvl is also recruited to FZD/LRP6 dimers and promotes the formation of large, subapical oligomeric complexes termed signalosomes (Bilic et al., 2007), which are internalised in a Caveolin-dependent manner (Yamamoto et al., 2006). Over time these signalosomes are incorporated into multivesicular bodies (MVBs), where Axin, Dvl and GSK3β are degraded (Taelman et al., 2010). The phospshorylation and internalisation of LRP5/6 is enhanced by R-spondins (Carmon et al., 2011), which are vertebrate specific, secreted proteins that promote Wnt signalling (de Lau et al., 2012; Kamata et al., 2004). Curiously, R-spondins also enhance degradation of LRP6 and β-catenin, suggesting that they act to cause a spike in Wnt signalling that is rapidly shut off.

FZD proteins are atypical G-protein coupled receptors – so much so that they have been assigned as a separate subfamily (Schulte, 2010). FZD proteins are able to catalyse the breakdown of Go proteins into Goα and Goβγ subunits (Katanaev and Buestorf, 2009), and Go is essential for both canonical and

non-canonical signalling in *Drosophila* and vertebrates (Katanaev et al., 2005; Liu et al., 2001). Indeed, genetic experiments in *Drosophila* suggest that Goα recruits Axin to the signalosome, whereas Goβγ recruits Dsh/Dvl, enhancing activation of the Wnt signalling pathway (Egger-Adam and Katanaev, 2009).

Finally, the presence of receptors at the membrane can be a regulatory point within the Wnt signalling cascade. The secreted protein Dickkopf-1 (Dkk1) has long been known to be an inhibitor of Wnt signalling (Glinka et al., 1998). Dkk1 binds to LRP6 using the same β-propeller motifs as Wnt ligands, thus acting as a competitive inhibitor (Bourhis et al., 2010). Furthermore, Dkk1 binding causes internalisation of LRP6 in association with the protein Kremen (Krm; (Mao et al., 2002). Krm plays a complex role in the regulation of LRP6, as not only is it required for Dkk1-mediated inhibition of Wnt signalling, but it also acts to increase the levels of LRP6 at the cell membrane in the absence of Dkk1 (Hassler et al., 2007). This dual activity has been proposed to create a sharp on/off boundary of Wnt signalling in response to a Dkk1 gradient (Cselenyi and Lee, 2008). Thus the levels of FZD and LRP5/6 protein present at the cell membrane play a key role in regulating the ability of cells to respond to Wnt ligands.

1.2.3.2 Alternative Receptors

Besides FZD and LRP5/6 several other transmembrane proteins transduce Wnt signals. The receptor tyrosine kinase (RTK) ROR2 activates non-canonical Wnt signalling and enhances convergent extension in *Xenopus* animal caps (Hikasa et al., 2002; Oishi et al., 2003). The "non-canonical" ligand Wnt5a binds to ROR2, inducing receptor dimerization and RTK signalling (Liu et al., 2008). In addition to potentiating non-canonical signals, this activation of ROR2 is known to inhibit the intracellular canonical Wnt pathway (Mikels and Nusse, 2006).

RYK is an atypical receptor tyrosine kinase with a WIF1-like extracellular domain and non-functional kinase domains (Yoshikawa et al., 2001). RYK binding to Wnt5a activates calcium signalling to co-ordinate neuronal pathfinding (Yoshikawa et al., 2003); (Li et al., 2009), and during convergent extension in *Xenopus* RYK enhances non-canonical signalling by internalising FZD$_7$ (Kim et al., 2008).

RYK also plays a role in β-catenin-dependent signalling, because a ternary complex of RYK, FZD_8 and Wnt3a or Wnt1 is able to activate luciferase reporters in HEK293 cells (Lu et al., 2004) and induce neuronal differentiation of neural progenitor cells in vitro (Lyu et al., 2008). In the latter example the intracellular domain of RYK was cleaved and localised to the nucleus in a similar manner to that seen for FZD, although the functional consequences of this event is unclear. Finally, RYK and the E3 Ubiquitin ligase Mindbomb1 (Mib1) interact to activate canonical signalling (Berndt et al., 2011). These observations contradict previous findings in *Drosophila*, where the RYK homologue Derailed could not bind to either Wg (Wnt1) or Wnt4 (Yoshikawa et al., 2001). A possible explanation for this is that *Drosophila* has 3 RYK homologues, and the RYK-Wnt interaction could exist in one of the untested homologues.

1.2.4 Destruction Complex Mediated Degradation of β-catenin

The destruction complex represses Wnt signalling in the absence of ligand by first phosphorylating and then ubiquitinating β-catenin, which is subsequently degraded by the proteasome. It is composed of five core proteins: Axin, Adenomatous Polyposis Coli (APC), Glycogen Synthase Kinase 3β (GSK3β), Casein Kinase 1 (CK1) and β-Transducin Repeat Containing Protein (βTrCP) (MacDonald et al., 2009). Loss of any of these proteins leads to accumulation of β-catenin and transcription of Wnt target genes.

1.2.4.1 The Axin Scaffold

Axin was named for its ability to inhibit axis formation in *Xenopus* when it is overexpressed (Zeng et al., 1997). Axin is a largely unstructured, flexible protein with binding sites for many of the destruction complex components (Fig. 1.3). Axin binds to APC via an N-terminal RGS domain, and to GSK3β with a central α-helix (Dajani et al., 2003; Spink et al., 2000). β-catenin binds to Axin at a site just distal to GSK3β (Ikeda et al., 1998), and CK1 and protein phosphatase 2A (PP2A) bind more distally still (Hsu et al., 1999; Liu et al., 2002).
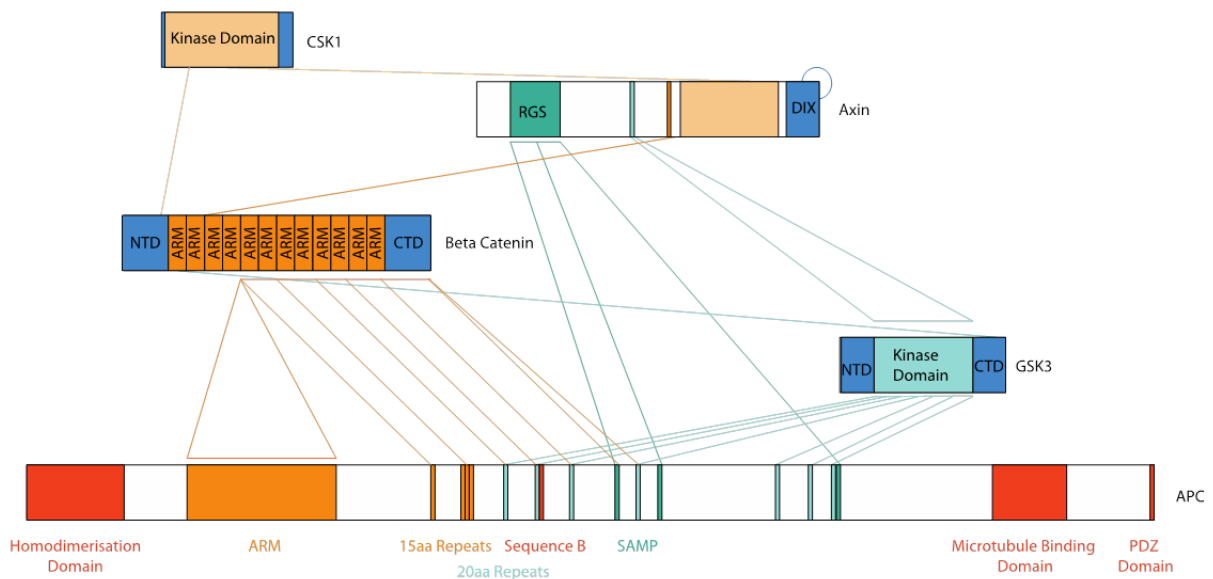
Fig. 1.7 Physical Interactions Between Members of The Destruction Complex

Diagram showing the relative size and domain composition of the destruction complex proteins.

Physical interactions are represented by lines. Axin homodimerises via its DIX domain.

NTD = N terminal domain

CTD = C terminal domain

ARM = Armadillo repeat

RGS = Regulation of G-protein signaliing

DIX = dishevelled and axin

The C-terminus of Axin contains a DIX domain that allows it to form homopolymers and create large destruction complex foci (Luo et al., 2005), although the polymerisation of Axin is not required for its ability to inhibit Wnt signalling. Axin increases the local concentration of β-catenin and its kinases and greatly enhances β-catenin turnover (Stamos and Weis, 2013). In fact, the addition of Axin to *in vitro* kinase assays increases the phosphorylation of β-catenin by as much as 20,000 fold (Dajani et al., 2003).

1.2.4.2 Phosphorylation, Ubiquitination and Degradation of *β-catenin*

In resting cells a large portion of the total β-catenin forms cadherin complexes at the membranes and does not participate in Wnt signalling (van de Wetering et al., 2001). The remaining cytosolic β-catenin is phosphorylated within the destruction complex by CK1 proteins at Serine45 (S45; (Amit et al., 2002; Liu et al., 2002; Stamos and Weis, 2013). This phosphoserine acts as a priming site for GSK3β, which then phosphorylates T41, S37 and S33 sequentially (Hagen et al., 2002; Yost et al., 1996). Point mutation at any of these sites results in stabilised β-catenin that stimulates transcription of Wnt target genes.

In addition to phosphorylating β-catenin, GSK3β has a wide range of substrates within the cell (Atkins et al., 2013)—in fact only 5% of cellular GSK3β is bound to Axin (Li et al., 2012; Ng et al., 2009). GSK3β phosphorylates both Axin and APC, increasing their affinity for β-catenin (Salic et al., 2000; Willert et al., 1999; Yamamoto et al., 1999). In this manner GSK3β acts as a feed-forward mechanism to enhance phosphorylation of β-catenin. While most studies focus on GSK3β, knock out work in mice has shown that GSK3α and β are functionally redundant in the regulation of Wnt signalling (Doble et al., 2007). Thus much of what is known for GSK3β is probably true for GSK3α.

Once phosphorylated, β-catenin is ubiquitinated by the E3 ligase β-TrCP (Kitagawa et al., 1999). Polyubiquitinated β-catenin is then degraded by the proteasome (Orford et al., 1997). Recent work has demonstrated that ubiquitinated β-catenin remains bound to Axin and that the proteasome is recruited to the destruction complex to degrade β-catenin (Li et al., 2012).

1.2.4.3 The Role of APC In The Destruction Complex

APC has long been known to be a critical regulator of the Wnt signalling pathway. Mutations in APC occur in around 80% of colon cancers and are thought to be the driving oncogenic force by constitutively activating the Wnt pathway. Many different colorectal carcinoma cell lines with truncated APC proteins have been used to demonstrate that loss of APC causes nuclear localisation of β-catenin and hyperactivation of the Wnt pathway (Minde et al., 2011). However, despite focussed research, the mechanistic role of APC in the regulation of Wnt signalling is still unclear (Stamos and Weis, 2013).

APC is a large, 310 kDa protein with a flexible unstructured central region that contains docking sites for destruction complex components. This region has four 15 amino acid (aa) repeats, seven 20 amino acid repeat segments that bind to β-catenin (Eklof Spink, 2001; Rubinfeld et al., 1997), and three SAMP repeats that bind to Axin (Behrens et al., 1998). The role of APC in the regulation of β-catenin phosphorylation is unclear. Su and colleagues showed that addition of APC to *in vitro* reactions did not stimulate β-catenin phosphorylation by CK1α or GSK3β (Su et al., 2008). Instead it protected phospho-β-catenin from Protein Phosphatase 2A. Conflicting data from the Klein lab showed that APC did in fact stimulate the activity of GSK3β *in vitro* (Valvezan et al., 2012)*.* However, this study only used a partial fragment of APC, and thus may not reflect the function of the intact protein.

It is more likely that APC acts to positively regulate the ubiquitination of β-catenin. The second and third 20 aa repeats in APC are required for ubiquitination of β-catenin (Su et al., 2008). SW480 and DLD-1 cell lines have truncated APC that lacks the second, or second and third, 20aa repeats respectively. β-catenin in these cell lines is not ubiquitinated, although it does still bind to β-TrCP, raising the possibility that APC could be required to catalyse the addition of ubiquitin to β-catenin (Yang et al., 2006a).

In addition to regulating the post-translation modification of β-catenin, APC has been proposed to act as a sink, sequestering β-catenin in the cytoplasm and therefore dampening Wnt induced transcription (Roberts et al., 2011).

Determining the precise role of APC in the destruction complex will be a key step towards our understanding of how free β-catenin is degraded in the absence of Wnt signalling.

1.2.5 Nuclear Regulation Of Canonical Wnt Signalling

Free β-catenin rapidly enters the nucleus and promotes transcription of Wnt target genes by binding to TCF proteins. In the absence of signal, TCF proteins bind co-repressors of the TLE/Groucho family and suppress expression of Wnt target genes.

1.2.5.1 The 'Wnt Off' State

Wnt target genes often contain a Wnt Responsive Element (WRE) in their regulatory regions, characterised by the motif WWCAAG where W represents A or T. These WREs are bound by members of the T-Cell Factor/Lymphoid Enhancer Factor (TCF/LEF) family, of which there are 4 in vertebrates (TCF1, 3, 4 and LEF1) and one each in *Drosophila* (dTCF/Pan) and *C. elegans* (POP1; (Mao and Byers, 2011). TCF/LEF proteins have three domains: an N-terminal β-catenin-binding domain, a high mobility group (HMG) domain that binds to DNA and promotes severe bending, and a cysteine (c)-clamp that is present in some but not all TCF proteins and confers DNA binding to extra sites (Atcha et al., 2007; Love et al., 1995; Molenaar et al., 1996). While the action of each TCF must be considered on a gene-by-gene basis, the different TCFs do seem to have different preferences: LEF1 is predominantly an activator of transcription while TCF3 is mostly repressive. TCF1 and TCF4 act as activators and repressors in equal measure (MacDonald et al., 2009). ChIP-seq studies of TCF4 in colorectal carcinoma cells showed that over 70% of TCF binding sites are more than 10 kb from the nearest transcription start site (TSS; (Hatzis et al., 2008). The remaining sites are distributed in an approximately 3 kb region surrounding the TSS, but are not as tightly clustered as peaks for other transcription factors. Only 10-15% of all TCF binding sites are co-bound in the presence of β-catenin, emphasising the role of TCF proteins in the regulation of other biological functions (Schuijers et al., 2014).
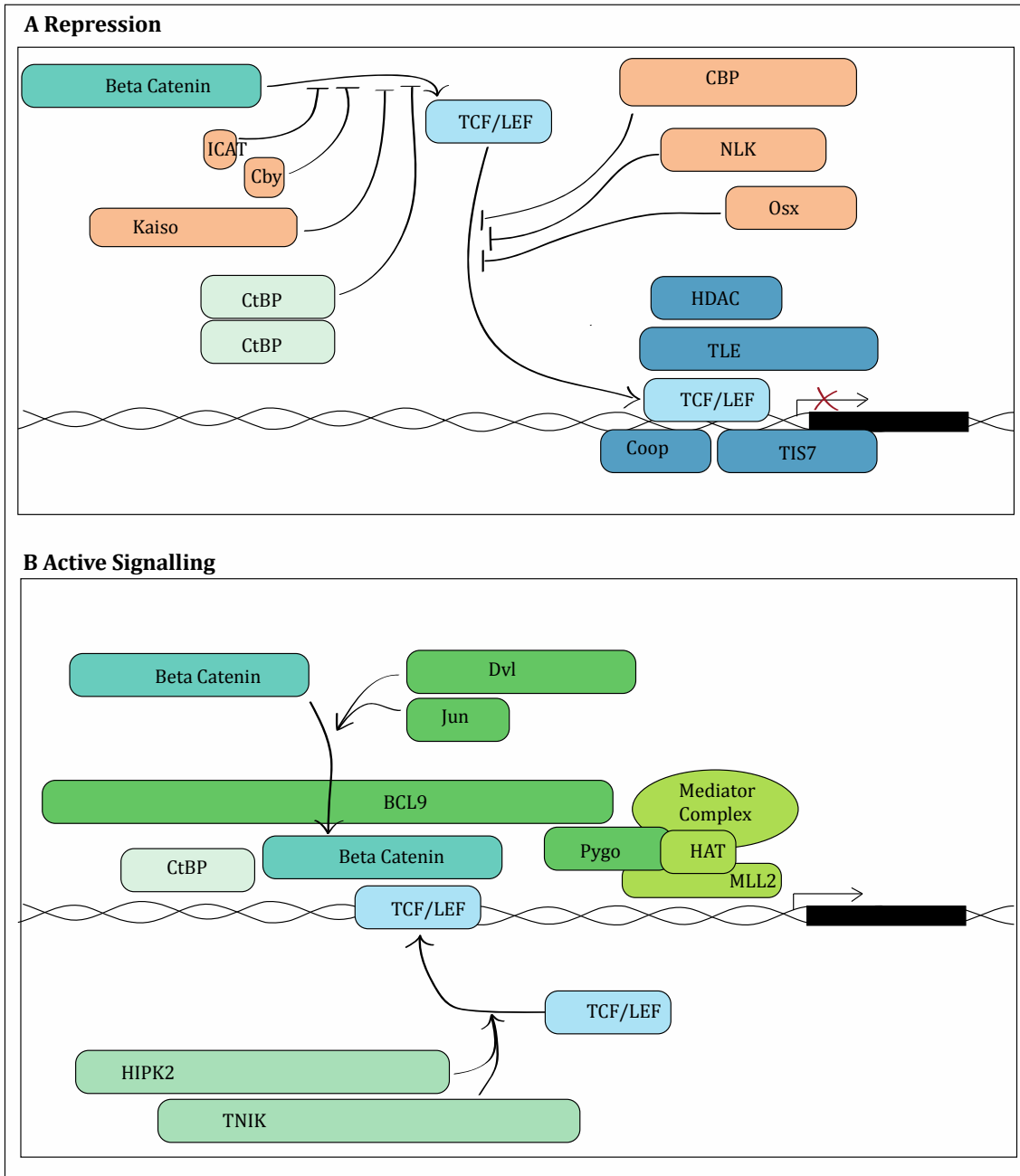
Fig. 1.8 Nuclear Regulation Of Wnt Signalling

A: In the absence of Wnt signalling TCF/LEF proteins bind to co-repressors that recruit histone deacetylases. Additional protein-protein interactions prevent the association of TCF/LEF proteins with DNA, or beta-catenin with TCF/LEF proteins.

B: Stablised beta-catenin binds to BCL9 and Pygopus to form a chain of adaptors that recruitshistone acetylases and the mediator complex to activate transcription. Phosphorylation of TCF/LEF proteins enhances their association with DNA, while Dvl and Jun enhance binding of beta-catenin to TCF/LEF.

The expression of TCF proteins is highly complex, as each TCF has alternative promoters and is alternatively spliced to give rise to different isoforms in a tissue-specific manner (van de Wetering et al., 1996). The most striking example of this is the skipping of exon1 in LEF1, resulting in the loss of the β-catenin binding domain and formation of a natural dominant negative that inhibits Wnt signalling (Hovanes et al., 2001). However more recent work in osteoblasts has demonstrated that Lef1-ΔN is still able to bind β-catenin and enhance luciferase activity (Hoeppner et al., 2011), highlighting cell-type specific differences in the regulation of TCF activity.

The Wnt target gene *Sia* contains a WRE in its promoter region. Deletion of the WRE causes an increase in activity of a *Sia* reporter gene in the absence of Wnt ligand, indicating that TCF/LEF proteins act to suppress Wnt target genes (Brannon et al., 1997). Since this early observation it has become clear that TCF/LEF proteins play a vital role in the inhibition of Wnt target genes by binding the repressive protein Groucho (Cavallo et al., 1998; Roose et al., 1998). Vertebrates have four Groucho homologues, known as either Groucho-related genes (Grg1-4) or transducin-like enhancer of split (TLE) proteins (Cadigan, 2012).

TLE proteins consist of five domains, the first two of which are involved in Wnt signalling. The N-terminal Q domain mediates homotetramerisation of TLE proteins, a property that is required for their function (Song et al., 2004), and it is this domain that binds to TCF proteins (Brantjes et al., 2001). The GP domain binds to histone deacetylases (HDACs), including Rpd3/HDAC3 (Chen et al., 1999). Treatment of cells with the HDAC inhibitor trichostatin A (TSA) reduces the ability of TLE to repress luciferase reporters indicating that this may be the major mechanism by which TLE proteins act.

Non-TLE proteins also act to repress Wnt target genes. Co-repressor of Pan (Coop), TIS7 and some myeloid translocation genes (MTGs) bind TCF and recruit HDACs in a similar manner to TLE to repress Wnt target genes (Moore et al., 2008; Song et al., 2010; Vietor et al., 2005).

In contrast, Osterix regulates Wnt signalling by preventing the association of TCF1 with DNA (Zhang et al., 2008), while Kaiso stops β-catenin from binding promoter sequences (Park et al., 2005). HIC1 recruits TCF4 into HIC1 bodies, sequestering it from the rest of the cell (Valenta et al., 2006). This is of particular interest because ARID1a also binds to HIC1 (Van Rechem et al., 2009). Finally, post-translational modification of TCF proteins can regulate their activity. Creb-binding protein (CBP) acetylates dTCF in *Drosophila* and reduces its capacity to bind Armadillo (Waltzer and Bienz, 1998). In HEK293 cells phosphorylation of TCF4 or LEF1 by Nemo-like kinase (NLK) reduces activation of luciferase reporters and prevents binding of β-catenin/TCF complexes to DNA (Ishitani et al., 2003).

Several proteins have been identified that prevent β-catenin from binding to TCF/LEF proteins. Chibby (Cby) and inhibitor of β-catenin and TCF binding (ICAT) bind to β-catenin and compete with LEF1 and TCF3 respectively (Graham et al., 2002; Takemaru et al., 2003). APC shuttles between the cytoplasm and the nucleus, and has been proposed to mediate nuclear export of β-catenin (Henderson, 2000; Sierra et al., 2006). However, APC proteins tethered to the cell membrane or mitochondria are able to completely rescue APC mutant cells, arguing against a requirement for APC shuttling (Roberts et al., 2012). As these experiments used overexpressed APC, it may be that high levels of APC are able to compensate for a lack of shuttling. Therefore experiments using inducible or shuttling mutants are required to resolve the requirement of APC in the nucleus.

1.2.5.2 The 'Wnt On' State

Wnt signalling causes β-catenin to accumulate in the nucleus within 30 minutes (Li et al., 2012). Mathematical modelling suggests that this rapid influx is mediated by active transport, although the proteins responsible are unknown (Tan et al., 2014). Once nuclear, β-catenin binds to the N-terminal β-catenin Binding Domain (BBD) of TCF/LEF proteins and displaces TLE (Daniels and Weis, 2005). This displacement is consistent with work of Sierra and colleagues, who used ChIP time course experiments to show that TLE1 and β-catenin never bind the c-myc enhancer at the same time (Sierra et al., 2006).

TCF/LEF proteins are essential for expression of Wnt target genes. Knock down of TCF1 in *Xenopus* completely blocks the Wnt pathway, while mutation of TCF binding sites in luciferase reporters renders them incapable of responding to Wnt signals (Liu et al., 2005; Veeman et al., 2003).

Once bound to TCF and DNA, β-catenin recruits a wide range of factors to initiate transcription. For example, β-catenin recruits Pygopus (Pygo) and BCL9/Legless to form a "chain of adaptors" (Städeli and Basler, 2005). BCL9 acts as a bridging factor, binding to the first ARM repeat of β-catenin via its homology domain 1 (HD1) and to the PHD domain of Pygo via HD2 (see Fig. 1.4; (Hoffmans and Basler, 2004; Kramps et al., 2002). Pygo in turn then recruits the Med12 and Med13 subunits of the Mediator complex via its NH2 domain to promote transcription (Carrera et al., 2008). Alternatively the NH2 domain has been shown to bind <u>h</u>istone <u>a</u>cetyl <u>t</u>ransferases (HATs) and the <u>h</u>istone <u>m</u>ethyl<u>t</u>ransferase (HMT) MLL2, both of which remodel chromatin to promote transcription (Chen et al., 2010).

The N-terminus of β-catenin also recruits <u>C</u> terminal <u>b</u>inding <u>p</u>rotein (CtBP), which plays a dual role in the regulation of transcription. While monomeric, CtBP enhances β-catenin mediated transcription. Conversely, CtBP homodimers act to repress β-catenin, though the mechanism behind this switch is not clear (Bhambhani et al., 2011). Finally TCF/LEF proteins can also recruit cofactors to enhance Wnt signalling. <u>T</u>randuction <u>β</u> <u>l</u>ike <u>p</u>rotein 1 (TBL1) and TBLR1 bind to TCF and are required for activation luciferase reporters (Li and Wang, 2008). Phosphorylation by <u>h</u>omeodomain <u>i</u>nteracting <u>p</u>rotein <u>k</u>inase 2 (HIPK2) reduces the ability of TCFs to repress signalling (Hikasa and Sokol, 2011), while phosphorylation by <u>T</u>raf2/<u>N</u>ck <u>i</u>nteracting <u>k</u>inase (TNIK) actively promotes β-catenin mediated transcription (Mahmoudi et al., 2009).

In addition to displacing TLE repressors from TCFs, it has been proposed that active Wnt signalling causes the replacement of repressive TCF/LEF proteins with permissive ones. Over the course of several hours, repressive TCF3 is lost from WREs in response to Wnt signalling (Shy et al., 2013). Furthermore, repressive TCF1 is exported from the nucleus by the Wnt/Calcium pathway in

cancer cell lines while TCF4 is not, changing the balance of stimulatory/repressive TCF proteins within the nucleus (Najdi et al., 2009). This switch in TCF proteins represents a feed-forward loop whereby prolonged Wnt signalling promotes further activation of the pathway.

Several proteins that play a role in the cytoplasmic regulation of the Wnt pathway are known to enter the nucleus and affect β-catenin-mediated transcription. Dvl binds to β-catenin/TCF4 complexes, recruits c-jun and is essential for Wnt stimulated transcription in HEK293T cells (Gan et al., 2008). There is some evidence that the intracellular domains of FZD and RYK are cleaved following ligand binding and can enter the nucleus to promote transcription (Lyu et al., 2008; Mathew et al., 2005). Finally, as noted earlier, a subset of cellular APC exists within the nucleus. APC is able to bind WREs together with CtBP, but not at the same time as β-catenin (Sierra et al., 2006). Sierra and colleagues make the interesting observation that during continuous Wnt stimulation β-catenin/TCF complexes are displaced from chromatin by APC/CtBP complexes, which are in turn replaced by repressive TCF/TLE complexes. Presumably, β-catenin then displaces TLE and the cycle continues. This is one of the few studies to assess the dynamics of Wnt signalling and the changes at WREs over time. More of these investigations, perhaps with respect to chromatin modifications, could shed light onto the long-term effects of Wnt stimulation.

1.2.5.3 Chromatin Modifications During Wnt Signalling

In order to promote transcription β-catenin recruits a range of chromatin modifiers. CBP and p300 are histone acetyl transferases (HATs) that bind to the C-terminal part of β-catenin (Takemaru and Moon, 2000). In depth study of the *naked cuticle* and *notum* loci showed that TCFs, acetyl H3 and H4, and CBP binding is centred on the WRE (Parker et al., 2008), and that loss of CBP inhibits Wnt signalling. Protein arginine methyltransferase 2 (PRMT2) binds to β-catenin and is required for Wnt signalling (Blythe et al., 2010). PRMT2 methylates histones at arginine residues, a modification that promotes transcription.

Recently, genome-wide investigation of β-catenin binding sites by ChIP-seq has shown that the majority of β-catenin sites contain the pro-transcriptional H3K4me3 mark (Watanabe et al., 2014), which have been shown to be deposited by the mixed myeloid leukaemia 1 and 2 (MLL1 and 2) complexes (Sierra et al., 2006). The action of MLL1/2 at β-catenin target genes requires ubiquitination of Histone H2, which is interesting because ubiquitinated H2 is able to recruit the BAF complex (Shema-Yaacoby et al., 2013). A link between β-catenin and the BAF complex is already well established: β-catenin binds directly to Brg1, and Brg1 is required for Wnt signalling in certain tissues (Barker et al., 2001); see section 1.1.3.6). Furthermore, telomerase reverse transcriptase (TERT) binds to β-catenin and Brg1 and is required for transcription of Wnt target genes (Park et al., 2009).

1.2.6 Wnt Signalling During *Xenopus* Development

The Wnt signalling pathway plays a key role in the embryogenesis of all animals studied so far. Wnt signals are required for a range of developmental processes including establishing the dorsal-ventral axis, hindbrain patterning, and bone formation. Here I discuss the role of Wnt signalling during early *Xenopus* development and in human disease.

1.2.6.1 The Nieuwkoop Centre and Establishment of the Dorsal-Ventral Axis

The future dorsal side of *Xenopus* embryos is determined upon fertilisation (Elinson and Holowacz, 1995), when sperm entry causes polymerisation of microtubules, which rotate the cellular cortex relative to the cytoplasm (Rowning et al., 1997). This cortical rotation and the accompanying microtubule network are required for establishment of dorsal structures, as ablation of microtubule polymerisation (such as by UV light) results in ventralised embryos (Grant and Wacaster, 1972). Furthermore, this ventralisation can be rescued by physically tilting embryos to mimic cortical rotation (Scharf and Gerhart, 1980), giving rise to the model that cortical rotation acts to localise dorsal determinants. These determinants activate the Wnt/β-catenin signalling pathway (Marikawa and Elinson, 1999), although the molecular identity of these factors is still unclear (Houston, 2012).

This maternal Wnt signal establishes the dorsal-vegetal Nieuwkoop centre during the early blastula (De Robertis and Kuroda, 2004). The Nieuwkoop centre was identified as an inducer of dorsal mesoderm by a series of seminal experiments. When dissected dorsal vegetal regions were juxtaposed with animal cap tissue, embryoids with mesodermal cells and a dorsal-ventral axis were formed, demonstrating that signalling by the Nieuwkoop centre is capable of establishing a Spemann's organiser (see below)(Gerhart, 1999). At the molecular level β-catenin and VegT act together in the Nieuwkoop centre to drive expression of Xnr5 and Xnr6 (Takahashi et al., 2000). These and other nodal proteins (Xnr1, 2, 4, Agius et al., 2000) are secreted by the Nieuwkoop centre and are potent morphogens, inducing dorsal mesoderm at high concentrations and ventral mesoderm at low concentrations (Jones et al., 1995). Intriguingly the BMP inhibitor *Chordin* is required for induction of dorsal mesoderm by Xnr1 (Vonica and Gumbiner, 2007), indicating that the establishment of the organiser by the Nieuwkoop centre involves the integration of multiple signalling pathways.

Whether the Nieuwkoop centre is a *bona fide* inducer of the organiser has been questioned. Excision of Nieuwkoop centre cells results in wounding-activated FGF signalling (LaBonne and Whitman, 1997), which together with maternal Wnt signalling could establish an organiser-like tissue in the explanted cells (Vonica and Gumbiner, 2007). Therefore these explants would not be acting in the same way as endogenous Nieuwkoop centres, and interpretation of these transplant experiments should be treated with caution.

Most Wnt target genes are not expressed prior to the mid-blastula transition (MBT, ~stage 8), despite the presence of nuclear β-catenin from the 16-cell stage (Larabell et al., 1997a; Lemaire et al., 1995; Smith et al., 1995). However, changes are made to the chromatin at Wnt target genes. For example, at the *Siamois* (*Sia*) promoter β-catenin recruits protein arginine methyltransferase 2 (Prmt2) to create a poised chromatin state (Blythe et al., 2010). *Siamois* and *twin* are key Wnt-target genes during the blastula stages. *Sia* and *twin* induce expression of organiser specific genes such as *goosecoid* (*gsc*) and *chordin (chrd)*(Carnac et al., 1996), and when injected into ventral blastomeres induces a complete secondary

axis (Lemaire et al., 1995). Thus both the maternal Wnt pathway and its immediate targets act to establish the dorsal side of the embryo.

Like *Sia* and *Twin, Xenopus Nodal related 3 (Xnr3)* is a target of maternal Wnt signalling (McKendry et al., 1997). Unlike other nodal related proteins, Xnr3 does not activate Smad signalling due to a mutation in the cysteine knot (Smith et al., 1995). Instead, Xnr3 acts as an inhibitor of BMP signalling and induces neural tissue in the ectoderm (Glinka et al., 1996), and promotes convergent-extension movements by signalling through the FGF receptor (Yokota, 2003). Thus the effects of Xnr3 are complementary to those of the organiser (see below).

1.2.6.2 Spemann's Organiser and Patterning of the Dorsal Ventral Axis

Spemann's organiser elaborates the dorsal-ventral axis during *Xenopus* gastrulation, and when transplanted is sufficient to induce a complete secondary axis. Somewhat counter intuitively, the organiser establishes dorsal character by secreting inhibitors of cell-cell signalling. These inhibitors antagonise signals produced by ventral tissue, giving rise to gradients of Wnt, BMP and Nodal ligands that are high on the ventral side of the embryo and low on the dorsal side (reviewed by Niehrs, 2004). In addition to patterning the mesoderm, inhibition of BMP in overlying ectoderm is crucial for the induction of neural tissue (Zimmerman et al., 1996).

As described in section 1.2.2.3, extracellular inhibitors of the Wnt pathway such as Cer, sFRPs and Cresc are secreted from the organiser and inhibit Wnt signalling. Cerberus is particularly interesting because it binds to Wnt, BMP and Nodal ligands, acting as a triple repressor {Piccolo:1999bc}. Some of these extracellular regulators, such as sFRP3 and Cresc, also act as chaperones to enhance the diffusion of Wnt ligands, and thus act to perpetuate the dorsal-ventral gradient (Mii and Taira, 2009).

This phenomenon is not limited to extracellular regulators of the Wnt pathway. For example the dorsal-ventral gradient of chordin is controlled by a complex interplay between tolloid (a secreted protease that degrades chordin), sizzled (an sFRP that is a competitive inhibitor for tolloid) and twisted gastrulation (tsg, a protein that enhances the activity of both chordin and BMPs)(described by De

Robertis, 2009). The diffusion of these factors within the embryo causes a gradient of chordin activity that is more finely controlled than would be generated by diffusion alone.

1.2.6.2 The Role of Wnt In Neural Patterning and Neural Crest Specification

Neural tissue in *Xenopus* is specified during gastrulation by BMP-antagonists emanating from Spemann's organiser (De Robertis and Kuroda, 2004). During this time a posterior-anterior gradient of Wnt signalling exists in the presumptive brain and conveys posterior fate (Kiecker and Niehrs, 2001). A decrease in Wnt signalling using Dkk1 mRNA or a Wnt3a morpholino causes expansion of anterior markers (Elkouby et al., 2010; McGrew et al., 1997). Similarly, overexpression of Wnt from stage 10 using inducible constructs or plasmid DNA posteriorises the head region, leading to expansion of the hindbrain and loss of anterior structures such as the eyes and cement gland (Domingos et al., 2001; Elkouby et al., 2010).

Neural crest (NC) cells are specified at the lateral borders of the neural plate by signals secreted by the paraxial mesoderm (Elkouby and Frank, 2010). Once specified, NC cells undergo an epithelial-mesenchymal transition (EMT), migrate throughout the embryo and differentiate into many different cell types (Pegoraro and Monsoro-Burq, 2012). Wnt signalling plays a key role in NC specification, as overexpression of Wnt ligands causes an increase in NC cells, whereas depletion reduces the number of NC cells (LaBonne and Bronner-Fraser, 1998). Surprisingly, recent work shows that the earliest stages of neural crest specification also require an inhibition of Wnt signalling (Ben Steventon and Mayor, 2012). Therefore assessing the role of Wnt signalling in neural crest specification is not trivial and requires consideration of the developmental stage at which experiments are carried out.

1.2.6.3 Wnt Signalling in Disease

APC was one of the first tumour suppressor genes to be cloned (Kinzler et al., 1991), and is mutated in a large number of colon cancers (Clevers, 2006). Loss of APC causes hyperactivation of the Wnt pathway (Rubinfeld et al., 1997), which is thought to be a key step in the progression of cancers. Similarly, other mutations that activate the Wnt pathway, such as loss of the GSK3β phosphorylation site in β-catenin, are thought to drive tumourigenesis in the colon (Morin et al., 1997).

Aberrant Wnt signalling is also found in several other tumour types, such as pancreatic, ovarian and liver cancers (Barker and Clevers, 2006), and are important for tumour progression.

Dysregulation of the Wnt pathway in human disease is not restricted to cancer. Loss of Wnt signalling is associated with reduced bone mass in patients with osteoporosis pseudoglioma (Gong et al., 2001), whereas gain of function mutations in LRP6 cause an increase in bone formation (Boyden et al., 2002). Mutations in TCF/LEF proteins are associated with sebaceous tumours, diabetes and Crohn's disease (Beisner et al., 2014; Grant et al., 2006; Takeda et al., 2006). Haploinsufficiency of β-catenin causes post-natal developmental delay and mental retardation (Dubruc et al., 2014). Inactivation of the Wnt pathway is thought to be a key step in the development of Parkinson's disease, reducing the neuroprotective capabilities of astrocytes (L'Episcopo et al., 2014). Finally the Wnt pathway plays a complex role in schizophrenia that is poorly understood. Some drugs used to treat mental disorders activate the Wnt pathway, while others act to repress it (Panaccione et al., 2013). Why opposite effects on the same pathway are both able to treat schizophrenia is unclear, though it is likely that these drugs are targeting multiple cellular processes simultaneously.

Due to the wide spectrum of diseases in which the Wnt pathway is involved, there is a great deal of interest in developing drugs to manipulate Wnt signalling. Thus an improved understanding of which proteins regulate the Wnt pathway and the molecular mechanisms by which they act will be informative for drug design and developing treatments.

1.2.7 Non-Canonical Wnt Signalling

In addition to "canonical" signalling, binding of Wnt ligands to FZD receptors activates many β-catenin-independent intracellular pathways, commonly referred to as non-canonical Wnt signalling pathways. I will give a brief overview of these signalling events.

The ability of Wnt ligands to activate more than one pathway was first seen in *Xenopus,* where overexpression of Wnt5a disrupted convergent extension movements during gastrulation (Moon et al., 1993). Since then many proteins involved the establishment of planar cell polarity (PCP) – the orientation of apical surfaces across a tissue – have been identified, but the mechanism by which they establish polarity is still unclear (Wallingford, 2012). Ligand binding to FZD receptors causes activation of Rho and Rac, which subsequently reorganise the actin cytoskeleton to cause changes in cell shape (Habas et al., 2003). How this activity is linked to the establishment of polarity remains unknown. As well as mediating convergent extension movements, the PCP pathway is required for planar polarity of epithelia, contact inhibition in migrating neural crest cells and axonal guidance during neuronal outgrowth (Mayor and Theveneau, 2013).

Binding of Wnt ligands to receptors can also cause an influx of Calcium ions (Ca^{2+}). Intracellular Ca^{2+} activates a wide range of cellular responses such as the activation of protein kinase C (PKC), calcineurin and calcium/calmodulin dependent kinase II (CaMKII; (van Amerongen, 2012). In *Xenopus* animal caps, Wnt5a-dependent Ca^{2+} signalling stimulated nuclear translocation of nuclear factor of activated T-cells (NFAT), which was able to suppress canonical Wnt signalling (Saneyoshi et al., 2002).

The Wnt signalling pathway is complex, and the preferential activation of different branches is poorly understood. By dissecting each aspect of the pathway separately we can build up a bigger picture of the molecular activities that occur during active Wnt signalling.

1.3 Aims of the Thesis

I am interested in the control of signalling pathways during embryogenesis, and how they direct tissue specification through the regulation of gene expression. Previous work in the lab has shown that Dri3 regulates TGFβ signalling during mesoderm development (Callery et al., 2005). I was therefore interested in whether other ARID family members were capable of controlling intercellular signalling. ARID1a was a clear candidate as work in *Drosophila* indicated that it could repress the Wnt signalling pathway (Collins and Treisman, 2000).

ARID1a is the largest subunit of the BAF complex. The nucleosome remodelling capabilities of the BAF complex have been well studied *in vitro*, however its functional role within the cell is less clear. Most work to date has focussed upon the core ATPase Brg1 and there are few physiological studies of other BAF complex subunits.

The Wnt pathway has been extensively studied since its discovery. Many of the cytoplasmic proteins that regulate the Wnt/β-catenin pathway have been characterised; however events in the nucleus are less well understood. Therefore ARID1a offers an interesting opportunity to discover more about the nuclear regulation of the Wnt pathway and to investigate the *in vivo* function of the BAF complex. There are 3 aims of this thesis: to assess the effects of gain of function and loss of function of *ARID1a* on *Xenopus* development; to test whether ARID1a regulates the Wnt signalling pathway in a vertebrate model; and to investigate the molecular mechanisms by which ARID1a is acting.

Chapter 2: Materials And Methods

2.1 *Xenopus* Embryological Tools and Techniques

2.1.2 Solutions and Reagents

10X Marc's Modified Ringers (MMR) Solution:

NaCl	1 M
KCl	20 mM
$MgSO_4$	10 mM
$CaCl_2$	20 mM
HEPES (pH 7.8)	50 mM
EDTA	1 mM

10X Normal Amphibian Medium (NAM):

NaCl	1.1 M
KCl	20 mM
$Ca(NO_3)_2$	10 mM
$MgSO_4$	10 mM
EDTA	1 mM
$NaHCO_3$	10 mM
Sodium Phosphate (pH 7.4)	20 mM

Cysteine Solution (for de-jellying embryos):

L-cysteine hydrochloride monohydrate (Sigma-Aldrich)	2.2% (w/v)
Sodium Hydroxide (Fisher Scientific)	To pH 7.9-8.0
NAM	0.1X

10X Calcium-Magnesium-Free Medium (CMFM):

NaCl	880 mM
KCl	10 mM
$NaHCO_3$	24 mM
Tris (pH 7.6)	75 mM

1X MEMFA:

MOPS (pH 7.4)	100 mM
EGTA	2 mM
$MgSO_4$	1 mM
Formalin (Sigma)	10% (v/v)

1X Immunofluorescence Blocking Solution (IBS):

PBS	1X
Bovine Serum Albumin (Sigma-Aldrich)	0.1% (w/v)
Triton-X (Promega)	0.1% (v/v)
Goat Serum (Sigma)	10% (v/v)

1X PBST

PBS	1X
Tween-20 (Sigma)	0.1% (v/v)

20X Saline-Sodium Citrate (SSC) buffer:

NaCl	175.3 g
Sodium Citrate	88.2 g
NaOH	To pH 7.0
Distilled Water	To a final volume of 1 L

1X Bleaching Solution

SSC	0.5X
Formamide (Sigma)	5% (v/v)
37% Hydrogen Peroxide Solution (Sigma)	2% (v/v)

1X Hybridisation Buffer

Formamide	50% (v/v)
SSC	5X
Torula RNA (Sigma)	1 mg/ml
Heparin (Sigma)	100 µg/ml

Denhart's Solution	1X
Tween-20	0.1% (v/v)
CHAPS (Sigma)	0.1% (w/v)
EDTA	10 mM

2X Maleic Acid Buffer (MAB):

Maleic Acid (Sigma)	200 mM
NaCl (ph 7.5)	300 mM

10% Blocking Solution

Make up a 10% stock (w/v) of Blocking Reagent (Roche) in 1X MAB. Heat the solution to 65°C for several hours and shake vigorously to ensure it dissolves. Store at −20°C.

1X Alkaline Phosphatase (AP) Buffer:

Tris (Sigma)	100 μM
NaCl	100 μM
Tween-20	0.1% (v/v)
$MgCl_2$	40 mM

1X Bouin's Fixative:

Formalin	25% (v/v)
Acetic Acid	5% (v/v)

NB: The picric acid was omitted as it can become dangerously explosive if dried out, and is not necessary for the fixation process.

2.1.2 In Vitro Fertilisation

Female *Xenopus* were primed, boosted and transferred to 1X Marc's Modified Ringers (MMR) solution to lay. Eggs were collected from the salt solution using a plastic pasteur pipette.

Adult male *Xenopus* were sacrificed by injection of MS222 anaesthetic (0.32 g/ml)(Sigma) followed by decapitation with a guillotine and pithing of the brain and brain stem with a pair of forceps, in accordance with Schedule 1 killing

guidelines. The testes were then dissected and transferred to 60% L-15 (PAA) and kept at 4℃.

For *in vitro* fertilisation, the 1X MMR solution was removed from the eggs. A piece of testis was cut and crushed in a 1.5 ml tube (Eppendorf) using a micropestle (Ambion). This solution was mixed with the eggs and left for 3-7 minutes for the sperm to diffuse. The dish was flooded with 0.1X Normal Amphibian Medium (NAM) and left for up to 30 minutes, or until the embryos turned with the pigmented pole facing upwards. The embryos were de-jellied using cysteine solution, and washed thoroughly in 0.1X NAM. Embryos were cultured in 0.1X NAM at 14°C, 18°C or room temperature (~22-24°C).

2.1.3 mRNA In Vitro Synthesis

To synthesise mRNA, plasmids were first linearised using an appropriate restriction enzyme (see Table 2.1). The following reaction was assembled and incubated at 37°C for 1-2 hours:

- 10-20 µg plasmid
- 10 µl 10X restriction enzyme buffer
- 2.5 µl BSA solution
- 2.5 µl restriction enzyme
- Water, to 100 µl

The reactions were then processed using a PCR Purification Kit (Qiagen) and eluted in 30 µl of water. mRNA synthesis was carried out using the mMESSAGE mMACHINE kit (Ambion). The following reaction was assembled and incubated at 37°C for 2-4 hours. To synthesis ARID1a mRNA, 1 µl of GTP was included in the reaction.

- 2 µl 10X buffer
- 10 µl 2X NTP/Cap
- 2 µl polymerase mix
- 1 µg linearised plasmid
- Water, to 20 µl

2 μl of Turbo DNase (Ambion) was added to the reaction, and the plasmid DNA digested for 30 minutes at 37°C. Then 30 ul of water and 30 μl LiCl (Ambion) was added and the reaction mixed, and placed at −20°C for at least 2 hours. The mRNA solution was then centrifuged at 4°C at 14000 rpm for 30 minutes. The resultant pellet was then washed in 80% ethanol, and centrifuged at 4°C at 14000 rpm for 30 minutes. Then ethanol was removed and the pellet air dried at room temperature for 20 minutes, before being suspended in 20 μl water. The mRNA was then quantitated using a NanoDrop, and analysed by running 0.5 μl on a 1% agarose gel, checking for the presence of a single band at approximately the correct size.

2.1.4 Microinjection

Glass needles were prepared from 1.2 mm capillaries (Harvard Apparatus) using a needle puller (Sutter Instruments). The settings were:

    Pull: 55

    Velocity: 55

    Time: 10

The tips of the needles were broken with forceps, and the needles were mounted onto an IM 300 Microinjector (Narishige). By injecting water into mineral oil (Sigma-Aldrich) the needles were calibrated using a graticule to deliver either 10 nl (diameter of 26.7) or 5 nl (diameter of 21.2).

50 mm dishes (Sterilin) coated with 1% agarose (Ultra-Pure Agarose, Invitrogen) made up in 0.1X NAM, and prior to injection embryos were transferred onto these plates in 3% Ficoll solution (Sigma-Aldrich, made up in 0.1X NAM). Following injection embryos were left in Ficoll solution overnight, before being transferred back into 0.1X NAM the following day.

2.1.5 Animal Cap Dissections

To dissect the animal pole regions of *Xenopus* blastulae, the embryos were first transferred to agarose-coated dishes containing 0.75X NAM. Using forceps, the vitelline membrane was removed, and then the animal cap was excised. The dissected animal caps were then transferred to clean agaorse-coated dishes (in 0.75X NAM) using a glass pipette and allowed to heal. Once all caps had been cut, or when sibling embryos reached the desired stage, the caps were transferred to 1.5 ml tubes and snap frozen on dry ice.

To dissociate animal caps into single cells, the above procedure was modified slightly. Prior to embryo dissection, coverslips or 8 well glass dishes (LabTek) were coated with 1.5 μg/ml recombinant human E-cadherin (R+D Systems) diluted in 0.75X NAM, and left overnight at 4°C. They were then washed in 0.75X NAM immediately before use.

Embryos were dissected and caps cultured in 1X Calcium-Magnesium-Free Medium (CMFM). Dishes were coated with low-melting point agarose (Agarose MP, Roche) dissolved in 1X CMFM. Once the excised animal caps had begun to disperse, the outer, pigmented epithelium was removed with forceps as it does not easily dissociate. 200 μl of the dissociated cells were then transferred into 400 μl 0.75X NAM and pipetted up and down a few times to ensure even distribution of cells on the slide. The cells were then lefts to adhere for a minimum of 1 hour at room temperature.

2.1.6 Immunofluorescence Of Dissociated Cells and Animal Caps

Cells were dissociated and cultured on E-cadherin coated wells as described above. They were then fixed by adding an equal volume of 2X MEMFA for 10 minutes at room temperature, followed by 1X MEMFA for a further 5 minutes. The cells were then washed twice in 1X Phosphate Buffered Saline (PBS), and either at 4°C or processed immediately.

Whole animal caps were dissected as described above and cultured in 0.75X NAM until the required stage. They were then transferred to Bijou bottles and fixed for 20 minutes in MEMFA, followed by a 5 minute wash in PBS. They were then transferred into Dent's fixative and kept at -20°C overnight or longer.

Prior to the immunofluorescence protocol detailed below, the animal caps were rehydrated in 5 minute washes of 75%, 50%, 25% methanol, followed by two 5 minute washes in PBST.

The following procedure was followed for immunostaining of fixed cells or intact animal caps. All washes were 250 μl, and antibody incubations were in 80 μl.

1) Replace PBS with PBS + 0.5% Triton-X for 10 minutes

2) Wash in PBS 3 times for 5 minutes each

3) Block for 1 hour at room temperature in Immunofluorescence Blocking Solution (IBS)

4) Add primary antibody (diluted in IBS) for 1 hour at room temperature, or overnight at 4°C

5) Wash in IBS 3 times for 10 minutes each

6) Incubate with secondary antibodies diluted in IBS for 1 hour in the dark

7) Wash with PBS 3 times for 10 minutes each

8) Mount with 80 l Prolong Gold (with or without DAPI, Invitrogen)

Prepared cells were imaged with an LSM710 confocal microscope (Leica) and images were captured using ZEN software.

2.1.7 RNA Extraction From *Xenopus* Tissue

RNA was extracted from embryos as described below. Embryos were frozen in batches of 10 on dry ice, and stored at −80°C until use.

1) Embryos were thawed on ice, then homogenised in 500 μl Trizol (Invitrogen) by pipetting up and down, and then vortexing for approximately 5 minutes.

2) Meanwhile, Phase-Lock tubes (5 Prime) were prepared by centrifuging at 14,000 rpm for 1 minute

3) 100 μl chloroform (Sigma) was added to the homogenised embryos and mixed by inverting the tubes vigorously. The homogenate was then transferred to the prepared Phase-Lock tubes

4) The tubes were centrifuged for 30 minutes at 14,000 rpm at 4°C

5) The upper phase was transferred to Safe-Lock tubes (Eppendorf) and an equal volume of cold isopropanol was added (approximately 300 µl). The tubes were shaken to mix, and then centrifuged for 30 minutes at 14,000 rpm at 4°C

6) The supernatant was removed, and the pellet washed in 150 µl of cold 80% ethanol, followed by centrifugation for 10 minutes at 14,000 rpm at 4°C

7) The ethanol was removed as thoroughly as possible, and the pellets air dried at 37°C for 5-10 minutes. 30 µl of water was then added to each tube and kept on ice for 1 hour for the RNA to dissolve.

8) The RNA pellet was suspended by pipetting up and down, and then 30 µl of LiCl was added. The tubes were then either stored at -20°C overnight, or immediately continued on to the next step.

9) The RNA was centrifuged for 30 minutes at 14,000 rpm at 4°C.

10) The pellet was washed with cold 80% ethanol as in step 6, then air dried as in step 7.

11) The RNA pellet was then suspended in 21 µl of water and left for 1 hour on ice to fully dissolve.

1 µl of RNA was quantitated using a NanoDrop (Thermo Scientific), and RNA quality was assessed by running on a 1% agarose gel (see section 2.3.3).

The same protocol was used to extract RNA from excised animal cap tissue, with the following changes:

- 10-15 caps were frozen for each extraction.
- Caps were homogenised in 500 µl Trizol and 100 µl chloroform.
- RNA pellets were suspended in 11 µl water

2.1.8 Protein Extraction

Between 5 and 10 embryos were frozen on dry ice for each protein extraction. Frozen embryos were stored at −80°C until use. Embryo protein lysate was obtained by the followed method:

1) Phosphosafe extraction buffer (Millipore) was prepared by dissolving one protease inhibitor tablet (mini-EDTA free, Roche) in 1 ml. This stock was then diluted 1:10 in Phosphosafe buffer.
2) Embryos were homogenized in 100 µl diluted Phosphosafe per embryo by pipetting up and down. The lysate was left on ice for 15 minutes.
3) The yolk in the lysate was removed by adding an equal volume of 1,1,2-Trichloro-Trifluoroethane (FREON, Sigma) and mixing thoroughly, followed by centrifugation for 15 minutes at 14,000 rpm at 4°C
4) The upper phase was transferred into a new safelock tube and either used immediately or stored at −80°C.

Proteins concentration was obtained using a NanoDrop and a Protein Assay Kit (660 nm, Pierce).

2.1.9 Synthesis of Digoxygenin-Labelled Probes

Digoxygenin-labelled antisense RNA probes were used to detect gene expression patterns using *in situ* hybridisation (see below). To synthesise these probes, plasmids were first linearised using an appropriate restriction enzyme (see Table 2.1). The following reactions were assembled, and incubated at 37°C for 1-2 hours:

• 10 µg plasmid
• 10 µl 10X restriction enzyme buffer
• 2.5 µl BSA solution
• 2.5 µl restriction enzyme
• Water, to 100 µl

The reactions were then processed using a PCR Purification Kit (Qiagen) and eluted in 30 µl of water. Linearisation was tested by running the digestion

product on a 1% agarose gel. To synthesise the probe, the following was then assembled and incubated at 37°C for 2-4 hours:

- 2 μl 10X Transcription buffer (Roche)
- 2 μl Dig RNA Labelling Mix (Roche)
- 1 μl Ribolock RNase Inhibitor (Thermo Scientific)
- 1 μg linearised plasmid DNA
- 2 μl polymerase (Roche)
- Water, to 20 μl

Following incubation, 2 μl of Turbo DNase (Ambion) was added to the reaction, and the plasmid DNA digested for 30 minutes at 37°C. Then 30 μl of water and 30 μl LiCl (Ambion) was added and the reaction mixed, and placed at −20°C for at least 2 hours. The mRNA solution was then centrifuged at 4°C at 14000 rpm for 30 minutes. The resultant pellet was then washed in 80% ethanol, and centrifuged at 4°C at 14000 rpm for 10 minutes. Then ethanol was removed and the pellet air-dried at 37°C for 5-10 minutes, before being suspended in 21 μl water. The antisense probe was then quantitated using a NanoDrop, and analysed by running 0.5 μl on a 1% agarose gel, checking for the presence of a single band at approximately the correct size.

2.1.10 In Situ Hybridisation

Embryos were fixed in 5 ml glass vials in 1X MEMFA for 2 hours at room temperature or overnight at 4°C. Embryos older than stage 30 were killed with MS222 prior to fixation.

After fixation, the embryos were washed in 1X PBS for 5 minutes and then dehydrated in 100% methanol for 2 hours at room temperature. The alcohol was removed and replaced with fresh methanol, and the embryos stored at −20°C until use. The *in situ* hybridisation reaction was carried out as below.

For steps 1-4, the embryos were kept in 5 ml glass vials.

1) Embryos were rehydrated by washing in 75% ethanol, 50% ethanol, 25% ethanol and PBST, for 5 minutes each.

2) For blastula stage embryos, the animal pole was pierced with a pair of forceps. This prevents reagents becoming trapped in the blastocoel.

3) The pigment was then removed by incubating the embryos in bleach solution. They were placed on a light box and covered in foil until all the pigment had gone. This typically took 2-3 hours.

4) The embryos were washed twice in PBST for 5 minutes each, followed by fixation for 20 minutes in 1X MEMFA. They were then washed twice in PBST for 5 minutes each.

The embryos were then transferred to *in situ* baskets. These baskets were made from 2 ml tubes with the lids and bottoms cut off with a sharp scalpel, and plastic mesh melted over the bottom of the tubes. The baskets allowed for quick and easy transfer of embryos between solutions, and reduced the risk of damaging or losing embryos during aspiration of solutions.

5) Once in the baskets, the embryos were washed in 25% Hybridisation Buffer (diluted with water) for 10 minutes at room temperature.

6) The embryos were transferred to Hybridisation Buffer and incubated at 65°C for 3-5 hours.

7) 250-500 μl of antisense digoxygenin-labelled RNA probes, diluted to 1 μg/ml in Hybridisation Buffer, was added to the embryos and incubated at 65°C overnight.

8) Embryos were then washed in 2X SSC for 20 minutes at 65°C. Repeat for a total of 3 washes. This step was then repeated using 0.2X SSC.

9) Next, the embryos were washed in 1X MAB for 5 minutes at room temperature. Repeat for a total of 2 washes.

10) Embryos were then blocked in 2% Blocking Solution for 1 hour at room temperature

11) The anti-digoxygenin antibody (Roche) was diluted 1:2000 in 2% Blocking Solution containing 10% sheep serum. 250-500 μl was added to each basket, and the reaction was placed at 4°C overnight.

12) The third day if the *in situ* protocol consisted entirely of 1 hour washes in 1X MAB for 1 hour each at room temperature, followed by a final wash overnight at 4°C.

13) The next day, the embryos were equilibrated in AP Buffer for 5 minutes at room temperature

Here the embryos were transferred to a 24 well tissue culture dish (Corning) in AP Buffer. This allowed easy visualisation of the developing stain.

14) The AP buffer was replaced with BM Purple development solution (Roche). The plate was covered with foil and the stain allowed to develop. If no stain was visible by the end of the day the reaction was transferred to 4°C and continued overnight

15) The reaction was stopped by washing twice in 1X MAB

16) The stained embryos were fixed in Bouin's Solution overnight at 4°C

17) Finally the embryos were washed 3 times in PBS for 5 minutes each, and then stored in PBS at 4°C.

For imaging, embryos were transferred to 50 mm dishes coated in 1% agarose, filled with 1X PBS. Images were taken with a Leica M165 FC microscope using LAS V3 software.

Some embryos were cleared to allow visualisation of internal structures. These embryos were transferred glass dishes and covered with Murray's Clear, a solution with the same refractive index as a *Xenopus* embryo, thus rendering the embryos mostly transparent. Images were then captured using the same set up as above.

2.2 Tissue Culture Techniques

2.2.1 Solutions and Reagents

Protein Lysis Buffer:

HEPES pH 7.4	40 mM
NaCl	120 mM
EDTA	1 mM
Sodium Fluoride	50 mM
Sodium Orthovanadate	1.5 mM
Triton-X	1% (v/v)
(Mini) Protease Inhibitor (Roche)	1 tablet

PBST:

PBS	1X
Tween-20	0.1% (v/v)

IF Blocking Buffer:

PBS	1X
BSA	0.1% (w/v)
Triton-X	0.1% (v/v)
Goat Serum	10% (v/v)

2.2.2 Cell Maintenance

Human Embryonic Kidney 293 (HEK293) cells were maintained in Dulbecco's Modified Eagle Medium (DMEM) plus 10% foetal bovine serum (FBS), 1% Pen/Strep and 6 mM L-glutamine (DMEM +++).

Cells were split by first washing in PBS (Gibco) and then incubated with trypsin solution (Gibco) for 3-5 minutes at 37°C. The cells were then collected in DMEM and centrifuged at 1000 rpm for 3 minutes. The pelleted cells were re-suspended in 10 ml DMEM +++ and then diluted into tissue culture plates as desired.

2.2.3 RNA Extraction

RNA was extracted from confluent dishes of HEK293 cells. The media was removed using a vacuum pump and cells were washed in PBS. The PBS was removed and the cells frozen at −80°C.

Cells were thawed on ice. 500 μl of trizol was added and the cells allowed to homogenise for 5-10 minutes. The homogenate was collected and transferred to 1.5 ml Eppendorf tubes and 100 μl of chloroform was added. The samples were then processed as described in section 2.1.7.

2.2.4 Protein Lysis

Dishes of confluent cells were taken from the incubator and placed immediately on ice. They were then washed in cold PBS, before the addition of Protein Lysis Buffer:

Plate size	Volume of lysis buffer
6-well plate	200 μl
10 cm dish	500 μl
15 cm dish	1 ml

Using rubber cell scrapers, the cells were harvested into either 1.5 ml Eppendorf tubes, or 50 ml falcon tubes and left on ice for 15 minutes to allow lysis to occur. If required, samples were snap-frozen on dry ice or in liquid nitrogen and stored at −80°C.

Samples were thawed in ice water, and then centrifuged at 13,000 rpm for 30 minutes to pellet cytoskeletal debris. The supernatant was then gathered for use in future experiments. Protein concentrations were determined using the Pierce Protein Assay Kit and a Nanodrop.

2.2.5 Transfection of HEK Cells

Transfection of HEK cells was performed using Lipofectamine reagent (Invitrogen) according to the manufacturer's recommendations. Briefly, cells were grown in DMEM + 10% FBS + L-Glutamine, but without antibiotics prior to transfection. The required amount of DNA was diluted in Optimem medium (Gibco) and left for 5 minutes. Lipofectamine reagent was then added, and the mixture allowed to combine for 20 minutes to 1 hour. This solution was then added to the cells, and the cells were grown overnight.

The following morning, the media was replaced with normal DMEM+++ media.

2.2.6 Live Imaging Of FRT/GFP-ARID1a Cells

FRT/GFP-ARID1a cells were seeded onto 8 well dishes (Lab-Tek) and maintained in DMEM+++. They were treated with 20 ng/ml doxycycline (Sigma) overnight to induce expression of GFP-ARID1a. Nuclei were labelled using 5 μM DRAQ5 (Biostatus). Cells were imaged using an LSM710 confocal microscope (Leica) and processed using ZEN software.

2.2.7 Immunofluorescence of Tissue Culture Cells

Cells were seeded onto 8 well dishes (LabTek) and grown as described above. Cells were fixed by adding an equal volume of 20% formalin in 2X PBS to each well for 10 minutes, then a further 10 minutes in 10% formalin in PBS. The cells were then dehydrated in 100% ethanol and stored at −80°C (this dehydration step was sometimes omitted).

All further washes were 250 μl unless otherwise stated.

If dehydrated, the cells were rehydrated in successive washes of 75%, 50%, and 25% ethanol, followed by PBST for 5 minutes each. Next, the cells were incubated in IF Blocking Buffer for 1 hour at room temperature. The Blocking Buffer was replaced with primary antibodies diluted in 80 μl IF Blocking Buffer and incubated overnight at 4°C.

The cells were then washed in Blocking Buffer 3 times for 15 minutes each. The final wash was removed and replaced with secondary antibodies conjugated to flourophores, diluted in 80 μl IF Blocking Buffer for 2 hours at room temperature. The secondary antibody solution was removed and the cells were washed in Blocking Buffer 3 times for 15 minutes. Then the Blocking Buffer was removed, and the samples were covered in 80 μl Prolong Gold Mounting Medium containing DAPI (Promega). If using slides with a removable casket this was discarded and a coverslip was placed over the cells.

The cells were imaged on an LSM710 confocal microscope (Leica) using ZEN software.

2.2.8 Creating Stable Cell Lines

N-terminally GFP-tagged *Xenopus* ARID1a was cloned into the pcDNAFRT/TO vector by the Cloning Facility at the Protein Phosphorylation Unit, University of Dundee.

Generation of pFRT/GFP-ARID1a cells was carried out by Lina Herhaus (Sapkota Lab, University of Dundee). T-REx-293 cells (Invitrogen) were maintained in DMEM+++ containing 15 μg/ml blastidicidin (InvivoGen) and 100 μg/ml zeocin (Fischer Scientific). For transfection, cells were grown to 60% confluency in a 10 cm dish, in DMEM+++ lacking blasticidin and zeocin. 9 μg of plasmid pOG44 (which contains the flippase gene) and 1 μg of pcDNAFRT/TO/GFP-ARID1a was added to 25 μl of polyethyleneimine (PEI; 1 mg/ml) in 1 ml DMEM+++. After 15 minutes, the transfection mixture was added to the cells and grown overnight. The cells were split 1:3 and allowed to grow for a day before the media was changed to DMEM+++ containing 15 μg/ml blasticidin and 100 μg/ml hygromycin B (Hyclone Laboratories). Surviving colonies were picked and expanded under selection.

2.2.9 Immunoprecipitations

For immunoprecipitation experiments, cell lysates were prepared in Protein Lysis Buffer as described in section 2.2.1. 10% of the lysate was set aside as input material, and the rest used for the immunoprecipitation experiments. The lysate was blocked with a 1:1 solution of immobilised protein G on agarose beads (Thermo Scientific):Sepharose CL4B beads (Sigma) for 1 hour at 4°C on a rotor (approximately 10% the volume of the lysate). The lysate was then spun at 13,000 rpm at 4°C for 1 minute to pellet the beads, and the supernatant was transferred to a new tube. The primary antibody was added at a 1:100 dilution, along with a protein G agarose/sepharose CL4B mixture as above, and the lysate incubated on a rotor at 4°C overnight.

The lysate was then spun at 10,000 g for 1 minute at 4°C, and the supernatant removed. The beads were washed 3 times in Protein Lysis Buffer. 50 – 100 μl of 1X SDS loading buffer was added and the beads were heated to 70°C for 10 minutes, with gentle shaking. The mixture was then spun at 13,000 rpm for 1 minute to pellet the beads, and the supernatant analysed by western blotting (see section 2.3.6).

2.2.10 Luciferase Assays

Luciferase assays were carried out using the Super8 TOPFLASH and FOPFLASH reporter plasmids (Addgene plasmids 12456 and 12457 respectively; (Veeman et al., 2003). Cells were seeded into 24 well plates, and transfected as described above. For each well, 10 ng Renilla plasmid and 100 ng of either the TOPFLASH or FOPFLASH reporter plasmids were transfected with up to 500 ng of plasmid of interest. The following morning, the cells were washed in serum-free medium and starved for at least four hours before the addition of either 100 μl L-cell conditioned medium or 100 μl Wnt-conditioned medium (gift from K. Dingwell). After 24 hours the cells were processed using the Dual Luciferase Reporter Assay Kit (Promega). The cells were washed in PBS, then 100 μl of 1X Passive Lysis buffer was added and the plate placed on a shaker for at least 15 minutes at room temperature. For each reaction, 20 μl was transferred to a Nunclon 96 well

plate (Thermo Scientific). The luciferase activity was then read using a Synergy2 plate reader (Biotek).

2.2.11 Mass Spectrometry

For each mass spectrometry experiment, between ten and twenty 15 cm dishes of FRT/GFP-ARID1a cells were grown to confluency and treated with 20 ng/ml doxycycline overnight. Each dish was lysed in 1 ml HEPES lysis buffer + 2.5 mg/ml DSP (Sigma) and left for 30 minutes on ice. The cross-linking reaction was quenched by adding 250 µl 1 M Tris-HCL pH 7.4 for a further 15 minutes. The lysate was then centrifuged at 15,000 rpm at 4°C for 30 minutes, then filtered through a 0.45 µM column.

The lysate was then blocked using 15 µl CL4B beads and 15 µl protein G agarose beads for 2 hours on a rotor at 4°C. The beads were pelleted by centrifugation, and the lysate was taken. 15 µl of CL4B beads and 15 µl of GFP-TRAP beads (Chromotek) were added, and then incubated at 4°C on a rotor for 2 hours. The beads were then collected by centrifugation, and washed four times in HEPES lysis buffer + 0.2 M NaCl, followed by a final wash in 10 mM Tris-HCL pH 7.4. The beads were then incubated in 100 µl LDS sample buffer + 0.1 M DTT and heated to 95°C for 10 minutes.

The beads were removed by passing through a Spin-X column (Thermo Scientific). 50 mM iodoacetamide was then added for 30 minutes to alkylate cysteine residues and completely disrupt disulphide bonds. The proteins were then run on a gradient gel in TGX buffer at 180 V. The gel was stained using colloidal blue (Novex) for two hours, and then washed with water overnight.

The gel was cut with a scalpel into different segments (Fig. 4.6) and each processed individually. Each segment was cut into ~0.5 mm cubes and put into a 1.5 ml Eppendorf tube. The gel slices were then incubated with 500 µl of the following for 10 minutes each on a shaker at room temperature: water, 50% acetonitrile, 100 mM NH_4HCO_3, 50% acetonitrile + 50 mM NH_4HCO_3. The final wash was repeated at 60°C until all blue colour had been removed. The gel pieces were shrunk using 300 µl of acetonitrile and then dried using a speed-vac. The proteins were then digested by adding 60 µl 25 mM Triethylammonium

bicarbonate + 5 ug/ml trypsin at 30°C on a shaker. After 30 minutes, a further 170 μl Triethylammonium bicarbonate was added and the reaction left overnight.

The next day, 200 μl acetonitrile was added to each sample and then shook for 15 minutes at 30°C. The supernatant was then transferred to new tubes and frozen at -80°C for 30 minutes, then dried using a speed-vac. Meanwhile, 100 μl 50% acetonitrile/2.5% formic acid was added to the gel pieces. The supernatant was then added to the dried samples above and dried using a speed-vac. The prepared samples were stored at -20°C until they were processed for mass spectrometry.

Raw data from the mass spectrometry runs were matched to the human proteome or *Xenopus* translatome. Mascot scores were generated using the formula $-10Log(P)$, where P is the probability that the peptide matching is a random event. Therefore a mascot score of 67 gives a false discovery rate (FDR) of 5%.

2.3 Molecular Biology Techniques

2.3.1 cDNA Synthesis

To synthesise cDNA, 1 µg of total RNA was denatured at 75°C for 5 minutes in a volume of 4 µl of water. The following reaction was then assembled, and added to the denatured RNA:

Reagent	Desired Concentration	Volume Added / µl	Manufacturer
M-MLV RT 5X Buffer	1X	2	Promega
10 mM dNTPs	1 mM	1	
100 µM Random Hexamers	10 µM	1	Sigma
MMLV-RT RNase (H-) Mutant (200 units/µl)	4 units	0.2	Promega
Water		1.8	

The reactions were then briefly vortexed to mix, followed by a quick centrifugation. cDNA was then synthesised using a BioRad T100 Thermal Cycler and the steps below:

- 25°C for 15 minutes
- 37°C for 15 minutes
- 55°C for 45 minutes
- 85°C for 15 minutes
- 4°C indefinitely

Upon completion of the final cycle, 40 µl of water was added to the reaction, and the synthesised cDNA was stored at −20°C until required.

2.3.2 Polymerase Chain Reaction (PCR)

Amplification of DNA for cloning and diagnostics was carried out using a BioRad T100 Thermal Cycler. Several different polymerases were used over the course of this work, and they are detailed here. In all cases 10 µM primer pairs were made by diluting 100 µM forward and reverse primer stocks 1:10 in water.

Red-Taq (Sigma) and KAPA2 (KAPA):

These two polymerases were used for amplification of short stretches of DNA (<2kb) where fidelity was not a primary concern: mostly, these polymerases were used for diagnostic PCRs or the synthesis of standards for use in quantitative PCR (qPCR). The reactions were identical for both polymerases:

- 5 µl 2X polymerase mix

- 0.2 µl 10 uM primer pair

- 0.2 µl DNA (typically 5 ng plasmid DNA or 50 ng cDNA)

- 4.6 µl water

Temperature	Time	Number of Cycles
95°C	30 s	
58°C	30 s	X 30
72°C	30 s	
4°C	indefinite	

Pfu Ultra (Agilent)

Pfu Ultra is a high fidelity enzyme that produces blunt end products, and so was used for cloning *Xenopus* ARID1a from cDNA. Reactions were assembled as below:

- 5 µl 10X Pfu Ultra AD buffer

- 0.4 µl 25 mM dNTPs

- 1 µl template DNA

- 1 µl 10 µM primer pair

- 1 µl Pfu Ultra

- 41.6 µl water

Temperature / °C	Time	Cycles
95	2 minutes	1
95	30 seconds	
64	30 seconds	35
72	6 minutes	
72	10 minutes	1

Phusion (NEB)

Phusion polymerase is a highly progressive and accurate polymerase, and so was ideal for amplifying DNA that would subsequently be used for producing expression constructs. Reactions were carried out as below:

- 2 μl template DNA

- 10 μl 5X High Fidelity buffer

- 1.25 μl 10 mM dNTP

- 1.5 μl 10 μM primer pair

- 0.5 μl Phusion polymerase

- 34.75 μl water

Temperature / °C	Time	Cycles
95	2 minutes	1
95	30 seconds	35
64	30 seconds	
72	30 seconds/kb	
72	10 minutes	1
4	indefinite	

2.3.3 Agarose Gel Electrophoresis

DNA and RNA was visualised using agarose gel electrophoresis. For a typical 1% gel 0.3 g of UltraPure Agarose (Invitrogen) was dissolved in 30 ml TAE buffer by heating in a microwave. 1 μl of RedSafe was added to the gel to allow visualisation of nucleic acids and the gel poured into a mould. The appropriate volume of Gel Loading Dye (NEB) was added to samples where required, and a 1 kb or 100 bp ladder (NEB) was loaded onto the gel. Gels were run for 20-25 minutes at 120 V.

2.3.4 Entry Vector Cloning

For the creation of expression constructs, desired regions of DNA were amplified by PCR and incorporated into Entry vectors (pENTR/D-TOPO, Invitrogen). The advantage of the Entry Vector system is that one template plasmid can be used to

quickly generate many expression constructs containing different immunoreactive tags.

To use the Entry vector system, forward and reverse primers were designed using Primer 3, complementary to the gene of interest with one additional consideration: four residues - CACC - were added to the 5' end of the forward primer, ideally just prior to the start codon. This was to allow the incorporation of the PCR product into the Entry vector via a TOPO-isomerase-directed insertio. Pfu Ultra- or Phusion-derived PCR products were purified using a PCR Purification kit (Qiagen) and their concentration determined using a NanoDrop 1000 (Sigma Biotechnologies). The amount of PCR product to be used was then obtained using the following formula:

$$\frac{ng\ vector\ \times\ kb\ size\ of\ insert}{kb\ size\ of\ vector} + \frac{vector}{insert} = \ ng\ insert$$

$$\frac{7.5\ \times\ kb\ size\ of\ insert}{2.58} + \frac{1}{1} = \ ng\ insert$$

The optimal vector:insert ratio is between 0.5:1 and 2:1. I most frequently used 1:1.

For the cloning reaction, 0.5 μl pENTR/D-TOPO, 0.5 μl salt solution (Entry vector cloning kit, Invitrogen), and the calculated volume of PCR product were mixed in a total volume of 2.5 μl and incubated at 22°C for 1 hour. A negative control reaction containing no PCR product was always included.

The plasmids were then transformed into either One Shot (Invitrogen) or highly competent bacteria (C2987, NEB) by mixing 2 μl of the reaction with 50 μl bacterial suspension and leaving on ice for 30 minutes, followed by 40 seconds at 42°C. 250 μl SOC (NEB) was added to the bacteria, and they were grown at 37°C for 1 hour with continual shaking. The bacteria were then spread onto L-agar plates containing 100 μg/ml kanamycin and grown overnight at 37°C.

Colonies were picked using a pipette tip and transferred to 4 ml of Luria Broth (LB) containing 100 μg/ml kanamycin and grown at 37°C with shaking overnight. The following day, the plasmids were isolated using a Mini-Prep Kit (Qiagen) following the manufacturer's protocol. To ensure that the plasmids contained the desired insert, each was verified by sequencing (Cogenics).

To generate useable expression constructs from sequence-verified Entry vectors, a subsequent Gateway Cloning (Invitrogen) step had to be carried out. In this reaction the gene of interest inserted in the Entry vector is recombined into a Destination vector of choice, many of which contain in frame tags such as Green Fluorescent Protein (GFP) or the Haemagglutinin (HA) moiety. To this end, 0.75 μl of the Entry vector (100 ng/μl), 0.75 μl of the desired Destination vector (100 ng/μl), 2.5 μl of TE and 1 μl Gateway LR Clonase II Enzyme Mix (Invitrogen) were combined and incubated at 25°C for 1 hour. 0.5 μl proteinase K solution (provided with the LR Clonase Kit) was then added to degrade the recombinase, and the reaction was heated to 37°C for 10 minutes. 2 μl of this reaction was then transformed as described above, except that the bacteria were grown on L-agar plates containing 100 μg/ml ampicillin rather than kanamycin. The following day colonies were picked and grown in 100 ml LB containing 100 μg/ml ampicillin overnight, and then the plasmids were isolated using a Midi Prep Kit (Qiagen) and verified by sequencing (Cogenics).

2.3.5 qPCR

Quantitative real-time Polymerase Chain Reactions (qPCR) were carried out to assess the expression levels of different genes. For these experiments, cDNA was prepared as described from the requisite samples. Primer pair solutions were made by diluting forward and reverse stock primers (100 μM) 1:10, to give a final concentration of 10 μM of each primer.

Before beginning a qPCR experiment, a standard curve was made for each new set of primers. The following PCR reaction was set up:

- 25 μl KAPA2

- 1 μl primer pair

- 1 μl appropriate cDNA

- 23 μl water

And the following programme was run:

Temperature/°C	Time	Cycles
95	2 minutes	
95	30 seconds	
55	30 seconds	20
72	30 seconds	
4	Indefinite	

After completion, 10 μl of this PCR reaction was taken and run again through the same programme. The products from this second round were then run on a 2% agarose gel to confirm that DNA of the correct size was created, and that the primer pair produced only a single band. The remaining 40 μl was used to create a standard curve by serial ten-fold dilutions, beginning at 10^{-3} down to 10^{-10}.

For the qPCR, the following was assembled for each sample. Every sample was done in duplicate:

- 5 μl 2X LightCycler 480 SYBR Green I Master (Roche)

- 0.5 μl primer pair

- 2 μl water

7 μl of this master mix was then put into each well of a 96-well plate as desired, using a repeater pipette (Pipetman). 3 μl cDNA or diluted standards was then added to each sample using a multichannel pipette (Pipet-Lite XLS, Rainin). Once complete, the plate was covered using a Clear Adhesive Seal (Rainin), and then centrifuged at 1000 rpm for 1 minute. The qPCR was carried out using a LightCycler II (Roche).

LightCycler 480 SW1.5 software provided concentrations of the amplified products using the standard curve included in the run. These data were then exported to Excel (Microsoft), and analysed in the following way: technical replicates were averaged and divided by the averages of the chosen housekeeping gene (most commonly histone H4 or ornithine decarboxylase) measured for the same sample.

2.3.6 Western Blotting

2.3.6.1 Solutions and Reagents
SDS Running Buffer

Trizma Base	30	gm
Glycine	144	gm
SDS	10	gm
Dist. Water	1	l

Wet Transfer Buffer

Reagent	Volume/Mass
Tris Base	6 g
Glycine	28 g
Methanol	400 ml
10% SDS	2 ml
Dist. Water	To 2 l

TBST

TRIS (50mM Ph7.5)	6	gm
NaCl (150Mm)	8	gm
Tween 20 (0.20%)	2	ml
Dist. Water	1	l

2.3.6.2 Running Gels and Membrane Transfer

All western blots were carried out using pre-cast TGX gradient gels (BioRad, 1 mm Mini-Protean anykD) and SDS running buffer.

Samples to be analysed by western blotting were prepared as described above. 4X SDS loading buffer (Licor) was prepared by adding 10% 2-mercaptoethanol (Sigma). The buffer was added to the samples and heated to 80°C for 10 minutes. Samples were loaded onto the gel, and run at 70-100 mA until the dye front had left the bottom of the gel. 8 μl of Precision Plus Protein Dual Colour Standards (BioRad) was used as a ladder.

Once separated, the proteins were then transferred onto PVDF membrane (Immobilon-FL, Millipore) by wet transfer, running at 100 V for 30 minutes, or for larger proteins at 20 V overnight at 4°C.

2.3.6.3 Detection By Chemiluminescence

For chemiluminescence visualisation of proteins the membrane was blocked in Milk Solution (5% milk powder [Marvel] in PBST) for 1 hour at room temperature, or overnight at 4°C. Primary antibodies were then added, diluted in Milk Solution between one hundred- and one thousand-fold (see Table 2.4 and Table 2.5) for 2 hours at room temperature, or more typically overnight at 4°C.

The membranes were then washed 3 times in Milk Solution for 10-20 minutes, followed by incubation with HRP-conjugated secondary antibodies diluted 1:1000 in milk solution for 2 hours at room temperature. The membranes were then washed 3 times in Milk Solution for 10-20 minutes, followed by two 5-minute washes in TBS.

Chemiluminscence detection solution was prepared by mixing both components of the Super Signal West Dura Kit (Thermo Scientific) in equal amounts and waiting approximately one minute. The membranes were removed from PBS and covered with the prepared detection solution for one minute, before pouring off. The chemiluminescent signal was then detected using a BioRad Chemi-Doc XRS.

2.3.6.4 Detection Using The Odyssey Imager

For visualisation using the Odyssey Imager (Licor) the membranes were blocked using Odyssey buffer (BioRad) for 1 hour at room temperature, or overnight at 4°C. The membranes were then incubated with the primary antibodies diluted in TBST solution for 2 hours at room temperature, or overnight at 4°C.

The primary antibody solution was then removed and the membranes washed 3 times for 10 minutes each in TBST at room temperature. Secondary antibodies were added in TBST + 0.1% SDS for 2 hours at room temperature, then the membranes were washed 3 times in TBST for 10 minutes each, followed by rinsing in TBS. The membranes were then placed onto the Licor detector plate, and the fluorescence captured using Image Studios software (Licor).

2.4 Tables

Table 2.1 Plasmids

Plasmid Name	Gene Insert	Vector	Source	Linearising Enzyme	Transcribing Enzyme
Expression Vectors					
ARID1a	ARID1a	pCS2+	ATW	DraI	SP6
GFP-ARID1a	GFP-ARID1a	pCS2+	ATW	DraI	SP6
HA-ARID1a	HA-ARID1a	pCS2+	ATW	DraI	SP6
ΔUTR-ARID1a	ARID1a	pCS2+	ATW	DraI	SP6
GFP	GFP	pCS2+	Mary Wu	NotI	SP6
pCSKA XWnt-8	Wnt8	pCSKA	Richard Harland	BamHI	SP6
Beta-Catenin	Beta-catenin	pSP64T	Stefan Schneider-Hanson	BamHI	SP6
pSP64T-eFGF(i)	FGF4	pSP64T	S. Schulte-Merker	EcoRI	SP6
DDX5	DDX5	pCS2+	ATW	NotI	SP6
Myc-DDX5	Myc-DDX5	pCS2+	ATW	NotI	SP6
BCL7a	BCL7a	pCS2+	ATW	NotI	SP6
Myc-BCL7a	Myc-BCL7a	pCS2+	ATW	NotI	SP6
In Situ Hybridisation Vectors					
Sox3	Sox3	pBS SK+	Lab Stocks	SmaI	T7
Slug	Snai2	pMX363	Mary Wu	BglII	SP6
21.3C	ARID1a	pCMV-SPORT6	E. Callery	NcoI	T7
Other					
ARID1a pGEM-T Easy	ARID1a	pGEM-T Easy	ATW	N/A	N/A
ARID1a pENTR	ARID1a	pENTR	ATW	N/A	N/A
ARID1a pFRT	GFP-ARID1a	pcDNA5 /FRT/TO	Cloning facility at Protein Phosphorylation Unit, Univeristy of Dundee	N/A	N/A
pOG44	Flp	pOG44	Sapkota Lab	N/A	N/A
TOPFLASH		pTA-luc	R. Moon. Addgene plasmid 12456	N/A	N/A
FOPFLASH		pTA-luc	R. Moon. Addgene plasmid 12457		N/A
BCL7a pENTR	BCL7a	pENTR	ATW	N/A	N/A
DDX5 pENTR	DDX5	pENTR	ATW	N/A	N/A

Table 2.2 Morpholinos

Table 2.2 Morpholinos

Name	Type	Sequence 5'-3'
ARID1a _CO	Mismatch control for ARID1a TB1	CATcGAcGAgAGAcAAAAGcAC
ARID1a _TB	Translation blocking	CATGGAGGACAGAGAAAAGGAC
ARID1a _SC1	Mismatch control for ARID1a SB1	AAaAAcACTTgACTcTACCTcTTGC
ARID1a _SC2	Mismatch control for ARID1a SB2	ATATGcAcACATCTcTGcAcCAAAT
ARID1a_ SB1	Splice blocking	AATAAGACTTCACTGTACCTGTTGC
ARID1a _SB2	Splice blocking	ATATGGAGACATCTGTGGAGCAAAT
DDX5 CO1	Mismatch control for DDX5 TB1	CCaTGTCaTTAAATaCGGaCATaGC
DDX5 TB1	Translation blocking	CCCTGTCGTTAAATCCGGGCATGGC

Table 2.3 Primers

Name	Sequence 5'-3'
Cloning	
ARID1a pENTR Forward	CACCATGGCCTCTCCTCCTACTCTCTAC
ARID1a pENTR Reverse	TCATGACTGGCCAATCAAGAAGA
ARID1a 5'UTR Forward	TCCAGCTCCAGTTCCTGTCT
BCL7a pENTR Forward	CACCATGTCAGGACGATCTGTCAG
BCL7a pENTR Reverse	AGTTTCTCTGAAGCCCCTGG
DDX5 pENTR Forward	CACCATGCCCGGATTTAACGACAG
DDX5 pENTR Reverse	AGTCACCACTGCAGTTACCT
Sequencing And Morpholino Verification	
ARID1a Seq 1	AAAGGAGCCGAAGGTTATAC
ARID1a Seq 2	TTCTCACCTCACACTTCCCC
ARID1a Seq 3	CGAGGGTACATGCAGAGGAA
ARID1a Seq 4	AATGTGGGCACTTCAAGCAG
ARID1a Seq 5	AAAGAGTGTCTGCTGCTCCT
ARID1a Seq 6	GTTGGGCCGCTTACAAGAAT
ARID1a Seq 7	AGTTTCAGCAGAGTCAGGCT
ARID1a Exon 2 Forward	GTCCATGCAAGGAAGACCAC
ARID1a Exon 4 Reverse	TGGTTGCATTCCCATACTCA
qPCR	
ODC Forward	GCCATTGTGAAGACTCTCTCCA
ODC Reverse	TTCGGGTGATTCCTTGCCAC
H4 Forward	CGGGATAACATTCAGGGTATCACT
H4 Reverse	ATCCATGGCGGTAACTGTCTTCCT
ARID1a Forward	AGAAATTGTATGGGACCTTG
ARID1a Reverse	TGTCACCTTGAGCTAGATTG
Siamois Forward	TCAACCCTTATCCAGACTTT
Siamois Reverse	ATGTCTGGCTCTTCTGTTCT
Xnr3 Forward	TCCACTTGTGCAGTTCCACAG
Xnr3 Reverse	ATCTCTTCATGGTGCCTCAGG
Xbra Forward	GAGCATGGAGCACAAACAGA
Xbra Reverse	CAATTCAGCCCAGGAAATA
Goosecoid Forward	TGTTGTGGAGCAGTTCAAGC
Goosecoid Reverse	CCAGTGCTTCCAGTTGTTCA
BCL7a Forward	GAAACAAGAAGTCGGGCGAA
BCL7a Reverse	CACTTTGGGCTCTGCAACAG
DDX5 Forward	TGGAAGCGATTAAACGGCAG
DDX5 Reverse	ATCTCCCCGCTGTAGGAATG
ARID1a HEK Forward	GGTAATGATGTCCCTCAAGT
ARID1a HEK Reverse	GATCCAGTAGCGTTCTCTGT

Table 2.4 Primary Antibodies

Antibody Name	Protein Recognised	Species Raised In	Manufacturer	Dilution
HA-7	Haemagglutinin epitope	Mouse	Sigma	1:1000-1:5000
H-90	ARID1A	Rabbit	Santa-Cruz Biotechnology	1:1000
PSG3	ARID1A	Mouse	Santa-Cruz Biotechnology	1:1000
H-88	BRG1	Rabbit	Santa-Cruz Biotechnology	1:1000
G-7	BRG1	Mouse	Santa-Cruz Biotechnology	1:1000
H-102	CTNB1	Rabbit	Santa-Cruz Biotechnology	1:1000/1:200
AP7459c	DDX5/p68	Rabbit	Abgent	1:200
S268B	GFP	Sheep	Sapkota Lab	1:5000
9E10	Myc	Mouse	Santa-Cruz Biotechnology	1:2000

Table 2.5 Secondary Antibodies

Antibody Name	Protein Recognised	Species Raised In	Manufacturer	Dilution
Stabilised Peroxidase Conjugated Goat Anti-Rabbit (32460)	Rabbit IgG	Goat	Thermo Scientific	1:1000
Stabilised Peroxidase Conjugated Goat Anti-Mouse (32430)	Mouse IgG	Goat	Thermo Scientific	1:1000
Odyssey Goat Anti-Mouse IRDye 800CW (926-32210)	Mouse IgG	Goat	LiCor	1:15000
Odyssey Goat Anti-Mouse IRDye 680LT (926-68020)	Mouse IgG	Goat	LiCor	1:20000
Odyssey Goat Anti-Rabbit IRDye 800CW (926-32211)	Rabbit IgG	Goat	LiCor	1:15000
Odyssey Goat Anti-Mouse IRDye 680 (926-32221)	Rabbit IgG	Goat	LiCor	1:15000

Chapter 3: *ARID1a* During *Xenopus* Development

3.1 Introduction

Xenopus is an excellent model organism for studying embryogenesis. Females can be induced to lay eggs by injection of H̲uman C̲horionic G̲onadotropin (HCG). This procedure is not harmful, and the frogs can be re-used every 3 months. Each spawn produces hundreds of eggs, which when fertilised develop synchronously. These embryos can be accurately staged and collected at the desired times. Gene expression can be readily manipulated by microinjection of mRNA or antisense morpholino oligonucleotides. Furthermore, the detailed fate map of the early blastula allows targeting of different tissues by injection of specific blastomeres. While this is cruder than genetic approaches available in the mouse, this method is significantly faster and can be carried out on a large scale. Finally, the large size of *Xenopus* embryos makes them amenable to dissection. Classic transplantation experiments established many of the paradigms of *Xenopus* embryology, and are still valuable techniques in modern research.

I have assessed the expression pattern of *ARID1a* during *Xenopus* embryogenesis. I then examined the effects of loss and gain of function of *ARID1a* on *Xenopus* development.

3.2 Results

3.2.1 Cloning of *Xenopus laevis ARID1a*

Xenopus laevis is pseudotetraploid, owing to a hybridisation event between two species ~40 million years ago (Bisbee et al., 1977; Evans et al., 2004). This property has meant that sequencing the *X. laevis* genome has proven exceptionally challenging, and to date only partial scaffolds exist. In order to clone *Xenopus ARID1a* I sought to design primers against the open reading frame. Unfortunately, no genomic sequence nor e̲xpressed s̲equence t̲ag (EST) containing the entire *ARID1a* coding sequence was available.

I therefore adopted a different strategy, designing primers against *ARID1a* using sequence from the closely related species *X. tropicalis,* which has a sequenced genome. Using these primers I carried out PCR on cDNA from stage 1 *X. laevis* embryos and cloned the resultant product into an Entry vector (Invitrogen). *X. laevis ARID1a* was then subcloned into pCS2+ using the Gateway system, producing expression vectors that were either untagged, or contained an N-terminal HA or GFP tag that were then verified by sequencing.

X. laevis ARID1a is 6159 base pairs long, coding for a 2053 amino acid protein with a predicted mass of 220 kDa (Fig. 3.1, top line). The *X. laevis* ARID1a protein has two predicted domains: an ARID region from residue 812 to 932, and a Domain of Unknown Function (DUF3518) spanning residues 1742-1998. The DUF domain corresponds to the previously described Eyelid Homology Domain (EHD) in the *Drosophila* Osa protein. I looked for sequence similarities by aligning the *X. laevis* ARID1a protein with ARID1a proteins from *X. tropicalis,* human, mouse, fly and yeast (Fig. 3.1). The *Xenopus laevis* ARID1a protein is 97.7% identical to the *Xenopus tropicalis* protein, and is well conserved with the human and mouse ARID1a proteins (87.2% and 87.1% identical, respectively). As expected, conservation with fly and yeast is lower (73.3% and 73.0% identity, respectively), with the ARID and DUF as the most highly conserved regions. Due to the degree of conservation observed between these proteins, I conclude that I have successfully cloned the entire open reading frame for *X. laevis ARID1a*. From here on I will refer to *Xenopus laevis* as *Xenopus* and *X. laevis ARID1a* as *ARID1a* unless otherwise stated.
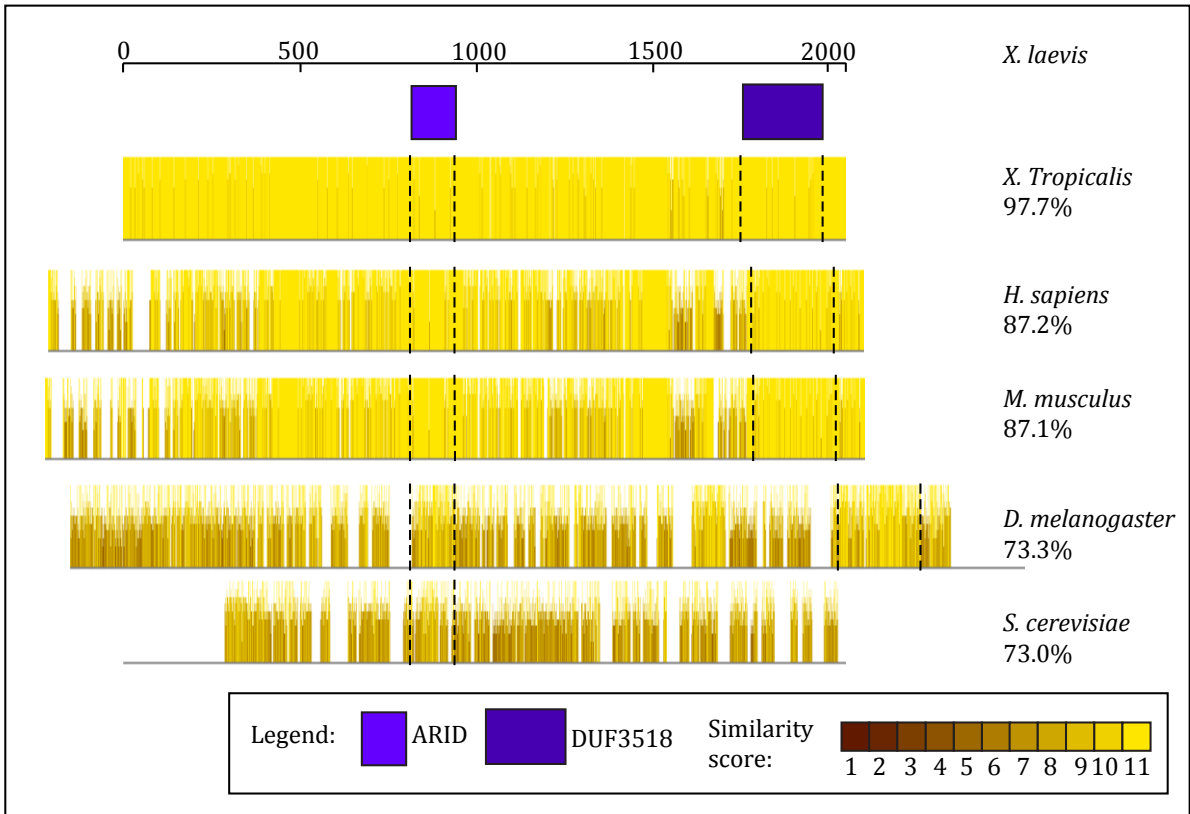
Fig. 3.1: Species Comparison of ARID1a Proteins

Protein sequences for ARID1a from 5 different species were aligned against the *in silico* translated sequence for *X. laevis ARID1a* using Clustal X and were visualised using Jalview. They are displayed with the ARID region overlapping. The similarity score is a representation of the degree of conservation for each residue - with 11 being identical and 1 being completely unconserved. The heights of the bars correspond to the similarity score.

3.2.2 Expression Pattern Of *ARID1a* During *Xenopus* Embryogenesis

To understand what functions *ARID1a* carries out within the embryo, it was first important to know when and where it is expressed throughout development. To assess this I carried out quantitative PCR (qPCR) using cDNA synthesised from embryos collected at different developmental stages (Fig 3.2 A).

ARID1a transcripts were detectable throughout embryogenesis. Following fertilisation levels of *ARID1a* mRNA dropped, perhaps indicating decay of maternally deposited transcripts. During gastrulation the expression of *ARID1a* increased, and continued to rise until stage 16 and thereafter remained high. These experiments were also normalised to *Ornithine decarboxylase (ODC)* and showed a similar trend (data not shown).

To complement these qPCR data I carried out *in situ* hybridisation to assess the spatial expression pattern of *ARID1a*. In the fertilised zygote *ARID1a* transcripts were localised to the animal pole, with very little expression visible in the vegetal hemisphere (Fig 3.2 B and B'). By mid-gastrulation *ARID1a* was expressed throughout the ectoderm and involuting mesoderm (Fig. 3.2 C and C'). At stage 19, *ARID1a* expression was clearly visible in the epidermis and developing neural tissue, and at stage 25 had become further restricted, with strong staining in the developing eye, brain and migrating streams of neural crest cells (Fig 3.2 D, E). In stage 33 embryos *ARID1a* was highly expressed in cranial structures such as the eye, brain, branchial arches and otic vesicles. Staining was also observed in a lateral stripe immediately ventral to the somites, though it is unclear what this tissue is. Sectioning would reveal whether this is real or background staining, and could also clarify where in the embryo *ARID1a* is expressed during gastrulation.

The yolky vegetal region of early *Xenopus* embryos stains poorly during the *in situ* hybridisation procedure (Sive et al., 2010). To assess whether the animal pole localisation I observed was real or an artefact of the procedure, I bisected stage 1 embryos and assayed the expression of *ARID1a* in either the animal or vegetal hemispheres by qPCR (Fig 3.2 G). *ARID1a* transcripts were twofold higher in animal hemispheres than in vegetal hemispheres.
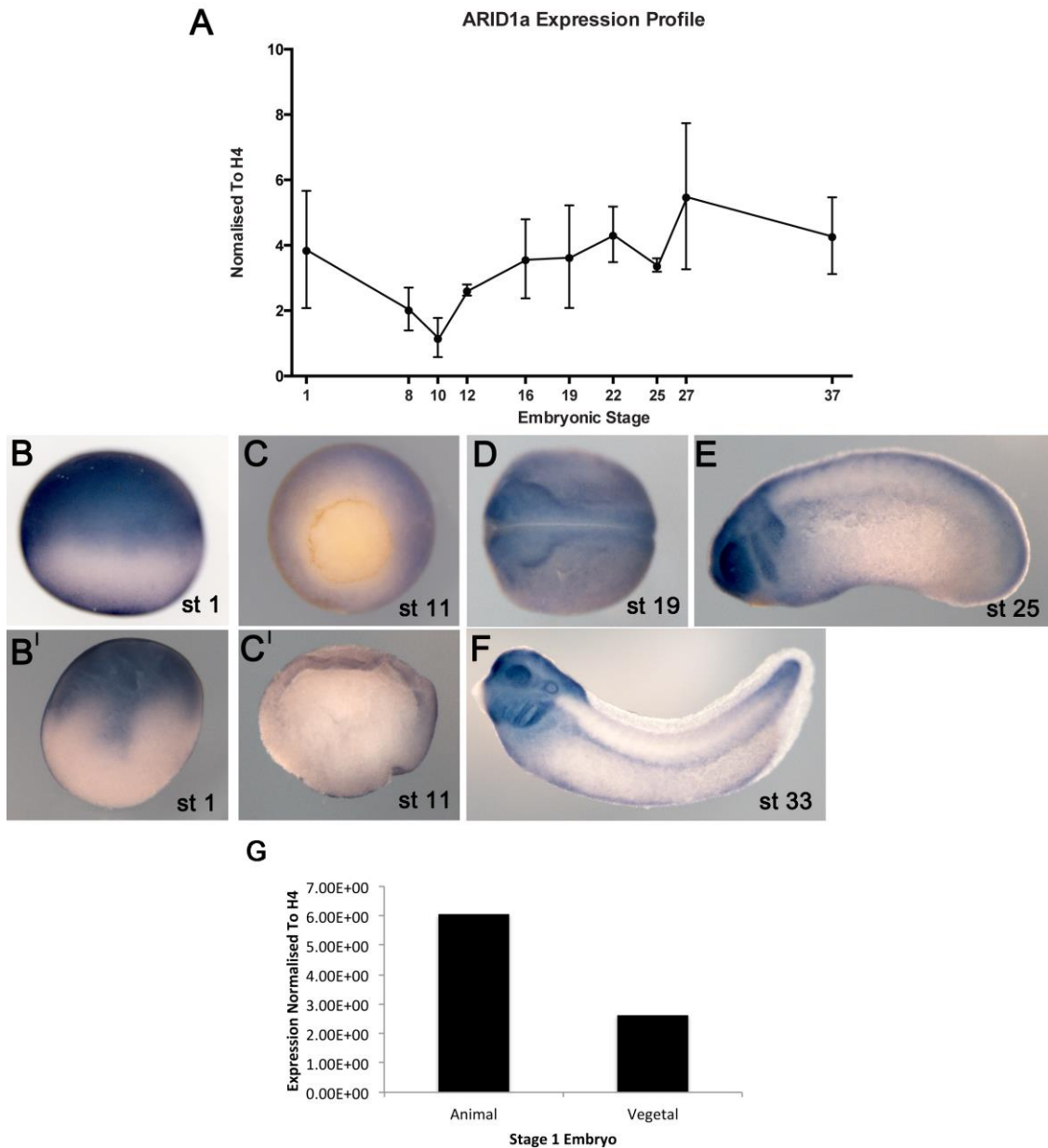
Fig. 3.2: Expression Of *ARID1a* In *Xenopus* Embryos

A: qPCR timecourse of *ARID1a* expression over the first four days of *Xenopus* development. Data are shown normalised to *histone H4*, and are the average of 3 independent experiments.

B-F: In situ hybridisation for *ARID1a* carried out on different developmental stages. B' and C' are bisected embryos corresponding to B and C respectively. B, B' are lateral views with the animal pole at the top of the image. C is a vegetal view with the dorsal side on the right, C' is a lateral view with the animal pole uppermost and the dorsal side to the right. D is a dorsal view with the anterior to the left. E and F are lateral views with the anterior to the left. Staining is ubiquitous until neurula stages (D), when *ARID1a* becomes more strongly expressed in the neural tissue. From tailbud stages onwards (E,F) staining is visible in the migrating neural crest, branchial arches, eyes, otic vesicles and cranial regions..

G: qPCR of bisected *Xenopus* zygotes. Expression of *ARID1a* is higher in the animal hemisphere, confirming the localisation observed in B and B'. Data are shown normalised to *histone H4.* Data are representative of two independent experiments.

This is less than would be expected based on the apparent difference seen by *in situ* hybridisation, though it does confirm that *ARID1a* is expressed more strongly in the animal hemisphere.

3.2.3 Depletion of *ARID1a* Using Translation-Blocking Morpholinos

To study the function of *ARID1a* during *Xenopus* embryogenesis I used a translation blocking mopholino to deplete ARID1a protein (ARID1a_TB, designed by E. Callery, Smith Lab. Fig. 3.3 A). A 5-base mismatch morpholino was used as a control (ARID1a_CO). I first validated these ARID1a morpholinos using *in vitro* transcription-translation reactions (Fig. 3.3 B). The mismatch control morpholino had no effect on ARID1a protein synthesis (lane 2) whereas 20 ng ARID1a_TB1 caused a marked reduction in ARID1a protein (lane 3). A construct lacking the morpholino recognition sequence was unaffected by the translation blocking morpholino (lane 4).

Embryos were injected with either 10 ng ARID1a_CO or 10 ng ARID1a_TB at the one cell stage. Those injected with ARID1a_CO appeared phenotypically normal throughout development (Fig. 3.3 C, E), whereas embryos injected with ARID1a_TB had diminished forebrains and were significantly delayed in their development (Fig. 3.3 D). Furthermore, 53% of the ARID1a_TB morphants developed oedema around the heart, although the hearts were still beating. Injection of a higher dose (20 ng) caused a more severe phenotype: the morphants underwent gastrulation and neurulation as normal but failed to progress to the tailbud stage. This arrest was coupled with epidermal shedding and embryo death (Fig. 3.3 F). This lethal phenotype indicates that *ARID1a* is required for embryogenesis.

To assess whether *ARID1a*_TB caused apoptosis I carried out TUNEL assays on stage 18 embryos injected with 20 ng of either ARID1a_CO or ARID1a_TB morpholino (Fig. 3.4 A-C). As expected, there was no detectable cell death in the control morphants (Fig. 3.4 A). Treatment of control morphants with DNase prior to the TUNEL assay provided a positive control (Fig. 3.4 B), with staining throughout the epidermis.

A

	5' UTR	Exon 1
ARID1a	...TCCCCGTCCTTTTCTCTGTCCTCC	ATGGCTGCTCAGGTGGCC...
ARID1a_TB	CAGGAAAAGAGACAGGAGG	TAC
ARID1a_CO	CACGAAAACAGAGAGCAGC	TAC

B

No Plasmid
ARID1a + CO
ARID1a + TB
ΔUTR-ARID1a + TB

◄ ARID1a

150 kDa

ARID1a_CO — ARID1a_TB

C 10 ng 20/20
D 10 ng 19/36
E 20 ng 28/29
F 20 ng 38/44
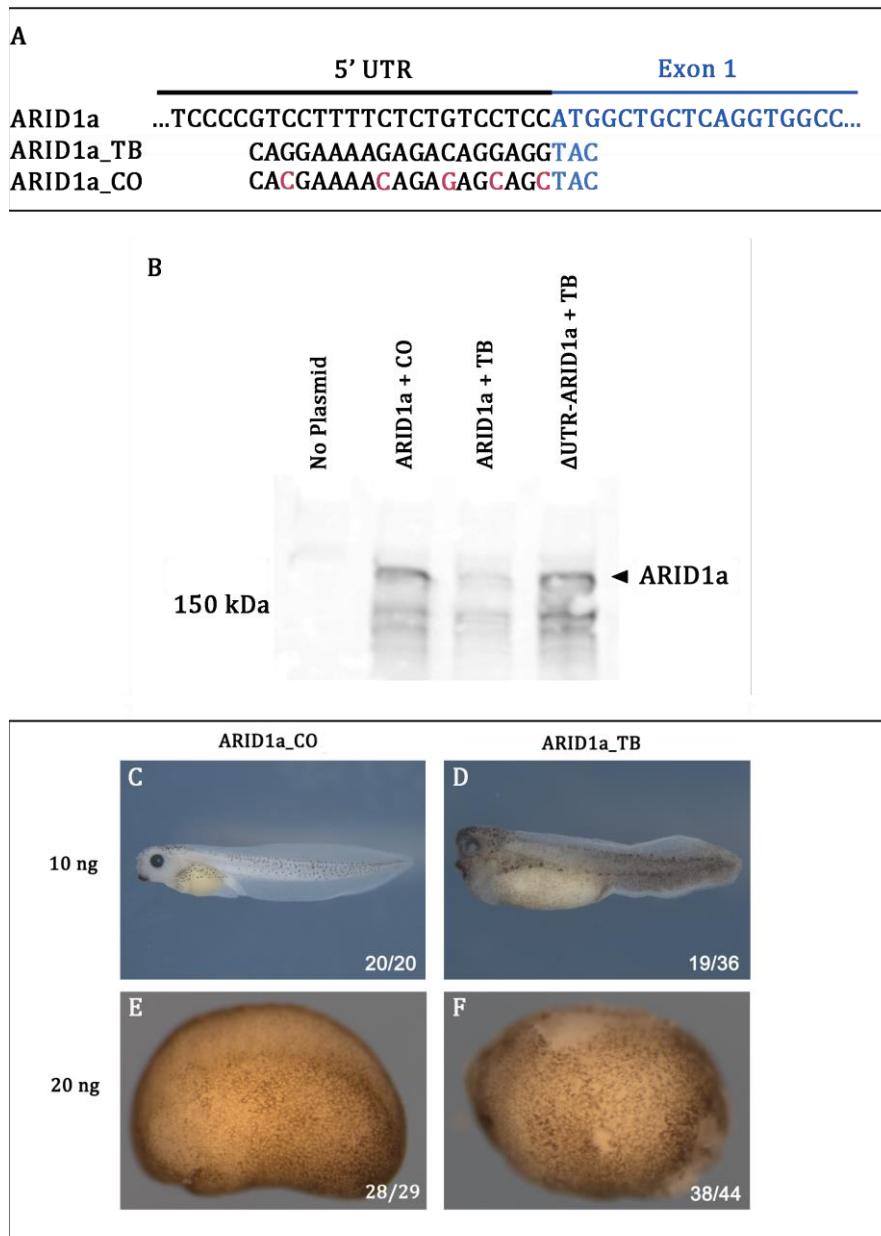
Fig. 3.3: Loss Of ARID1a Was Embryonic Lethal

A: Diagram showing the position of the control and translation blocking morpholinos relative to the *ARID1a* gene. ARID1a_TB: translation blocking morpholino. ARID1a_CO: mismatch control morpholino.

B: Morpholino validation. ARID1a protein was produced by *in vitro* transcription-translation reactions using biotinylated lysines and then run on a polyacrylamide gel. A western blot using streptavidin was then carried out. Due to the large nature of ARID1a only small amounts of protein were produced, Lane 1: no plasmid. No ARID1a detectable. Lane 2: ARID1a plasmid with 20 ng ARID1a_CO morpholino. ARID1a detectable as an ~220 kDa band. Lane 3: ARID1a plasmid with 20 ng ARID1a_TB morpholino. Marked reduction in the amount of ARID1a protein present. Lane 4: an ARID1a plasmid lacking the morpholino recognition sequence. 20 ng ARID1a_TB has no effect on the expression of this protein.

C-F: embryos injected with either control or translation blocking morpholinos. All images are lateral views with the anterior of the embryo to the left.

C, E: ARID1a_CO morpholino has no effect on *Xenopus* development.

D, F: Injection of 10 ng ARID1a_TB caused oedema around the heart and shortened forebrains (D). Injection of 20 ng ARID1a_TB caused embryonic death and epidermal shedding (F).

20 ng ARID1a_CO1   20 ng ARID1a_CO1 +DNase   20 ng ARID1a_TB1
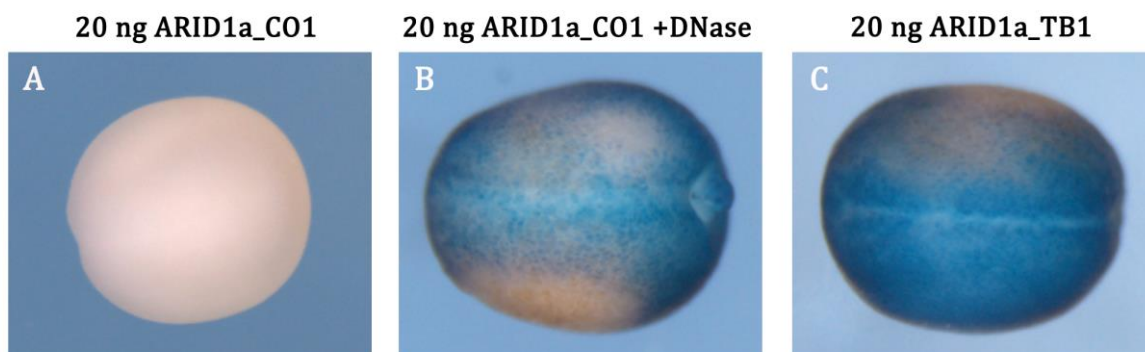
Fig. 3.4 Loss Of ARID1a Caused Widespread Apoptosis

A-C: TUNEL staining (blue) to show apoptotic cells. There is no apoptosis in control morphants at stage 17 (A). Treatment of control morphants with DNaseI created nicked ends that could be recognised by the TUNEL antibodies and acted as a positive control (B). Injection of embryos with ARID1a_TB caused a large degree of apoptosis, particularly around the neural tube and dorsal epidermis (C).

Embryos were all fixed at the same time. Images are dorsal views with the anterior to the left.

Embryos injected with ARID1a_TB were heavily stained throughout the epidermis and neural tube, indicating that there was significant cell death caused by this morpholino (Fig. 3.4 C). This large degree of apoptosis could be caused by, or be the cause of, the developmental arrest (see section 3.3).

The apoptosis observed here could be due to toxic, off target effects of the morpholino rather than being a consequence of loss of ARID1a. In zebrafish a common test for morpholino toxicity is to co-inject a p53 morpholino to abrogate the phenotype – however injection of p53 morpholinos into *Xenopus* embryos disrupts mesodermal patterning (Takebayashi-Suzuki, 2003). Instead I attempted rescue experiments co-injecting 1 ng *ARID1a* mRNA along with 20 ng ARID1a_TB, however the embryos still underwent epidermal shedding and died. As rescue experiments are notoriously difficult, it may be that I did not use the correct dose of *ARID1a* mRNA, or that it did not diffuse efficiently as it is such a large transcript. As the mismatch morpholino has no effect on embryonic development even at very high doses (50 ng), and the previously demonstrated requirement for *ARID1a* during embryonic development (see Chapter 1) it is likely that the embryonic death phenotype observed here is real and not caused by a toxic translation blocking morpholino.

3.2.4: Depletion of *ARID1a* Using Splice Blocking Morpholinos

Due to the GC-rich nature of the 5' UTR of *ARID1a* it was not possible to create a second translation blocking morpholino, so instead I designed a pair of splice blocking morpholinos against Intron 2. The draft *Xenopus laevis* genome was searched using *ARID1a* sequence from the cDNA that I cloned. Two genes matched *ARID1a,* which I termed *ARID1aa* and *ARID1ab.* Unusually, the putative exon sequences for these two genes were exactly identical, although the intronic sequences did vary. The 5' UTR was identical for both genes, so the translation blocking morpholino described earlier would knock down both *ARID1aa* and *ARID1ab* with equal efficiency. To design splice blocking morpholinos I verified the sequence of Intron 2 experimentally by carrying out PCR on genomic DNA from 10 pooled embryos. Only one intronic sequence was retrieved from this experiment, which matched *ARID1aa.* Due to the highly unusual nature of the

complete exonic conservation between *ARID1aa* and *ARID1ab,* and the fact that I only retrieved intronic sequence for *ARID1aa*, I concluded that *ARID1ab* was probably an artefact of the genome assembly and did not represent a real gene. Since carrying out this work a new *X. laevis* genome has been published and only *ARID1aa* is present.

I designed morpholinos ARID1a_SB1 and ARID1a_SB2 across the Exon 2-Intron 2 and Intron 2-Exon 3 boundaries of *ARID1aa* respectively (Fig. 3.5 A). These morpholinos had a 2 and 3 base pair mismatch with *ARID1ab* respectively, and so if this allele is expressed they would have a reduced efficiency blocking efficient splicing of the mRNA. The morpholinos should cause the retention of Intron 2, which would introduce a premature stop codon and lead to a truncated protein product. To test this I designed primers spanning Exon2-4 (Fig. 3.5 A) and carried out PCR on cDNA derived from stage 20 embryos injected with either control or splice blocking morpholinos (Fig. 3.5 B). Stage 20 was chosen because by this time maternal transcripts of *ARID1a* would have been depleted. As maternal transcripts not affected by splice blocking morpholinos, carrying out the experiment at this later time point prevented false negatives that might be found at earlier stages. A band 400 bp in size was amplified from uninjected embryos or control morphants, corresponding to correctly spliced *ARID1a* mRNA. Injection of ARID1a_SB1 alone, or together with ARID1a_SB2 reduced the intensity of this band, and a new band >1 kb in size was detected. This band appears to be slightly smaller than expected, but that may be due to the high percentage agarose gel used to visualise the PCR products. Sequencing of this product showed that it matched Intron2 of *ARID1a* and that a premature stop codon had been introduced, indicating that these morpholinos are capable of depleting *ARID1a*.

Injection of ARID1a_SB1 or ARID1a_SB2 alone into stage 1 embryos had no effect on development, even at high doses. However, co-injection of ARID1a_SB1 and ARID1a_SB2 together caused embryos to develop small heads and ventral oedema similar to that observed with low doses of ARID1a_TB (Fig. 3.5 B). Additionally, melanocyte migration was mildly affected, with more diffuse scattering over the body walls and in the anterior head.
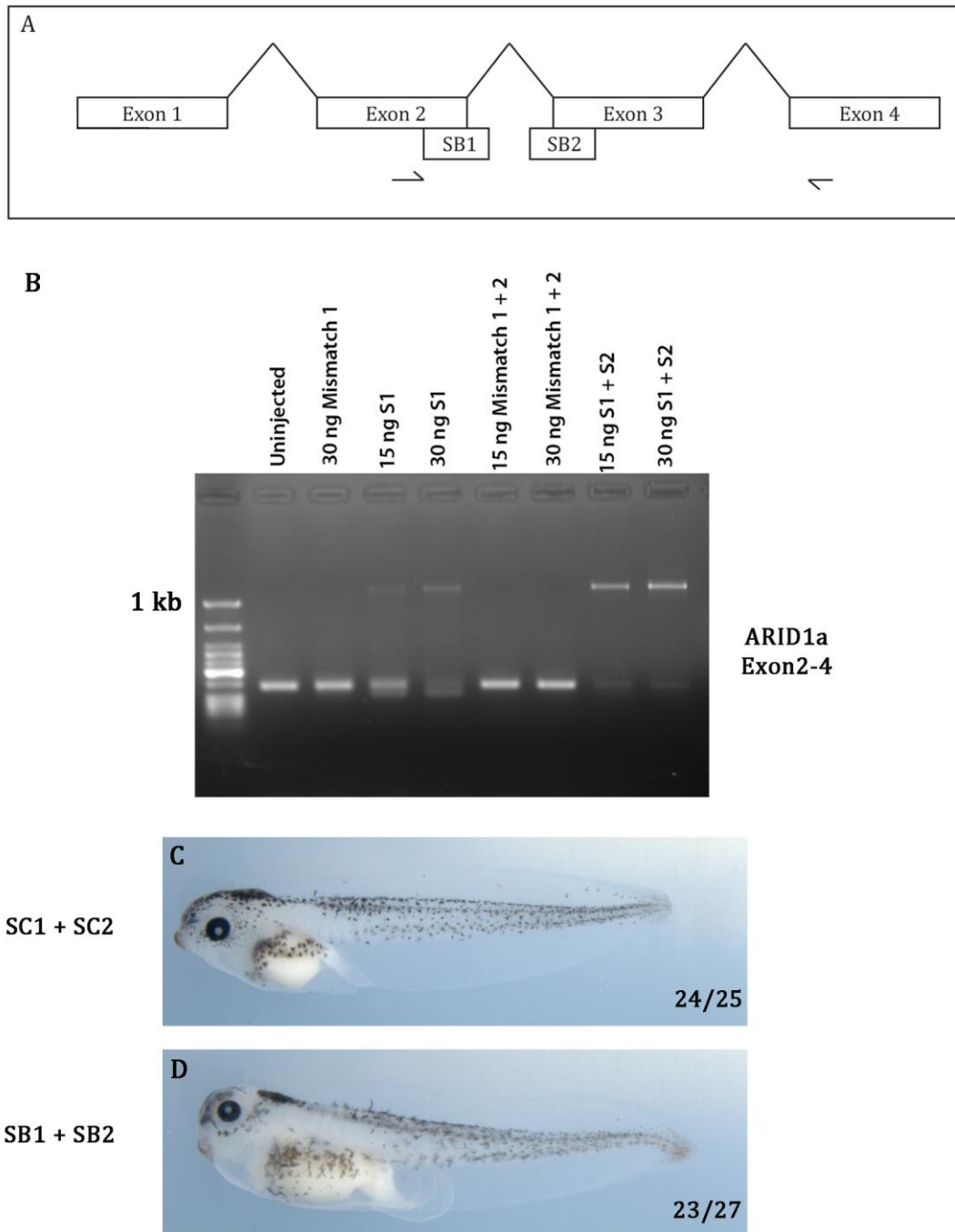
Fig. 3.5: Splice Block Morpholinos Knock Down *ARID1a*

A: Schematic representation of the first 4 exons of *ARID1a.* The location of the splice blocking morpholinos and the primers (half arrows) used in B are shown.

B: PCR validation of the splice blocking morpholinos measured at stage 20. Injection of SB1 and SB2 caused a decrease in correctly spliced mRNA (lanes 1, 2, 5, 6) and gain of a larger PCR product representing mRNA containing the second intron (lanes 3, 4, 7, 8).

C: Injection of the two control morpholinos SC1 and SC2 had no effect on *Xenopus* development.

D: Injection of the two splice blocking morpholinos SB1 and SB2 caused a mild phenotype, with oedema around the heart, shortened brain structures and mild melanocyte defects. Embryos are lateral views with the anterior to the left.
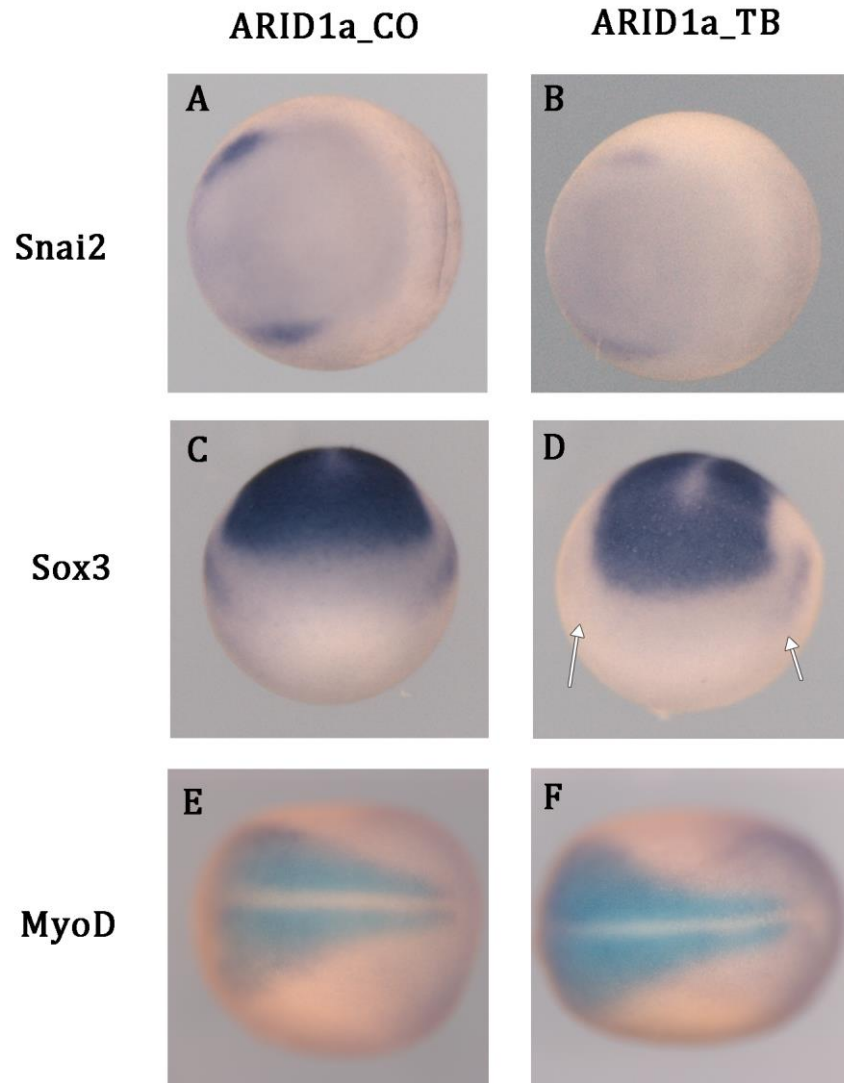
Fig. 3.6 Neural Crest Specification Is Impaired In *ARID1a* Morphants

(A, B): Dorsal view with the anterior to the left of *in situ* hybridisation for *Snai2* on stage 13 embryos injected with 20 ng of either control or translation blocking morpholino. Depletion of *ARID1a* severely reduced expression of *Snai2* in the neural crest (B).

(C, D): Anterior view with dorsal side uppermost of in situ hybridisation for *Sox3* on stage 13 embryos injected with 20 ng of either control or translation blocking morpholino. Depletion of *ARID1a* reduced placodal expression of *Sox3* (D, white arrows) but did not affect expression in the neural tube.

(E, F): Dorsal view with the anterior to the left of in situ hybridisation for *MyoD* on stage 14 embryos injected with 20 ng of either control or translation blocking morpholino. Depletion of *ARID1a* had no effect on MyoD expression.

3.2.5 Assay of Neural and Neural Crest Genes By *In Situ* Hybridisation

As *ARID1a* is strongly expressed in neural tissue, I assayed the effects of knock down of *ARID1a* on neural development. Embryos were injected with either control or translation-blocking morpholino and fixed at stage 13. Expression of the pan-neural marker *Sox3*, the neural crest marker *Snai2* and the myogenic gene *MyoD* were assessed by *in situ* hybridisation (Fig. 3.6). Knock down of *ARID1a* caused a striking reduction in *Snai2* expression (Fig. 3.6 compare A with B), indicating a loss of neural crest cell specification. Expression of *Sox3* in neural tissue was not affected, but there was a subtle reduction in placodal staining (Fig. 3.6 D, arrows). *MyoD* was unaffected by knock down of *ARID1a* (Fig. 3.6 E, F). These data indicate that *ARID1a* is required for neural crest specification in *Xenopus*. Carrying out *in situs* at different developmental stages, and with additional specific markers such as *twist* for neural crest cells and *Six1* or *Pax8* for the placodes (Schlosser and Ahrens, 2004) would further explore the extent to which *ARID1a* controls the specification of these tissues.

Injection of morpholinos into one of the two blastomeres at the 2 cell stage is a useful way to explore changes in gene expression – the uninjected side acts as an internal control and can help to distinguish between changes in expression level and timing. Unfortunately, injection of ARID1a_TB morpholino into one of the two blastomeres at the 2 cell stage caused embryonic lethality, perhaps due to developmental delay of one half of the embryo during gastrulation.

3.2.6 Overexpression of *ARID1a* In *Xenopus* Embryos

ARID1a is part of the BAF complex and is predominantly nuclear (Hargreaves and Crabtree, 2011). To verify that exogenous ARID1a is localised to the nucleus I carried out immunofluorescence on dissociated animal cap cells injected with *ARID1a* mRNA. The commercial antibodies tested were unable to detect endogenous or overexpressed *Xenopus* ARID1a, so instead I injected *HA-ARID1a* mRNA and stained cells with an anti-HA antibody (Fig. 3.7 A-F). Some background fluorescence was detected as cytoplasmic speckles in cells from both conditions (Fig. 3.7 B, E). Strong nuclear fluorescence was seen in cells from

embryos injected with *HA-ARID1a* mRNA, indicating that exogenous ARID1a is nuclear in *Xenopus* cells (Fig. 3.7 E, F).

Preliminary experiments injecting *ARID1a* mRNA into animal blastomeres or equatorially had little effect on embryonic development. As *ARID1a* has been suggested to be a Wnt inhibitor I injected *ARID1a* mRNA into the dorsal blastomeres at the 4 cell stage to see whether axis specification was affected (Fig. 3.7 G, H). Injection of *GFP* mRNA into the dorsal blastomeres had either no effect, or caused a slight bend in the tail (Fig. 3.7 G). Injection of *GFP-ARID1a* mRNA dorsally caused loss of anterior structures including the eyes and cement glands (Fig. 3.7 H).
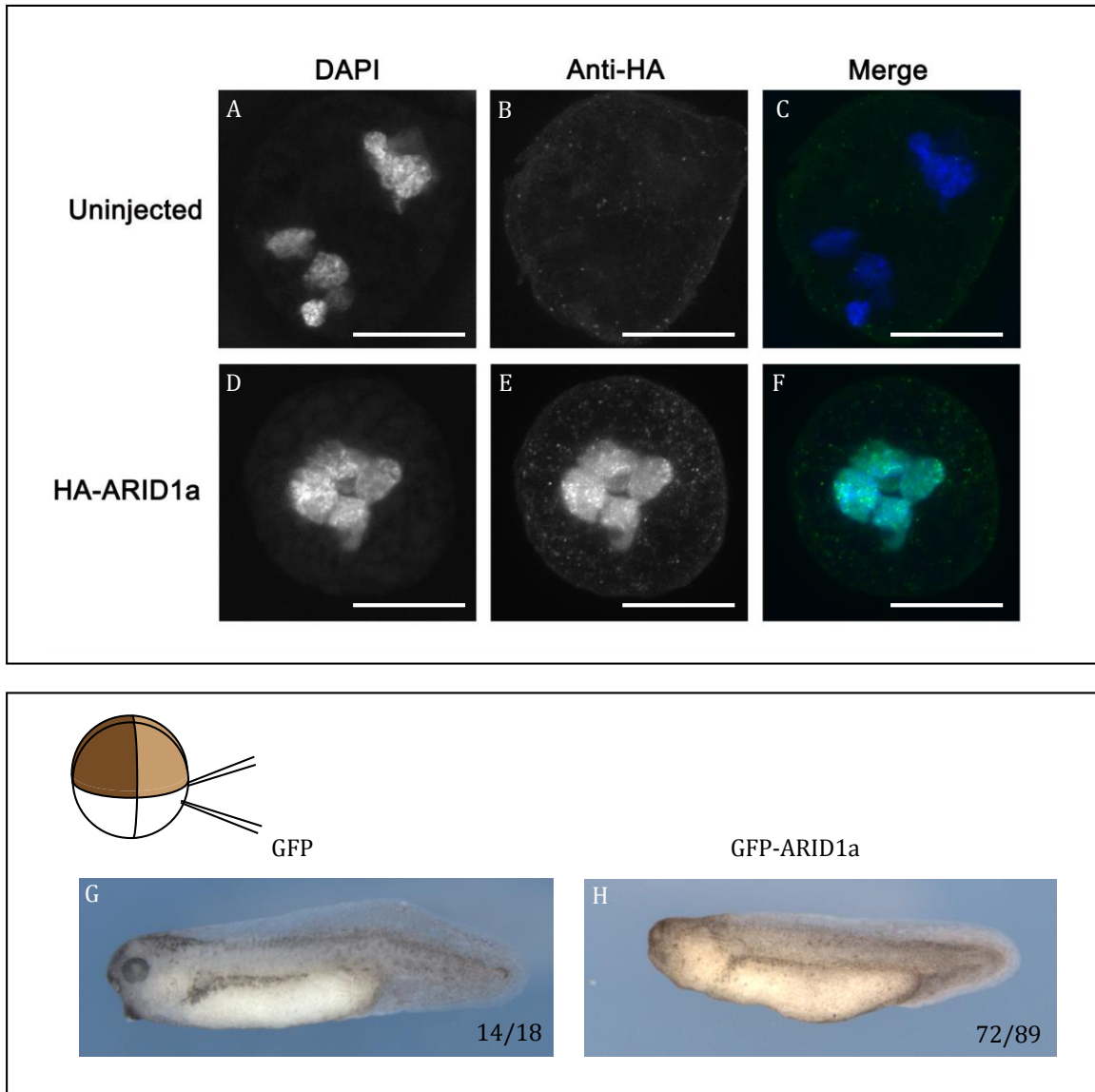
Fig. 3.7: *ARID1a* **Overexpression Caudalises** *Xenopus* **Embryos**

A-F: Immunofluorescence of dissociated animal cap cells using an anti-HA antibody from embryos injected with or without 1 ng *HA-ARID1a* mRNA. Magnification is 40X. Images are of single cells. DAPI was used to visualise nuclei (A, D). Cells from uninjected embryos show some background HA staining (B). HA-ARID1a is localised to the nucleus in *Xenopus* cells (E). Scale bars represent 20 μm.

G, H: Injection of mRNA into the 2 dorsal blastomeres at the 4 cell stage as shown on the diagram. Injection of *GFP* mRNA had little or no effect on development (G). Injection of *GFP-ARID1a* mRNA caused a loss of anterior head structures (H). Images are lateral views with the anterior to the left.

108

3.3 Discussion

ARID1a encodes the largest subunit of the BAF complex. The function of *ARID1a* has been briefly investigated in mouse, but no detailed studies exist in vertebrates. Experiments with the *Drosophila* homologue of *ARID1a, Osa,* showed that it was embryonic lethal and that *Osa* may act as an inhibitor of Wg signalling. I have shown that *ARID1a* is deposited as maternal mRNA in *Xenopus* and is expressed throughout embryogenesis. I have also investigated the effects of loss of function and gain of function of *ARID1a* during *Xenopus* development.

3.3.1 Depletion Of *ARID1a*

Loss of *ARID1a* in mice, *Drosophila* and *C. elegans* is embryonic lethal (Gao et al., 2008; Large and Mathies, 2014; Treisman et al., 1997). In *Xenopus* depletion of *ARID1a* caused developmental arrest and embryonic death at the end of the neurula stages (Fig. 3.3). This occurred later than the lethality observed in *ARID1a*$^{-/-}$ mice, which die during gastrulation (Gao et al., 2008). This difference is likely due to maternally deposited *ARID1a* mRNA, and possibly protein. Morpholinos are not efficient at inhibiting maternal transcripts, and cannot affect proteins that have already been synthesised, and this residual ARID1a may be sufficient to delay the onset of embryonic lethality. Without an antibody that recognises *Xenopus* ARID1a it was not possible to test when ARID1a protein was significantly depleted.

The splice blocking morpholinos and translation blocking morpholinos did not produce identical phenotypes (Fig. 3.3 and 3.4). Injection of a high dose of splice blocking morpholinos caused a similar phenotype to a low dose of translation blocking morpholino, although there are differences. The forebrain of embryos injected with ARID1a_TB was more severely reduced than those injected with ARID1a_SB1+SB2, and the onset of the phenotype occured earlier. A likely explanation for the difference between the morpholinos is that ARID1a_TB is able to prevent translation of maternally deposited mRNA, whereas ARID1a_SB is not. Therefore the splice blocking morpholinos will only deplete zygotically transcribed *ARID1a,* and no phenotype will be evident until the maternal transcripts and their protein products have been degraded.

The neural crest marker *Snai2* was severely reduced in *ARID1a* morphants (Fig. 3.5 B). This loss of expression could represent a direct requirement for *ARID1a* in the specification of neural crest cells. Alternatively, neural crest specification is sensitive to Wnt signalling with too much or too little signalling leading to loss of the neural crest (Ben Steventon and Mayor, 2012; LaBonne and Bronner-Fraser, 1998). In *Drosophila Osa* has been implicated as an inhibitor of Wg signalling (Collins and Treisman, 2000). If this function exists in vertebrates, then loss of *ARID1a* would cause an increase in Wnt signalling, which would lead to a loss of neural crest specification and *Snai2* expression.

3.3.2 Overexpression Of *ARID1a*

The *Xenopus* fatemap is a valuable tool for investigating gene function. By injecting mRNA into dorsal blastomeres it is possible to target expression to the organiser and future dorsal-anterior structures such as the head. Overexpression of *ARID1a* in the dorsal blastomeres caused a loss of anterior structures, indicating that these embryos have been posteriorised. Such phenotypes are associated with an increase in Wnt3a signalling (Elkouby et al., 2010), which is inconsistent with a possible role of *ARID1a* as a repressor of Wnt signalling (Collins and Treisman, 2000). However, the observed phenotype may not be a direct effect of *ARID1a* on the Wnt signalling pathway, as Wnt antagonists, retinoic acid signalling and fibroblast growth factor (FGF) signalling are all able to caudalise neural tissue (Kudoh et al., 2002). Secondly, the organiser itself contributes to both the notochord and anterior head structures (Sakai, 2007), therefore changes in the organiser could lead to a loss of anterior head structures. *In situ* hybridisation of markers for the processes described above could discern between these possibilities.

Chapter 4: ARID1a Is An Inhibitor Of Wnt Signalling

4.1 Introduction

The *Drosophila* homologue of *ARID1a, Osa,* has been suggested to inhibit the Wg pathway in wing disc clones (Collins and Treisman, 2000). Since this discovery fourteen years ago, the link between *ARID1a* and Wnt signalling has remained unexplored. As depletion and overexpression of *ARID1a* in *Xenopus* caused phenotypes consistent with changes Wnt signalling (Chapter 3), I used the animal cap assay to directly assess what effects *ARID1a* has on the Wnt pathway.

4.2 Results

4.2.1 The Animal Cap Assay

The animal pole ectoderm of blastula stage *Xenopus* embryos, known as the animal cap, is an excellent system for studying signalling pathways. Animal ectoderm cells are naïve and able to differentiate into many cell types from neuronal and mesodermal lineages (Guille, 1999). During development, animal pole cells are not exposed to inducing signals and become epidermis "by default". They are, however, competent to respond to a range of signalling molecules such as Wnt, activin and FGF (Green et al., 1992; Guger and Gumbiner, 1995; Lamb et al., 1993; Larabell et al., 1997b). By excising the animal pole ectoderm prior to the MBT and culturing *ex vivo*, signalling pathways can be directly analysed away from the noisy context of the whole embryo. Furthermore, as most genes are not expressed before the MBT changes in target gene expression are likely to be direct interference with the pathway itself.

Injection of *Wnt8* or *β-catenin* mRNA induces ectopic expression of Organiser genes *Siamois (Sia)* and *Xenopus nodal related 3* (*Xnr3*; (Carnac et al., 1996; Nelson and Gumbiner, 1998). I have used these genes as readouts of Wnt signalling in animal caps to assess the effects of *ARID1a* on the Wnt pathway.

4.2.2 Depletion Of *ARID1a* Enhances Wnt Signalling In Animal Caps

If *ARID1a* is acting as a repressor of the Wnt pathway in *Xenopus* then depletion of ARID1a should cause an increase in Wnt signalling. Embryos were injected with 2 pg *Wnt8* mRNA at the one cell stage to stimulate the Wnt pathway, together with either 10 ng ARID1a_CO or ARID1a_TB morpholino (Fig. 4.1). Animal caps were cut at stage 8 and cultured until stage 10. RNA was then extracted, cDNA synthesised and qPCR carried out for the Wnt-target genes *Sia* and *Xnr3.* Injection of ARID1a_CO or ARID1a_TB alone failed to induce either *Sia* or *Xnr3* (Fig. 4.1 A and B). Injection of *Wnt8* mRNA alone or together with the control morpholino induced transcription to an equal degree, whereas concomitant depletion of ARID1a using the translation blocking morpholino caused a marked upregulation of both *Sia* and *Xnr3* expression

I next sought to determine where in the Wnt pathway ARID1a was acting. As ARID1a is localised to the nucleus I tested whether depletion of ARID1a was able to enhance β-catenin mediated stimulation of the Wnt pathway. 200 pg of *β-catenin* mRNA was co-injected with either 10 ng ARID1a_CO or ARID1a_TB morpholino (Fig. 4.1 C and D). Injection of either the mismatch or translation blocking morpholinos did not induce expression of *Sia* or *Xnr3,* whereas injection of *β-catenin* alone or together with ARID1a_CO caused transcription of both genes. Co-injection of ARID1a_TB and *β-catenin* mRNA caused an increase in *Sia* and *Xnr3* expression compared to *β-catenin* alone. Therefore *ARID1a* is acting downstream of β-catenin, as loss of *ARID1a* caused a de-repression of β-catenin-mediated transcription. These data show that ARID1a is an inhibitor of the Wnt pathway.

Due to large variations between the biological replicates for these experiments (this section and the remainder of Chapter 4) it was not possible to carry out statistical analysis. However, the same trend was observed for each of the three replicates, and normalisation with an alternative housekeeping genes (ornithine decarboxylase, ODC) showed the same result (data not shown).
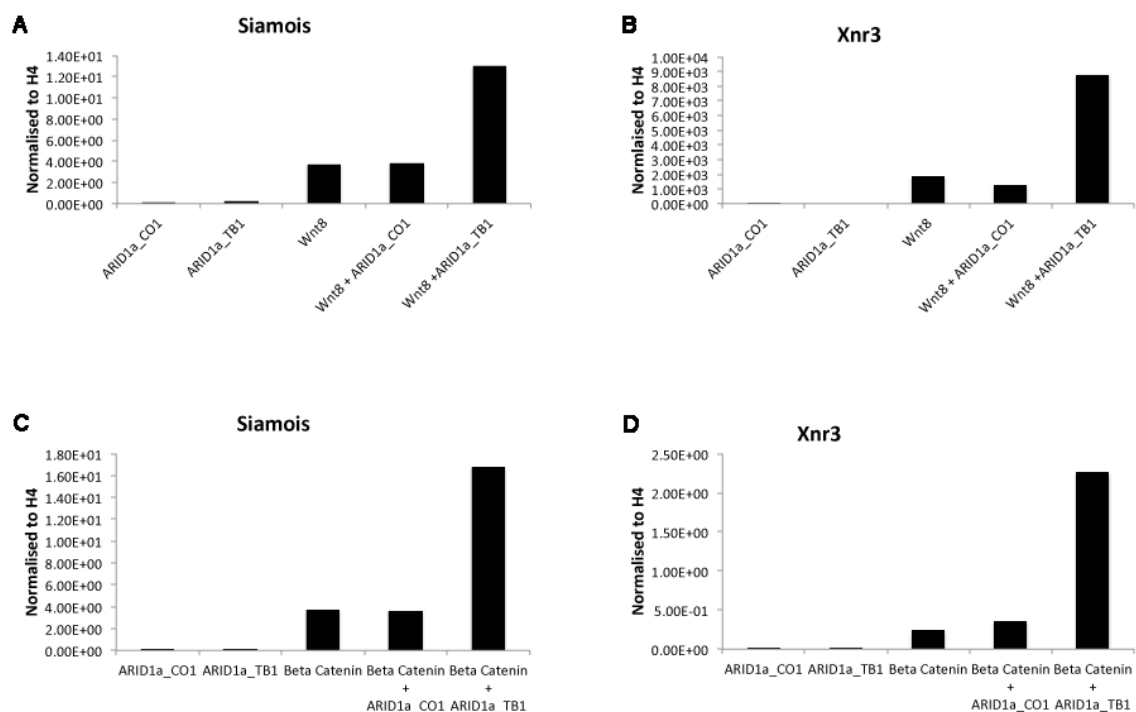
Fig. 4.1 Loss Of ARID1a De-Represses Wnt Signalling

Animal cap assays. Embryos were injected at the 1 cell stage with 2 pg *Wnt8* mRNA (A,B) or 200 pg *β-catenin* mRNA (C,D). 10 animal caps were cut at stage 8 for each treatment and cultured until stage 10, then processed for qPCR. The expression of *Sia*(A,C) and *Xnr3* (B,D) was measured by qPCR.

Depletion of ARID1a by morpholino injection caused an increase in *Sia* and *Xnr3* expression. Data are presented normalised to *histone H4.* Each experiment is representative of 3 biological replicates. Due to large variations between biological replicates it was not possible to conduct statistical analysis, however the same trend was observed in each experiment. The same data were also normalised to ODC and the same trend was observed.

113

4.2.3 Overexpression of *ARID1a* Inhibits Wnt Signalling In Animal Caps

If *ARID1a* is an inhibitor of Wnt signalling, then overexpression of *ARID1a* should inhibit expression of *Sia* and *Xnr3*. I therefore carried out reciprocal experiments to those above, stimulating the Wnt pathway and overexpressing *ARID1a*.

Embryos were injected at the one cell stage with 2 pg *Wnt8* mRNA with or without 2 ng *ARID1a* mRNA and qPCR carried out. In the absence of *Wnt8* mRNA no expression of *Sia* or *Xnr3* was detectable (Fig. 4.2 A, B). Co-injection of *ARID1a* mRNA with *Wnt8* mRNA caused a 2-fold reduction in *Sia* expression when compared to *Wnt8* alone (Fig. 4.2 A). *Xnr3* was more markedly affected, with expression almost completely abolished by the overexpression of *ARID1a* (Fig. 4.2 B). These data show that *ARID1a* is capable of repressing the Wnt pathway in *Xenopus*.

As *ARID1a* was acting below the level of β-catenin in depletion experiments, I next asked whether overexpression of *ARID1a* was capable of repressing β-catenin-induced transcription. 200 pg *β-catenin* mRNA was injected into 1 cell embryos with or without 2 ng *ARID1a* mRNA and animal caps processed for qPCR. As before, *Sia* and *Xnr3* were only induced when *β-catenin* was present (Fig. 4.2 C, D). When *ARID1a* was co-expressed with *β-catenin,* both *Sia* and *Xnr3* were almost undetectable. Therefore *ARID1a* is a Wnt inhibitor in *Xenopus*, acting below the level of *β-catenin* in the pathway.

4.2.4 N-Terminal Tags Do Not Affect The Biological Activity Of ARID1a

For several experiments it was beneficial to use forms of ARID1a tagged with either HA or GFP. I therefore wanted to assess whether these N-terminal tags would affect the activity of ARID1a, and I chose the animal cap assay from Section 4.2.3 to test this. Embryos were injected with 200 pg *β-catenin* mRNA alongside 2 ng of *ARID1a, HA-ARID1a* or *GFP-ARID1a* mRNA. Animal caps were cut and the expression of *Sia* and *Xnr3* measured by qPCR. As shown in Fig. 4.3, both tagged and untagged forms of ARID1a were equally able to repress β-catenin-mediated transcription in animal caps. I therefore conclude that these N-terminal tags do not affect the ability of ARID1a to regulate the Wnt pathway.
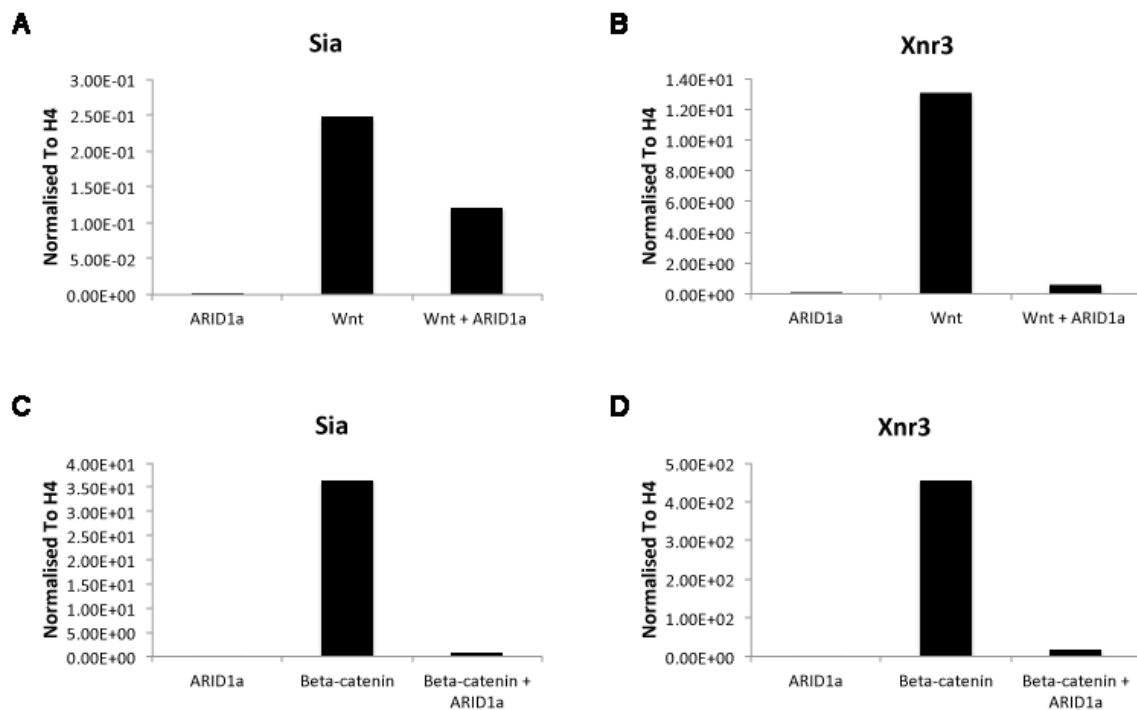
Fig. 4.2 Overexpression of ARID1a Inhibits Wnt Signalling

Animal cap assays. Embryos were injected at the 1 cell stage with 2 pg *Wnt8* mRNA (A,B) or 200 pg *β-catenin* mRNA (C,D). 10 animal caps were cut at stage 8 for each treatment and cultured until stage 10, then processed for qPCR. The expression of *Sia*(A,C) and *Xnr3* (B,D) was measured by qPCR.

Overexpression of *ARID1a* by mRNA injection caused loss of *Sia* and *Xnr3* expression. Data are presented normalised to *histone H4.* Each experiment is representative of 3 biological replicates. Due to large variations between biological replicates it was not possible to conduct statistical analysis, however the same trend was observed in each experiment. The same data were also normalised to ODC and the same trend was observed.
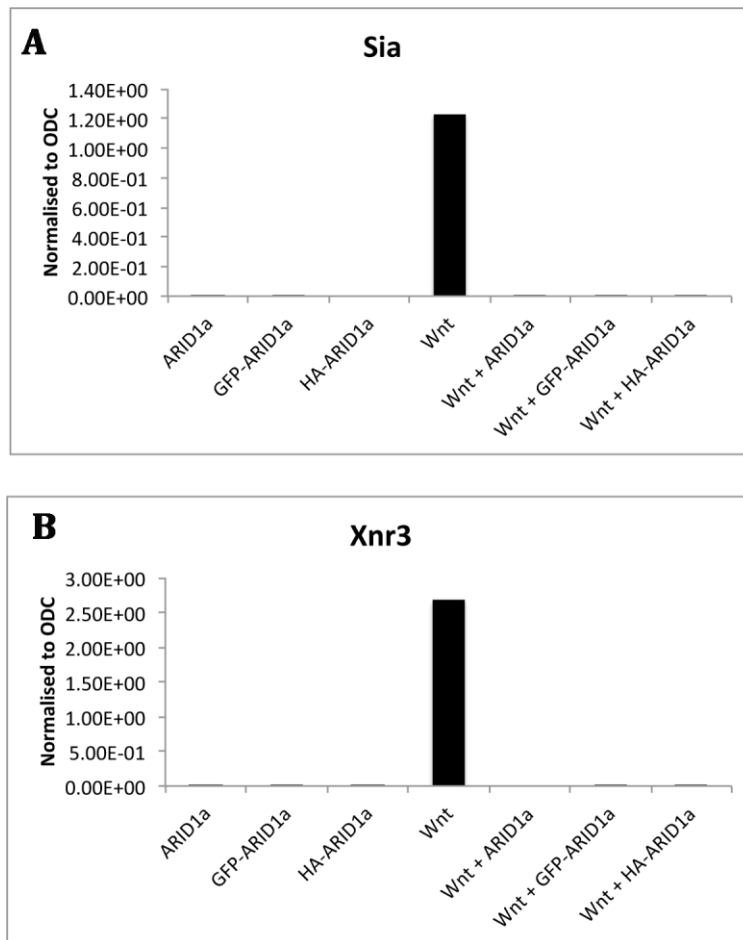
Fig. 4.3: N-Terminal Tags Do Not Affect The Ability Of ARID1a To Repress Wnt Signalling

Embryos were injected with or without 2 pg *Wnt8* mRNA and 2 ng of either *ARID1a*, *GFP-ARID1a* or *HA-ARID1a* mRNA. Animal caps were cut at stage 8, harvested at stage 10 and expression of *Sia* (A) and *Xnr3* (B) was measured by qPCR.

Both tagged and untagged forms of ARID1a repressed expression of *Sia* (A) and *Xnr3* (B) in response to Wnt signalling. Data are presented normalised to *histone H4.* Data are representative of two independent experiments.

4.2.5 *ARID1a* Inhibits The Formation Of Secondary Axes

As *ARID1a* inhibited Wnt signalling in the *in vitro* animal cap assay, I sought to confirm this property using the *in vivo* secondary axis assay. Stimulation of the Wnt pathway in the ventral blastomeres at the 4-cell stage induces a Spemann organiser, which causes the embryos to develop a complete second body axis.

Injection of 200 pg *β-catenin* mRNA into a single ventral blastomere at the 4-cell stage was sufficient to induce a complete secondary axis (Fig. 4.4 B). *GFP* mRNA was included as a lineage tracer. Co-injection of 2 ng *GFP-ARID1a* mRNA with 200 pg *β-catenin* mRNA markedly reduced the secondary axis to structures ranging from a slight bulge to a short outgrowth lacking any head structures (Fig. 4.4 C). Indeed, only 2/135 embryos had a complete secondary axis (Fig. 4.4 D), demonstrating that *ARID1a* is an effective inhibitor of β-catenin in this assay. Embryos injected ventrally with *ARID1a* mRNA alone did not exhibit a phenotype.

4.2.6 *ARID1a* And The Nuclear Localisation Of β-Catenin

As ARID1a is nuclear (Fig. 3.6) and acts downstream of β-catenin (Fig. 4.2, 4), then it is possible that ARID1a directly interferes with the nuclear accumulation of β-catenin. To test this I carried out immunofluorescence on animal caps.

2 ng *HA-ARID1a* mRNA was injected together with 200 pg *β-catenin* mRNA at the one cell stage. Animal caps were cut at stage 8 and cultured until stage 10, then immunofluorescence was carried out (Fig. 4.5). Animal caps from uninjected embryos showed β-catenin staining around the cell periphery corresponding to adherens junctions, and no nuclear fluorescence (Fig. 4.5 left column). Injection of *β-catenin* mRNA caused some nuclear fluorescence (Fig. 4.5 centre column), while co-injection of *HA-ARID1a* mRNA (right column) had little effect. These experiments were inconsistent and I never observed the strong nuclear β-catenin fluorescence described elsewhere (Vincan, 2008), despite using 2 different antibodies for β-catenin. Quantification of nuclear β-catenin fluorescence using Imaris software revealed no consistent trend between experiments.

A: Diagram showing the injection site on 4-cell embryos.

Beta catenin + GFP

GFP-ARID1a + Beta-Catenin

B: 41/51

C: 119/135

D

Percentage Of Injected Embryos

- Normal
- Partial
- Complete

GFP — n=21

Beta-Catenin — n=51

Beta-Catenin + ARID1a — n=135
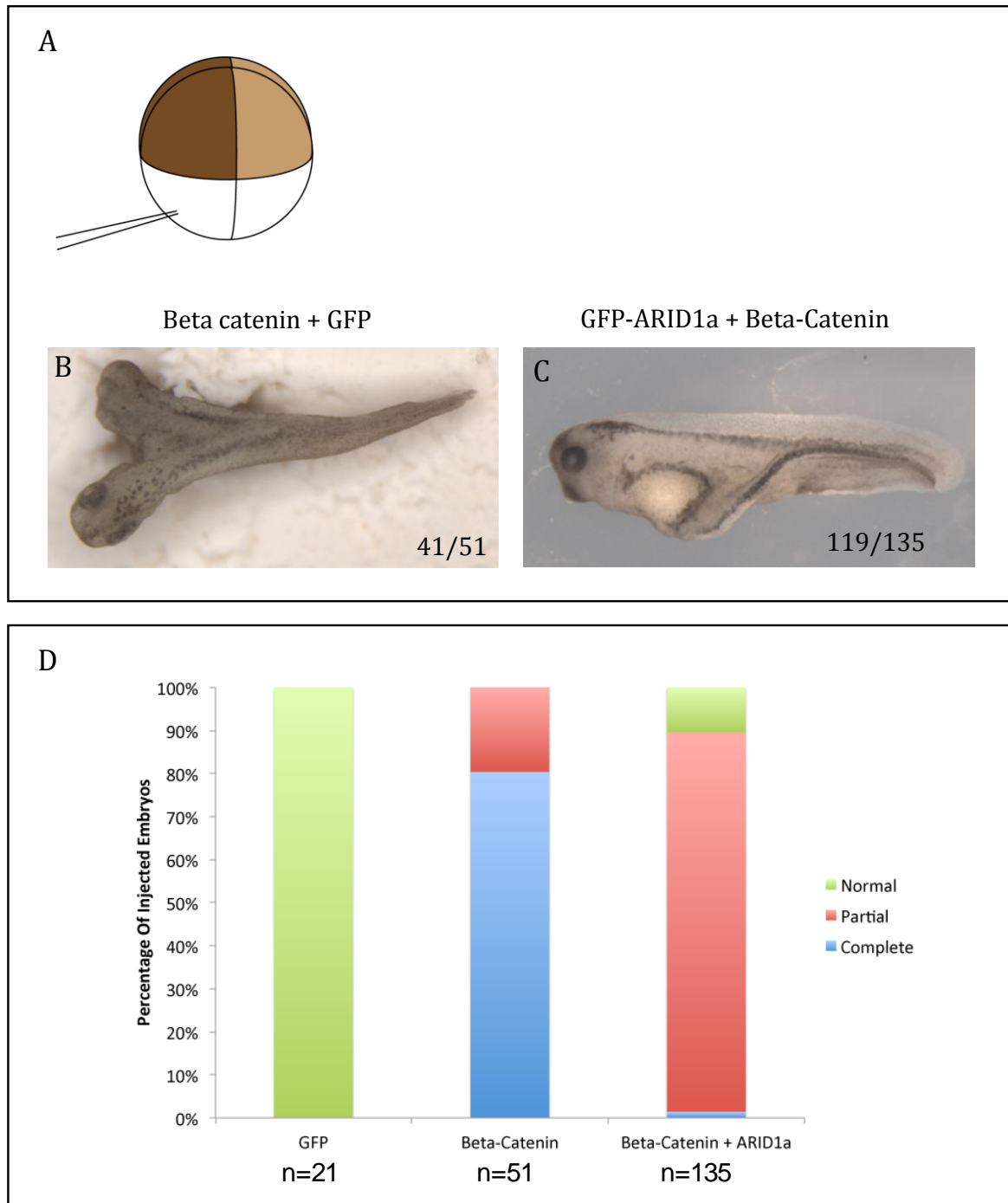
Fig. 4.4 ARID1a Inhibits Secondary Axis Formation

Overexpression of *ARID1a* in *Xenopus* inhibited secondary axis formation.

A: Diagram showing the injection site on 4-cell embryos.

B: Injection of 200 pg *β-catenin* mRNA with 200 pg *GFP* mRNA as a control produced complete secondary axes with defined head structures. Dorsal view with anterior to the left.

C: Co-injection of 2 ng *GFP-ARID1a* mRNA with 200 pg *β-catenin* mRNA significantly reduced secondary axis formation. Most embryos displayed similar or lesser secondary axes than the one shown. Lateral view with the anterior to the left.

D: Quantitation of phenotypes from the above experiment. Values are shown as percentages of the total samples for each treatment. GFP column represents 21 embryos that were all indistinguishable from uninjected sibling embryos.
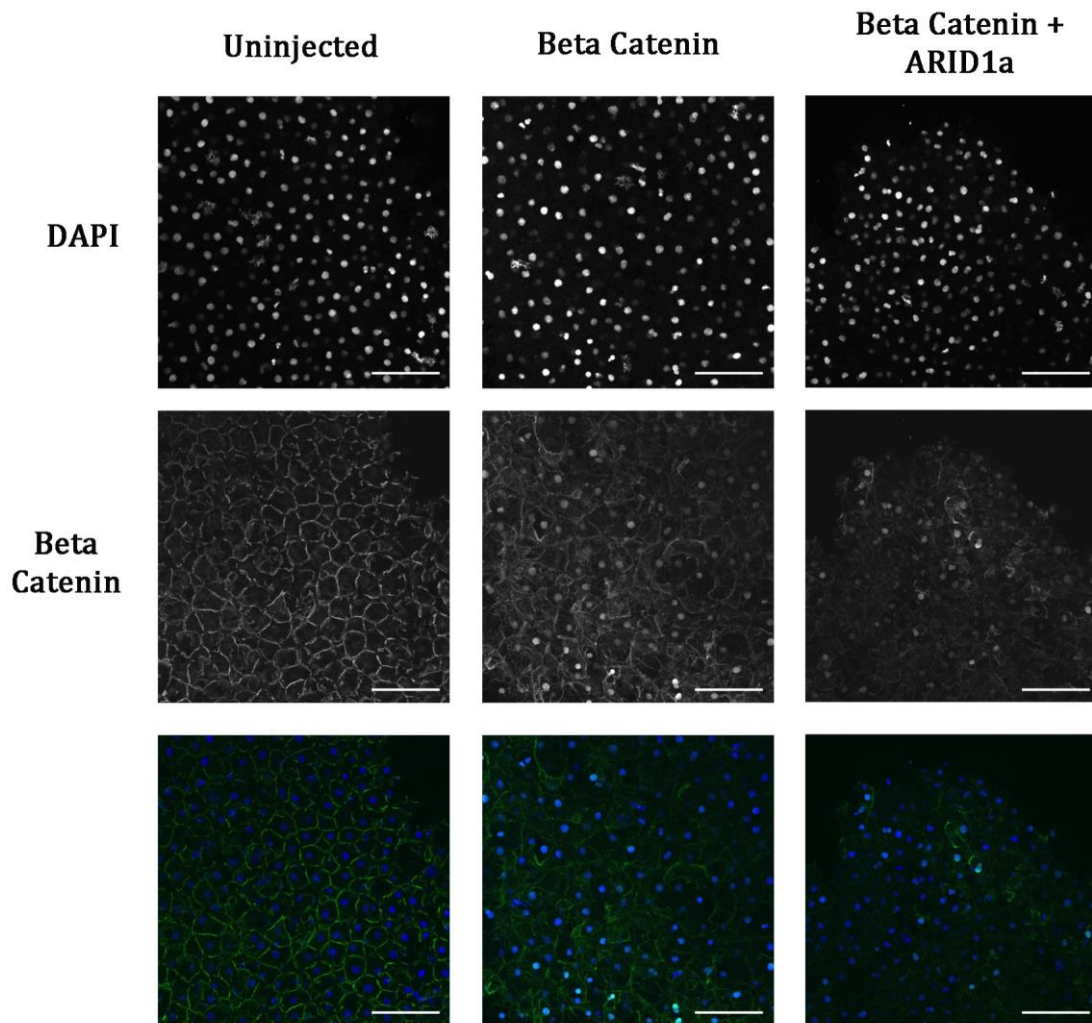
Fig. 4.5: Nuclear Localisation Of β-Catenin In The Presence of ARID1a
Immunofluorescence of stage animal caps cut at stage 8 and fixed at stage 10. Embryos were injected at the one cell stage with 200 pg *β-catenin* mRNA with (middle column) or without (right hand column) 2 ng *ARID1a* mRNA.

The caps were stained with DAPI to visualise nuclei (top row) and an anti-β-catenin antibody (middle row). Injection of *β-catenin* mRNA resulted in nuclear detection of β-catenin (central image). Co-injection of *β-catenin* and *ARID1a* mRNA produced ambiguous results, with no consistently measurable change in nuclear β-catenin. Scale bars represent 100 μm.

Despite using several different β-catenin antibodies and fixation conditions, clear nuclear localisation of β-catenin was not observed consistently as reported elsewhere. Quantification of these experiments using Imaris software revealed no consistent trend in the effect of ARID1a on β-catenin localisation. I am therefore hesitant to make any conclusions from these data.

These experiments were carried out in parallel to those described in Section 4.2.4, and induction of *Sia* and *Xnr3* was always observed upon injection of *β-catenin* mRNA. The difficulties experienced here could be circumvented by injecting an epitope-tagged form of β-catenin, which would allow the use of alternative antibodies that work well for immunofluorescence.

4.2.7 ARID1a Does Not Regulate FGF or Activin Signalling

As ARID1a inhibits Wnt signalling, I next asked whether it was able regulate other signalling pathways. I therefore carried out animal cap assays using fibroblast growth factor (FGF) and transforming growth factor β (TGFβ) signalling. FGF signalling in animal caps induces *Brachyury* (*Xbra*), whereas TGFβ signalling causes expression of *goosecoid* (*gsc*). I used these target genes to assess the effects of overexpression and depletion of *ARID1a* on FGF and TGFβ signalling.

Embryos were injected with 50 pg *FGF4* mRNA and either 10 ng ARID1a_CO, 10 ng ARID1a_TB or 2 ng *ARID1a* mRNA. Animal caps were cut and the expression of *Xbra* measured by qPCR (Fig. 4.6 A). *Xbra* was not expressed in the absence of FGF signalling, and was induced by FGF4. Neither depletion nor overexpression of *ARID1a* affected the level of *Xbra* expression. Therefore ARID1a does not regulate FGF signalling in the early embryo.

I next carried out similar experiments using Activin as an agonist for the TGFβ pathway. Embryos were injected with either 10 ng ARID1a_CO, 10 ng ARID1a_TB or 2 ng *ARID1a* mRNA and left to develop until stage 8. Animal caps were then cut and treated with 16 U/ml activin until sibling embryos had reached stage 11. *gsc* expression was then measured using qPCR. No *gsc* expression was detectable in untreated caps, whereas addition of activin induced *gsc* (Fig. 4.6 B). Knock down or overexpression of *ARID1a* did not have any effect on *gsc* expression, showing that ARID1a does not affect TGFβ signalling.

These experiments indicate that ARID1a specifically regulates Wnt signalling, and is not a general inhibitor of signalling-mediated transcription.

A Xbra

B Gsc
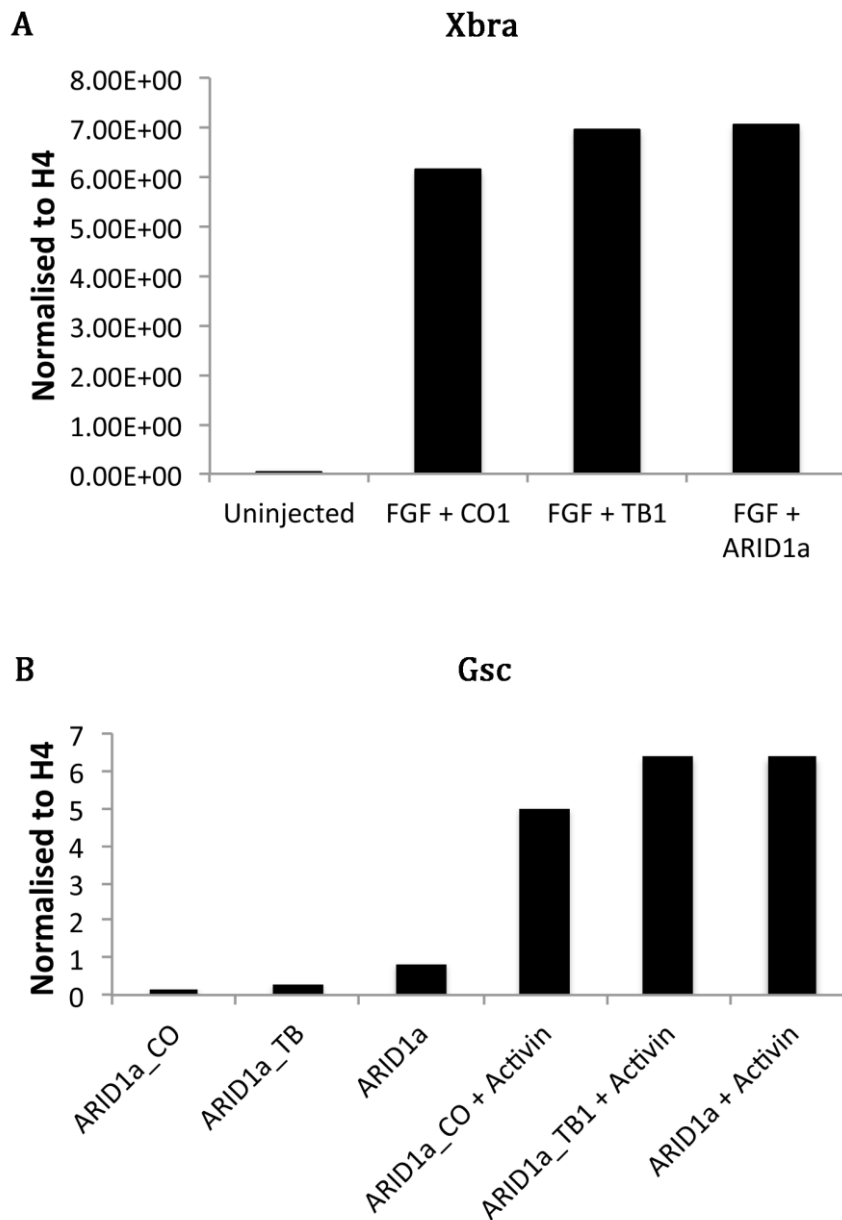
Fig. 4.6 ARID1a Does Not Affect FGF or TGFb Signalling

Animal cap assays. 10 caps were cut for each treatment at stage 8 and cultured to stage 10, then gene expression measured by qPCR.

A: Embryos were injected with 50 pg *FGF4* mRNA alongside either 10 ng *ARID1a* morpholinos or 2 ng mRNA. Loss or gain of function of *ARID1a* did not affect *Xbra* expression.

B: Embryos were injected with either 10 ng *ARID1a* morpholino or 2 ng mRNA. Caps cut at stage 8 were treated with 16 U/ml activin until stage 10. Loss of gain of function of *ARID1a* did not affect expression of *gsc*.

Data are presented normalised to *histone H4.* They were also normalised to ODC and exhibited a similar trend. Data are representative of 3 independent experiments however due to large variations between biological replicates it was not possible to carry out statistical analysis.

4.3 Discussion

4.3.1 *ARID1a* Inhibits The Wnt Pathway

Using both loss and gain of function approaches I have shown that *ARID1a* is an inhibitor of the Wnt pathway in *Xenopus.* This is the first time that *ARID1a* has been demonstrated to affect Wnt signalling in vertebrates, although previous work in *Drosophila* has suggested that *Osa* inhibits Wg signalling (Collins and Treisman, 2000). This work used the Gal4-UAS system to clonally overexpress *Osa* in the wing disc and then measure expression of the target gene *Nubbin* by *in situ* hybridisation. However, it is not possible to tell whether *Osa* is directly repressing Wg in these experiments: change in expression of *Osa* could result in differences in Wg-regulating proteins, which would in turn give rise to the observed changes in *Nubbin.* The animal cap assay I used in my experiments measured gene expression shortly after the onset of zygotic transcription, therefore there is insufficient time for changes in Wnt-regulatory gene expression to take effect. Instead, the observed changes in Wnt-target gene expression were likely due to direct interaction of ARID1a with Wnt pathway components or by changing the chromatin state of Wnt-responsive genes.

ARID1a could repress Wnt signalling by mediating the export of β-catenin from the nucleus. My attempts to address this possibility remain inconclusive (Fig. 4.5). ARID1a is thought to shuttle between the nucleus and cytoplasm (Guan et al., 2012), and could therefore act as a chaperone to facilitate nuclear export of β-catenin. Alternatively ARID1a could be acting as part of the BAF complex to create a repressive chromatin state that prevents the transcription of β-catenin target genes. For more detail see section 7.1.

Other members of the BAF complex are regulators of Wnt signalling. Loss of SNF5 in mice is sufficient to activate the Wnt pathway (Mora-Blanco et al., 2014). This observation is in agreement with the current work, indicating that the BAF complex acts to repress Wnt signalling. Conversely, Brg1 binds to β-catenin and enhances transcription (Barker et al., 2001; Griffin et al., 2011). How two proteins that are part of the same complex can have opposite effects on Wnt

signalling is not known, however the modular composition of the BAF complex may provide an answer. It is possible that the presence of either ARID1a or SNF5 changes BAF complexes into Wnt repressors, and without them Brg1 is capable of promoting β-catenin-mediated transcription. As different conformations of the BAF complex exist within the same cell (Wang et al., 2004b), it is possible that Wnt signalling causes a switch between two BAF complexes at target promoters. It is also possible that a switch between ARID1a and ARID1b containing complexes at Wnt-target gene promoters could act to regulate gene expression (see Chapter 7 for further discussion). Detailed ChIP time course experiments could provide evidence to support or refute this model.

4.3.2 *ARID1a* Does Not Affect FGF or TGFβ Signalling In Early Embryos

ARID1a is an enhancer of steroid hormone signalling (Inoue et al., 2002) and an inhibitor of the Wnt pathway (Collins and Treisman, 2000); this work). I therefore tested whether *ARID1a* was able to regulate other signalling pathways. Data from animal cap experiments showed that *ARID1a* did not affect either the FGF or TGFβ signalling pathways (Fig. 4.6). The latter result is intriguing, as Brg1 is required for maximal TGFβ responses in tissue culture (Xi et al., 2008). In this system, Brg1 and ARID1b form a complex with Smad3 to activate transcription. It would be interesting to see whether *ARID1b* is able to regulate TGFβ signalling in *Xenopus.*

Chapter 5: Mass Spectrometry Approach To Identify Interactors of ARID1a

5.1 Introduction

In order to investigate the molecular mechanism by which ARID1a was acting I performed a mass spectrometry screen to identify interacting proteins. This screen was designed and carried out in collaboration with L. Herhaus and G. Sapkota at the MRC Protein Phosphorylation Unit, University of Dundee. Preliminary experiments using *Xenopus* embryo lysate were inconclusive, so instead I expressed *Xenopus ARID1a* in Human Embryonic Kidney 293 (HEK293) cells and looked for conserved interactors.

HEK cells were used because they have an intact and well-characterised Wnt signalling pathway (Gujral and MacBeath, 2010). Additionally, the commercially available T-REx cells offered a convenient system for generating cells lines stably expressing an inducible form of GFP-tagged ARID1a, which was desirable for the mass spectrometry screen (see section 5.2.2). An N-terminal GFP tag was used for several reasons: firstly, no antibodies tested recognised endogenous *Xenopus* ARID1a; secondly, GFP-ARID1a represses Wnt signalling to the same extent as untagged ARID1a (Fig. 4.3); finally, GFP tags have been used extensively by the Sapkota lab and they have generated a comprehensive list of GFP-interacting proteins that can be discarded from any pull down experiment. Together with the Sapkota lab I used these tools to identify interaction partners for *Xenopus* ARID1a.

5.2 Results

5.2.1 *Xenopus* ARID1a Represses Wnt Signalling in HEK293 Cells

It was first important to test whether HEK293 cells were a suitable system for the mass spectrometry screen. ARID1a was detected by PCR and western blot in HEK293 cells (Fig. 5.1 A, B) indicating that ARID1a is physiologically relevant to these cells.

Next, I established that *Xenopus* GFP-ARID1a was capable of inhibiting Wnt signalling in HEK293 cells using the TOPFLASH dual luciferase reporter assay (see Section 2.2.10). Cells were transfected with *GFP* or *Xenopus GFP-ARID1a* alongside the luciferase constructs, and then treated with either Wnt-conditioned media (WCM, a gift from K. Dingwell) or control L-cell-conditioned media (LCM). Transfection of *GFP-ARID1a* caused a 5-fold reduction in Wnt activity compared to *GFP,* showing that *Xenopus* ARID1a is capable of inhibiting Wnt signalling in HEK293 cells (Fig. 5.1 C). No luciferase activity was detected using the control FOPFLASH plasmid (Fig. 5.1 D).

5.2.2 Generation and Characterisation of Inducible GFP-ARID1a HEK293 Cells

While transfection is a very efficient way of expressing a gene of interest in tissue culture cells, it often leads to very high and heterogeneous expression. Stable cell lines have lower heterogeneity in expression of introduced genes, and also provide a convenient tool for large-scale work. Therefore HEK293 cells were generated that expressed *GFP-ARID1a* under the control of a doxycycline-inducible promoter. The strategy used is outlined in Fig. 5.2 A.

HEK293 T-rex cells constitutively express the tetracycline repressor (TetR) protein, which in the absence of doxycycline binds to the TetO2 promoter and represses transcription (Hillen and Berens, 1994). Doxycycline allosterically inhibits TetR, allowing transcription from the TetO2 promoter (Fig. 5.2 B). T-rex cells were transfected with *GFP-ARID1a* and Flp recombinase and selected for using blasticidin and hygromycin B. These cells were called FRT/GFP-ARID1a.
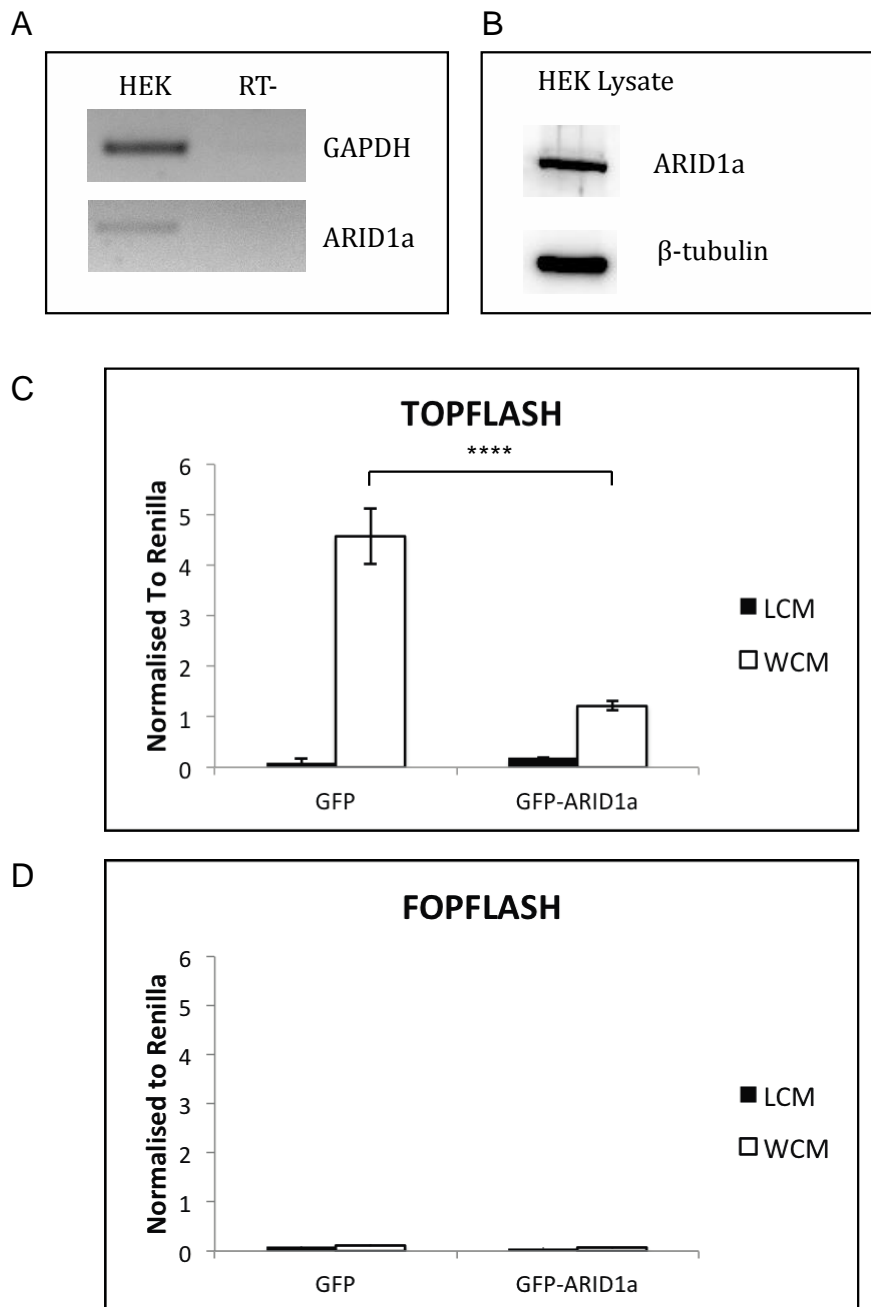
Fig. 5.1: *Xenopus* ARID1a Inhibits Wnt Signalling In HEK Cells
A: PCR of GAPDH and ARID1a using cDNA synthesised from HEK total RNA.
B: Western blot showing expression of endogenous ARID1a in HEK cell lysates.
β-tubulin is shown as a loading control.
C: TOPFLASH analysis of HEK cells. Cells were transfected with plasmids encoding either GFP or GFP-ARID1a (*Xenopus*) alongside Renilla luciferase and the TOPFLASH reporter plasmid. The cells were treated for 16 hours with Wnt3a-conditioned media (WCM) to induce Wnt signalling, or L-cell conditioned media (LCM) as a negative control. Luciferase activity was then measured using the Dual Luciferase Assay Kit. GFP-ARID1a significantly reduced WCM-induced luciferase activity. Data are from three experiments.
D: FOPFLASH luciferase activity. Experimental set up is identical to C, except that the FOPFLASH reporter was used in place of the TOPFLASH reporter. As expected, no FOPFLASH activity was observed under any conditions.
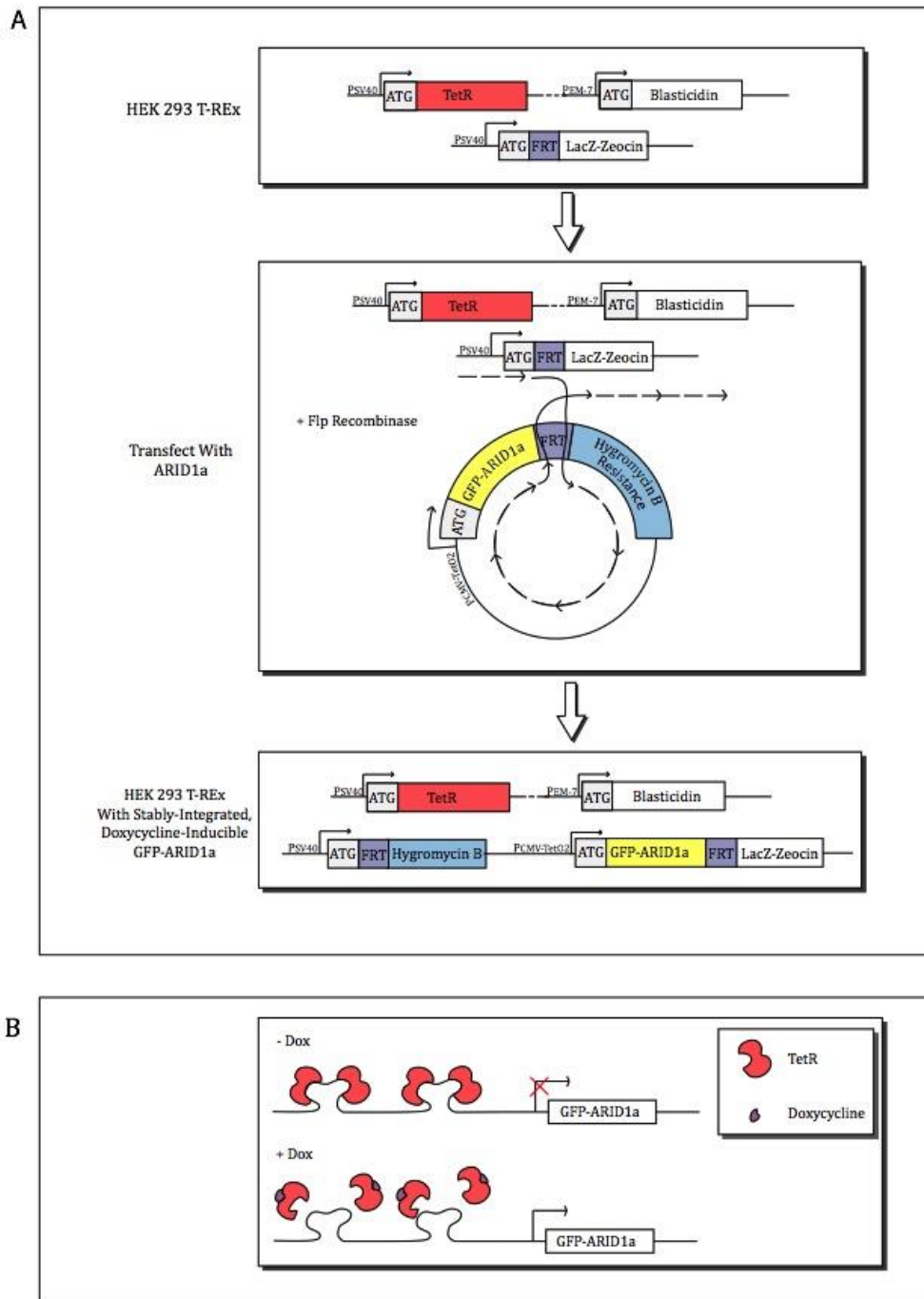
Fig. 5.2: Generating FRT/GFP-ARID1a Cells

A: Schematic representation of parental T-rex cells, recombination with transfected plasmid and the resultant FRT/GFP-ARID1a cells. Recombination between the FRT sites causes insertion of GFP-ARID1a and the Hygromycin B resistance gene, while simultaneously disrupting the Zeocin resistance gene. FRT/GFP-ARID1a cells constitutively express TetR, Blasticidin and Hygromycin B resistance genes, and express GFP-ARID1a in response to doxycycline.

B: Schematic representation of the doxycycline inducible system. In the absence of doxycycline the TetR protein binds to the pO2 promoter that regulates GFP-ARID1a expression and represses transcription. Doxycycline allosterically inhibits TetR, preventing it from binding the promoter and allows GFP-ARID1a to be expressed.

In order to confirm that FRT/GFP-ARID1a cells were able to express GFP-ARID1a they were treated with doxycycline overnight and then imaged using fluorescence microscopy. However, no fluorescent signal was detectable using a conventional inverted microscope, so I instead used a confocal microscope (Fig. 5.3). Nuclei were visualised by staining the cells with DRAQ5 (Fig. 5.3 A, D). In the absence of doxycycline, no GFP fluorescence was detectable (Fig. 5.3 B) whereas cells treated with doxycycline showed weak nuclear signal (Fig. 5.3 E). This localisation is consistent with my previous findings in *Xenopus*. Treatment with doxycycline sometimes caused the cells to adopt a more spindle-shaped morphology (compare A with D), which could be due to changes in gene expression caused by an increase in ARID1a expression.

To verify that full-length GFP-ARID1a was being produced, and to determine the onset of expression, a western blot time course was carried out (Fig. 5.4 A). An ~250kDa band corresponding to GFP-ARID1a was detectable after 3 hours of treatment with doxycycline. At subsequent time points the expression of GFP-ARID1a increased, along with the appearance of an ~25 kDa band. The initiator methionine of ARID1a is cleaved (Gauci et al., 2009), so this smaller band could represent a degradation product of the fusion protein. These results show that FRT/GFP-ARID1a cells contain a stable insert of *Xenopus GFP-ARID1a* that is expressed only in the presence of doxycycline. However, it is notable that these cells grow much more slowly than the parental HEK T-rex cells, even in the absence of selective antibiotics – a phenotype consistent with the ability of ARID1*a* to repress the cell cycle (Nagl et al., 2007). Thus while no GFP-ARID1a was detected in the absence of doxycycline it is possible that there is some basal expression of GFP-ARID1a in these cells.

Finally I tested whether doxycycline treatment was capable of inhibiting Wnt signalling in FRT/GFP-ARID1a cells using the TOPFLASH assay (Fig. 5.4 B). Cells treated with doxycycline showed a two-fold reduction in luciferase activity when compared with untreated cells, indicating that GFP-ARID1a was expressed at sufficient levels to inhibit Wnt signalling.
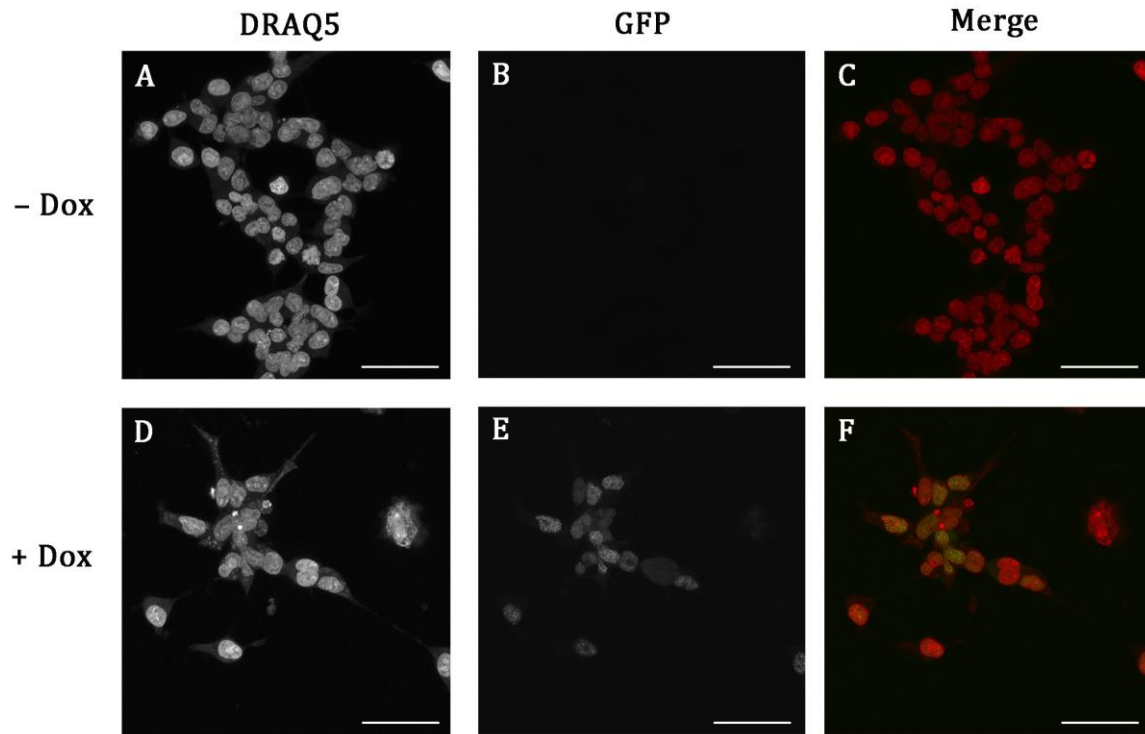
Fig. 5.3 Live Imaging Of FRT/GFP-ARID1a Cells
FRT/GFP-ARID1a cells treated with (D-F) or without (A-C) doxycycline. Nuclei were
visualised using DRAQ5 (A, D). Treatment of cells with doxycycline induced GFP-ARID1a
expression (E) which was localised to the nucleus (F).
Scale bars represent 50 μm.
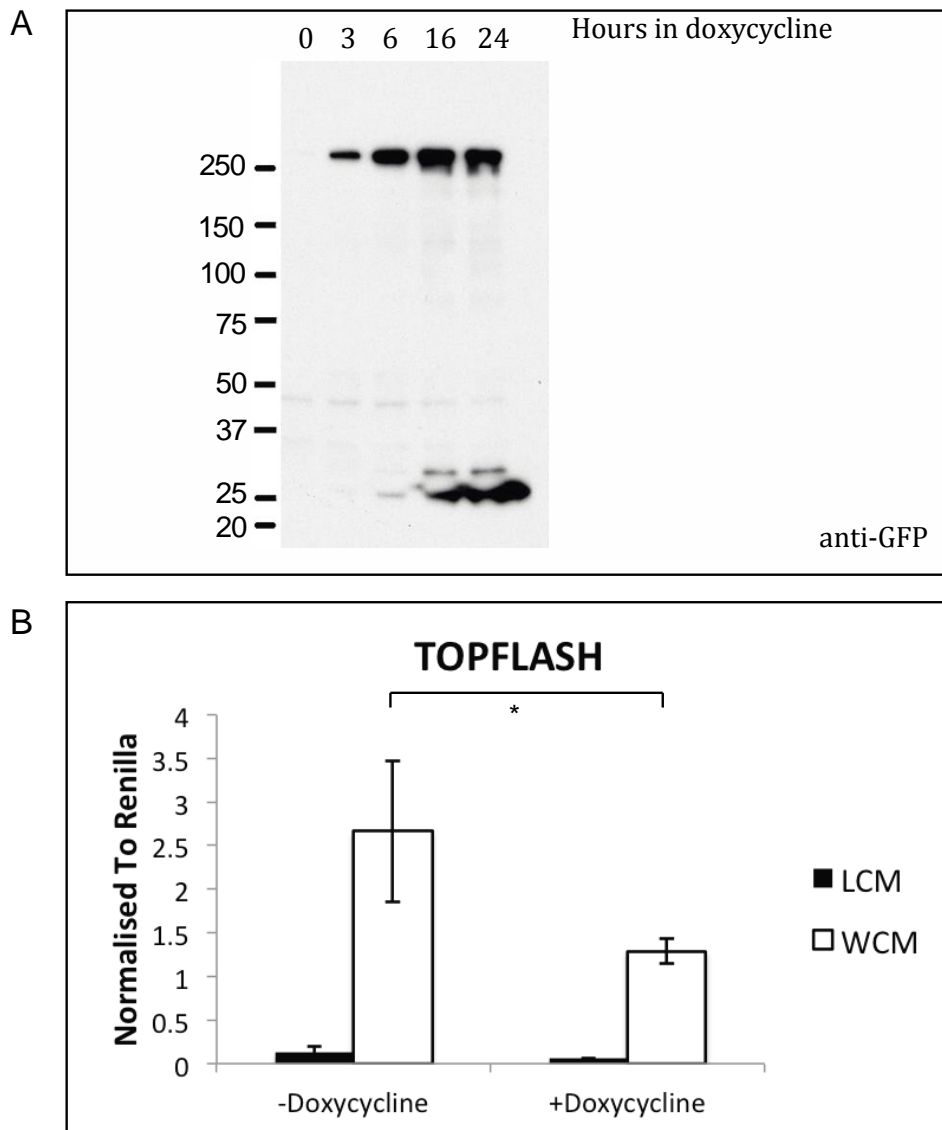
Fig. 5.4: FRT/GFP-ARID1a Cells Respond to Doxycycline
A: FRT/GFP-ARID1a cells were treated with 20 ng/ml docycyline as indicated and then processed for western blot. GFP-ARID1a expression began at 3 hours and was maximal from 16 hours onwards. Anti-sheep antibody was used 1:2000.
B: TOPFLASH assay in FRT/GFP-ARID1a cells. Cells were transfected with the TOPFLASH reporter and Renilla luciferase plasmids. The cells were treated with or without 20 ng/ml doxycycline and either L-cell conditioned media (LCM) or Wnt conditioned media (WCM) overnight. Luciferase activity was measured using the Dual Luciferase Assay kit. Treatment with doxycycline caused an approximately 2 fold reduction in luciferase activity. While this reduction is less than observed using transfected plasmids (Fig. 5.1) the reduction is still statistically significant.

5.2.3 The Mass Spectrometry Screen

5.2.3.1 Carrying Out The Screen

The original strategy for the mass spectrometry screen was to induce FRT/GFP-ARID1a cells with doxycycline and isolate GFP-ARID1a to use produce as bait to probe *Xenopus* embryo lysate for interaction partners. FRT/GFP-ARID1a cells were treated with doxycycline and GFP-ARID1a was immunoprecipitated using GFP-TRAP beads. The precipitate was then incubated with stage 9 *Xenopus* lysate, and proteins analysed by mass spectrometry. Stage 9 was chosen because it corresponded to the time the animal cap experiments in chapter 4 were carried out. Components of the BAF complex were identified from this experiment, however all of the remaining proteins were either cytoskeletal, ribosomal or unidentifiable (see Appendix for complete list of proteins). Trying to discern which proteins represented real interactions from this noisy system was not possible, so instead I decided to examine interactions between *Xenopus* GFP-ARID1a and human proteins within FRT/GFP-ARID1a cells.

The experimental approach for the mass spectrometry screen is outlined in Fig. 5.5. FRT/GFP-ARID1a cells were treated with doxycycline for 16 hours, as this was the time from which GFP-ARID1a was maximally expressed (Fig. 5.4 A). As a negative control, FRT/GFP cells were used in parallel, which express GFP in response to doxycycline (developed in the Sapkota Lab). GFP or GFP-ARID1a was then immunoprecipitated using an anti-GFP antibody in the presence of the weak cross-linking agent DSP. The isolated complexes were run on a gradient gel and visualised using colloidal blue staining (Fig. 5.6 A). Immunoprecipitation of GFP from FRT/GFP cells pulled down the bait protein (white arrowhead) and very few other interacting proteins, demonstrating that the antibody against is GFP specific and that GFP does not bind to many proteins within the cell. Immunoprecipitation of GFP-ARID1a from FRT/GFP-ARID1a cells yielded the bait (black arrowhead) along with many other bound proteins. To avoid masking of interactors by particularly abundant peptides the gel was cut into 14 pieces (Fig. 5.6 B) and each one individually processed for mass spectrometry analysis. This was repeated for a final of 3 biological replicates.

Induce expression of GFP-ARID1a by doxycycline treatment

ARID1a

Immunoprecipate ARID1a and interactors

Separate on acrylamide gel

Cut gel into pieces and trypsinise

MALDI-TOF

Carry out mass spectrometry
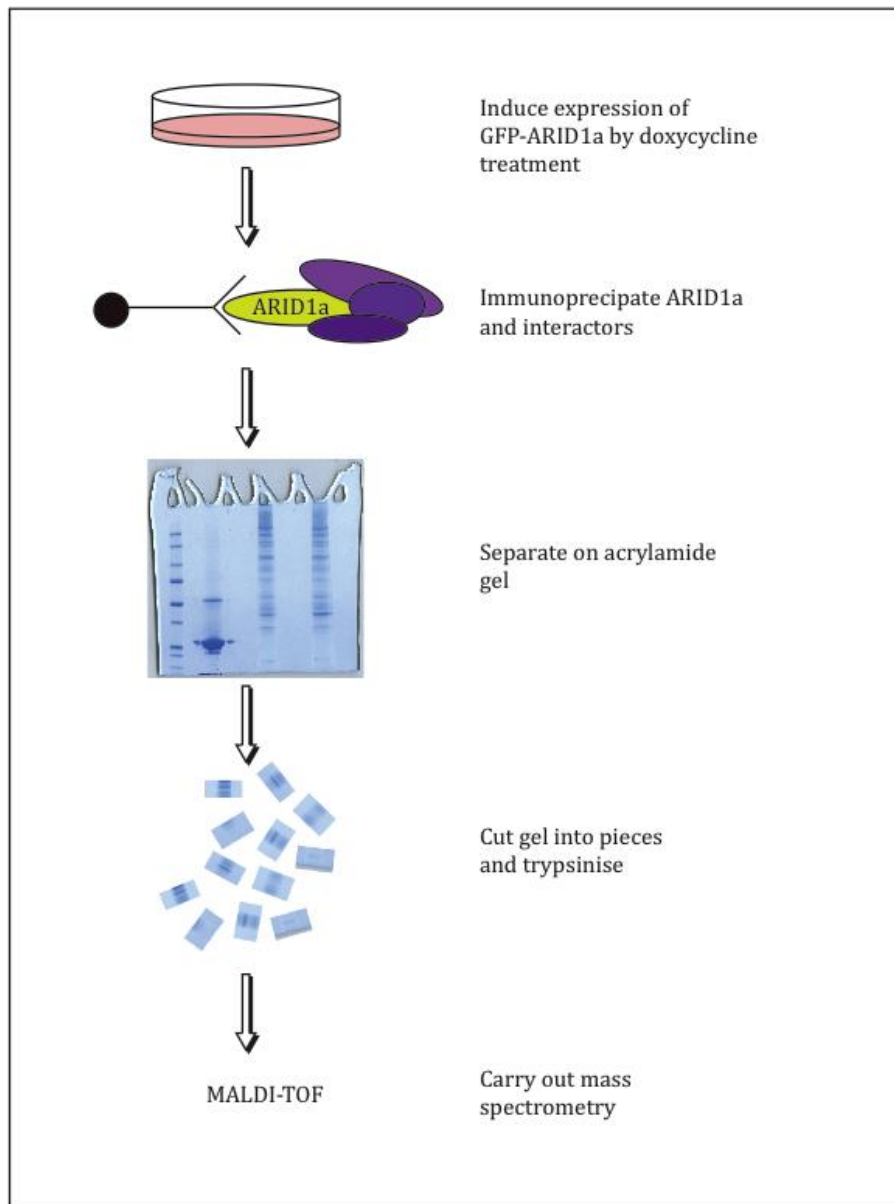
Fig. 5.5: Diagram Of Mass Spectrometry Experiments
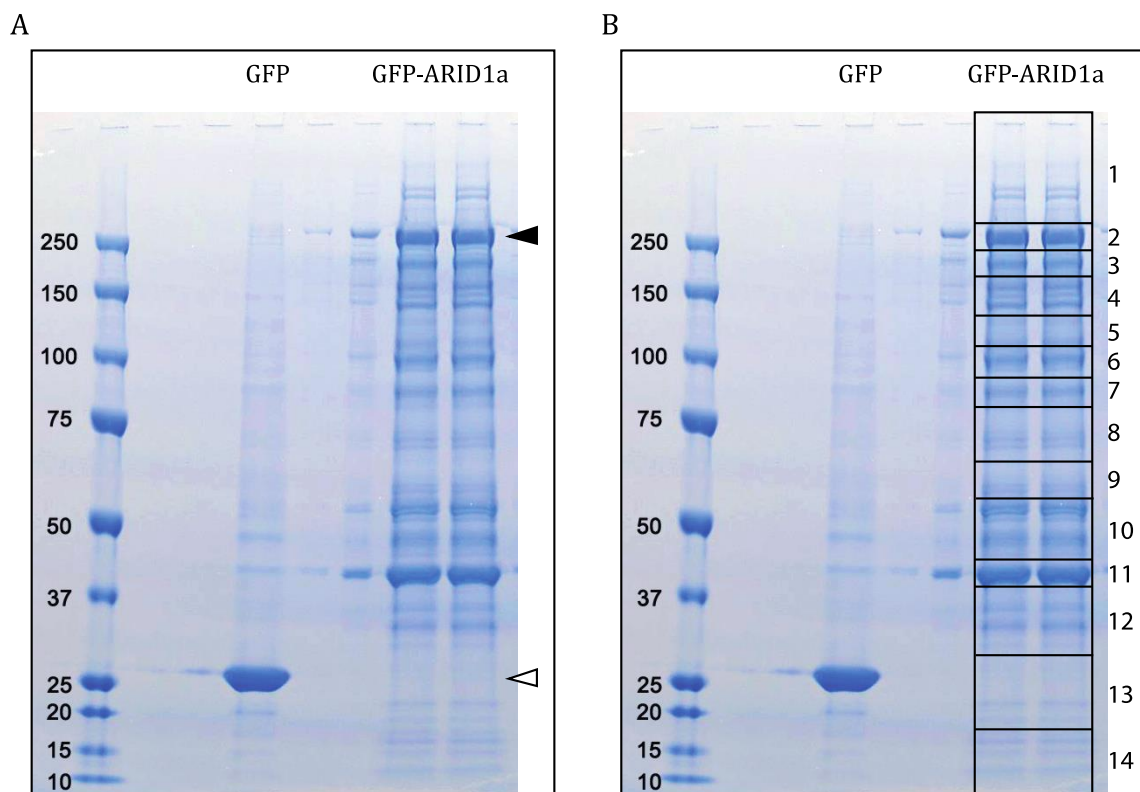
Fig. 5.6: Visualisation Of ARID1a Interacting Proteins

A: Immunoprecipitation of GFP or GFP-ARID1a from FRT/GFP or FRT/GFP-ARID1a respectively, run on a 4-12% gradient gel and stained using colloidal blue. The GFP bait (white arrow) and GFP-ARID1a bait (black arrow) are clearly visible.

B: The GFP-ARID1a lane was cut into 14 pieces as indicated, and each one processed separately.

5.2.3.2 Analysis Of Identified Proteins

Each MALDI-TOF run yielded over 1000 proteins with matching peptides. To remove any erroneously identified proteins the following computational filtering steps were carried out. Firstly, proteins known to bind to GFP were subtracted from the dataset. This list has been compiled by the Sapkota lab from many experiments and represents a comprehensive GFP interactome (see Appendix). Secondly, all proteins with a mascot score of less than 70 were discarded. The mascot score is a measure of the false discovery rate (FDR), and a score of 70 represents an FDR of 5% (www.matrixscience.com). Finally, the remaining proteins were cross-referenced with the Contaminant Repository for Affinity Purification database (CRAPome), and likely contaminants were removed (for list of identified proteins see Appendix).

From the three screens I identified 182, 70 and 54 proteins that bind to GFP-ARID1a respectively (see Appendix for protein lists). Gene Ontology (GO) analysis of the pooled proteins was then carried out using the Panther database (Fig. 5.7 A). 26.7% of the identified proteins are involved in transcriptional regulation, consistent with the role of the BAF complex as a chromatin remodeller. 20.5% of the proteins were characterised as having structural molecule activity. These proteins are predominantly cytoskeletal and ribosomal, and probably represent non-specific interactions with ARID1a. Finally, 34.1% of the total protein pool was annotated as proteins with binding activity. Of these proteins, over half have chromatin or nucleic acid-binding properties, which is a good indicator that they may be involved in the function of the BAF complex.

The three datasets were then overlaid to identify proteins that were common to all three mass spectrometry replicates (Fig. 5.7 B). This resulted in a list of 34 core proteins, which are displayed in Table 5.1. All of the BAF complex components were present, indicating that *Xenopus* ARID1a is capable of being incorporated into mammalian BAF complexes. This is also a good indicator that the mass spectrometry experiments have produced useful data, as the expected proteins are present as the most abundant peptides.

A

- transporter activity
- translation regulator activity
- protein binding transcription factor activity
- enzyme regulator activity
- catalytic activity
- receptor activity
- nucleic acid binding transcription factor activity
- antioxidant activity
- structural molecule activity
- binding

B

Set 1
Set 2
Set 3
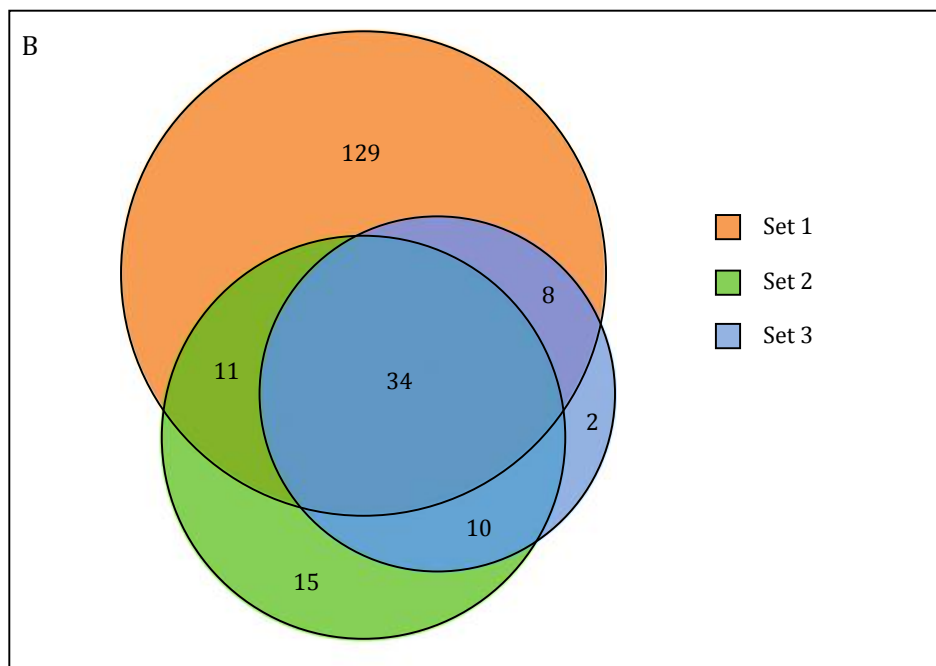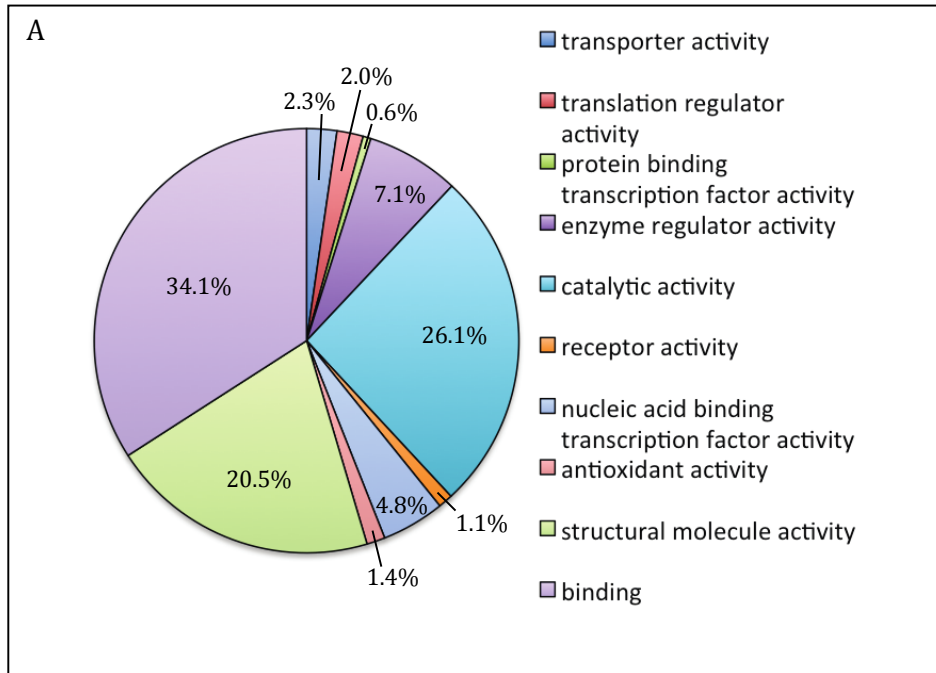
Fig. 5.7: Mass Spectrometry Identifies Interactors of ARID1a in HEK293 Cells

A: Gene Ontology analysis for all the 3 mass spectrometry experiments after filtering. Generated using the Panther Classification System.

B: Overlay of the 3 datasets. 34 proteins are common to all 3 replicates.

Ranking	Protein ID	Summary Of Function
Nuclear		
1	SMARCC2	BAF Component
2	SMARCA4	BAF Component
3	SMARCC1	BAF Component
4	SMARCD1	BAF Component
5	ACTL6A	BAF Component
6	SMARCA2	BAF Component
7	SMARCB1	BAF Component
9	SMARCE1	BAF Component
10	SMARCD2	BAF Component
11	SMARCD3	BAF Component
12	SNRPA1	Spliceosome Component
13	ARID1A	BAF Component
19	DPF1	nBAF Component*
20	HIST2H3A	Histone
25	ACTL6B	BAF Component
33	DDX5	Transcriptional Cofactor
Cytoskeleton		
8	DPF2	Transcription Factor*
14	ACTN3	Actin Binding
15	FLOT1	Endocytosis
18	LIMA1	Actin Binding
21	RPS18	Ribosomal Protein
22	RPL12	Ribosomal Protein
23	ARPC4	Actin Binding
24	CAPZB	Actin Binding
26	PRPH	Adhesion Protein
27	FLOT2	Endocytosis
28	PSMD2	Proteasome Component*
29	INA	Intermediate Filament
30	ARPC1A	Actin Binding
32	ARPC3	Actin Binding
34	PPIA	Protein Folding
Unknown		
16	BCL7A	No Known Function
17	BCL7C	No Known Function
31	BAG2	Substrate Release From Chaperones

Table 5.1: Core Interactors Of ARID1a As Identified By Mass Spectrometry

The 34 proteins core interactors identified by mass spectrometry. The summary of function and localisation are derived from Uniprot, and the ranking is generated from average mascot scores. *: these proteins have both cytoplasmic and nuclear localisation. They are organised by the predominant compartment.

5.2.3.3 Proteins Of Interest

Of the 34 proteins present in all three screens, four are of particular interest. SNRPA1 is a component of the splicing machinery. As the BAF complex interacts with splicing factors the presence of SNRPA1 in this screen agrees with what is already known (Batsché et al., 2005). Whether the BAF complex influences the splicing of Wnt target genes or of Wnt pathway components has not been investigated, so further studies are required to explore this possibility.

BCL7a and BCL7c are uncharacterised proteins and that have not appeared in any other mass spectrometry screen carried out by the Sapkota lab. BCL7a is present in only 9 out of 411 experiments in the CRAPome database, while BCL7c is present in 10. These two proteins are therefore highly likely to be *bona fide* interactors of ARID1a, and may have functional roles in the BAF complex.

DDX5 is present in the nucleus and has been implicated in Wnt signalling (Yang et al., 2006b). It is therefore a strong candidate for a co-regulator of the Wnt pathway with ARID1a, and I chose to investigate DDX5 further. I also chose BCL7a as a second candidate, as nothing is known about it.

5.2.4 Verifying The Interaction Between ARID1a, BCL7a and DDX5

I cloned *BCL7a* and *DDX5* from *Xenopus* cDNA into pCS2+ vectors containing an N-terminal myc tag. HEK cells were co-transfected with either myc-BCL7a or myc-DDX5 together with GFP or GFP-ARID1a, and immunoprecipitations carried out using an anti-GFP antibody (Fig. 5.8). GFP-ARID1a successfully precipitated both BCL7a (Fig. 5.8 A) and DDX5 (Fig. 5.8 B), while GFP alone could not. These experiments verify the mass spectrometry screen and identify BCL7a and DDX5 as interactors of ARID1a. Both BCL7a and DDX5 were expressed more strongly when co-transfected with GFP-ARID1a compared with GFP (Fig. 5.8 Input lanes). Due to the large molecular weight of the *GFP-ARID1a* plasmid the molar ratio of *BCL7a/DDX5:GFP-ARID1a* was likely higher than that for GFP, which would result in stronger expression. While this difference could explain why GFP did not immunoprecipitate BCL7a or DDX5, GFP is expressed much more strongly than GFP-ARID1a in these experiments. Therefore if an interaction between GFP and BCL7a or DDX5 existed it is probable that it would have been detected.
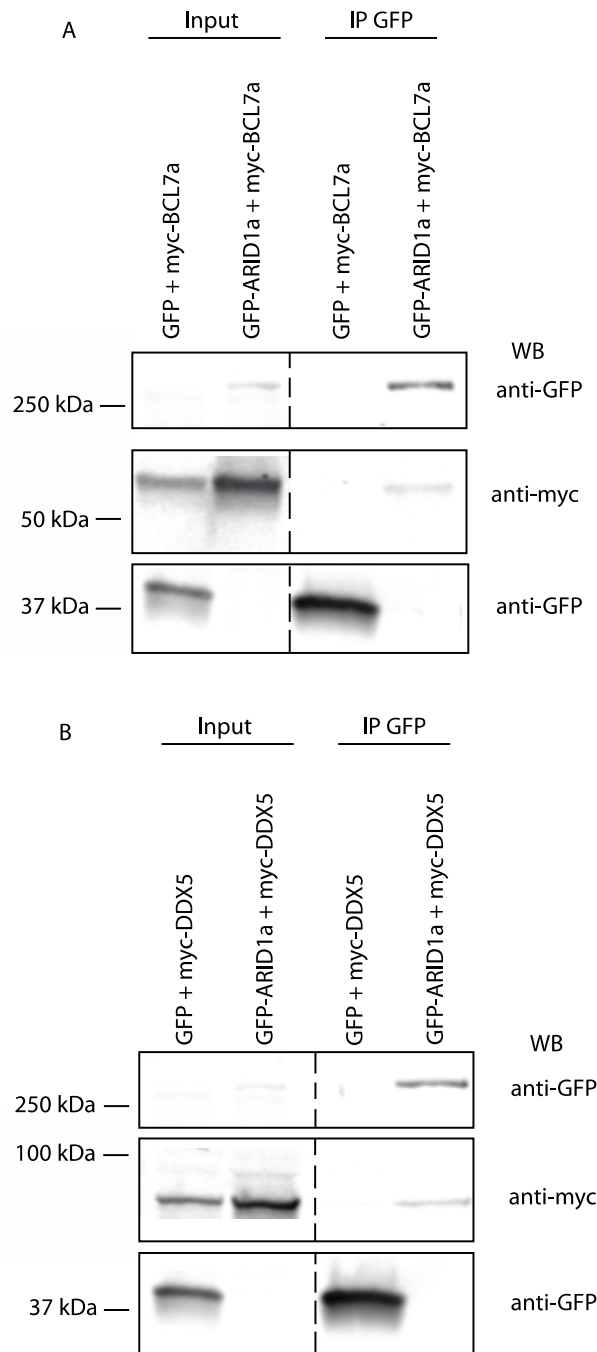
Fig. 5.8 Co-Immunoprecipitation Of GFP-ARID1a, BCL7a and DDX5

Co-immunoprecipitation experiments carried out in HEK cells. Cells were transfected with plasmids encoding *Xenopus* proteins as indicated and left overnight before harvesting.

A) Interaction between GFP-ARID1a and myc-BCL7a. myc-BCL7a is precipitated by GFP-ARID1a (centre panel, rightmost lane) but not GFP (centre panel, 3rd lane). Note that there is more myc-BCL7a in the input lane for cells transfected with GFP-ARID1a than GFP: this is probably due to the large size of the GFP-ARID1a plasmid affecting the molar ratio of the two transfected plasmids.

B) Myc-DDX5 is precipitated by GFP-ARID1a (centre panel, rightmost lane) but not GFP (centre panel, 3rd lane). Note that there is more myc-DDX5 in the GFP-ARID1a input lane than the GFP input lane for the reasons described in (A).

5.3 Discussion

5.3.1 The Mass Spectrometry Approach

As mentioned above, the initial approach for the mass spectrometry screen was to identify proteins from *Xenopus* embryo lysate using bait purified from FRT/GFP-ARID1a cells. This approach was used rather than injecting embryos with *GFP-ARID1a* mRNA because mRNA does not diffuse well in the embryo, and using purified bait eliminated any heterogeneity that would have been introduced by microinjection.

However, analysis of the *Xenopus* mass spectrometry proved problematic. Matching of peptides to the translatome is stringent, and as the *X. laevis* genome is still incomplete the translatome is of poor quality. It is therefore possible that real proteins of interest are present within the dataset, but are not computationally accessible at this time. A second difficulty with carrying out mass spectrometry in *Xenopus* is the high abundance of "sticky" yolk proteins that bind to bait non-specifically in many experiments. Although efforts were made to minimise the presence of yolk within embryo lysates, a large amount of non-specific binding occurred when lysates were incubated with GFP.

These two issues combined meant that extracting useful data from this mass spectrometry experiment was not possible, and instead I chose to look for proteins in FRT/GFP-ARID1a cells. This new approach had certain caveats. This screen was testing for interactions between *Xenopus* bait and human proteins that physiologically would never take place. However, as *Xenopus* ARID1a was able to inhibit Wnt signalling in FRT/GFP-ARID1a cells (Fig. 5.1), then functional interactions were taking place between frog and human proteins. Therefore the proteins identified in this screen could facilitate the ARID1a-mediated repression of Wnt signalling observed in this thesis.

Due to the nature of this cross-species approach some interaction sites may not be conserved, and therefore some binding partners may have been missed. The proteins identified here are likely to be the most conserved interactors, which could provide insight in to the evolution of the BAF complex.

5.3.2 Mass Spectrometry Hits

5.3.2.1 The BAF Complex

Each BAF complex component was found in the core 34 proteins, which is an excellent indicator that *Xenopus* GFP-ARID1a is incorporated into a functional complex in FRT/GFP-ARID1a cells. ARID1b was not identified, which is consistent with the fact that ARID1a and ARID1b exist in mutually exclusive BAF complexes (Wang et al., 2004b). DPF1, a member of the neural-specific BAF complex, was present in the dataset. This is to be anticipated, as despite their name HEK cells are actually derived from a neural lineage (Shaw et al., 2002).

A histone H3 protein, HIST2H3A, was identified in all 3 experiments. While association of GFP-ARID1a with histones is expected, eight other histones were removed from the dataset during the filtering process. Whether this particular histone represents a preferred binding partner for ARID1a is not clear.

5.3.2.2 Actin Binding Proteins

6 proteins in the list have actin binding properties, and all of them are localised to the cytoplasm. It is therefore tempting to dismiss them as cytoskeletal contaminants, and indeed that may well be the case. However, the BAF complex binds to filamentous actin (F-actin; (Rando et al., 2002). F-actin is required for PolII transcription (Yoo et al., 2006), while monomeric actin is an essential subunit for several nuclear complexes, including the BAF complex (Zhao et al., 1998). It is therefore feasible that interactions with actin-binding proteins facilitates binding of the BAF complex to actin, though the exact functional significance of this interaction remains unknown.

5.3.2.3 Possible Contaminant Proteins

7 proteins are likely to be contaminants. Flotillin 1 (FLOT1) and FLOT2 are localised to the plasma membrane where they create a microdomain that mediates endocytosis (Otto and Nichols, 2011). As flotillins associate with the cytoskeletal cortex (Ludwig et al., 2010), and cytoskeletal proteins are often contaminants in mass spectrometry experiments (Gingras et al., 2007), then it is probable that FLOT1 and 2 are not physiologically associated with ARID1a.

Peripherin (PRPH) is an integral membrane glycoprotein that is required for photoreceptor morphology (Boon et al., 2008). Similar to FLOT1 and FLOT2, the membrane localisation of PRPH makes it an unlikely binding partner for ARID1a. However, ARID1a has been reported in the cytoplasm at low levels (Guan et al., 2012). While unlikely, it is therefore possible that these proteins interact physiologically.

RPS18 and RPL12 are ribosomal subunits, and are most likely bound to nascent GFP-ARID1a that is still being translated. Twelve other proteins of the RPS and RPL families were removed when the dataset was compared to the CRAPome, indicating that such ribosomal proteins are common in mass spectrometry experiments and should be treated with caution. Likewise, PPIA is a chaperone involved in protein folding (Liu et al., 2013) and PSMD2 is a proteasome component. Both are likely to be involved in the synthesis and turnover of ARID1a rather than its cellular function. Therefore these proteins are not likely to be co-effectors of ARID1a.

5.3.3 Verification Of The Mass Spectrometry Screen

The mass spectrometry screen identified an interaction between *Xenopus* ARID1a and human BCL7a and human DDX5. This interaction was verified by co-immunoprecipitation between *Xenopus* proteins (Fig. 5.8). Ideally the reciprocal experiment of immunoprecipitating myc-tagged BCL7a or DDX5 and blotting for GFP-ARID1a would have been carried out. Preliminary experiments did not detect GFP-ARID1a, although the protocol could have been optimised further. Verification of the interaction by a third method such as proximity ligation assays (PLA) would also have been beneficial. However, as both BCL7a and DDX5 were identified in all three mass spectrometry replicates, and they co-immunoprecipitated with ARID1a, I am confident that these two proteins are *bona fide* interactors of ARID1a. I spent the remainder of my PhD investigating the role of BCL7a and DDX5 in the regulation of the Wnt pathway.

Chapter 6: Characterisation of BCL7a and DDX5 In *Xenopus*

6.1 Introduction

6.1.1 BCL7a

<u>B</u>-cell <u>C</u>LL/<u>l</u>ymphoma protein <u>7a</u> (BCL7a) was identified as a three-way translocation fusion gene in a Burkitt Lymphoma cell line (Zani et al., 1996). In this instance, the first exon of BCL7a had been replaced with the first exon of Myc, though whether a protein was produced was not tested. Since then, loss of BCL7a has been correlated with aggressive lymphoma, indicating that BCL7a is a anti-malignancy factor (Blenk et al., 2007; Carbone et al., 2008). In adult humans BCL7a expression is restricted to lymphocytes lineages (Ramos-Medina et al., 2013), although the expression pattern during embryogenesis has not been tested in any species. To date, no biochemical or functional investigation of BCL7a exists.

6.1.2 DDX5

<u>DEAD</u>-bo<u>x</u> helicase <u>5</u> (DDX5), also known as p68, is an RNA helicase with diverse functions (Janknecht, 2010). DDX5 binds to the spliceosome and mediates alternative splicing (Guil et al., 2003; Lin et al., 2005). Its RNA helicase ability is also required for ribosome biogenesis (Jalal et al., 2007) and Drosha-mediated micro-RNA processing (Fukuda et al., 2007). DDX5 promotes transcription by binding to to <u>C</u>REB-<u>b</u>inding <u>p</u>rotein (CBP) and PolII (Rossow and Janknecht, 2003). Like ARID1a, DDX5 positively regulates expression of o<u>e</u>strogen <u>r</u>eceptor (ER) targets (Watanabe et al., 2001), and can act as a cofactor for several other transcription factors such as MyoD and p53 (Bates et al., 2005; Caretti et al., 2006).

DDX5 is an activator of β-catenin. DDX5 and β-catenin physically interact and bind to Wnt target gene promoters (Clark et al., 2013; Shin et al., 2007). Furthermore, phosphorylation of DDX5 by <u>p</u>latelet-<u>d</u>erived <u>g</u>rowth <u>f</u>actor (PDGF)

is sufficient to cause nuclear localisation of β-catenin and subsequent transcription (Yang et al., 2006b). Consistent with a role in Wnt signalling, overexpression of DDX5 together with β-catenin causes an increase in TOPLFASH activity over β-catenin alone (Shin et al., 2007). However one report showed that DDX5 does not promote nuclear localisation of β-catenin, nor does it activate the Wnt pathway. Furthermore, siRNA-mediated knock down of DDX5 had no effect on Wnt signalling (Stucke et al., 2008). Why this study differs from other work in the field is unclear, though despite the controversy the proposed role of DDX5 as a regulator of β-catenin makes it an interesting protein for my research.

6.2 Results

6.2.1 Expression Pattern of *BCL7a* and *DDX5*

First I assessed the expression of *BCL7a* and *DDX5* during *Xenopus* development. qPCR was carried out using cDNA collected from a range of embryonic stages (Fig. 6.1). *BCL7a* was present as maternally deposited mRNA (Fig. 6.1 A). Expression was maintained at low levels throughout embryogenesis except for a spike during gastrulation, where *BCL7a* expression was 3 fold higher than at other stages. *DDX5* mRNA was also expressed maternally (Fig. 6.1 B). DDX5 levels showed little change until stage 35, when a two-fold increase in expression was observed.

The expression of both genes was then visualised using *in situ* hybridisation. Unfortunately no *BCL7a* staining was observed, which may be due to its low expression levels during development. *DDX5* was ubiquitous at stage 11 (Fig. 6.1 C). The vegetal hemisphere was not stained in this image, however *DDX5* expression was observed in samples that were allowed to develop further.
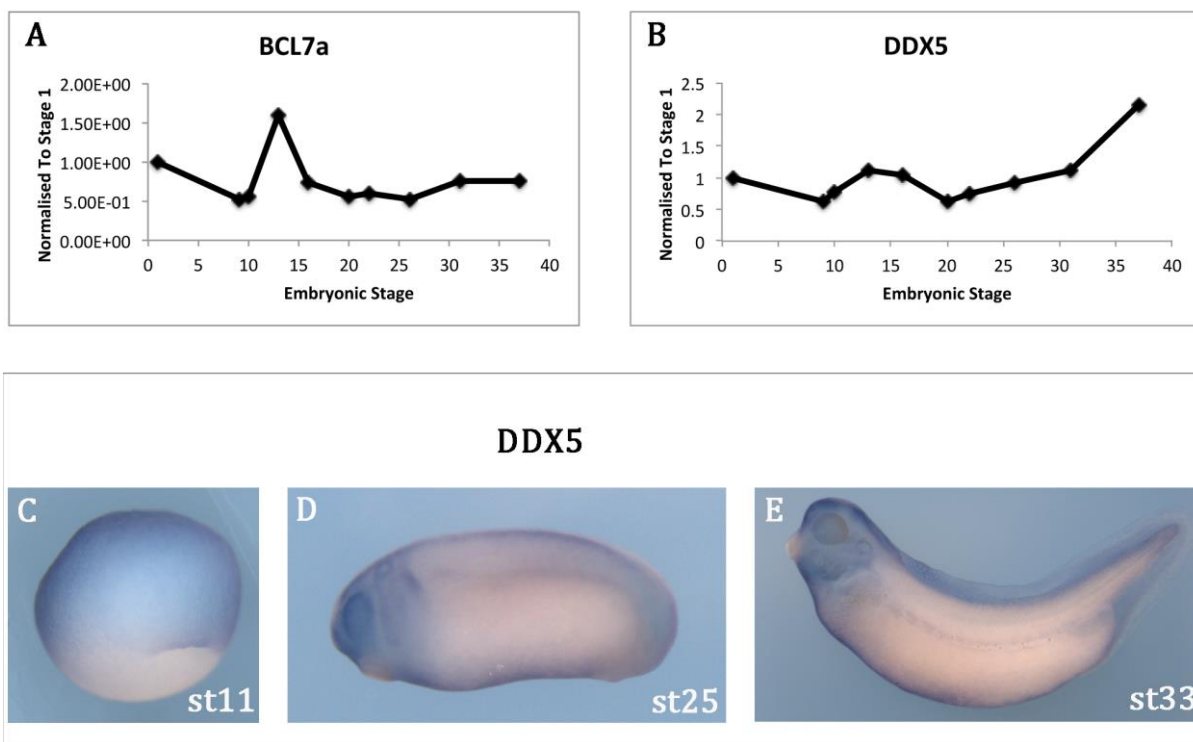
Fig. 6.1 Expression Pattern Of BCL7a and DDX5

A, B: qPCR for *BCL7a* (A) and *DDX5* (B) during *Xenopus* development. Data are normalised to stage 1. Representative of two independent experiments.

C-E: In situ hybridisation for *DDX5* on *Xenopus* embryos.

C: Lateral view of stage 11 embryo, with the animal pole uppermost. *DDX5* was ubiquitous throughout the ectoderm.

D: Lateral view of a stage 25 embryo with the anterior to the left. *DDX5* was expressed in the eye and neural crest streams, with faint staining in the posterior tailbud region.

E: Lateral view of a stage 32 embryo, with the anterior to the left. DDX5 was expressed throughout the cranial region, including eyes, otic vesicle and branchial arches. Unfortunately no staining was observed using a BCL7a probe.

During the tailbud stage *DDX5* was present in the eye and migrating streams of neural crest cells (Fig. 6.1 D), and in the tailbud. At stage 33 *DDX5* was expressed throughout the head including the eye and otic vesicles (Fig. 6.1 E). The tailbud staining was also present at this stage.

The expression pattern of *DDX5* is remarkably similar to that of *ARID1a* (compare with Fig. 3.2). However, there are subtle differences. Firstly, at stage 25 *DDX5* was visible within the otic vesicle whereas *ARID1a* staining was not detected in the vesicle until later stages. Secondly, the branchial arches are clearly visible in embryos stained for *ARID1a* expression, but are less well demarcated by the *DDX5* probe. The tight co-localisation of *ARID1a* and *DDX5* transcripts suggests a functional relationship between the two genes.

6.2.2 Overexpression of *BCL7a* and *DDX5* Results In Different Phenotypes

To test whether ARID1a, DDX5 and BCL7a co-localised within the cell I carried out immunofluorescence on dissociated animal cap cells. Embryos were injected with 2 ng *HA-ARID1a* and 250 pg of either *myc-BCL7a* or *myc-DDX5* and harvested at stage 8 (Fig. 6.2 C-L). These experiments showed that exogenous BCL7a and DDX5 were localised to the nucleus, as seen by overlapping fluorescence with DAPI. ARID1a co-localised with both BCL7a and DDX5, supporting the *in vitro* data from Chapter 5 that these proteins physically interact.

I then overexpressed *BCL7a* and *DDX5* in *Xenopus* by injecting mRNA into the two dorsal blastomeres at the 4-cell stage (Fig. 6.2). Injection of 250 pg *BCL7a* mRNA had little effect on embryo development (Fig. 6.2 A). Some embryos developed mild oedema around the heart or exhibited a slight developmental delay, but otherwise developed normally. In contrast embryos injected with 250 pg *DDX5* mRNA exhibited severe defects (Fig. 6.2 B). These embryos developed short body axes and were significantly delayed in their development. This phenotype falls into the "shortened axis" synphenotype group, and is similar to those caused by loss of organiser genes such as *Lim1* and *Xnr3* (Rana et al., 2006).
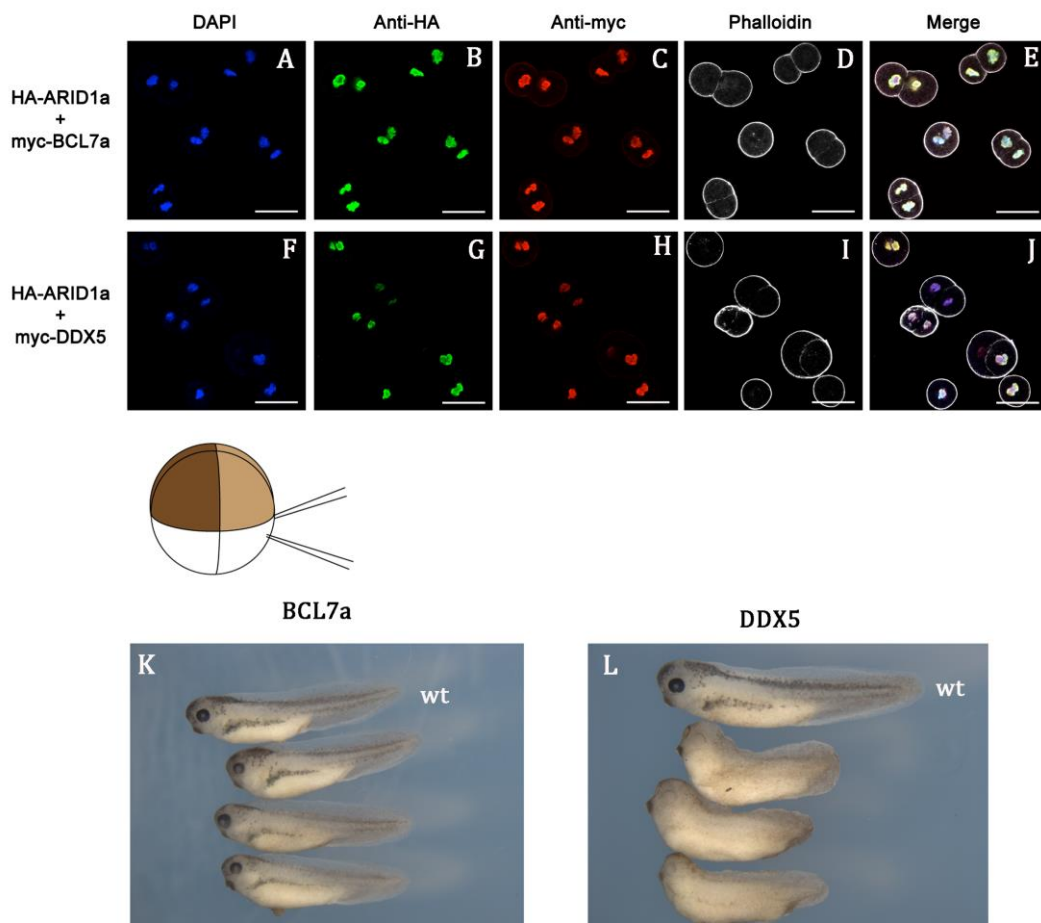
Fig. 6.2: Co-Localisation Of DDX5 and BCL7a and ARID1a

A-J: Immunofluorescence of dissociated animal cap cells injected with HA-ARID1a and myc-BCL7a (A-E) or myc-DDX5 (F-J). Nuclei were visualised using DAPI (A, F) and the cell periphery by phalloidin (D, I). Both BCL7a and DDX5 co-localise with ARID1a (E, J). Scale bars represent 50 μm.

K, L: lateral views of embryos injected dorsally with BCL7a (K) or DDX5 (L) mRNA. Injection of BCL7a mRNA had little to no effect on development (K). Injection of DDX5 caused shortening of the body axis and loss of neural crest derived melanocytes. An uninjected embryo is included in both images for comparison (wt).

146

6.2.3 BCL7a and DDX5 Inhibit Wnt Signalling In *Xenopus*

The aim of the mass spectrometry screen was to identify interactors of ARID1a that could explain how it is able to inhibit Wnt signalling. I therefore tested whether BCL7a or DDX5 were able to repress expression of *Sia* and *Xnr3* when overexpressed in the animal cap assay.

Embryos were injected at the one cell stage with 2 pg *Wnt8* mRNA along with 250 pg of either *BCL7a* or *DDX5* mRNA and target gene expression measured by qPCR (Fig. 6.3). Both BCL7a and DDX5 reduced expression of *Sia* by >2 fold and *Xnr3* by >4 fold (Fig. 6.3 A, B). These assays show that, like ARID1a, both BCL7a and DDX5 act to inhibit Wnt signalling in *Xenopus.*

As ARID1a acts below the level of β-catenin, I next confirmed that BCL7a and DDX5 were also acting at this level of the pathway. Both BCL7a and DDX5 repressed *Sia* and *Xnr3* to the same extent as ARID1a in this assay (Fig. 6.3 C, D).

I next used the TOPFLASH assay to test whether BCL7a and DDX5 could repress Wnt signalling in HEK293 (Fig. 6.3 E). Cells were transfected with the TOPFLASH and Renilla luciferase plasmids alongside *Xenopus BCL7a, DDX5* or *GFP-ARID1a. GFP* was used as a negative control. GFP-ARID1a and DDX5 both reduced luciferase activity to similar degree when compared with GFP transfected cells. However, BCL7a had no effect on TOPFLASH activity. Unfortunately the data from these experiments are not statistically significant. This is probably due to the large variance observed between the data sets (Fig. 6.3, the error bars are unusually large). Why this experiment had higher variance than other luciferase experiments I have carried out is unclear, though it could be that the batch of assay kit I used was getting old. If more biological replicates were carried the variance between experiments may be reduced, and the significance of the data could be more easily queried. However, there is clearly a qualitative difference between cells transfected with BCL7a and those transfected with DDX5, indicating that BCL7a – in contrast to *Xenopus* animal cap tissue – is unable to repress β-catenin-mediated signalling in HEK cells.
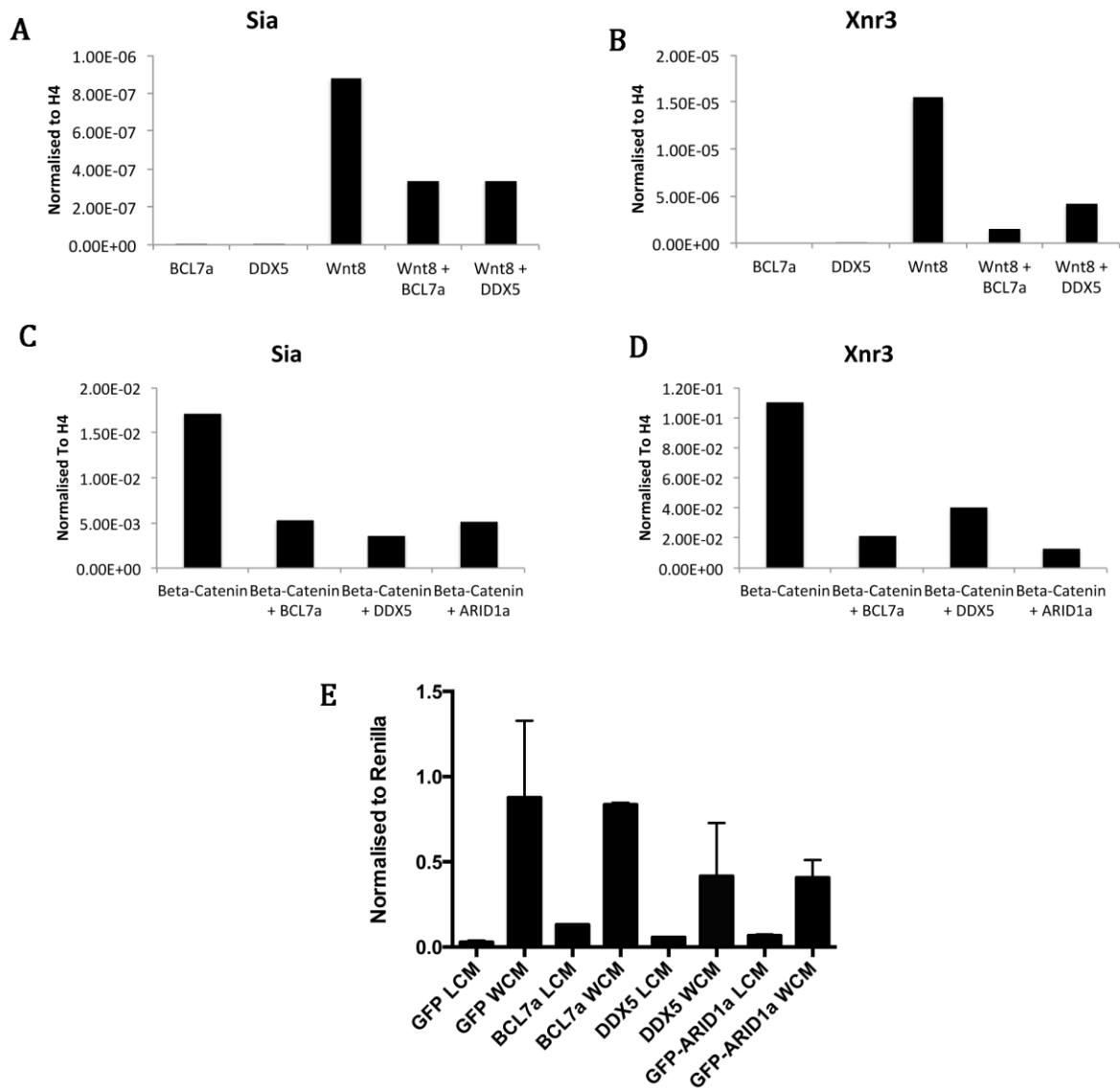
Fig. 6.3 DDX5 and BCL7a Inhibit Wnt Signalling

A-C: Animal cap assays. Embryos were injected at the 1 cell stage with either 2 pg *Wnt8* mRNA (A, B) or 200 pg *β-catenin* mRNA (C,D) alongside 250 pg of either *BCL7a* or *DDX5* mRNA. Animal caps were cut at stage 8 and incubated until stage 10 and qPCR carried out to measure the expression of *Sia* (A, C) and *Xnr3* (B, D). Data are normalised to *histone H4* expression. Data are representative of 3 independent experiments, however due to large variations between replicates it was not possible to carry out statistical analysis on these data.

E: TOPFLASH luciferase assay. HEK cells were transfected as indicated alongside TOPFLASH and Renilla reporter plasmids. Cells were treated with either L-cell conditioned media (LCM) or Wnt conditioned media (WCM) overnight and then luciferase activity measured. GFP-ARID1a and DDX5 caused an approximately 2 fold reduction in luciferase activity, whereas BCL7a had no effect. Data are the average of three experiments and are presented normalised to Renilla luciferase. Unfortunately these differences are not statistically significant (see text for discussion).

6.2.4 Loss Of DDX5 Causes Phenotypes Similar To Loss of ARID1a

As BCL7a did not have a phenotype when overexpressed (Fig. 6.2) and had different potentials to repress Wnt signalling between *Xenopus* and HEK cells (Fig. 6.3), I therefore focused on DDX5. I designed a translation blocking morpholino (DDX5_TB) to deplete DDX5 in *Xenopus* embryos and an associated 5 base pair mismatch control (DDX5_CO). Injection of 20 ng DDX5_CO had no effect on development (Fig. 6.4 A). Injection of the translation blocking morpholino caused ventral oedema and malformation of head structures (Fig. 6.4 B). These embryos had smaller eyes and flattened forebrains. This phenotype is similar to that seen for low doses of ARID1a_TB suggesting that *DDX5* and *ARID1a* regulate similar processes during embryogenesis.

I then attempted to validate the morpholinos by carrying out western blots against endogenous DDX5 (Fig. 6.4 C). Unfortunately the antibody I used did not recognise *Xenopus* DDX5 (lanes 1-3). DDX5 protein was detected in HEK293 cell lysate, indicating that this antibody is capable of detecting DDX5 (lane 4), however the epitopes it recognises must not be well conserved between the human and *Xenopus* proteins. Due to time constraints I was not able to attempt validation by other methods such as *in vitro* transcription-translation reactions, injecting mRNA coding for epitope-tagged DDX5 (such as HA-DDX5 or GFP-DDX5), or rescue experiments co-injecting DDX5_TB with *DDX5* mRNA. Before continuing with these experiments it will be crucial to demonstrate that the DDX5_TB morpholino specifically knocks down DDX5.

DDX5_CO   **DDX5_TB**

A   B

C

Uninjected DDX5_CO DDX5_TB HEK293

1   2   3   4

75 kDa
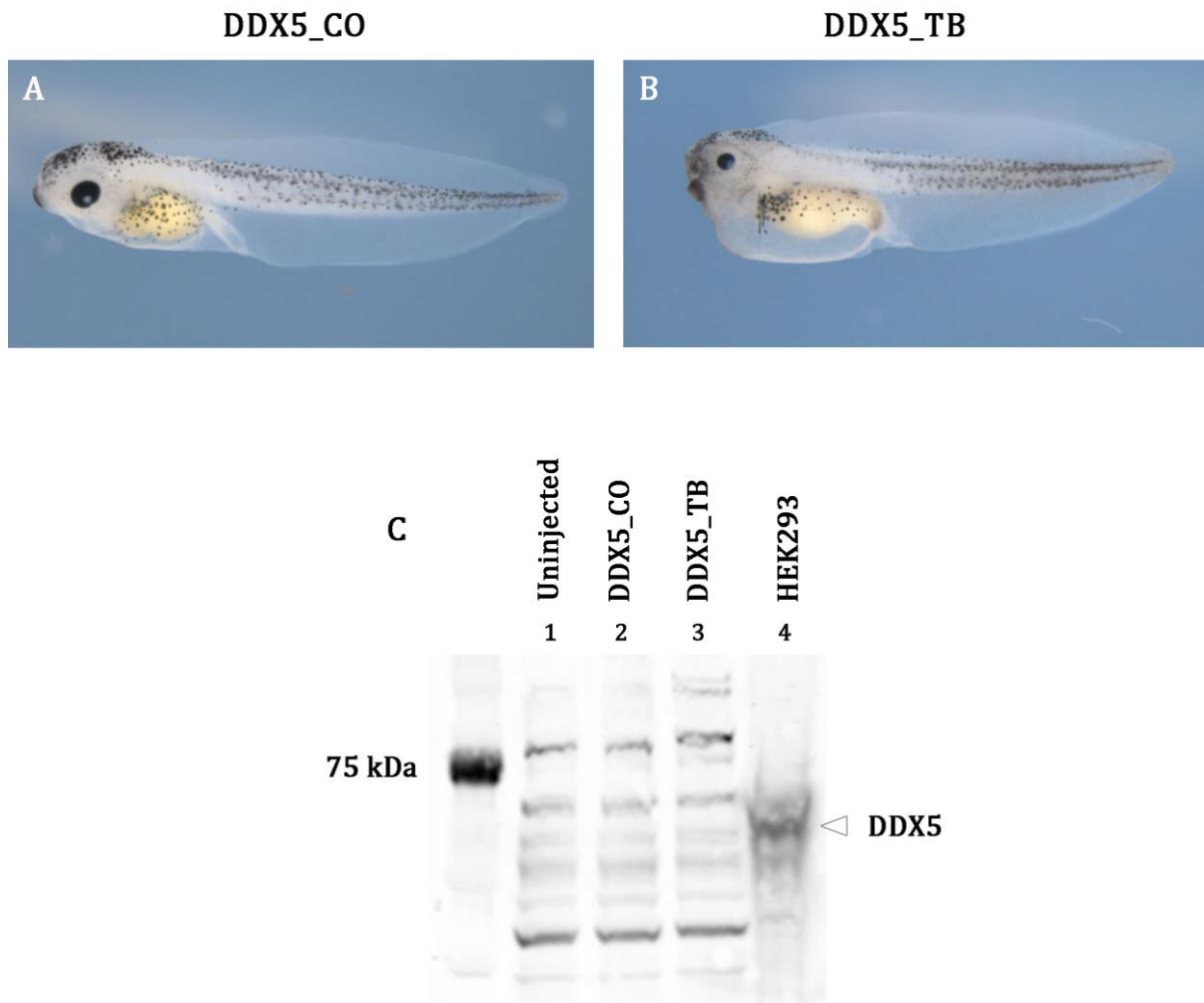
◁ DDX5

Fig. 6.4 Morpholino Knock Down Of *DDX5*

A: Embryos were injected with 20 ng mismatch control morpholino at the one cell stage an allowed to develop. Control morphants developed without gross phenotypic changes.

B: Embryos were injected with 20 ng translation blocking morpholino at the one cell stage. DDX5 morphants developed oedema around the heart, small eyes and facial abnormalities.

C: Western blot against endogenous DDX5 against *Xenopus* embryo lysate (lanes 1-3) or HEK293 cells (lane 4). DDX5 protein was only detected in HEK293 cells and not in *Xenopus* lysates (Arrowhead. Compare lane 4 with lanes 1-3).

150

6.2.5 ARID1a Can Repress β-catenin-Mediated Transcription In The Absence Of DDX5

As overexpression of DDX5 inhibited Wnt signalling, then the reciprocal experiment should cause an increase in expression of Wnt target genes. I therefore carried out animal cap assays by injecting 20 ng of either DDX5_TB or DDX_CO morpholino together with 200 pg *β-catenin* mRNA and then measuring gene expression by qPCR (Fig. 6.5). Injection of DDX5_TB had no effect on the expression of *Sia* (A) or *Xnr3* (B) in the absence of *β-catenin*. Injection of the translation blocking morpholino enhanced expression of both *Sia* and *Xnr3* compared with the control morpholino in the presence of exogenous β-catenin, although to a lesser extent than depletion of *ARID1a.* This upregulation is consistent with DDX5 being a repressor of β-catenin in this assay.

As both ARID1a and DDX5 had the same effect on β-catenin dependent transcription and they physically interact, I next asked whether ARID1a was capable of repressing β-catenin-mediated signalling in the absence of DDX5. To this end I co-injected *β-catenin* and *ARID1a* mRNA along with either DDX5_CO or DDX5_TB morpholinos. Overexpression of *ARID1a* was sufficient to inhibit expression of both *Sia* and *Xnr3* in the absence of DDX5, indicating that DDX5 is not required for ARID1a to inhibit Wnt signalling.

These experiments are preliminary, and require repeating before firm conclusions can be drawn.

A

Sia

| Beta-catenin | − | − | + | + | + | + | + | + |

B

Xnr3

| Beta-catenin | − | − | + | + | + | + | + | + |
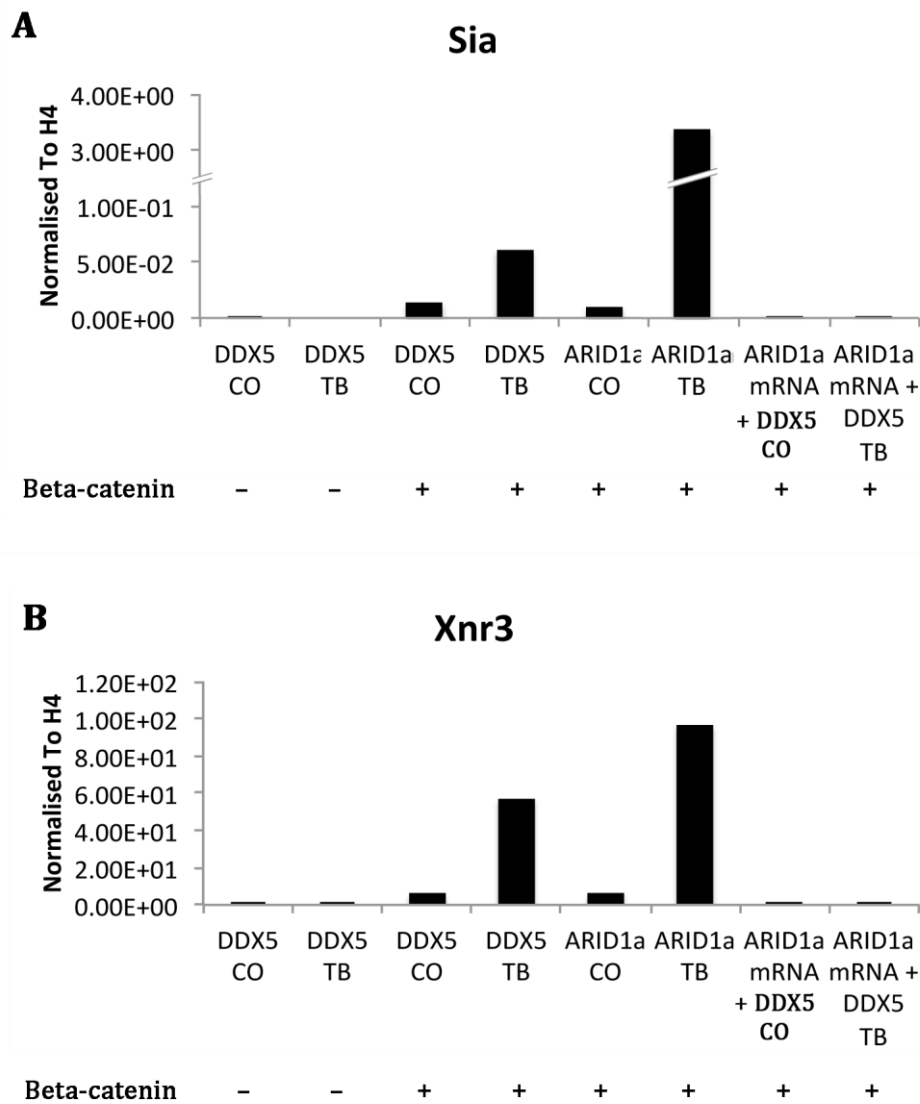
Fig. 6.5 Morpholino Depletion Of DDX5 Caused An Increase In Wnt Signalling

Animal cap assays. Embryos were injected at the one cell stage with 200 pg *β-catenin* mRNA plus either 20 ng DDX5 control or translation-blocking morpholino, 20 ng ARID1a control or translation-blocking morpholino, 2 ng *ARID1a* mRNA or 2 ng *ARID1a* mRNA plus 20 ng DDX5 morpholino. The expression of *Sia* (A) and *Xnr3* (B) were measured by qPCR. Data are normalised to *histone H4*. The data are from a single preliminary experiment.

6.3 Discussion

6.3.1 BCL7a As A Member of the BAF Complex

BCL7a bound to ARID1a and they co-localised in the nucleus. However, overexpression of *BCL7a* had no effect on *Xenopus* development. This may because the BCL7a protein is highly regulated in *Xenopus*, or that in these experiments it was expressed in tissues that lack essential co-factors for BCL7a function. This lack of a phenotype is not consistent with the repression of Wnt target genes *Sia* and *Xnr3* as seen by the animal cap assays. Furthermore, BCL7a was an effective inhibitor of Wnt in *Xenopus* but not in HEK293 cells. These three systems – whole embryos, explanted animal caps and tissue culture cells – have different properties, which may explain these differences. Perhaps *Xenopus* BCL7a is unable to interact with human proteins that regulate nuclear Wnt signalling, or HEK293 cells lack a critical co-factor. Whatever the mechanism, the role of BCL7a with respect to the BAF complex merits further study.

6.3.2 DDX As A Repressor Of The Wnt Pathway

In *Xenopus* animal cap assays DDX5 acted as an inhibitor of the Wnt pathway. Furthermore, TOPFLASH experiments in HEK293 cells showed that DDX5 repressed Wnt signalling to a similar degree as ARID1a. These data contradict the current literature, which states that DDX5 is an activator of Wnt signalling. Several groups have shown an interaction between DDX5 and β-catenin, and have demonstrated that gain of DDX5 function corresponds with activation of the Wnt pathway (Clark et al., 2013; Shin et al., 2007; Yang et al., 2006b). Why then, is there this discrepancy? Firstly, all of the studies cited so far have been carried out in colon cancer-derived cell lines, which are notorious for having dysregulated Wnt signalling pathways (Minde et al., 2011). However, experiments in mouse Gc1-Spg cells – which are derived from spermatogonial cells – have also shown that DDX5 activates the Wnt pathway (Arun et al., 2012), arguing against this property being an artefact of colon carcinoma cell lines.

In contrast to previous studies that were carried out in cell lines derived from adult tissues, my experiments were done using embryonic cell types. Another difference is that I used the *Xenopus* DDX5 protein, which while 85% conserved with human DDX5 may contain sufficient differences to switch it from an activator to a repressor of Wnt signalling. The crucial phosphorylation residue that allows DDX5 to interact with β-catenin is conserved between human and frog, indicating that this function could be maintained (Yang et al., 2006b). However, immunofluorescence of DDX5 showed it was nuclear in *Xenopus* animal cap cells (Fig. 6.2), suggesting that the mechanism that allows DDX5 to become cytoplasmic is not present in these cells. As only cytoplasmic DDX5 is able to bind to β-catenin (Shin et al., 2007) then nuclear retention of DDX5 would prevent it from activating β-catenin mediated signalling. This retention model could be tested by proximity ligation assays between β-catenin and DDX5, which would determine whether these proteins are interacting in *Xenopus* and if so in which cellular compartment. Furthermore, animal cap experiments similar to those described in Fig. 6.3 using human DDX5 would test whether *Xenopus* and human DDX5 have intrinsically different abilities to regulate Wnt signalling within the same system.

6.3.3 ARID1a May Not Require DDX5 To Regulate The Wnt Pathway

Preliminary animal cap experiments showed that ARID1a is able to repress β-catenin dependent transcription in the absence of DDX5 (Fig. 6.5). As mentioned above, the DDX5 morpholinos must be validated and these experiments repeated before drawing conclusions. If these data are confirmed, then the implication is that DDX5 is inhibiting Wnt signalling independently to ARID1a and not as part of the BAF complex. Alternatively, DDX5 may be acting to recruit the BAF complex to β-catenin target sites, and once ARID1a is overexpressed DDX5 becomes redundant. Further experiments are required to investigate the relationship between ARID1a and DDX5 with respect to Wnt signalling (see section 7.1.3 for more detail).

Chapter 7: Discussion And Future Directions

Despite years of research there is still much we do not know about how the Wnt pathway is regulated. In particular, events that occur in the nucleus before and after β-catenin translocation from the cytoplasm remain insufficiently understood. Nuclear β-catenin displaces TLE/Groucho from TCF/LEF proteins and recruits co-factors to alter the chromatin landscape, changing it from a transcriptionally repressive to a permissive state (see Chapter 1). One such chromatin remodelling complex is the BAF complex, which binds to β-catenin via the core ATPase Brg1 (Barker et al., 2001). However, other members of the BAF complex such as SNF5 act to supress Wnt signalling (Collins and Treisman, 2000; Mora-Blanco et al., 2014). Previous work on Osa, the *Drosophila* homologue of ARID1a, suggested that it inhibits the Wg pathway (Collins and Treisman, 2000). My study focussed on testing and expanding these findings, showing that ARID1a is a direct inhibitor of Wnt signalling in vertebrates.

Two proteins, BCL7a and DDX5, were identified as interaction partners for ARID1a by mass spectrometry. Individually, overexpression of these proteins prevented β-catenin mediated transcription in *Xenopus* indicating that they might act together with ARID1a to regulate transcription of Wnt target genes. I will now discuss potential mechanisms for how ARID1a could be functioning at the molecular level (Fig. 7), and suggest experiments that would validate or refute these models.

7.1 Possible Models For ARID1a and DDX5 Function

7.1.1 Creation of a Repressive Chromatin State

The BAF complex re-positions nucleosomes to both positively and negatively regulate gene expression (Tolstorukov et al., 2013). In *Drosophila* SAYP-containing BAP complexes lay down nucleosome "barriers" within the *ftz-f1* gene (Vorobyeva et al., 2012). These barriers are regions of tightly clustered

nucleosomes that interfere with PolII elongation and lead to reduced gene expression (Subtil-Rodríguez and Reyes, 2010). Such barriers are also removed by the BAF complex to allow transcription to take place (Schwabish and Struhl, 2007). Therefore ARID1a could act to repress Wnt signalling either by actively positioning nucleosome barriers within β-catenin target genes, or by preventing the BAF complex from disassembling barriers already present (Fig. 7 A). This model could be tested by DNase footprinting experiments, which would identify the location of nucleosomes within β-catenin target genes, and assess whether the position or occupancy of these nucleosomes is changed upon manipulation of ARID1a.

Alternatively, the BAF complex is able to recruit histone deacetylases (HDACs) (Sif et al., 2001). HDACs prevent transcription by condensing chromatin and denying transcription factors such as β-catenin access to DNA (Haberland et al., 2009). Therefore localisation of HDACs to β-catenin target genes by ARID1a could be sufficient to repress Wnt signalling (Fig. 7 B).

Both of these models assume that ARID1a is present at β-catenin target genes, and that it is inhibiting β-catenin dependent transcription as part of the BAF complex. Neither of these assumptions have been directly tested. Chromatin immunoprecipitation (ChIP) followed by sequencing or qPCR would show whether ARID1a is present at β-catenin target genes. A time course experiment similar to that carried out by Sierra and colleagues (Sierra et al., 2006), where cells were stimulated with Wnt and ChIP-qPCR carried out at short time intervals, would provide information as to when ARID1a is present on chromatin with respect to β-catenin. ChIP experiments using antibodies that recognise histone acetylation and methylation marks could also be used to test the second hypothesis directly, as it predicts that perturbation of ARID1a would result in measurable changes in histone modifications.
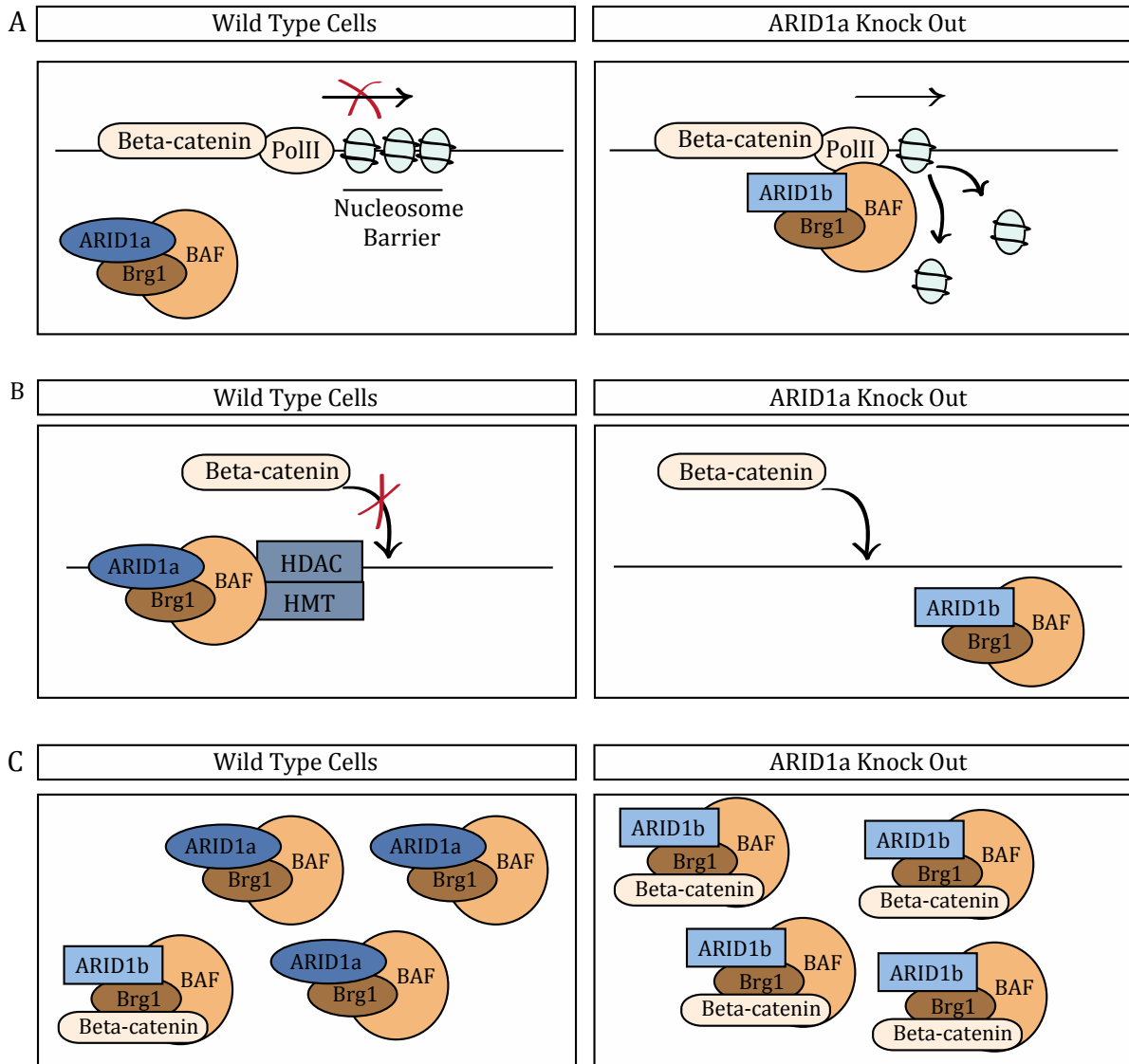
Fig. 7 Models Of BAF250a Repression of Beta Catenin

A: ARID1a may establish nucleosome barriers within target genes, or prevent their disassembly by the BAF complex. These barriers prevent efficient transcription. Upon ARID1a knock down these nucleosomes are no longer positioned within the gene, or are now able to be displaced by ARID1b containing complexes. With the barrier removed, PolII is able to transcribe target genes.

B: ARID1a creates a repressive chromatin state by recruiting histone modifying enzymes that prevent β-catenin from binding to target genes, and thereby inhibit transcription. Loss of ARID1a prevents association of these enzymes with beta-catenin sites, and β-catenin is able to bind DNA and promote transcription.

C: ARID1a prevents Brg1 from binding β-catenin, and therefore sequesters the BAF complex away from β-catenin target genes, preventing their transcription. Loss of ARID1a increases the amount of Brg1 able to bind β-catenin, sensitising cells to the Wnt pathway.

7.1.2 ARID1a Could Prevent Brg1 From Associating With β-catenin

Brg1, the core ATPase of the BAF complex, binds to β-catenin (Barker et al., 2001). However, β-catenin was not identified in my mass spectrometry screen for ARID1a interacting proteins. This may be because the weak cross-linking agent used did not allow detection of proteins that were not directly bound to ARID1a, or ARID1a may prevent association between Brg1 and β-catenin. If the latter were the case, ARID1a-containing complexes would not be recruited to Wnt target genes; instead β-catenin dependent transcription would be mediated by complexes containing the alternative subunit ARID1b. ARID1a and ARID1b are mutually exclusive subunits of the BAF complex (Wang et al., 2004), and have opposite roles in several cellular processes, such as control of the cell cycle (Nagl et al., 2007). It is therefore possible ARID1a and ARID1b have opposing roles in Wnt signalling, although ARID1b has not been tested in this regard.

If Brg1 were limiting, this could explain the changes in Wnt target gene transcription that I observed. Depletion of ARID1a would increase the pool of Brg1 bound to ARID1b (and therefore available to bind β-catenin), sensitising cells to Wnt signals (Fig. 7 C). Likewise, overexpression of ARID1a would sequester Brg1 from ARID1b and prevent interaction with β-catenin, leading to a loss of Wnt target gene transcription. This model can be directly tested by carrying out co-immunoprecipitations between Brg1, β-catenin, ARID1a and ARID1b. It would also be interesting to carry out animal cap experiments similar to those in Chapter 4 to test the effects of ARID1b on Wnt signalling.

7.1.3 ARID1a, BCL7a and DDX5

To date, no studies have investigated the molecular properties of BCL7a. It has no identifiable domains and few known binding partners. The experiments described in my thesis show that BCL7a is capable of inhibiting Wnt/β-catenin signalling in *Xenopus* animal cap assays, but was not able to inhibit Wnt signalling in HEK293 cells. Further experiments with both *Xenopus* and human BCL7a such as secondary axis induction and depletion experiments would contribute towards resolving this discrepancy.

DDX5 was identified as an interaction partner for ARID1a from the mass spectrometry screen, and was shown to inhibit Wnt signalling to a similar degree as ARID1a. However, preliminary work showed that DDX5 was not required for ARID1a-mediated repression of β-catenin (Fig. 6.5). If these findings are confirmed by further repeats, then it may be that ARID1a and DDX5 regulate β-catenin independently, or that DDX5 represses β-catenin by recruiting ARID1a-containing complexes. DDX5 can bind to DNA together with proteins such as MyoD and p53 (Bates et al., 2005; Caretti et al., 2006), therefore it is possible that DDX5 binds DNA together with ARID1a. Additionally, BAF complexes have little specificity for DNA sequence and are often recruited to specific genes by cofactors (Tolstorukov et al., 2013), though whether DDX5 is capable of this has yet to be tested. Reciprocal experiments depleting ARID1a and overexpressing DDX5 would determine whether DDX5 requires ARID1a to repress Wnt signalling. If not, then it is likely that these two proteins are regulating β-catenin independently.

In addition to inhibiting β-catenin dependent transcription, ARID1a and DDX5 share several other properties. Both have embryonic lethal phenotypes (Fukuda et al., 2007; Gao et al., 2008), both regulate transcription of target genes, for example in response to oestrogen signalling (Inoue et al., 2002; Watanabe et al., 2001) and both interact with the spliceosome (Batsché et al., 2005; Guil et al., 2003). Therefore it may be that DDX5 is a frequently recruited co-factor, or may even be an integral BAF subunit. Co-sedimentation experiments such as those described by Hargreaves and Crabtree (2011) could be used to test whether DDX5 is a *bona fide* subunit of the BAF complex.

7.2 Mass Spectrometry Screens In *Xenopus*

My first attempt at mass spectrometry was carried out in *Xenopus* and produced data that proved difficult to analyse. Many of the proteins identified were cytoplasmic contaminants, or annotated as being uncharacterised. Despite these issues, *Xenopus* has the potential to be a very powerful proteomic model organism in the near future. A single *Xenopus* embryo contains enough protein to

carry out mass spectrometry, although more will be needed for the immunoprecipitation style screens as carried out in this thesis (Wühr et al., 2014). A recent study used mass spectrometry to characterise proteins present during the first hours of *Xenopus* development (Smits et al., 2014). These recent studies successfully overcame the problem of removing the abundant yolk proteins that complicated the interpretation of my experiments. However, the issue of matching peptides to an incomplete proteome still remains. By more in depth exome sequencing a more detailed translatome can be derived, which will aid the interpretation of mass spectrometry experiments. Finally, recent work has adapted the INTACT system for use in *Xenopus* (Amin et al., 2014). This technique allows extraction of nuclei from a desired subset of cells within the embryo, allowing cell-type specific examination of nuclear proteins by mass spectrometry. Further elaboration of this system has great potential for expanding our understanding of how proteins interact to control development processes.

7.3 Links between ARID1a, Wnt and Cancer

Many members of the BAF complex are tumour suppressor genes (Yaniv, 2014) including ARID1a (Wang et al., 2004a). High throughput sequencing has identified *ARID1a* mutations in a range of cancers, including ovarian clear cell carcinoma (OCCC), gastric, pancreatic and breast cancer (Jones et al., 2010; Shain et al., 2012; Wang et al., 2011; Wiegand et al., 2010).

Wnt signalling plays a key role in the development and growth of ovarian cancers (Arend et al., 2013). However, activating mutations in the Wnt/β-catenin pathway are rare in ovarian clear cell carcinomas (Dubeau, 2008). The work presented in this thesis shows *ARID1a* is a repressor of Wnt signalling, therefore mutation of *ARID1a* in these carcinomas may provide the upregulation of Wnt signalling characteristic of ovarian tumours. Indeed loss of *ARID1a* is an early event in the progression of OCCC and therefore may act to establish an active-Wnt state that is permissive to cancer formation (Yamamoto et al., 2011). To date, no link has been made between the ability of *ARID1a* to regulate the

Wnt signalling pathways and its role as a tumour suppressor gene. It would therefore be valuable to know whether loss of *ARID1a* in human cancer causes an increase in paracrine Wnt signalling.

C-myc is a well studied oncogene (Conacci-Sorrell et al., 2014). ARID1a binds to the c-myc promoter and inhibits cell cycle progression (Nagl et al., 2006; Nagl et al., 2007). As c-myc is also a target of Wnt signalling (He et al., 1998), ARID1a may be acting at multiple levels to suppress tumour formation. Indeed, ARID1a reportedly binds to p53 and promotes transcription of target genes such as CDKN1a and SMAD3 (Guan et al., 2011). These observations indicate that ARID1a-containing BAF complexes may be key tumour suppressor "nodes" controlling various cell-cycle regulators to prevent proliferation. Further investigation into the molecular functions of ARID1a and its regulatory role within the BAF complex will provide greater understanding of the consequences of ARID1a mutations in human disease.

Appendix

Mass Spectrometry Screen: GFP Interacting Proteins

ACLY	GAPDH	KRT7	PKM2
ACTA1	GART	KRT8	PLEC
ACTB	GFAP	KRT9	POTEE
ACTN1	GMPS	KRT10	POTEF
ACTN2	GNB2	KRT13	POTEKP
ACTN4	GNB2L1	KRT14	PPA1
ACTR2	HIST2H2BF	KRT15	PPP1CA
ACTR3	HNRNPA1	KRT16	PPP1CC
ADD1	HNRNPA2B1	KRT17	PPP1R9B
ADD3	HNRNPA3	KRT18	PPP2CA
AHCY	HNRNPA3	KRT19	PPP2CB
ALB	HNRNPC	KRT24	PRKDC
ANXA2	HNRNPF	KRT25	PRKDC
ARPC2	HNRNPH1	KRT26	PSMC4
CAD	HNRNPK	KRT28	PTBP1
CAPZA1	HNRNPL	KRT32	RCC2
CAPZA2	HNRNPM	KRT37	RPLP0
CCT2	HNRNPU	KRT38	RPSA
CCT3	HSP90AA1	KRT71	RUVBL2
CCT4	HSP90AB1	KRT73	SDHA
CCT5	HSP90AB2P	KRT75	SEC23B
CCT7	HSP90AB4P	KRT76	SERBP1
CCT8	HSP90B1	KRT77	SPTBN1
CLTC	HSPA1A	KRT79	SPTBN2
CORO1C	HSPA1L	KRT80	TCP1
CRKL	HSPA5	KRT81	TMOD3
CTNNA1	HSPA6	KRT84	TP53
CTNNA2	HSPA8	MATR3	TRAP1
CTNNB1	HSPA9	MCM3	TRIM28
DARS	HSPD1	MCM5	TUBA1A
DBN1	HSPD1	MCM7	TUBA1B
DDX1	IPO5	MTHFD1	TUBA1C
DDX17	IQGAP1	MYH9	TUBA4B
DDX3X	IRS4	MYO1C	TUBB
DDX6	JUP	MYO6	TUBB2B
DES	KHSRP	NONO	TUBB3
DHX15	KIF5B	NPM1	TUBB4A
DSG2	KPNB1	PABPC1	TUBB4B
DSP	KRT1	PARP1	TUBB6
EEF1A1	KRT2	PCBP2	TUBB8
EEF2	KRT3	PCM1	TUFM
EIF4A1	KRT4	PDIA3	UBA1
EPPK1	KRT5	PDIA6	VIM
FASN	KRT6A	PFKP	XRCC5
FLNA	KRT6B		

Mass Spectrometry Screen: Proteins Identified From *Xenopus* Lysate

Protein MW (Da)	Mascot Score	Coverage	Gene Name
124428	1948	145%**	MGC80068 protein
56328	1764	207%**	ATP synthase, H+ transporting, mitochondrial F1 complex, beta polypeptide
58006	1461	162%**	SWI/SNF related, matrix associated, actin dependent regulator of chromatin, subfamily d, member 1
113202	1347	90%**	SWI/SNF related, matrix associated, actin dependent regulator of chromatin, subfamily a, member 4
50256	1305	129%**	tubulin, beta 2C
25245	1289	264%**	elogation factor 1 beta
55488	1267	161%**	similar to SWI/SNF related
25274	1191	211%**	elogation factor 1 beta
95821	1056	172%**	SWI/SNF related, matrix associated, actin dependent regulator of chromatin, subfamily c, member 2
136835	911	50%**	SWI/SNF related, matrix associated, actin dependent regulator of chromatin, subfamily c, member 1
72739	878	75%**	heavy-chain binding protein BiP
72489	869	71%**	heat shock 70kDa protein 5 (glucose-regulated protein, 78kDa)
43556	844	209%**	MGC80271 protein
28526	833	173%**	MGC81833 protein
16211	792	259%**	hypothetical protein MGC83076
50714	772	97%**	MGC97820 protein
50739	753	76%**	similar to alpha-Tubulin at 84B
50459	743	70%**	tubulin, beta 6
50559	743	70%**	hypothetical protein MGC52834
50754	737	72%**	hypothetical protein LOC446922
48468	730	195%**	SWI/SNF related, matrix associated, actin dependent regulator of chromatin, subfamily e, member 1
29831	720	133%**	40S ribosomal protein S4
50173	653	96%**	elongation factor 1 gamma
20810	610	210%**	hypothetical protein MGC64263
20938	608	209%**	similar to ribosomal protein L18a
17666	593	161%**	hypothetical protein MGC82306
18737	584	104%**	hypothetical protein MGC64285
22056	579	149%**	ribosomal protein L9
83304	576	56%**	heat shock 90kDa protein beta
45192	555	75%**	ribosomal protein L4
24981	549	153%**	ribosomal protein L10
51771	531	45%**	tubulin, alpha 8
50433	518	139%**	elongation factor 1-alpha O
50505	508	131%**	elongation factor 1 alpha, oocyte form
19868	495	131%**	hypothetical protein LOC100124811
46354	474	117%**	ribosomal protein L3
57612	469	55%**	keratin 5, gene 7
16434	459	117%**	ribosomal protein S16
15274	443	166%**	hypothetical protein MGC64320
96603	419	58%**	eukaryotic translation elongation factor 2
30092	418	74%**	ATP synthase, H+ transporting, mitochondrial F1 complex,

Protein MW (Da)	Mascot Score	Coverage	Gene Name
			gamma polypeptide 1
13101	399	134%**	ribosomal protein L30
224826	394	14%**	laryngeal-specific muscle myosin heavy chain
32610	387	80%**	hypothetical protein MGC82276
50633	386	112%**	elongation factor 1 gamma
22621	375	100%**	ribosomal protein S9
28830	370	54%**	ribosomal Protein, Small subunit (28.1 kD) (rps-6)
54298	359	56%**	MGC86299 protein
50540	355	40%**	mec-12 protein
15930	333	142%**	MGC86316 protein
50775	310	35%**	eukaryotic translation elongation factor 1 alpha 2
50088	309	24%**	hypothetical LOC496021
15571	308	129%**	MGC82841 protein
84539	293	17%**	MGC82579 protein
16655	269	141%**	ribosomal protein L22
24497	257	62%**	RAN, member RAS oncogene family
24280	256	55%**	ribosomal protein L13
50524	245	30%**	eukaryotic translation elongation factor 1 alpha, somatic form
24241	242	70%**	ribosomal protein L13
161626	241	14%**	hypothetical protein LOC443585
50355	237	29%**	hypothetical protein LOC100145396
30092	225	67%**	hypothetical protein LOC100126639
16434	216	135%**	ribosomal protein S14
14956	215	61%**	MGC82808 protein
13339	213	54%**	ribosomal protein S26
55820	212	31%**	keratin 8
33147	204	26%**	solute carrier family 25 (mitochondrial carrier; adenine nucleotide translocator), member 5
9811	189	89%**	ribosomal protein S27
15376	186	135%**	H3 histone, family 3B (H3.3B)
15376	186	135%**	MGC81913 protein
18296	173	37%**	MGC81889 protein
49150	167	26%**	hypothetical protein LOC100037222
58093	166	35%**	MGC81949 protein
13958	159	90%**	hypothetical protein MGC130860
46263	158	30%**	hypothetical protein LOC100145042
42225	153	26%**	similar to actin, alpha 1, skeletal muscle
42225	153	26%**	hypothetical protein LOC779096
60582	151	21%**	aspartyl-tRNA synthetase
54531	151	35%**	hypothetical protein LOC100037087
33351	148	15%**	solute carrier family 25 (mitochondrial carrier; adenine nucleotide translocator), member 4
48943	146	35%**	keratin 12
45615	134	8%**	hypothetical protein MGC68500
46364	129	18%**	hypothetical protein LOC100037184
45007	117	10%**	keratin 8, gene 2
49867	116	8%**	tubulin, beta 4
34208	111	39%**	60S ribosomal protein L5-B
100682	110	6%**	middle molecular weight neurofilament protein NF-M(1)
25109	110	61%**	MGC89303 protein
49716	103	19%**	elongation factor 1 alpha, oocyte form

Protein MW (Da)	Mascot Score	Coverage	Gene Name
13478	96	35%**	variant histone H2A.Zl1
11177	96	91%**	hypothetical protein LOC100049136
40295	94	21%**	NADH dehydrogenase (ubiquinone) 1 alpha subcomplex, 10, 42kDa
18581	93	69%**	ribosomal protein S11
48903	91	17%**	hypothetical LOC493206
13291	91	19%**	hypothetical LOC495401
44829	89	13%**	hypothetical protein LOC100125118
16917	89	24%**	hypothetical protein LOC414678
29282	87	29%**	tyrosine 3-monooxygenase/tryptophan 5-monooxygenase activation protein, epsilon polypeptide
193254	87	8%**	hypothetical LOC496448
42821	86	7%**	hypothetical protein MGC81067
30104	83	18%**	rps3a protein
55547	82	5%**	MGC97634 protein
193019	82	4%**	MGC80936 protein
98225	81	12%**	phosphorylase, glycogen; liver (Hers disease, glycogen storage disease type VI)
12139	80	32%**	hypothetical protein MGC80065
54509	77	8%**	RNA helicase p54
40337	75	5%**	solute carrier family 25 (mitochondrial carrier; phosphate carrier), member 3
17675	75	75%**	MGC89958 protein
24687	74	12%**	hypothetical protein MGC68604
65062	74	9%**	hypothetical protein LOC100189561
87585	72	2%**	hypothetical protein LOC100216266
34580	70	29%**	succinate-CoA ligase, alpha subunit

Mass Spectrometry Screen: Set 1

Protein MW (Da)	Mascot Score	Peptides matched	Coverage	Gene Symbol
185100	6055	257	55%	SMARCA4
133196	5223	270	64%	SMARCC2
123303	3829	238	69%	SMARCC1
42334	3496	220	68%	ACTC1
181794	3356	162	47%	SMARCA2
58481	3291	141	93%	SMARCD1
59112	2722	115	68%	SMARCD2
85630	2436	149	71%	LIMA1
42318	2435	137	46%	ACTBL2
46678	1774	79	73%	SMARCE1
55528	1704	68	73%	INA
80895	1617	90	67%	SCIN
44398	1569	64	78%	SMARCB1
31616	1399	61	63%	CAPZB
55210	1360	67	62%	SMARCD3
18229	1352	62	71%	PPIA
103917	1282	43	16%	ACTN3
47944	1152	70	71%	ACTL6A
22324	1132	72	80%	PRDX1
27025	1093	52	78%	EFHD1
86043	1091	55	43%	GSN
45268	1054	43	60%	DPF2
20761	1054	56	74%	ARPC3
47554	907	27	46%	FLOT1
61720	834	44	48%	CTTN
12639	719	24	71%	MIF
22853	697	41	43%	BCL7A
42381	696	40	37%	ACTA2
38151	686	23	55%	GNB1
22049	678	23	50%	PRDX2
242805	667	45	6%	ARID1A
26842	663	34	73%	RPS3
122858	651	43	12%	POTEI
23511	641	24	57%	BCL7C
229827	634	44	22%	MYH10
37961	625	28	40%	PPP1CB
71610	625	41	38%	ATAD3A
24792	617	18	55%	HPRT1
17114	611	33	64%	AIF1L
111016	579	34	28%	KIF23
16367	570	20	72%	ARPC5
19768	564	19	52%	ARPC4
249417	550	41	24%	SVIL
58168	534	19	37%	KPNA2
13981	529	19	50%	HIST1H2BM
100203	525	28	26%	CDH2
195682	519	25	18%	TJP1
16827	510	23	62%	CALM1

Protein MW (Da)	Mascot Score	Peptides matched	Coverage	Gene Symbol
118740	490	39	14%	POTEJ
27134	485	16	66%	HSD17B10
47434	477	24	48%	FLOT2
18719	468	26	63%	CFL1
53732	465	16	8%	PRPH
18296	459	26	31%	RPS27A
69618	452	30	37%	DDX5
66065	452	23	26%	PPP2R1A
17249	449	13	53%	SSBP1
61054	447	24	37%	PSMD3
116927	447	39	29%	MYO1D
73564	443	26	30%	DDX3Y
17090	436	17	58%	MYL6
97868	433	22	26%	PKP2
23928	424	20	68%	BAG2
28633	396	27	46%	PSMB5
16549	393	22	57%	RPS16
14087	391	18	57%	HIST2H2AA3
73399	381	24	26%	LZTS2
18487	369	11	39%	ACP1
61536	357	17	24%	NEFL
69620	357	14	23%	RBM14
43900	349	17	37%	DPF1
110601	346	23	21%	RAI14
32213	342	26	48%	PGAM5
21935	340	25	48%	LIN7C
80837	340	26	24%	NEXN
33059	339	22	43%	SLC25A5
23682	327	23	72%	SNAP23
30749	323	11	20%	PRDX4
23033	322	12	34%	RPS5
15378	321	13	50%	PFN2
36049	312	7	12%	MYADM
22548	312	15	64%	TAGLN2
197617	311	20	12%	KIAA1671
136532	308	23	18%	CGN
20704	307	14	42%	CNBP
17708	306	17	51%	RPS18
11360	298	19	52%	HIST1H4A
28017	295	13	39%	PRDX3
20468	293	21	31%	RPL11
134104	290	18	15%	TJP2
24792	286	26	55%	PCMT1
29326	286	19	44%	YWHAE
187743	285	12	6%	KIF14
117260	281	11	13%	MPRIP
27838	276	11	19%	PSMA6
85391	275	15	21%	LRCH2
123585	269	15	19%	WDR6
25996	261	18	44%	PSMA2
73098	260	23	17%	ATAD3B
76022	259	17	25%	GAS2L3

Protein MW (Da)	Mascot Score	Peptides matched	Coverage	Gene Symbol
67332	259	8	15%	CTPS1
61276	258	21	25%	YES1
17979	254	9	33%	RPL12
244289	253	25	16%	DOCK7
16434	250	9	31%	RPS14
48090	249	11	11%	ACTR3B
123552	245	16	13%	PPP1R9A
61237	245	13	21%	FYN
68721	240	6	10%	EWSR1
17309	235	16	53%	NME1
14970	234	6	32%	RPL23
17401	232	17	56%	NME2
24579	231	28	38%	RAN
100877	228	9	15%	PSMD2
18398	223	13	26%	PPIAL4A
19839	218	9	47%	MYL12A
53622	217	18	22%	FUS
33073	216	17	27%	SLC25A6
15004	215	15	45%	UBA52
13478	214	14	35%	RPS20
66653	212	12	11%	LMNB1
15597	209	15	178%**	RPS17L
16931	208	13	67%	ARPC5L
19824	207	8	47%	MYL12B
21852	207	15	45%	CSRP2
25133	207	9	34%	PRDX6
26794	202	17	33%	EFHD2
118469	199	16	18%	AMOT
70084	196	30	41%	XRCC6
26700	196	9	25%	PSMB1
47303	192	8	19%	ACTL6B
18839	191	11	40%	CFL2
14083	191	6	35%	HIST1H2AG
20050	190	18	48%	PARK7
28032	188	9	21%	YWHAQ
120772	186	13	12%	LUZP1
17049	185	11	45%	EIF5A
56961	185	8	13%	CAMK2D
12015	184	8	40%	TXN
26565	183	9	34%	PSMA5
29033	181	6	25%	EMD
10530	179	10	51%	DYNLL1
9797	179	10	14%	RPS27
115610	177	7	6%	PPP1R12A
20630	175	14	44%	CAV1
71666	175	21	29%	RACGAP1
12947	172	11	62%	RPL30
18817	172	6	25%	SKP1
84026	167	8	9%	IMMT
27095	167	10	37%	EIF6
93943	167	10	13%	NUP93
69874	164	10	18%	NF2

Protein MW (Da)	Mascot Score	Peptides matched	Coverage	Gene Symbol
63254	162	6	9%	COIL
198016	157	10	7%	KIDINS220
11190	154	7	30%	CSTB
24475	150	6	30%	RPS8
71279	147	14	22%	PLS3
46013	146	11	20%	SS18
18590	139	21	54%	RPS11
21172	137	9	25%	UBE2M
40525	134	8	17%	SLC25A3
8115	127	6	59%	GNG12
26421	127	6	19%	CHCHD3
85762	127	7	10%	PFKL
22993	124	8	40%	PSMB2
67762	124	16	16%	LMNB2
135242	123	10	9%	PLEKHG3
26095	120	15	25%	LIN7A
15725	119	10	31%	ATP6V0C
15436	118	24	63%	HIST2H3A
25151	118	17	41%	UCHL1
28643	116	12	26%	PSMA3
25304	115	13	54%	GRB2
28179	114	11	34%	YWHAB
22239	112	12	53%	BCL7B
14225	111	9	35%	HIST1H2AA
18783	109	9	34%	DCTPP1
27899	108	6	20%	YWHAZ
66701	106	10	14%	FARSB
55688	103	10	28%	C22orf28
30097	99	9	40%	LASP1
63958	96	6	11%	RANGAP1
122531	94	8	10%	AZI1
29264	93	11	23%	RPL7
41722	93	8	21%	ARPC1B
62021	93	7	19%	TAF15
28512	91	7	27%	SNRPA1
132585	91	9	11%	PKP4
70215	91	6	10%	PABPC3
18971	90	8	29%	PTGES3
106795	88	9	10%	PSMD1
13791	87	7	30%	RPS25
57585	85	6	7%	FARSA
58993	85	6	11%	LYN
6900	84	6	19%	RPS29
42113	83	7	21%	ARPC1A
8270	82	6	50%	RPL38
14905	80	8	42%	RPS12
57203	80	6	11%	DNAJC7
29822	78	13	24%	PSMA1
25044	76	9	34%	RPL10
71990	76	6	9%	SSX2IP
14944	75	8	57%	RPS15A
30288	74	7	8%	PSMB7

Protein MW (Da)	Mascot Score	Peptides matched	Coverage	Gene Symbol
10281	73	10	69%	BOLA2
15788	72	12	36%	RPL27
32856	71	8	19%	TPM3

Protein MW (Da)	Mascot Score	Peptides matched	Coverage	Gene Symbol

Mass Spectrometry Screen: Set 2

Protein MW (Da)	Mascot Score	Peptides matched	Coverage	Gene Symbol
133196	6089	281	63%	SMARCC2
185100	5358	225	57%	SMARCA4
123303	4865	276	67%	SMARCC1
58481	3109	107	72%	SMARCD1
47944	2832	125	86%	ACTL6A
181794	2828	150	34%	SMARCA2
44398	2790	109	80%	SMARCB1
42334	2382	140	44%	ACTC1
45268	1975	81	74%	DPF2
46678	1731	76	71%	SMARCE1
42318	1669	108	38%	ACTBL2
59112	1310	66	54%	SMARCD2
55210	1008	48	40%	SMARCD3
35903	880	24	37%	YBX1
28512	823	19	37%	SNRPA1
11360	795	34	54%	HIST1H4A
70263	785	34	17%	HSPA2
14087	693	24	57%	HIST2H2AA3
242805	682	43	9%	ARID1A
13896	621	19	41%	HIST1H2BJ
13944	614	20	41%	HIST1H2BL
103917	610	22	21%	ACTN3
47554	557	19	32%	FLOT1
283140	526	42	11%	HRNR
22853	525	29	43%	BCL7A
23511	512	15	56%	BCL7C
85630	424	34	28%	LIMA1
43900	403	21	41%	DPF1
15436	385	22	57%	HIST2H3A
14113	379	13	35%	HIST3H2A
46365	369	19	31%	RPL3
17708	354	17	50%	RPS18
15509	350	23	57%	HIST1H3A
42381	337	18	33%	ACTA2
17979	327	11	39%	RPL12
19768	320	10	41%	ARPC4
45995	314	23	34%	LANCL1
84531	313	15	20%	GYS1
14970	309	8	38%	RPL23
31616	296	11	37%	CAPZB
76216	292	32	31%	SFPQ
18296	286	16	42%	RPS27A
29807	286	15	41%	RPS4X
14225	281	13	35%	HIST1H2AA
93943	270	11	15%	NUP93
47303	263	8	16%	ACTL6B
32765	263	11	23%	RPL6
229827	245	22	10%	MYH10

Protein MW (Da)	Mascot Score	Peptides matched	Coverage	Gene Symbol
15376	245	20	57%	H3F3A
13987	230	8	35%	HIST2H2AB
87804	229	18	20%	DDX21
45768	225	11	28%	PSMC5
26842	218	7	21%	RPS3
68721	217	6	9%	EWSR1
27899	216	9	28%	YWHAZ
24304	215	10	29%	RPL13
44254	214	14	29%	DPF3
53732	212	8	8%	PRPH
24475	212	7	24%	RPS8
47434	204	11	16%	FLOT2
13501	204	10	62%	H2AFV
31590	202	17	41%	RPS2
29264	195	19	48%	RPL7
24245	195	9	28%	RPL15
29326	193	8	29%	YWHAE
58168	186	7	13%	KPNA2
100877	178	9	9%	PSMD2
16434	173	7	31%	RPS14
49002	169	6	15%	PSMC2
55528	162	13	18%	INA
28235	152	10	41%	RPL8
48090	147	10	14%	ACTR3B
36960	138	7	10%	HNRNPH3
21735	135	7	26%	RPL18
22239	134	7	50%	BCL7B
23531	132	6	22%	RPL14
17248	132	13	33%	RPL26
17212	127	10	42%	RPS13
39764	126	8	26%	H2AFY
46013	124	6	7%	SS18
26872	121	8	27%	ALYREF
69620	111	6	7%	RBM14
24579	105	6	20%	RAN
42113	103	7	19%	ARPC1A
23928	102	9	44%	BAG2
20761	101	10	26%	ARPC3
96250	101	12	16%	HNRNPUL1
15969	99	8	20%	RPS23
30148	94	9	25%	RPL7A
22324	92	7	23%	PRDX1
15795	88	6	31%	RPL28
69618	87	12	13%	DDX5
66065	86	7	10%	PPP2R1A
47719	84	5	13%	PSMD11
47126	84	6	17%	EIF4A3
29822	77	8	13%	PSMA1
42306	75	14	23%	RBMX
18229	74	9	43%	PPIA
12947	71	6	46%	RPL30

Mass Spectrometry Screen: Set 3

Protein MW (Da)	Mascot Score	Peptides matched	Coverage	Gene Symbol
185100	3970	161	49%	SMARCA4
133196	3964	202	63%	SMARCC2
123303	3524	206	69%	SMARCC1
42334	2983	187	50%	ACTC1
181794	2339	112	35%	SMARCA2
58481	2284	92	72%	SMARCD1
47944	1965	100	58%	ACTL6A
44398	1954	84	77%	SMARCB1
42318	1818	121	38%	ACTBL2
45268	1606	56	70%	DPF2
46678	1522	68	73%	SMARCE1
59112	1256	56	50%	SMARCD2
70263	885	31	15%	HSPA2
103917	794	25	12%	ACTN3
85630	701	58	46%	LIMA1
14087	663	17	50%	HIST2H2AA3
229827	648	38	19%	MYH10
118740	637	35	6%	POTEJ
55210	632	31	25%	SMARCD3
13942	611	15	35%	HIST1H2BB
13981	600	15	36%	HIST1H2BM
43900	599	22	42%	DPF1
22853	533	29	35%	BCL7A
76216	503	28	35%	SFPQ
242805	499	36	7%	ARID1A
47554	473	16	27%	FLOT1
11360	460	23	52%	HIST1H4A
45995	447	25	37%	LANCL1
28512	444	15	42%	SNRPA1
31616	422	18	41%	CAPZB
96250	332	14	17%	HNRNPUL1
38151	312	15	35%	GNB1
17979	308	9	24%	RPL12
19768	298	14	48%	ARPC4
15436	293	16	49%	HIST2H3A
73564	280	16	17%	DDX3Y
35903	277	11	31%	YBX1
44254	266	7	11%	DPF3
23511	259	7	48%	BCL7C
26842	258	9	27%	RPS3
55528	256	18	39%	INA
47303	255	8	16%	ACTL6B
18296	252	14	37%	RPS27A
15004	252	14	44%	UBA52
15509	244	14	49%	HIST1H3A
26872	238	9	34%	ALYREF
45768	231	10	21%	PSMC5
37961	230	9	24%	PPP1CB
53732	226	9	8%	PRPH
47434	224	10	23%	FLOT2

Protein MW (Da)	Mascot Score	Peptides matched	Coverage	Gene Symbol
46365	220	8	22%	RPL3
122858	215	12	7%	POTEI
16434	214	8	22%	RPS14
17708	214	9	41%	RPS18
20761	210	15	52%	ARPC3
29807	205	13	37%	RPS4X
100877	204	7	12%	PSMD2
80895	201	9	18%	SCIN
42381	196	14	25%	ACTA2
15376	196	13	49%	H3F3A
42113	192	11	36%	ARPC1A
29264	182	13	30%	RPL7
86043	162	10	12%	GSN
28235	156	8	28%	RPL8
283140	150	18	6%	HRNR
31590	149	13	32%	RPS2
23928	138	13	44%	BAG2
249417	137	13	8%	SVIL
24304	117	10	27%	RPL13
84531	116	7	14%	GYS1
24245	116	6	21%	RPL15
29326	111	6	21%	YWHAE
45581	108	8	25%	DNAJA1
15969	107	8	23%	RPS23
69618	102	6	8%	DDX5
15788	96	6	20%	RPL27
18229	75	9	53%	PPIA
51480	72	8	24%	TUBG1

Bibliography

Agius, E., Oelgeschläger, M., Wessely, O., Kemp, C. and De Robertis, E. M. (2000). Endodermal Nodal-related signals and mesoderm induction in Xenopus. *Development* **127**, 1173–1183.

Alessio, N., Squillaro, T., Cipollaro, M., Bagella, L., Giordano, A. and Galderisi, U. (2010). The BRG1 ATPase of chromatin remodeling complexes is involved in modulation of mesenchymal stem cell senescence through RB–P53 pathways. *Oncogene* **29**, 5452–5463.

Alexandre, C., Baena-Lopez, A. and Vincent, J.-P. (2014). Patterning and growth control by membrane-tethered Wingless. *Nature* **505**, 180–185.

Amin, N. M., Greco, T. M., Kuchenbrod, L. M., Rigney, M. M., Chung, M.-I., Wallingford, J. B., Cristea, I. M. and Conlon, F. L. (2014). Proteomic profiling of cardiac tissue by isolation of nuclei tagged in specific cell types (INTACT). *Development* **141**, 962–973.

Amit, S., Hatzubai, A., Birman, Y., Andersen, J. S., Ben-Shushan, E., Mann, M., Ben-Neriah, Y. and Alkalay, I. (2002). Axin-mediated CKI phosphorylation of β-catenin at Ser 45: a molecular switch for the Wnt pathway. *Genes & ….*

Aoyagi, S. and Hayes, J. J. (2002). hSWI/SNF-Catalyzed Nucleosome Sliding Does Not Occur Solely via a Twist-Diffusion Mechanism. *Molecular and Cellular Biology* **22**, 7484–7490.

Arend, R. C., Londoño-Joshi, A. I., Straughn, J. M. and Buchsbaum, D. J. (2013). The Wnt/β-catenin pathway in ovarian cancer: a review. *Gynecol. Oncol.* **131**, 772–779.

Armstrong, J. A., Papoulas, O., Daubresse, G., Sperling, A. S., Lis, J. T., Scott, M. P. and Tamkun, J. W. (2002). The Drosophila BRM complex facilitates global transcription by RNA polymerase II. *The EMBO Journal* **21**, 5245–5254.

Arun, G., Akhade, V. S., Donakonda, S. and Rao, M. R. S. (2012). mrhl RNA, a Long Noncoding RNA, Negatively Regulates Wnt Signaling through Its Protein Partner Ddx5/p68 in Mouse Spermatogonial Cells. *Molecular and Cellular Biology* **32**, 3140–3152.

Asp, P., Wihlborg, M., Karlén, M. and Farrants, A.-K. Ö. (2002). Expression of BRG1, a human SWI/SNF component, affects the organisation of actin filaments through the RhoA signalling pathway. *Journal of Cell Science* **115**, 2735–2746.

Atcha, F. A., Syed, A., Wu, B., Hoverter, N. P., Yokoyama, N. N., Ting, J. H. T., Munguia, J. E., Mangalam, H. J., Marsh, J. L. and Waterman, M. L. (2007). A Unique DNA Binding Domain Converts T-Cell Factors into Strong Wnt Effectors. *Molecular and Cellular Biology* **27**, 8352–8363.

Atkins, R. J., Stylli, S. S., Luwor, R. B., Kaye, A. H. and Hovens, C. M. (2013). Journal of Clinical Neuroscience. *Journal of Clinical Neuroscience* **20**, 1185–1192.

Baarsma, H. A., Königshoff, M. and Gosens, R. (2013). The WNT signaling pathway from ligand secretion to gene transcription: molecular mechanisms and pharmacological targets. *Pharmacol. Ther.* **138**, 66–83.

Bafico, A., Gazit, A., Pramila, T., Finch, P. W., Yaniv, A. and Aaronson, S. A. (1999). Interaction of frizzled related protein (FRP) with Wnt ligands and the frizzled receptor suggests alternative mechanisms for FRP inhibition of Wnt signaling. *J. Biol. Chem.* **274**, 16180–16187.

Baig, J., Chanut, F., Kornberg, T. B. and Klebes, A. (2010). The Chromatin-Remodeling Protein Osa Interacts With CyclinE in Drosophila Eye Imaginal Discs. *Genetics* **184**, 731–744.

Barker, N. and Clevers, H. (2006). Mining the Wnt pathway for cancer therapeutics. *Nat Rev Drug Discov* **5**, 997–1014.

Barker, N., Hurlstone, A., Musisi, H., Miles, A., Bienz, M. and Clevers, H. (2001). The chromatin remodelling factor Brg-1 interacts with β-catenin to promote target gene activation. *The EMBO Journal* **20**, 4935–4943.

Bartscherer, K., Pelte, N., Ingelfinger, D. and Boutros, M. (2006). Secretion of Wnt Ligands Requires Evi, a Conserved Transmembrane Protein. *Cell* **125**, 523–533.

Bates, G. J., Nicol, S. M., Wilson, B. J., Jacobs, A.-M. F., Bourdon, J.-C., Wardrop, J., Gregory, D. J., Lane, D. P., Perkins, N. D. and Fuller-Pace, F. V. (2005). The DEAD box protein p68: a novel transcriptional coactivator of the p53 tumour suppressor. *The EMBO Journal* **24**, 543–553.

Batsché, E., Yaniv, M. and Muchardt, C. (2005). The human SWI/SNF subunit Brm is a regulator of alternative splicing. *Nat Struct Mol Biol* **13**, 22–29.

Bazett-Jones, D. P., Côté, J., Landel, C. C., Peterson, C. L. and Workman, J. L. (1999). The SWI/SNF complex creates loop domains in DNA and polynucleosome arrays and can disrupt DNA-histone contacts within these domains. *Molecular and Cellular Biology* **19**, 1470–1478.

Bänziger, C., Soldini, D., Schütt, C., Zipperlen, P., Hausmann, G. and Basler, K. (2006). Wntless, a Conserved Membrane Protein Dedicated to the Secretion of Wnt Proteins from Signaling Cells. *Cell* **125**, 509–522.

Behrens, J., Jerchow, B.-A., Würtele, M., Grimm, J., Asbrand, C., Wirtz, R., Kühl, M., Wedlich, D. and Birchmeier, W. (1998). Functional interaction of an axin homolog, conductin, with β-catenin, APC, and GSK3β. *Science* **280**, 596–599.

Beisner, J., Teltschik, Z., Ostaff, M. J., Tiemessen, M. M., Staal, F. J., Wang, G.,

Gersemann, M., Perminow, G., Vatn, M. H., Schwab, M., et al. (2014). TCF-1 mediated Wnt Signaling regulates Paneth cell innate immune defense effectors HD-5 and -6: implications for Crohn's disease. *Am. J. Physiol. Gastrointest. Liver Physiol.*

Belo, J. A., Bachiller, D., Agius, E., Kemp, C., Borges, A. C., Marques, S., Piccolo, S. and De Robertis, E. M. (2000). Cerberus-like is a secreted BMP and nodal antagonist not essential for mouse development. *Genesis* **26**, 265–270.

Ben Steventon and Mayor, R. (2012). Developmental Biology. *Developmental Biology* **365**, 196–207.

Berendsen, A. D., Fisher, L. W., Kilts, T. M., Owens, R. T., Robey, P. G., Gutkind, J. S. and Young, M. F. (2011). Modulation of canonical Wnt signaling by the extracellular matrix component biglycan. *Proc. Natl. Acad. Sci. U.S.A.* **108**, 17022–17027.

Berndt, J. D., Aoyagi, A., Yang, P., Anastas, J. N., Tang, L. and Moon, R. T. (2011). Mindbomb 1, an E3 ubiquitin ligase, forms a complex with RYK to activate Wnt/ -catenin signaling. *J. Cell Biol.* **194**, 737–750.

Bhambhani, C., Chang, J. L., Akey, D. L. and Cadigan, K. M. (2011). The oligomeric state of CtBP determines its role as a transcriptional co-activator and co-repressor of Wingless targets. *The EMBO Journal* **30**, 2031–2043.

Bhanot, P., Brink, M., Samos, C. H., Hsieh, J.-C., Wang, Y., Macke, J. P., Andrew, D., Nathans, J. and Nusse, R. (1996). A new member of the frizzled family from Drosophila functions as a Wingless receptor. *Nature* **382**, 225–230.

Bilic, J., Huang, Y.-L., Davidson, G., Zimmermann, T., Cruciat, C.-M., Bienz, M. and Niehrs, C. (2007). Wnt induces LRP6 signalosomes and promotes dishevelled-dependent LRP6 phosphorylation. *Science* **316**, 1619–1622.

Bisbee, C. A., Baker, M. A., Wilson, A. C., Haji-Azimi, I. and Fischberg, M. (1977). Albumin phylogeny for clawed frogs (Xenopus). *Science* **195**, 785–787.

Blenk, S., Engelmann, J., Weniger, M., Schultz, J., Dittrich, M., Rosenwald, A., Müller-Hermelink, H. K., Müller, T. and Dandekar, T. (2007). Germinal center B cell-like (GCB) and activated B cell-like (ABC) type of diffuse large B cell lymphoma (DLBCL): analysis of molecular predictors, signatures, cell cycle state and patient survival. *Cancer Inform* **3**, 399–420.

Blythe, S. A., Cha, S.-W., Tadjuidje, E., Heasman, J. and Klein, P. S. (2010). beta-Catenin primes organizer gene expression by recruiting a histone H3 arginine 8 methyltransferase, Prmt2. *Developmental Cell* **19**, 220–231.

Boeger, H., Griesenbeck, J., Strattan, J. S. and Kornberg, R. D. (2004). Removal of Promoter Nucleosomes by Disassembly Rather Than Sliding In Vivo. *Molecular Cell*.

Boon, C. J. F., Hollander, den, A. I., Hoyng, C. B., Cremers, F. P. M., Klevering, B. J. and Keunen, J. E. E. (2008). The spectrum of retinal dystrophies caused by mutations in the peripherin/RDS gene. *Progress in Retinal and Eye Research* **27**, 213–235.

Bordonaro, M., Lazarova, D. L. and Sartorelli, A. C. (2008). Role of Tcf-DNA binding and the chromatin remodeling factor Brg-1 in the modulation of Wnt activity by butyrate. *Cell Cycle* **7**, 3472–3473.

Bourhis, E., Tam, C., Franke, Y., Bazan, J. F., Ernst, J., Hwang, J., Costa, M., Cochran, A. G. and Hannoush, R. N. (2010). Reconstitution of a frizzled8.Wnt3a.LRP6 signaling complex reveals multiple Wnt and Dkk1 binding sites on LRP6. *Journal of Biological Chemistry* **285**, 9172–9179.

Bouwmeester, T., Kim, S., Sasai, Y., Lu, B. and De Robertis, E. M. (1996). Cerberus is a head-inducing secreted factor expressed in the anterior endoderm of Spemann's organizer. *Nature* **382**, 595–601.

Boyden, L. M., Mao, J., Belsky, J., Mitzner, L., Farhi, A., Mitnick, M. A., Wu, D., Insogna, K. and Lifton, R. P. (2002). High bone density due to a mutation in LDL-receptor-related protein 5. *N Engl J Med* **346**, 1513–1521.

Brannon, M., Gomperts, M., Sumoy, L., Moon, R. T. and Kimelman, D. (1997). A β-catenin/XTcf-3 complex binds to thesiamois promoter to regulate dorsal axis specification in Xenopus. *Genes & Development* **11**, 2359–2370.

Brantjes, H., Roose, J., van de Wetering, M. and Clevers, H. (2001). All Tcf HMG box transcription factors interact with Groucho-related co-repressors. *Nucleic Acids Research* **29**, 1410–1419.

Bruno, M., Flaus, A., Stockdale, C., Rencurel, C., Ferreira, H. and Owen-Hughes, T. (2003). Histone H2A/H2B Dimer Exchange by ATP-Dependent Chromatin Remodeling Activities. *Molecular Cell* **12**, 1599–1606.

Bultman, S., Gebuhr, T., Yee, D., La Mantia, C., Nicholson, J., Gilliam, A., Randazzo, F., Metzger, D., Chambon, P. and Crabtree, G. (2000). A Brg1 Null Mutation in the Mouse Reveals Functional Differences among Mammalian SWI/SNF Complexes. *Molecular Cell* **6**, 1287–1295.

Cadigan, K. M. (2012). TCFs and Wnt/ b-catenin signaling: more than one way to throw the switch. *Curr. Top. Dev. Biol.* **98**, 1–34.

Cairns, B. R., Kim, Y.-J., Sayre, M. H., Laurent, B. C. and Kornberg, R. D. (1994). A multisubunit complex containing the SWI1/ADR6, SWI2/SNF2, SWI3, SNF5, and SNF6 gene products isolated from yeast. *Proc. Natl. Acad. Sci. U.S.A.* **91**, 1950–1954.

Cairns, B. R., Lorch, Y., Li, Y., Zhang, M., Lacomis, L., Erdjument-Bromage, H., Tempst, P., Du, J., Laurent, B. and Kornberg, R. D. (1996). RSC, an essential, abundant chromatin-remodeling complex. *Cell* **87**, 1249–1260.

Callery, E. M., Smith, J. C. and Thomsen, G. H. (2005). The ARID domain protein dril1 is necessary for TGF(beta) signaling in Xenopus embryos. *Developmental Biology* **278**, 542–559.

Carbone, A., Bernardini, L., Valenzano, F., Bottillo, I., De Simone, C., Capizzi, R., Capalbo, A., Romano, F., Novelli, A., Dallapiccola, B., et al. (2008). Array-based comparative genomic hybridization in early-stage mycosis fungoides: recurrent deletion of tumor suppressor genes BCL7A, SMAC/DIABLO, and RHOF. *Genes Chromosom. Cancer* **47**, 1067–1075.

Caretti, G., Schiltz, R. L., Dilworth, F. J., Di Padova, M., Zhao, P., Ogryzko, V., Fuller-Pace, F. V., Hoffman, E. P., Tapscott, S. J. and Sartorelli, V. (2006). The RNA Helicases p68/p72 and the Noncoding RNA SRA Are Coregulators of MyoD and Skeletal Muscle Differentiation. *Developmental Cell* **11**, 547–560.

Carmon, K. S., Gong, X., Lin, Q., Thomas, A. and Liu, Q. (2011). R-spondins function as ligands of the orphan receptors LGR4 and LGR5 to regulate Wnt/beta-catenin signaling. *Proc. Natl. Acad. Sci. U.S.A.* **108**, 11452–11457.

Carnac, G., Kodjabachian, L., Gurdon, J. B. and Lemaire, P. (1996). The homeobox gene Siamois is a target of the Wnt dorsalisation pathway and triggers organiser activity in the absence of mesoderm. *Development* **122**, 3055–3065.

Carrera, I., Janody, F., Leeds, N., Duveau, F. and Treisman, J. E. (2008). Pygopus activates Wingless target gene transcription through the mediator complex subunits Med12 and Med13. *Proc. Natl. Acad. Sci. U.S.A.* **105**, 6644–6649.

Carron, C., Pascal, A., Djiane, A., Boucaut, J.-C., Shi, D.-L. and Umbhauer, M. (2003). Frizzled receptor dimerization is sufficient to activate the Wnt/beta-catenin pathway. *Journal of Cell Science* **116**, 2541–2550.

Cavallo, R. A., Cox, R. T., Moline, M. M., Roose, J., Polevoy, G. A., Clevers, H., Peifer, M. and Bejsovec, A. (1998). Drosophila Tcf and Groucho interact to repress Wingless signalling activity. *Nature* **395**, 604–608.

Chandler, R. L., Brennan, J., Schisler, J. C., Serber, D., Patterson, C. and Magnuson, T. (2012). ARID1a-DNA Interactions Are Required for Promoter Occupancy by SWI/SNF. *Molecular and Cellular Biology* **33**, 265–280.

Chen, G., Fernandez, J., Mische, S. and Courey, A. J. (1999). A functional interaction between the histone deacetylase Rpd3 and the corepressor groucho in Drosophila development. *Genes & Development* **13**, 2218–2230.

Chen, J., Luo, Q., Yuan, Y., Huang, X., Cai, W., Li, C., Wei, T., Zhang, L., Yang, M., Liu, Q., et al. (2010). Pygo2 associates with MLL2 histone methyltransferase and GCN5 histone acetyltransferase complexes to augment Wnt target gene expression and breast cancer stem-like cell expansion. *Molecular and Cellular*

Biology **30**, 5621–5635.

Cheng, S.-W. G., Davies, K. P., Yung, E., Beltran, R. J., Yu, J. and Kalpana, G. V. (1999). c-MYC interacts with INI1/hSNF5 and requires the SWI/SNF complex for transactivation function. *Nature Genetics* **22**, 102–105.

Ching, W., Hang, H. C. and Nusse, R. (2008). Lipid-independent Secretion of a Drosophila Wnt Protein. *Journal of Biological Chemistry* **283**, 17092–17098.

Clapier, C. R. and Cairns, B. R. (2009). The Biology of Chromatin Remodeling Complexes. *Annu. Rev. Biochem.* **78**, 273–304.

Clark, E. L., Hadjimichael, C., Temperley, R., Barnard, A., Fuller-Pace, F. V. and Robson, C. N. (2013). p68/DdX5 Supports β-Catenin & RNAP II during Androgen Receptor Mediated Transcription in Prostate Cancer. *PLoS ONE* **8**, e54150.

Clevers, H. (2006). Wnt/β-Catenin Signaling in Development and Disease. *Cell* **127**, 469–480.

Collins, R. T. and Treisman, J. E. (2000). Osa-containing Brahma chromatin remodeling complexes are required for the repression of wingless target genes. *Genes & Development* **14**, 3140–3152.

Collins, R. T., Furukawa, T., Tanese, N. and Treisman, J. E. (1999). Osa associates with the Brahma chromatin remodeling complex and promotes the activation of some target genes. *The EMBO Journal* **18**, 7029–7040.

Colombres, M., Henríquez, J. P., Reig, G. F., Scheu, J., Calderón, R., Alvarez, A., Brandan, E. and Inestrosa, N. C. (2008). Heparin activates Wnt signaling for neuronal morphogenesis. *J. Cell. Physiol.* **216**, 805–815.

Conacci-Sorrell, M., McFerrin, L. and Eisenman, R. N. (2014). An Overview of MYC and Its Interactome. *Cold Spring Harbor Perspectives in Medicine* **4**, a014357–a014357.

Cong, F., Schweizer, L. and Varmus, H. (2004). Wnt signals across the plasma membrane to activate the beta-catenin pathway by forming oligomers containing its receptors, Frizzled and LRP. *Development* **131**, 5103–5115.

Corey, L. L., Weirich, C. S., Benjamin, I. J. and Kingston, R. E. (2003). Localized recruitment of a chromatin-remodeling activity by an activator in vivo drives transcriptional elongation. *Genes & Development* **17**, 1392–1401.

Côté, J., Peterson, C. L. and Workman, J. L. (1998). Perturbation of nucleosome core structure by the SWI/SNF complex persists after its detachment, enhancing subsequent transcription factor binding. *Proc. Natl. Acad. Sci. U.S.A.* **95**, 4947–4952.

Cselenyi, C. S. and Lee, E. (2008). Context-Dependent Activation or Inhibition of Wnt- -Catenin Signaling by Kremen. *Science Signaling* **1**, pe10–pe10.

Curtis, B. J., Zraly, C. B., Marenda, D. R. and Dingwall, A. K. (2011). Developmental Biology. *Developmental Biology* **350**, 534–547.

Czaja, W., Mao, P. and Smerdon, M. J. (2014). Chromatin remodelling complex RSC promotes base excision repair in chromatin of Saccharomyces cerevisiae. *DNA Repair* **16**, 35–43.

Dacwag, C. S., Bedford, M. T., Sif, S. and Imbalzano, A. N. (2009). Distinct Protein Arginine Methyltransferases Promote ATP-Dependent Chromatin Remodeling Function at Different Stages of Skeletal Muscle Differentiation. *Molecular and Cellular Biology* **29**, 1909–1921.

Dajani, R., Fraser, E., Roe, S. M., Yeo, M., Good, V. M., Thompson, V., Dale, T. C. and Pearl, L. H. (2003). Structural basis for recruitment of glycogen synthase kinase 3β to the axin—APC scaffold complex. *The EMBO Journal* **22**, 494–501.

Dallas, P. B., Pacchione, S., Wilsker, D., Bowrin, V., Kobayashi, R. and Moran, E. (2000). The Human SWI-SNF Complex Protein p270 Is an ARID Family Member with Non-Sequence-Specific DNA Binding Activity. *Molecular and Cellular Biology* **20**, 3137–3146.

Damelin, M., Simon, I., Moy, T. I., Wilson, B., Komili, S., Tempst, P., Roth, F. P., Young, R. A., Cairns, B. R. and Silver, P. A. (2002). The genome-wide localization of Rsc9, a component of the RSC chromatin-remodeling complex, changes in response to stress. *Molecular Cell* **9**, 563–573.

Daniels, D. L. and Weis, W. I. (2005). β-catenin directly displaces Groucho/TLE repressors from Tcf/Lef in Wnt-mediated transcription activation. *Nat Struct Mol Biol* **12**, 364–371.

Dann, C. E., Hsieh, J. C., Rattner, A., Sharma, D., Nathans, J. and Leahy, D. J. (2001). Insights into Wnt binding and signalling from the structures of two Frizzled cysteine-rich domains. *Nature* **412**, 86–90.

Das, A. V., James, J., Bhattacharya, S., Imbalzano, A. N., Antony, M. L., Hegde, G., Zhao, X., Mallya, K., Ahmad, F., Knudsen, E., et al. (2007). SWI/SNF Chromatin Remodeling ATPase Brm Regulates the Differentiation of Early Retinal Stem Cells/Progenitors by Influencing Brn3b Expression and Notch Signaling. *Journal of Biological Chemistry* **282**, 35187–35201.

Davidson, G., Wu, W., Shen, J., Bilic, J., Fenger, U., Stannek, P., Glinka, A. and Niehrs, C. (2005). Casein kinase 1 gamma couples Wnt receptor activation to cytoplasmic signal transduction. *Nature* **438**, 867–872.

de Lau, W. B. M., Snel, B. and Clevers, H. C. (2012). The R-spondin protein family. *Genome Biol.* **13**, 242.

De Robertis, E. M. (2009). Spemann's organizer and the self-regulation of embryonic fields. *Mechanisms of Development* **126**, 925–941.

De Robertis, E. M. and Kuroda, H. (2004). Dorsal-ventral patterning and neural induction in Xenopus embryos. *Annu. Rev. Cell Dev. Biol.* **20**, 285–308.

Dechassa, M. L., Sabri, A., Pondugula, S. and Kassabov, S. R. (2010). SWI/SNF Has Intrinsic Nucleosome Disassembly Activity that Is Dependent on Adjacent Nucleosomes. *Molecular Cell*.

Dechassa, M. L., Zhang, B., Horowitz-Scherer, R., Persinger, J., Woodcock, C. L., Peterson, C. L. and Bartholomew, B. (2008). Architecture of the SWI/SNF-Nucleosome Complex. *Molecular and Cellular Biology* **28**, 6010–6021.

Deindl, S., Hwang, W. L., Hota, S. K., Blosser, T. R., Prasad, P., Bartholomew, B. and Zhuang, X. (2013). ISWI Remodelers Slide Nucleosomes with Coordinated Multi-Base-Pair Entry Steps and Single-Base-Pair Exit Steps. *Cell* **152**, 442–452.

Doble, B. W., Patel, S., Wood, G. A., Kockeritz, L. K. and Woodgett, J. R. (2007). Functional Redundancy of GSK-3α and GSK-3β in Wnt/β-Catenin Signaling Shown by Using an Allelic Series of Embryonic Stem Cell Lines. *Developmental Cell* **12**, 957–971.

Domingos, P. M., Itasaki, N., Jones, C. M., Mercurio, S., Sargent, M. G., Smith, J. C. and Krumlauf, R. (2001). The Wnt/β-Catenin Pathway Posteriorizes Neural Tissue in Xenopus by an Indirect Mechanism Requiring FGF Signalling. *Developmental Biology* **239**, 148–160.

Domingos, P. M., Obukhanych, T. V., Altmann, C. R. and Hemmati-Brivanlou, A. (2002). Cloning and developmental expression of Baf57 in Xenopus laevis. *Mechanisms of Development* **116**, 177–181.

Doubravska, L., Krausova, M., Gradl, D., Vojtechova, M., Tumova, L., Lukas, J., Valenta, T., Pospichalova, V., Fafilek, B., Plachy, J., et al. (2011). Cellular Signalling. *Cellular Signalling* **23**, 837–848.

Dubeau, L. (2008). The cell of origin of ovarian epithelial tumours. *Lancet Oncol.* **9**, 1191–1197.

Dubruc, E., Putoux, A., Labalme, A., Rougeot, C., Sanlaville, D. and Edery, P. (2014). A new intellectual disability syndrome caused by CTNNB1haploinsufficiency. *Am. J. Med. Genet.* **164**, 1571–1575.

Egel, R., Beach, D. H. and Klar, A. J. (1984). Genes required for initiation and resolution steps of mating-type switching in fission yeast. *Proc. Natl. Acad. Sci. U.S.A.* **81**, 3481–3485.

Egger-Adam, D. and Katanaev, V. L. (2009). The trimeric G protein Go inflicts a double impact on axin in the Wnt/frizzled signaling pathway. *Dev. Dyn.* NA–NA.

Eklof Spink, K. (2001). Molecular mechanisms of beta-catenin recognition by

adenomatous polyposis coli revealed by the structure of an APC-beta-catenin complex. *The EMBO Journal* **20**, 6203–6212.

Elfring, L. K., Daniel, C., Papoulas, O., Deuring, R., Sarte, M., Moseley, S., Beek, S. J., Waldrip, W. R., Daubresse, G., DePace, A., et al. (1998). Genetic analysis of brahma: the Drosophila homolog of the yeast chromatin remodeling factor SWI2/SNF2. *Genetics* **148**, 251–265.

Elfring, L. K., Deuring, R., McCallum, C. M., Peterson, C. L. and Tamkun, J. W. (1994). Identification and characterization of Drosophila relatives of the yeast transcriptional activator SNF2/SWI2. *Molecular and Cellular Biology* **14**, 2225–2234.

Elinson, R. P. and Holowacz, T. (1995). Specifying the dorsoanterior axis in frogs: 70 years since Spemann and Mangold. *Curr. Top. Dev. Biol.* **30**, 253–285.

Elkouby, Y. M. and Frank, D. (2010). *Wnt/β-Catenin Signaling in Vertebrate Posterior Neural Development*. San Rafael (CA): Morgan & Claypool Life Sciences.

Elkouby, Y. M., Elias, S., Casey, E. S., Blythe, S. A., Tsabar, N., Klein, P. S., Root, H., Liu, K. J. and Frank, D. (2010). Mesodermal Wnt signaling organizes the neural plate via Meis3. *Development* **137**, 1531–1541.

Evans, B. J., Kelley, D. B., Tinsley, R. C., Melnick, D. J. and Cannatella, D. C. (2004). A mitochondrial DNA phylogeny of African clawed frogs: phylogeography and implications for polyploid evolution. *Molecular Phylogenetics and Evolution* **33**, 197–213.

Finch, P. W., He, X., Kelley, M. J., Uren, A., Schaudies, R. P., Popescu, N. C., Rudikoff, S., Aaronson, S. A., Varmus, H. E. and Rubin, J. S. (1997). Purification and molecular cloning of a secreted, Frizzled-related antagonist of Wnt action. *Proc. Natl. Acad. Sci. U.S.A.* **94**, 6770–6775.

Franch-Marro, X., Wendler, F., Griffith, J., Maurice, M. M. and Vincent, J. P. (2008). In vivo role of lipid adducts on Wingless. *Journal of Cell Science* **121**, 1587–1592.

Fryer, C. J. and Archer, T. K. (1998). Chromatin remodelling by the glucocorticoid receptor requires the BRG1 complex. *Nature* **393**, 88–91.

Fukuda, T., Yamagata, K., Fujiyama, S., Matsumoto, T., Koshida, I., Yoshimura, K., Mihara, M., Naitou, M., Endoh, H., Nakamura, T., et al. (2007). DEAD-box RNA helicase subunits of the Drosha complex are required for processing of rRNA and a subset of microRNAs. *Nat. Cell Biol.* **9**, 604–611.

Galli, L. M., Barnes, T., Cheng, T., Acosta, L., Anglade, A., Willert, K., Nusse, R. and Burrus, L. W. (2006). Differential inhibition of Wnt-3a by Sfrp-1, Sfrp-2, and Sfrp-3. *Dev. Dyn.* **235**, 681–690.

Gan, X. Q., Wang, J. Y., Xi, Y., Wu, Z. L., Li, Y. P. and Li, L. (2008). Nuclear Dvl, c-Jun, -catenin, and TCF form a complex leading to stabiLization of -catenin-TCF interaction. *J. Cell Biol.* **180**, 1087–1100.

Gao, X. and Hannoush, R. N. (2013). Single-cell imaging of Wnt palmitoylation by the acyltransferase porcupine. *Nat Chem Biol* **10**, 61–68.

Gao, X., Tate, P., Hu, P., Tjian, R., Skarnes, W. C. and Wang, Z. (2008). ES cell pluripotency and germ-layer formation require the SWI/SNF chromatin remodeling component BAF250a. *Proc. Natl. Acad. Sci. U.S.A.* **105**, 6656–6661.

Gauci, S., Helbig, A. O., Slijper, M., Krijgsveld, J., Heck, A. J. R. and Mohammed, S. (2009). Lys-N and Trypsin Cover Complementary Parts of the Phosphoproteome in a Refined SCX-Based Approach. *Anal. Chem.* **81**, 4493–4501.

Gerhart, J. C. (1999). Pieter Nieuwkoop's contributions to the understanding of meso-endoderm induction and neural induction in chordate development. *Int. J. Dev. Biol.* 1–9.

Gingras, A.-C., Gstaiger, M., Raught, B. and Aebersold, R. (2007). Analysis of protein complexes using mass spectrometry. *Nat Rev Mol Cell Biol* **8**, 645–654.

Glinka, A., Delius, H., Blumenstock, C. and Niehrs, C. (1996). Combinatorial signalling by Xwnt-11 and Xnr3 in the organizer ephithelium. *Mechanisms of Development* **60**, 221–231.

Glinka, A., Wu, W., Delius, H., Monaghan, A. P., Blumenstock, C. and Niehrs, C. (1998). Dickkopf-1 is a member of a new family of secreted proteins and functions in head induction. *Nature* **391**, 357–362.

Goljanek-Whysall, K., Mok, G. F., Fahad Alrefaei, A., Kennerley, N., Wheeler, G. N. and Munsterberg, A. (2014). myomiR-dependent switching of BAF60 variant incorporation into Brg1 chromatin remodeling complexes during embryo myogenesis. *Development* **141**, 3378–3387.

Gong, Y., Slee, R. B., Fukai, N., Rawadi, G., Roman-Roman, S., Reginato, A. M., Wang, H., Cundy, T., Glorieux, F. H., Lev, D., et al. (2001). LDL receptor-related protein 5 (LRP5) affects bone accrual and eye development. *Cell* **107**, 513–523.

Goodman, R. M., Thombre, S., Firtina, Z., Gray, D., Betts, D., Roebuck, J., Spana, E. P. and Selva, E. M. (2006). Sprinter: a novel transmembrane protein required for Wg secretion and signaling. *Development* **133**, 4901–4911.

Götz, M. and Huttner, W. B. (2005). The cell biology of neurogenesis. *Nat Rev Mol Cell Biol* **6**, 777–788.

Graham, T. A., Clements, W. K., Kimelman, D. and Xu, W. (2002). The crystal structure of the beta-catenin/ICAT complex reveals the inhibitory mechanism of ICAT. *Molecular Cell* **10**, 563–571.

Grant, P. and Wacaster, J. F. (1972). The amphibian gray crescent region--a site of developmental information? *Developmental Biology* **28**, 454–471.

Grant, S. F. A., Thorleifsson, G., Reynisdottir, I., Benediktsson, R., Manolescu, A., Sainz, J., Helgason, A., Stefansson, H., Emilsson, V., Helgadottir, A., et al. (2006). Variant of transcription factor 7-like 2 (TCF7L2) gene confers risk of type 2 diabetes. *Nature Genetics* **38**, 320–323.

Green, J. B., New, H. V. and Smith, J. C. (1992). Responses of embryonic Xenopus cells to activin and FGF are separated by multiple dose thresholds and correspond to distinct axes of the mesoderm. *Cell* **71**, 731–739.

Griffin, C. T., Curtis, C. D., Davis, R. B., Muthukumar, V. and Magnuson, T. (2011). The chromatin-remodeling enzyme BRG1 modulates vascular Wnt signaling at two levels. *Proc. Natl. Acad. Sci. U.S.A.* **108**, 2282–2287.

Guan, B., Gao, M., Wu, C.-H., Wang, T.-L. and Shih, I.-M. (2012). Functional analysis of in-frame indel ARID1A mutations reveals new regulatory mechanisms of its tumor suppressor functions. *Neoplasia (New York, NY)* **14**, 986.

Guan, B., Wang, T. L. and Shih, I. M. (2011). ARID1A, a Factor That Promotes Formation of SWI/SNF-Mediated Chromatin Remodeling, Is a Tumor Suppressor in Gynecologic Cancers. *Cancer Research* **71**, 6718–6727.

Guger, K. A. and Gumbiner, B. M. (1995). beta-Catenin has Wnt-like activity and mimics the Nieuwkoop signaling center in Xenopus dorsal-ventral patterning. *Developmental Biology* **172**, 115–125.

Guil, S., Gattoni, R., Carrascal, M., Abián, J., Stévenin, J. and Bach-Elias, M. (2003). Roles of hnRNP A1, SR proteins, and p68 helicase in c-H-ras alternative splicing regulation. *Molecular and Cellular Biology* **23**, 2927–2941.

Guille, M. (1999). Molecular Methods in Developmental Biology.

Gujral, T. S. and MacBeath, G. (2010). A System-Wide Investigation of the Dynamics of Wnt Signaling Reveals Novel Phases of Transcriptional Regulation. *PLoS ONE* **5**, e10024.

Habas, R., Dawid, I. B. and He, X. (2003). Coactivation of Rac and Rho by Wnt/Frizzled signaling is required for vertebrate gastrulation. *Genes & Development* **17**, 295–309.

Haberland, M., Montgomery, R. L. and Olson, E. N. (2009). The many roles of histone deacetylases in development and physiology: implications for disease and therapy. *Nat Rev Genet* **10**, 32–42.

Hagen, T., Di Daniel, E., Culbert, A. A. and Reith, A. D. (2002). Expression and characterization of GSK-3 mutants and their effect on beta-catenin phosphorylation in intact cells. *J. Biol. Chem.* **277**, 23330–23335.

Haller, K., Rambaldi, I., Daniels, E. and Featherstone, M. (2004). Subcellular localization of multiple PREP2 isoforms is regulated by actin, tubulin, and nuclear export. *J. Biol. Chem.* **279**, 49384–49394.

Han, D., Jeon, S., Sohn, D. H., Lee, C., Ahn, S., Kim, W. K., Chung, H. and Seong, R. H. (2008). SRG3, a core component of mouse SWI/SNF complex, is essential for extra-embryonic vascular development. *Developmental Biology* **315**, 136–146.

Hargreaves, D. C. and Crabtree, G. R. (2011). ATP-dependent chromatin remodeling: genetics, genomics and mechanisms. *Nature Publishing Group* 1–25.

Hassler, C., Cruciat, C. M., Huang, Y. L., Kuriyama, S., Mayor, R. and Niehrs, C. (2007). Kremen is required for neural crest induction in Xenopus and promotes LRP6-mediated Wnt signaling. *Development* **134**, 4255–4263.

Hatzis, P., van der Flier, L. G., van Driel, M. A., Guryev, V., Nielsen, F., Denissov, S., Nijman, I. J., Koster, J., Santo, E. E., Welboren, W., et al. (2008). Genome-Wide Pattern of TCF7L2/TCF4 Chromatin Occupancy in Colorectal Cancer Cells. *Molecular and Cellular Biology* **28**, 2732–2744.

Häcker, U., Lin, X. and Perrimon, N. (1997). The Drosophila sugarless gene modulates Wingless signaling and encodes an enzyme involved in polysaccharide biosynthesis. *Development* **124**, 3565–3573.

He, T.-C., Sparks, A. B., Rago, C., Hermeking, H., Zawel, L., da Costa, L. T., Morin, P. J., Vogelstein, B. and Kinzler, K. W. (1998). Identification of c-MYC as a target of the APC pathway. *Science* **281**, 1509–1512.

He, X., Semenov, M., Tamai, K. and Zeng, X. (2004). LDL receptor-related proteins 5 and 6 in Wnt/beta-catenin signaling: arrows point the way. *Development* **131**, 1663–1677.

Henderson, B. R. (2000). Nuclear-cytoplasmic shuttling of APC regulates beta-catenin subcellular localization and turnover. *Nat. Cell Biol.* **2**, 653–660.

Herr, P. and Basler, K. (2012). Developmental Biology. *Developmental Biology* **361**, 392–402.

Hikasa, H. and Sokol, S. Y. (2011). Phosphorylation of TCF Proteins by Homeodomain-interacting Protein Kinase 2. *Journal of Biological Chemistry* **286**, 12093–12100.

Hikasa, H., Shibata, M., Hiratani, I. and Taira, M. (2002). The Xenopus receptor tyrosine kinase Xror2 modulates morphogenetic movements of the axial mesoderm and neuroectoderm via Wnt signaling. *Development* **129**, 5227–

5239.

Hillen, W. and Berens, C. (1994). Mechanisms underlying expression of Tn10 encoded tetracycline resistance. *Annu. Rev. Microbiol.* **48**, 345–369.

Ho, L., Jothi, R., Ronan, J. L., Cui, K., Zhao, K. and Crabtree, G. R. (2009). An embryonic stem cell chromatin remodeling complex, esBAF, is an essential component of the core pluripotency transcriptional network. *Proc. Natl. Acad. Sci. U.S.A.* **106**, 5187–5191.

Ho, L., Miller, E. L., Ronan, J. L., Ho, W. Q., Jothi, R. and Crabtree, G. R. (2011). esBAF facilitates pluripotency by conditioning the genome for LIF/STAT3 signalling and by regulating polycomb function. *Nat. Cell Biol.* **13**, 903–913.

Hoeppner, L. H., Secreto, F. J., Razidlo, D. F., Whitney, T. J. and Westendorf, J. J. (2011). Lef1DeltaN binds beta-catenin and increases osteoblast activity and trabecular bone mass. *Journal of Biological Chemistry* **286**, 10950–10959.

Hoffmans, R. and Basler, K. (2004). Identification and in vivo role of the Armadillo-Legless interaction. *Development* **131**, 4393–4400.

Houston, D. W. (2012). Cortical rotation and messenger RNA localization in Xenopus axis formation. *Wiley Interdiscip Rev Dev Biol* **1**, 371–388.

Hovanes, K., Li, T. W., Munguia, J. E., Truong, T., Milovanovic, T., Lawrence Marsh, J., Holcombe, R. F. and Waterman, M. L. (2001). Beta-catenin-sensitive isoforms of lymphoid enhancer factor-1 are selectively expressed in colon cancer. *Nature Genetics* **28**, 53–57.

Hsieh, J.-C., Kodjabachian, L., Rebbert, M. L., Rattner, A., Smallwood, P. M., Samos, C. H., Nusse, R., Dawid, I. B. and Nathans, J. (1999). A new secreted protein that binds to Wnt proteins and inhibits their activites. *Nature* **398**, 431–436.

Hsu, W., Zeng, L. and Costantini, F. (1999). Identification of a Domain of Axin That Binds to the Serine/Threonine Protein Phosphatase 2A and a Self-binding Domain. *Journal of Biological Chemistry* **274**, 3439–3445.

Hurlstone, A. F., Olave, I. A., Barker, N., van Noort, M. and Clevers, H. (2002). Cloning and characterization of hELD/OSA1, a novel BRG1 interacting protein. *Biochem. J.* **364**, 255.

Ikeda, S., Kishida, S., Yamamoto, H., Murai, H., Koyama, S. and Kikuchi, A. (1998). Axin, a negative regulator of the Wnt signaling pathway, forms a complex with GSK-3beta and beta-catenin and promotes GSK-3beta-dependent phosphorylation of beta-catenin. *The EMBO Journal* **17**, 1371–1384.

Imbalzano, A. N., Kwon, H., Green, M. R. and Kingston, R. E. (1994). Facilitated binding of TATA-binding protein to nucleosomal DNA. *Nature* **370**, 481–485.

Imbalzano, A. N., Schnitzler, G. R. and Kingston, R. E. (1996). Nucleosome Disruption by Human SWI/SNF Is Maintained in the Absence of Continued ATP Hydrolysis. *Journal of Biological Chemistry* **271**, 20726–20733.

Inoue, H., Furukawa, T., Giannakopoulos, S., Zhou, S., King, D. S. and Tanese, N. (2002). Largest subunits of the human SWI/SNF chromatin-remodeling complex promote transcriptional activation by steroid hormone receptors. *J. Biol. Chem.* **277**, 41674–41685.

Ishitani, T., Ninomiya-Tsuji, J. and Matsumoto, K. (2003). Regulation of Lymphoid Enhancer Factor 1/T-Cell Factor by Mitogen-Activated Protein Kinase-Related Nemo-Like Kinase-Dependent Phosphorylation in Wnt/ -Catenin Signaling. *Molecular and Cellular Biology* **23**, 1379–1389.

Jalal, C., Uhlmann-Schiffler, H. and Stahl, H. (2007). Redundant role of DEAD box proteins p68 (Ddx5) and p72/p82 (Ddx17) in ribosome biogenesis and cell proliferation. *Nucleic Acids Research* **35**, 3590–3601.

Janknecht, R. (2010). Multi-talented DEAD-box proteins and potential tumor promoters: p68 RNA helicase (DDX5) and its paralog, p72 RNA helicase (DDX17). *Am J Transl Res* **2**, 223–234.

Jerabek, S., Merino, F., Schöler, H. R. and Cojocaru, V. (2014). Biochimica et Biophysica Acta. *BBA - Gene Regulatory Mechanisms* **1839**, 138–154.

Jones, C. M., Kuehn, M. R., Hogan, B. L., Smith, J. C. and Wright, C. V. (1995). Nodal-related signals induce axial mesoderm and dorsalize mesoderm during gastrulation. *Development* **121**, 3651–3662.

Jones, S., Wang, T.-L., Shih, I.-M., Mao, T.-L., Nakayama, K., Roden, R., Glas, R., Slamon, D., Diaz, L. A., Vogelstein, B., et al. (2010). Frequent mutations of chromatin remodeling gene ARID1A in ovarian clear cell carcinoma. *Science* **330**, 228–231.

Jordan, N. V., Prat, A., Abell, A. N., Zawistowski, J. S., Sciaky, N., Karginova, O. A., Zhou, B., Golitz, B. T., Perou, C. M. and Johnson, G. L. (2013). SWI/SNF Chromatin-Remodeling Factor Smarcd3/Baf60c Controls Epithelial-Mesenchymal Transition by Inducing Wnt5a Signaling. *Molecular and Cellular Biology* **33**, 3011–3025.

Kadam, S. and Emerson, B. M. (2003). Transcriptional specificity of human SWI/SNF BRG1 and BRM chromatin remodeling complexes. *Molecular Cell* **11**, 377–389.

Kadoch, C., Hargreaves, D. C., Hodges, C., Elias, L., Ho, L., Ranish, J. and Crabtree, G. R. (2013). Proteomic and bioinformatic analysis of mammalian SWI/SNF complexes identifies extensive roles in human malignancy. *Nature Genetics* **45**, 592–601.

Kamata, T., Katsube, K.-I., Michikawa, M., Yamada, M., Takada, S. and Mizusawa, H. (2004). R-spondin, a novel gene with thrombospondin type 1

domain, was expressed in the dorsal neural tube and affected in Wnts mutants. *Biochimica et Biophysica Acta (BBA) - Gene Structure and Expression* **1676**, 51–62.

Kassabov, S. R., Zhang, B., Persinger, J. and Bartholomew, B. (2003). SWI/SNF Unwraps, Slides, and Rewraps the Nucleosome. *Molecular Cell*.

Katanaev, V. L. and Buestorf, S. (2009). Frizzled Proteins are bona fide G protein-coupled receptors. *Nature Precedings*.

Katanaev, V. L., Ponzielli, R., Sémériva, M. and Tomlinson, A. (2005). Trimeric G protein-dependent frizzled signaling in Drosophila. *Cell* **120**, 111–122.

Kennison, J. A. and Tamkun, J. W. (1988). Dosage-dependent modifiers of polycomb and antennapedia mutations in Drosophila. *Proc. Natl. Acad. Sci. U.S.A.* **85**, 8136–8140.

Khavari, P. A., Peterson, C. L., Tamkun, J. W., Mendel, D. B. and Crabtree, G. R. (1993). BRG1 contains a conserved domain of the SWI2/SNF2 family necessary for normal mitotic growth and transcription. *Nature* **366**, 170–174.

Kiecker, C. and Niehrs, C. (2001). A morphogen gradient of Wnt/beta-catenin signalling regulates anteroposterior neural patterning in Xenopus. *Development* **128**, 4189–4201.

Kim, G.-H., Her, J.-H. and Han, J.-K. (2008). Ryk cooperates with Frizzled 7 to promote Wnt11-mediated endocytosis and is essential for Xenopus laevis convergent extension movements. *J. Cell Biol.* **182**, 1073–1082.

King, H. A., Trotter, K. W. and Archer, T. K. (2012). Chromatin remodeling during glucocorticoid receptor regulated transactivation. *Biochim. Biophys. Acta* **1819**, 716–726.

Kinzler, K. W., Nilbert, M. C., Su, L. K., Vogelstein, B., Bryan, T. M., Levy, D. B., Smith, K. J., Preisinger, A. C., Hedge, P. and McKechnie, D. (1991). Identification of FAP locus genes from chromosome 5q21. *Science* **253**, 661–665.

Kitagawa, M., Hatakeyama, S., Shirane, M., Matsumoto, M., Ishida, N., Hattori, K., Nakamichi, I., Kikuchi, A., Nakayama, K.-I. and Nakayama, K. (1999). An F-box protein, FWD1, mediates ubiquitin-dependent proteolysis of β-catenin. *The EMBO Journal* **18**, 2401–2410.

Kozmik, Z., Machoň, O., Králová, J., Krešlová, J., Pačes, J. and Vlček, Č. (2001). Characterization of Mammalian Orthologues of the Drosophila osa Gene: cDNA Cloning, Expression, Chromosomal Localization, and Direct Physical Interaction with Brahma Chromatin-Remodeling Complex☆. *Genomics* **73**, 140–148.

Kramps, T., Peter, O., Brunner, E., Nellen, D., Froesch, B., Chatterjee, S., Murone, M., Züllig, S. and Basler, K. (2002). Wnt/wingless signaling requires BCL9/legless-mediated recruitment of pygopus to the nuclear β-catenin-TCF complex. *Cell* **109**, 47–60.

Kudoh, T., Wilson, S. W. and Dawid, I. B. (2002). Distinct roles for Fgf, Wnt and retinoic acid in posteriorizing the neural ectoderm. *Development* **129**, 4335–4346.

Kuzmanov, A., Karina, E. I., Kirienko, N. V. and Fay, D. S. (2014). The Conserved PBAF Nucleosome-Remodeling Complex Mediates the Response to Stress in Caenorhabditis elegans. *Molecular and Cellular Biology* **34**, 1121–1135.

Kwon, H., Imbalzano, A. N., Khavari, P. A., Kingston, R. E. and Green, M. R. (1994). Nucleosome disruption and enhancement of activator binding by a human SW1/SNF complex.

L'Episcopo, F., Tirolo, C., Caniglia, S., Testa, N., Morale, M. C., Serapide, M. F., Pluchino, S. and Marchetti, B. (2014). Targeting Wnt signaling at the neuroimmune interface for dopaminergic neuroprotection/repair in Parkinson's disease. *Journal of Molecular Cell Biology* **6**, 13–26.

LaBonne, C. and Bronner-Fraser, M. (1998). Neural crest induction in Xenopus: evidence for a two-signal model. *Development* **125**, 2403–2414.

LaBonne, C. and Whitman, M. (1997). Localization of MAP Kinase Activity in EarlyXenopusEmbryos: Implications for Endogenous FGF Signaling. *Developmental Biology*.

Lahaye, L. L., Wouda, R. R., de Jong, A. W. M., Fradkin, L. G. and Noordermeer, J. N. (2012). WNT5 Interacts with the Ryk Receptors Doughnut and Derailed to Mediate Muscle Attachment Site Selection in Drosophila melanogaster. *PLoS ONE* **7**, e32297.

Lamb, T. M., Knecht, A. K., Smith, W. C., Stachel, S. E., Economides, A. N., Stahl, N., Yancopolous, G. D. and Harland, R. M. (1993). Neural induction by the secreted polypeptide noggin. *Science* **262**, 713–718.

Lans, H., Marteijn, J. A. and Vermeulen, W. (2012). ATP-dependent chromatin remodeling in the DNA-damage response. *Epigenetics Chromatin* **5**, 4.

Larabell, C. A., Torres, M., Rowning, B. A., Yost, C., Miller, J. R., Wu, M., Kimelman, D. and Moon, R. T. (1997a). Establishment of the dorso-ventral axis in Xenopus embryos is presaged by early asymmetries in beta-catenin that are modulated by the Wnt signaling pathway. *J. Cell Biol.* **136**, 1123–1136.

Larabell, C. A., Torres, M., Rowning, B. A., Yost, C., Miller, J. R., Wu, M., Kimelman, D. and Moon, R. T. (1997b). Establishment of the dorso-ventral axis in Xenopus embryos is presaged by early asymmetries in beta-catenin

that are modulated by the Wnt signaling pathway. *J. Cell Biol.* **136**, 1123–1136.

Large, E. E. and Mathies, L. D. (2014). Caenorhabditis elegans SWI/SNF Subunits Control Sequential Developmental Stages in the Somatic Gonad. *G3: Genes| Genomes| Genetics* **4**, 471–483.

Laurent, B. C. and Carlson, M. (1992). Yeast SNF2/SWI2, SNF5, and SNF6 proteins function coordinately with the gene-specific transcriptional activators GAL4 and Bicoid. *Genes & Development* **6**, 1707–1715.

Laurent, B. C., Treich, I. and Carlson, M. (1993). The yeast SNF2/SWI2 protein has DNA-stimulated ATPase activity required for transcriptional activation. *Genes & Development* **7**, 583–591.

Laurent, B. C., Treitel, M. A. and Carlson, M. (1991). Functional interdependence of the yeast SNF2, SNF5, and SNF6 proteins in transcriptional activation. *Proc. Natl. Acad. Sci. U.S.A.* **88**, 2687–2691.

Lee, D., Kim, J. W., Seo, T., Hwang, S. G., Choi, E.-J. and Choe, J. (2002). SWI/SNF complex interacts with tumor suppressor p53 and is necessary for the activation of p53-mediated transcription. *J. Biol. Chem.* **277**, 22330–22337.

Lee, K.-M., Sif, S., Kingston, R. E. and Hayes, J. J. (1999). hSWI/SNF Disrupts Interactions between the H2A N-Terminal Tail and Nucleosomal DNA †. *Biochemistry* **38**, 8423–8429.

Lei, I., Gao, X., Sham, M. H. and Wang, Z. (2012). SWI/SNF Protein Component BAF250a Regulates Cardiac Progenitor Cell Differentiation by Modulating Chromatin Accessibility during Second Heart Field Development. *Journal of Biological Chemistry* **287**, 24255–24262.

Lemaire, P., Garrett, N. and Gurdon, J. B. (1995). Expression cloning of Siamois, a Xenopus homeobox gene expressed in dorsal-vegetal cells of blastulae and able to induce a complete secondary axis. *Cell* **81**, 85–94.

Lessard, J., Wu, J. I., Ranish, J. A., Wan, M., Winslow, M. M., Staahl, B. T., Wu, H., Aebersold, R., Graef, I. A. and Crabtree, G. R. (2007). An Essential Switch in Subunit Composition of a Chromatin Remodeling Complex during Neural Development. *Neuron* **55**, 201–215.

Li, G., Levitus, M., Bustamante, C. and Widom, J. (2004). Rapid spontaneous accessibility of nucleosomal DNA. *Nat Struct Mol Biol* **12**, 46–53.

Li, J. and Wang, C.-Y. (2008). TBL1–TBLR1 and β-catenin recruit each other to Wnt target-gene promoter for transcription activation and oncogenesis. *Nat. Cell Biol.* **10**, 160–169.

Li, L., Hutchins, B. I. and Kalil, K. (2009). Wnt5a Induces Simultaneous Cortical Axon Outgrowth and Repulsive Axon Guidance through Distinct Signaling

Mechanisms. *Journal of Neuroscience* **29**, 5873–5883.

Li, V. S. W., Ng, S. S., Boersema, P. J., Low, T. Y., Karthaus, W. R., Gerlach, J. P., Mohammed, S., Heck, A. J. R., Maurice, M. M., Mahmoudi, T., et al. (2012). Wnt Signaling through Inhibition of b-Catenin Degradation inan Intact Axin1 Complex. *Cell* **149**, 1245–1256.

Lickert, H., Takeuchi, J. K., Both, Von, I., Walls, J. R., McAuliffe, F., Adamson, S. L., Henkelman, R. M., Wrana, J. L., Rossant, J. and Bruneau, B. G. (2004). Baf60c is essential for function of BAF chromatin remodelling complexes in heart development. *Nature* **432**, 107–112.

Lin, C., Yang, L., Yang, J. J., Huang, Y. and Liu, Z. R. (2005). ATPase/Helicase Activities of p68 RNA Helicase Are Required for Pre-mRNA Splicing but Not for Assembly of the Spliceosome. *Molecular and Cellular Biology* **25**, 7484–7493.

Lin, X. (2004). Functions of heparan sulfate proteoglycans in cell signaling during development. *Development* **131**, 6009–6021.

Liu, C., Li, Y., Semenov, M., Han, C., Baeg, G. H. and Tan, Y. (2002). Control of β-Catenin Phosphorylation/Degradation by a Dual-Kinase Mechanism. *Cell*.

Liu, C.-C., Pearson, C. and Bu, G. (2009). Cooperative folding and ligand-binding properties of LRP6 beta-propeller domains. *J. Biol. Chem.* **284**, 15299–15307.

Liu, F., van den Broek, O., Destrée, O. and Hoppler, S. (2005). Distinct roles for Xenopus Tcf/Lef genes in mediating specific responses to Wnt/beta-catenin signalling in mesoderm development. *Development* **132**, 5375–5385.

Liu, T., DeCostanzo, A. J., Liu, X., Wang Hy, Hallagan, S., Moon, R. T. and Malbon, C. C. (2001). G protein signaling from activated rat frizzled-1 to the beta-catenin-Lef-Tcf pathway. *Science* **292**, 1718–1722.

Liu, X., Zhao, Z. and Liu, W. (2013). Insights into the roles of cyclophilin A during influenza virus infection. *Viruses* **5**, 182–191.

Liu, Y., Rubin, B., Bodine, P. V. N. and Billiard, J. (2008). Wnt5a induces homodimerization and activation of Ror2 receptor tyrosine kinase. *J. Cell. Biochem.* **105**, 497–502.

Lorch, Y., Zhang, M. and Kornberg, R. D. (1999). Histone Octamer Transfer by a Chromatin-Remodeling Complex. *Cell*.

Love, J. J., Li, X., Case, D. A., Giese, K., Grosschedl, R. and Wright, P. E. (1995). Structural basis for DNA bending by the architectural transcription factor LEF-1. *Nature* **376**, 791–795.

Lu, W., Yamamoto, V., Ortega, B. and Baltimore, D. (2004). Mammalian Ryk is a Wnt coreceptor required for stimulation of neurite outgrowth. *Cell* **119**, 97–108.

Ludwig, A., Otto, G. P., Riento, K., Hams, E., Fallon, P. G. and Nichols, B. J. (2010). Flotillin microdomains interact with the cortical cytoskeleton to control uropod formation and neutrophil recruitment. *J. Cell Biol.* **191**, 771–781.

Luger, K., Mäder, A. W., Richmond, R. K., Sargent, D. F. and Richmond, T. J. (1997). Crystal structure of the nucleosome core particle at 2.8 Å resolution. *Nature* **389**, 251–260.

Luo, W., Zou, H., Jin, L., Lin, S., Li, Q., Ye, Z., Rui, H. and Lin, S.-C. (2005). Axin contains three separable domains that confer intramolecular, homodimeric, and heterodimeric interactions involved in distinct functions. *J. Biol. Chem.* **280**, 5054–5060.

Lyu, J., Yamamoto, V. and Lu, W. (2008). Cleavage of the Wnt receptor Ryk regulates neuronal differentiation during cortical neurogenesis. *Developmental Cell* **15**, 773–780.

MacDonald, B. T., Tamai, K. and He, X. (2009). Wnt/beta-catenin signaling: components, mechanisms, and diseases. *Developmental Cell* **17**, 9–26.

Mahmoudi, T., Li, V. S. W., Ng, S. S., Taouatas, N., Vries, R. G. J., Mohammed, S., Heck, A. J. and Clevers, H. (2009). The kinase TNIK is an essential activator of Wnt target genes. *The EMBO Journal* **28**, 3329–3340.

Mao, B., Wu, W., Davidson, G., Marhold, J., Li, M., Mechler, B. M., Delius, H., Hoppe, D., Stannek, P. and Walter, C. (2002). Kremen proteins are Dickkopf receptors that regulate Wnt/β-catenin signalling. *Nature* **417**, 664–667.

Mao, C. D. and Byers, S. W. (2011). Cell-context dependent TCF/LEF expression and function: alternative tales of repression, de-repression and activation potentials. *Crit. Rev. Eukaryot. Gene Expr.* **21**, 207–236.

Mao, T.-L. and Shih, I.-M. (2013). The roles of ARID1A in gynecologic cancer. *Journal of gynecologic oncology* **24**, 376–381.

Marikawa, Y. and Elinson, R. P. (1999). Relationship of vegetal cortical dorsal factors in the Xenopus egg with the Wnt/beta-catenin signaling pathway. *Mechanisms of Development* **89**, 93–102.

Mathew, D., Ataman, B., Chen, J., Zhang, Y., Cumberledge, S. and Budnik, V. (2005). Wingless signaling at synapses is through cleavage and nuclear import of receptor DFrizzled2. *Science* **310**, 1344–1347.

Matsumoto, S., Banine, F., Struve, J., Xing, R., Adams, C., Liu, Y., Metzger, D., Chambon, P., Rao, M. S. and Sherman, L. S. (2006). Brg1 is required for murine neural stem cell maintenance and gliogenesis. *Developmental Biology* **289**, 372–383.

Mayor, R. and Theveneau, E. (2013). The role of the non-canonical Wnt–planar

cell polarity pathway in neural crest migration. *Biochem. J.* **457**, 19–26.

McGrew, L. L., Hoppler, S. and Moon, R. T. (1997). Wnt and FGF pathways cooperatively pattern anteroposterior neural ectoderm in Xenopus. *Mechanisms of Development* **69**, 105–114.

McKendry, R., Hsu, S. C., Harland, R. M. and Grosschedl, R. (1997). LEF-1/TCF proteins mediate wnt-inducible transcription from the Xenopus nodal-related 3 promoter. *Developmental Biology* **192**, 420–431.

Mii, Y. and Taira, M. (2009). Secreted Frizzled-related proteins enhance the diffusion of Wnt ligands and expand their signalling range. *Development* **136**, 4083–4088.

Mikels, A. J. and Nusse, R. (2006). Purified Wnt5a Protein Activates or Inhibits β-Catenin–TCF Signaling Depending on Receptor Context. *PLoS Biol* **4**, e115.

Minde, D. P., Anvarian, Z., Rüdiger, S. G. and Maurice, M. M. (2011). Messing up disorder: how do missense mutationsin the tumor suppressor protein APC lead tocancer? *Molecular Cancer* **10**, 101.

Miyamoto, K. and Gurdon, J. B. (2012). Transcriptional regulation and nuclear reprogramming: roles of nuclear actin and actin-binding proteins. *Cell. Mol. Life Sci.* **70**, 3289–3302.

Mohrmann, L. and Verrijzer, C. P. (2005). Composition and functional specificity of SWI2/SNF2 class chromatin remodeling complexes. *Biochimica et Biophysica Acta (BBA) - Gene Structure and Expression* **1681**, 59–73.

Mohrmann, L., Langenberg, K., Krijgsveld, J., Kal, A. J., Heck, A. J. R. and Verrijzer, C. P. (2004). Differential Targeting of Two Distinct SWI/SNF-Related Drosophila Chromatin-Remodeling Complexes. *Molecular and Cellular Biology* **24**, 3077–3088.

Molenaar, M., van de Wetering, M., Oosterwegel, M., Peterson-Maduro, J., Godsave, S., Korinek, V., Roose, J., Destrée, O. and Clevers, H. (1996). XTcf-3 transcription factor mediates beta-catenin-induced axis formation in Xenopus embryos. *Cell* **86**, 391–399.

Moon, R. T., Campbell, R. M., Christian, J. L., McGrew, L. L., Shih, J. and Fraser, S. (1993). Xwnt-5A: a maternal Wnt that affects morphogenetic movements after overexpression in embryos of Xenopus laevis. *Development* **119**, 97–111.

Moore, A. C., Amann, J. M., Williams, C. S., Tahinci, E., Farmer, T. E., Martinez, J. A., Yang, G., Luce, K. S., Lee, E. and Hiebert, S. W. (2008). Myeloid Translocation Gene Family Members Associate with T-Cell Factors (TCFs) and Influence TCF-Dependent Transcription. *Molecular and Cellular Biology* **28**, 977–987.

Mora-Blanco, E. L., Mishina, Y., Tillman, E. J., Cho, Y.-J., Thom, C. S., Pomeroy,

S. L., Shao, W. and Roberts, C. W. M. (2014). Activation of β-catenin/TCF targets following loss of the tumor suppressor SNF5. *Oncogene* **33**, 933–938.

Morin, P. J., Sparks, A. B., Korinek, V., Barker, N., Clevers, H., Vogelstein, B. and Kinzler, K. W. (1997). Activation of β-catenin-Tcf signaling in colon cancer by mutations in β-catenin or APC. *Science* **275**, 1787–1790.

Muchardt, C. and Yaniv, M. (1993). A human homologue of Saccharomyces cerevisiae SNF2/SWI2 and Drosophila brm genes potentiates transcriptional activation by the glucocorticoid receptor. *The EMBO Journal* **12**, 4279–4290.

Mueller-Planitz, F., Klinker, H. and Becker, P. B. (2013). Nucleosome sliding mechanisms: new twists in a looped history. *Nat Struct Mol Biol* **20**, 1026–1032.

Nagl, N. G., Wang, X., Patsialou, A., Van Scoy, M. and Moran, E. (2007). Distinct mammalian SWI/SNF chromatin remodeling complexes with opposing roles in cell-cycle control. *The EMBO Journal* **26**, 752–763.

Nagl, N. G., Zweitzig, D. R., Thimmapaya, B., Beck, G. R. and Moran, E. (2006). The c-myc gene is a direct target of mammalian SWI/SNF-related complexes during differentiation-associated cell cycle arrest. *Cancer Research* **66**, 1289–1293.

Najdi, R., Syed, A., Arce, L., Theisen, H., Ting, J.-H., Atcha, F., Nguyen, A. V., Martinez, M., Holcombe, R. F., Edwards, R. A., et al. (2009). A Wnt kinase network alters nuclear localization of TCF-1 in colon cancer. *Oncogene* **28**, 4133–4146.

Neigeborn, L. and Carlson, M. (1984). Genes affecting the regulation of SUC2 gene expression by glucose repression in Saccharomyces cerevisiae. *Genetics* **108**, 845–858.

Nelson, R. W. and Gumbiner, B. M. (1998). Beta-catenin directly induces expression of the Siamois gene, and can initiate signaling indirectly via a membrane-tethered form. *Ann. N. Y. Acad. Sci.* **857**, 86–98.

Neumann, S., Coudreuse, D. Y. M., van der Westhuyzen, D. R., Eckhardt, E. R. M., Korswagen, H. C., Schmitz, G. and Sprong, H. (2009). Mammalian Wnt3a is Released on Lipoprotein Particles. *Traffic* **10**, 334–343.

Ng, S. S., Mahmoudi, T., Danenberg, E., Bejaoui, I., de Lau, W., Korswagen, H. C., Schutte, M. and Clevers, H. (2009). Phosphatidylinositol 3-Kinase Signaling Does Not Activate the Wnt Cascade. *Journal of Biological ....*

Niehrs, C. (2004). Regionally specific induction by the Spemann-Mangold organizer. *Nat Rev Genet* **5**, 425–434.

Ninkovic, J., Steiner-Mezzadri, A., Jawerka, M., Akinci, U., Masserdotti, G., Petricca, S., Fischer, J., Holst, von, A., Beckers, J., Lie, C. D., et al. (2013). The BAF Complex Interacts with Pax6 in Adult Neural Progenitors to

Establish a Neurogenic Cross-Regulatory Transcriptional Network. *Stem Cell* **13**, 403–418.

Oh, J., Sohn, D. H., Ko, M., Chung, H., Jeon, S. H. and Seong, R. H. (2008). BAF60a interacts with p53 to recruit the SWI/SNF complex. *J. Biol. Chem.* **283**, 11924–11934.

Oishi, I., Suzuki, H., Onishi, N., Takada, R., Kani, S., Ohkawara, B., Koshida, I., Suzuki, K., Yamada, G., Schwabe, G. C., et al. (2003). The receptor tyrosine kinase Ror2 is involved in non-canonical Wnt5a/JNK signalling pathway. *Genes Cells* **8**, 645–654.

Orford, K., Crockett, C., Jensen, J. P., Weissman, A. M. and Byers, S. W. (1997). Serine phosphorylation-regulated ubiquitination and degradation of beta-catenin. *J. Biol. Chem.* **272**, 24735–24738.

Otto, G. P. and Nichols, B. J. (2011). The roles of flotillin microdomains - endocytosis and beyond. *Journal of Cell Science* **124**, 3933–3940.

Pal, S., Yun, R., Datta, A., Lacomis, L., Erdjument-Bromage, H., Kumar, J., Tempst, P. and Sif, S. (2003). mSin3A/histone deacetylase 2-and PRMT5-containing Brg1 complex is involved in transcriptional repression of the Myc target gene cad. *Molecular and Cellular Biology* **23**, 7475–7487.

Panaccione, I., Napoletano, F., Forte, A. M., Kotzalidis, G. D., Del Casale, A., Rapinesi, C., Brugnoli, C., Serata, D., Caccia, F., Cuomo, I., et al. (2013). Neurodevelopment in schizophrenia: the role of the wnt pathways. *Curr Neuropharmacol* **11**, 535–558.

Park, J.-H., Park, E.-J., Lee, H.-S., Kim, S. J., Hur, S.-K., Imbalzano, A. N. and Kwon, J. (2006). Mammalian SWI/SNF complexes facilitate DNA double-strand break repair by promoting gamma-H2AX induction. *The EMBO Journal* **25**, 3986–3997.

Park, J.-I., Kim, S. W., Lyons, J. P., Ji, H., Nguyen, T. T., Cho, K., Barton, M. C., Deroo, T., Vleminckx, K. and McCrea, P. D. (2005). Kaiso/p120-Catenin and TCF/β-Catenin Complexes Coordinately Regulate Canonical Wnt Gene Targets. *Developmental Cell* **8**, 843–854.

Park, J.-I., Venteicher, A. S., Hong, J. Y., Choi, J., Jun, S., Shkreli, M., Chang, W., Meng, Z., Cheung, P., Ji, H., et al. (2009). Telomerase modulates Wnt signalling by association with target gene chromatin. *Nature* **460**, 66–72.

Parker, D. S., Ni, Y. Y., Chang, J. L., Li, J. and Cadigan, K. M. (2008). Wingless signaling induces widespread chromatin remodeling of target loci. *Molecular and Cellular Biology* **28**, 1815–1828.

Patsialou, A., Wilsker, D. and Moran, E. (2005). DNA-binding properties of ARID family proteins. *Nucleic Acids Research* **33**, 66–80.

Pegoraro, C. and Monsoro-Burq, A. H. (2012). Signaling and transcriptional

regulation in neural crest specification and migration: lessons from xenopus embryos. *Wiley Interdiscip Rev Dev Biol* **2**, 247–259.

Perrimon, N., Engstrom, L. and Mahowald, A. P. (1989). Zygotic lethals with specific maternal effect phenotypes in Drosophila melanogaster. I. Loci on the X chromosome. *Genetics* **121**, 333–352.

Peterson, C. L. and Herskowitz, I. (1992). Characterization of the yeast SWI1, SWI2, and SWI3 genes, which encode a global activator of transcription. *Cell* **68**, 573–583.

Pfeiffer, S., Ricardo, S., Manneville, J.-B., Alexandre, C. and Vincent, J.-P. (2002). Producing Cells Retain and Recycle Wingless in Drosophila Embryos. *Curr. Biol.* **12**, 957–962.

Polach, K. J. and Widom, J. (1995). Mechanism of protein access to specific DNA sequences in chromatin: a dynamic equilibrium model for gene regulation. *Journal of Molecular Biology* **254**, 130–149.

Puri, P. L. and Mercola, M. (2012). BAF60 A, B, and Cs of muscle determination and renewal. *Genes & Development* **26**, 2673–2683.

Ramos-Medina, R., Montes-Moreno, S., Maestre, L., Cañamero, M., Rodríguez-Pinilla, M., Martínez-Torrecuadrada, J., Piris, M. Á., Majid, A., Dyer, M. J. S., Pulford, K., et al. (2013). BCL7A protein expression in normal and malignant lymphoid tissues. *Br. J. Haematol.* **160**, 106–109.

Rana, A. A., Collart, C., Gilchrist, M. J. and Smith, J. C. (2006). Defining synphenotype groups in Xenopus tropicalis by use of antisense morpholino oligonucleotides. *PLoS Genet* **2**, e193.

Rando, O. J., Zhao, K., Janmey, P. and Crabtree, G. R. (2002). Phosphatidylinositol-dependent actin filament binding by the SWI/SNF-like BAF chromatin remodeling complex. *Proc. Natl. Acad. Sci. U.S.A.* **99**, 2824–2829.

Reichsman, F., Smith, L. and Cumberledge, S. (1996). Glycosaminoglycans can modulate extracellular localization of the wingless protein and promote signal transduction. *J. Cell Biol.* **135**, 819–827.

Reyes, J. C., Barra, J., Muchardt, C., Camus, A., Babinet, C. and Yaniv, M. (1998). Altered control of cellular proliferation in the absence of mammalian brahma (SNF2α). *The EMBO Journal* **17**, 6979–6991.

Roberts, C. W., Galusha, S. A., McMenamin, M. E., Fletcher, C. D. and Orkin, S. H. (2000). Haploinsufficiency of Snf5 (integrase interactor 1) predisposes to malignant rhabdoid tumors in mice. *Proc. Natl. Acad. Sci. U.S.A.* **97**, 13796–13800.

Roberts, D. M., Pronobis, M. I., Poulton, J. S., Kane, E. G. and Peifer, M. (2012). Regulation of Wnt signaling by the tumor suppressor adenomatous polyposis

coli does not require the ability to enter the nucleus or a particular cytoplasmic localization. *Molecular biology of ....*

Roberts, D. M., Pronobis, M. I., Poulton, J. S., Waldmann, J. D., Stephenson, E. M., Hanna, S. and Peifer, M. (2011). Deconstructing the ßcatenin destruction complex: mechanistic roles for the tumor suppressor APC in regulating Wnt signaling. *Molecular Biology of the Cell* **22**, 1845–1863.

Roose, J., Molenaar, M., Peterson, J., Hurenkamp, J., Brantjes, H., Moerer, P., van de Wetering, M., Destrée, O. and Clevers, H. (1998). The Xenopus Wnt effector XTcf-3 interacts with Groucho-related transcriptional repressors. *Nature* **395**, 608–612.

Rossow, K. L. and Janknecht, R. (2003). Synergism between p68 RNA helicase and the transcriptional coactivators CBP and p300. *Oncogene* **22**, 151–156.

Rowning, B. A., Wells, J., Wu, M., Gerhart, J. C., Moon, R. T. and Larabell, C. A. (1997). Microtubule-mediated transport of organelles and localization of beta-catenin to the future dorsal side of Xenopus eggs. *Proc. Natl. Acad. Sci. U.S.A.* **94**, 1224–1229.

Rubinfeld, B., Albert, I., Porfiri, E., Munemitsu, S. and Polakis, P. (1997). Loss of β-Catenin Regulation by the APC Tumor Suppressor Protein Correlates with Loss of Structure Due to Common Somatic Mutations of the Gene. *Cancer Research*.

Rulifson, E. J., Wu, C.-H. and Nusse, R. (2000). Pathway specificity by the bifunctional receptor frizzled is determined by affinity for wingless. *Molecular Cell* **6**, 117–126.

Ryme, J., Asp, P., Böhm, S., Cavellán, E. and Farrants, A.-K. Ö. (2009). Variations in the composition of mammalian SWI/SNF chromatin remodelling complexes. *J. Cell. Biochem.* **108**, 565–576.

Sakai, M. (2007). Cell-autonomous and inductive processes among three embryonic domains control dorsal-ventral and anterior-posterior development of Xenopus laevis. *Development, Growth & Differentiation* **50**, 49–62.

Salic, A., Lee, E., Mayer, L. and Kirschner, M. W. (2000). Control of beta-catenin stability: reconstitution of the cytoplasmic steps of the wnt pathway in Xenopus egg extracts. *Molecular Cell* **5**, 523–532.

Samartzis, E. P., Samartzis, N., Noske, A., Fedier, A., Caduff, R., Dedes, K. J., Fink, D. and Imesch, P. (2012). Loss of ARID1A/BAF250a-expression in endometriosis: a biomarker for risk of carcinogenic transformation? *Mod. Pathol.* **25**, 885–892.

Saneyoshi, T., Kume, S., Amasaki, Y. and Mikoshiba, K. (2002). The Wnt/calcium pathway activates NF-AT and promotes ventral cell fate in Xenopus embryos. *Nature* **417**, 295–299.

Sawa, H., Kouike, H. and Okano, H. (2000). Components of the SWI/SNF complex are required for asymmetric cell division in C. elegans. *Molecular Cell* **6**, 617–624.

Schaniel, C., Ang, Y.-S., Ratnakumar, K., Cormier, C., James, T., Bernstein, E., Lemischka, I. R. and Paddison, P. J. (2009). Smarcc1/Baf155 Couples Self-Renewal Gene Repression with Changes in Chromatin Structure in Mouse Embryonic Stem Cells. *Stem Cells* N/A–N/A.

Scharf, S. R. and Gerhart, J. C. (1980). Determination of the dorsal-ventral axis in eggs of Xenopus laevis: Complete rescue of uv-impaired eggs by oblique orientation before first cleavage. *Developmental Biology*.

Schlosser, G. and Ahrens, K. (2004). Molecular anatomy of placode development in Xenopus laevis. *Developmental Biology* **271**, 439–466.

Schnitzler, G. R., Cheung, C. L., Hafner, J. H., Saurin, A. J., Kingston, R. E. and Lieber, C. M. (2001). Direct Imaging of Human SWI/SNF-Remodeled Mono- and Polynucleosomes by Atomic Force Microscopy Employing Carbon Nanotube Tips. *Molecular and Cellular Biology* **21**, 8504–8511.

Schubert, H. L., Wittmeyer, J., Kasten, M. M., Hinata, K., Rawling, D. C., Héroux, A., Cairns, B. R. and Hill, C. P. (2013). Structure of an actin-related subcomplex of the SWI/SNF chromatin remodeler. *Proc. Natl. Acad. Sci. U.S.A.* **110**, 3345–3350.

Schuijers, J., Mokry, M., Hatzis, P., Cuppen, E. and Clevers, H. (2014). Wnt-induced transcriptional activation is exclusively mediated by TCF/LEF. *The EMBO Journal* **33**, 146–156.

Schulte, G. (2010). International Union of Basic and Clinical Pharmacology. LXXX. The Class Frizzled Receptors. *Pharmacological Reviews* **62**, 632–667.

Schwabish, M. A. and Struhl, K. (2007). The Swi/Snf Complex Is Important for Histone Eviction during Transcriptional Activation and RNA Polymerase II Elongation In Vivo. *Molecular and Cellular Biology* **27**, 6987–6995.

Seo, S., Richardson, G. A. and Kroll, K. L. (2005). The SWI/SNF chromatin remodeling protein Brg1 is required for vertebrate neurogenesis and mediates transactivation of Ngn and NeuroD. *Development* **132**, 105–115.

Shain, A. H., Giacomini, C. P., Matsukuma, K., Karikari, C. A., Bashyam, M. D., Hidalgo, M., Maitra, A. and Pollack, J. R. (2012). Convergent structural alterations define SWItch/Sucrose NonFermentable (SWI/SNF) chromatin remodeler as a central tumor suppressive complex in pancreatic cancer. *Proc. Natl. Acad. Sci. U.S.A.* **109**, E252–E259.

Shaw, G., Morse, S., Ararat, M. and Graham, F. L. (2002). Preferential transformation of human neuronal cells by human adenoviruses and the origin of HEK 293 cells. *FASEB J.* **16**, 869–871.

Shema-Yaacoby, E., Nikolov, M., Haj-Yahya, M., Siman, P., Allemand, E., Yamaguchi, Y., Muchardt, C., Urlaub, H., Brik, A., Oren, M., et al. (2013). Systematic Identification of Proteins Bindingto Chromatin-Embedded Ubiquitylated H2B Reveals Recruitment of SWI/SNF to Regulate Transcription. *CELREP* **4**, 601–608.

Shin, S., Rossow, K. L., Grande, J. P. and Janknecht, R. (2007). Involvement of RNA Helicases p68 and p72 in Colon Cancer. *Cancer Research* **67**, 7572–7578.

Shy, B. R., Wu, C.-I., Khramtsova, G. F., Zhang, J. Y., Olopade, O. I., Goss, K. H. and Merrill, B. J. (2013). Regulation of Tcf7l1 DNA Bindingand Protein Stability as Principal Mechanisms of Wnt/b-Catenin Signaling. *CELREP* **4**, 1–9.

Sierra, J., Yoshida, T., Joazeiro, C. A. and Jones, K. A. (2006). The APC tumor suppressor counteracts beta-catenin activation and H3K4 methylation at Wnt target genes. *Genes & Development* **20**, 586–600.

Sif, S., Saurin, A. J., Imbalzano, A. N. and Kingston, R. E. (2001). Purification and characterization of mSin3A-containing Brg1 and hBrm chromatin remodeling complexes. *Genes & Development* **15**, 603–618.

Simone, C. (2006). SWI/SNF: The crossroads where extracellular signaling pathways meet chromatin. *J. Cell. Physiol.* **207**, 309–314.

Simone, C., Forcales, S. V., Hill, D. A. and Imbalzano, A. N. (2004). p38 pathway targets SWI-SNF chromatin-remodeling complex to muscle-specific loci - Nature Genetics. *Nature*.

Singh, A. P. and Archer, T. K. (2014). Analysis of the SWI/SNF chromatin-remodeling complex during early heart development and BAF250a repression cardiac gene transcription during P19 cell differentiation. *Nucleic Acids Research* **42**, 2958–2975.

Singhal, N., Esch, D., Stehling, M. and Schöler, H. R. (2014). BRG1 Is Required to Maintain Pluripotency of Murine Embryonic Stem Cells. *Biores Open Access* **3**, 1–8.

Singhal, N., Graumann, J., Wu, G., Araúzo-Bravo, M. J., Han, D. W., Greber, B., Gentile, L., Mann, M. and Schöler, H. R. (2010). Chromatin-Remodeling Components of the BAF Complex Facilitate Reprogramming. *Cell* **141**, 943–955.

Sive, H. L., Grainger, R. M. and Harland, R. M. (2010). *Early Development of Xenopus Laevis*.

Skibinski, A., Breindel, J. L., Prat, A., Galván, P., Smith, E., Rolfs, A., Gupta, P. B., LaBaer, J. and Kuperwasser, C. (2014). The Hippo Transducer TAZInteracts with the SWI/SNF Complexto Regulate Breast Epithelial Lineage Commitment. *CELREP* **6**, 1059–1072.

Smith, C. L., Horowitz-Scherer, R., Flanagan, J. F., Woodcock, C. L. and Peterson, C. L. (2003). Structural analysis of the yeast SWI/SNF chromatin remodeling complex. *Nat Struct Biol* **10**, 141–145.

Smith, W. C., McKendry, R., Ribisi, S., Jr and Harland, R. M. (1995). A nodal-related gene defines a physical and functional domain within the Spemann organizer. *Cell* **82**, 37–46.

Smits, A. H., Lindeboom, R. G. H., Perino, M., van Heeringen, S. J., Veenstra, G. J. C. and Vermeulen, M. (2014). Global absolute quantification reveals tight regulation of protein expression in single Xenopus eggs. *Nucleic Acids Research* **42**, 9880–9891.

Song, H., Goetze, S., Bischof, J., Spichiger-Haeusermann, C., Kuster, M., Brunner, E. and Basler, K. (2010). Coop functions as a corepressor of Pangolin and antagonizes Wingless signaling. *Genes & Development* **24**, 881–886.

Song, H., Hasson, P., Paroush, Z. and Courey, A. J. (2004). Groucho oligomerization is required for repression in vivo. *Molecular and Cellular Biology* **24**, 4341–4350.

Sotiropoulos, A., Gineitis, D., Copeland, J. and Treisman, R. (1999). Signal-regulated activation of serum response factor is mediated by changes in actin dynamics. *Cell* **98**, 159–169.

Spink, K. E., Polakis, P. and Weis, W. I. (2000). Structural basis of the Axin-adenomatous polyposis coli interaction. *The EMBO Journal* **19**, 2270–2279.

Staahl, B. T., Tang, J., Wu, W., Sun, A., Gitler, A. D., Yoo, A. S. and Crabtree, G. R. (2013). Kinetic Analysis of npBAF to nBAF Switching Reveals Exchange of SS18 with CREST and Integration with Neural Developmental Pathways. *Journal of Neuroscience* **33**, 10348–10361.

Stamos, J. L. and Weis, W. I. (2013). The -Catenin Destruction Complex. *Cold Spring Harbor Perspectives in Biology* **5**, a007898–a007898.

Städeli, R. and Basler, K. (2005). Dissecting nuclear Wingless signalling: Recruitment of the transcriptional co-activator Pygopus by a chain of adaptor proteins. *Mechanisms of Development* **122**, 1171–1182.

Stucke, V. M., Gorses, D. and Hofmann, F. (2008). DEAD-box RNA helicase p68 is not required for nuclear translocation of β-catenin in colon cancer cells. *Cell Cycle* **7**, 830–832.

Su, Y., Fu, C., Ishikawa, S., Stella, A., Kojima, M., Shitoh, K., Schreiber, E. M., Day, B. W. and Liu, B. (2008). APC Is Essential for Targeting Phosphorylated b-Catenin to the SCF. *Molecular Cell* **32**, 652–661.

Subtil-Rodríguez, A. and Reyes, J. C. (2010). BRG1 helps RNA polymerase II to overcome a nucleosomal barrier during elongation, in vivo. *EMBO Rep.* **11**,

751–757.

Sudarsanam, P., Iyer, V. R., Brown, P. O. and Winston, F. (2000). Whole-genome expression analysis of snf/swi mutants of Saccharomyces cerevisiae.

Szerlong, H., Hinata, K., Viswanathan, R., Erdjument-Bromage, H., Tempst, P. and Cairns, B. R. (2008). The HSA domain binds nuclear actin-related proteins to regulate chromatin-remodeling ATPases. *Nat Struct Mol Biol* **15**, 469–476.

Taelman, V. F., Dobrowolski, R., Plouhinec, J.-L., Fuentealba, L. C., Vorwald, P. P., Gumper, I., Sabatini, D. D. and De Robertis, E. M. (2010). Wnt Signaling Requires Sequestration of Glycogen Synthase Kinase 3 inside Multivesicular Endosomes. *Cell* **143**, 1136–1148.

Takada, R., Satomi, Y., Kurata, T., Ueno, N., Norioka, S., Kondoh, H., Takao, T. and Takada, S. (2006). Monounsaturated Fatty Acid Modification of Wnt Protein: Its Role in Wnt Secretion. *Developmental Cell* **11**, 791–801.

Takahashi, K. and Yamanaka, S. (2006). Induction of pluripotent stem cells from mouse embryonic and adult fibroblast cultures by defined factors. *Cell* **126**, 663–676.

Takahashi, S., Yokota, C., Takano, K., Tanegashima, K., Onuma, Y., Goto, J. and Asashima, M. (2000). Two novel nodal-related genes initiate early inductive events in Xenopus Nieuwkoop center. *Development* **127**, 5319–5329.

Takebayashi, S.-I., Lei, I., Ryba, T., Sasaki, T., Dileep, V., Battaglia, D., Gao, X., Fang, P., Fan, Y., Esteban, M. A., et al. (2013). Murine esBAF chromatin remodeling complex subunits BAF250a and Brg1 are necessary to maintain and reprogram pluripotency-specific replication timing of select replication domains. *Epigenetics Chromatin* **6**, 42.

Takebayashi-Suzuki, K. (2003). Interplay between the tumor suppressor p53 and TGF signaling shapes embryonic body axes in Xenopus. *Development* **130**, 3929–3939.

Takeda, H., Lyle, S., Lazar, A. J. F., Zouboulis, C. C., Smyth, I. and Watt, F. M. (2006). Human sebaceous tumors harbor inactivating mutations in LEF1. *Nat. Med.* **12**, 395–397.

Takemaru, K.-I. and Moon, R. T. (2000). The transcriptional coactivator CBP interacts with β-catenin to activate gene expression. *J. Cell Biol.* **149**, 249–254.

Takemaru, K.-I., Yamaguchi, S., Lee, Y. S., Zhang, Y., Carthew, R. W. and Moon, R. T. (2003). Chibby, a nuclear β-catenin-associated antagonist of the Wnt/Wingless pathway. *Nature* **422**, 905–909.

Takeuchi, J. K. and Bruneau, B. G. (2009). Directed transdifferentiation of

mouse mesoderm to heart tissue by defined factors. *Nature* **459**, 708–711.

Takeuchi, J. K., Lickert, H., Bisgrove, B. W., Sun, X., Yamamoto, M., Chawengsaksophak, K., Hamada, H., Yost, H. J., Rossant, J. and Bruneau, B. G. (2007). Baf60c is a nuclear Notch signaling component required for the establishment of left–right asymmetry. *Proc. Natl. Acad. Sci. U.S.A.* **104**, 846–851.

Tamai, K., Semenov, M., Kato, Y., Spokony, R., Liu, C., Katsuyama, Y., Hess, F., Saint-Jeannet, J.-P. and He, X. (2000). LDL-receptor-related proteins in Wnt signal transduction. *Nature* **407**, 530–535.

Tamai, K., Zeng, X., Liu, C., Zhang, X., Harada, Y., Chang, Z. and He, X. (2004). A mechanism for Wnt coreceptor activation. *Molecular Cell* **13**, 149–156.

Tamkun, J. W., Deuring, R., Scott, M. P., Kissinger, M., Pattatucci, A. M., Kaufman, T. C. and Kennison, J. A. (1992). brahma: a regulator of Drosophila homeotic genes structurally related to the yeast transcriptional activator SNF2/SWI2. *Cell* **68**, 561–572.

Tan, C. W., Gardiner, B. S., Hirokawa, Y., Smith, D. W. and Burgess, A. W. (2014). Analysis of Wnt signaling β-catenin spatial dynamics in HEK293T cells. *BMC Systems Biology* **8**, 1–18.

Tanaka, K. (2002). Drosophila Segment Polarity Gene Product Porcupine Stimulates the Posttranslational N-Glycosylation of Wingless in the Endoplasmic Reticulum. *Journal of Biological Chemistry* **277**, 12816–12823.

Tando, T., Ishizaka, A., Watanabe, H., Ito, T., Iida, S., Haraguchi, T., Mizutani, T., Izumi, T., Isobe, T., Akiyama, T., et al. (2010). Requiem Protein Links RelB/p52 and the Brm-type SWI/SNF Complex in a Noncanonical NF- B Pathway. *Journal of Biological Chemistry* **285**, 21951–21960.

Terriente-Félix, A. and de Celis, J. F. (2009). Osa, a subunit of the BAP chromatin-remodelling complex, participates in the regulation of gene expression in response to EGFR signalling in the Drosophila wing. *Developmental Biology* **329**, 350–361.

Tolstorukov, M. Y., Sansam, C. G., Lu, P., Koellhoffer, E. C., Helming, K. C., Alver, B. H., Tillman, E. J., Evans, J. A., Wilson, B. G. and Park, P. J. (2013). Swi/Snf chromatin remodeling/tumor suppressor complex establishes nucleosome occupancy at target promoters. *Proc. Natl. Acad. Sci. U.S.A.* **110**, 10165–10170.

Treisman, J. E., Luk, A., Rubin, G. M. and Heberlein, U. (1997). eyelid antagonizes wingless signaling during Drosophila development and has homology to the Bright family of DNA-binding proteins. *Genes & Development* **11**, 1949–1962.

Tuoc, T. C., Boretius, S., Sansom, S. N., Pitulescu, M.-E., Frahm, J., Livesey, F. J. and Stoykova, A. (2013). Chromatin Regulation by BAF170 Controls

Cerebral Cortical Size and Thickness. *Developmental Cell* **25**, 256–269.

Uren, A., Reichsman, F., Anest, V., Taylor, W. G., Muraiso, K., Bottaro, D. P., Cumberledge, S. and Rubin, J. S. (2000). Secreted frizzled-related protein-1 binds directly to Wingless and is a biphasic modulator of Wnt signaling. *J. Biol. Chem.* **275**, 4374–4382.

Valenta, T., Lukas, J., Doubravska, L., Fafilek, B. and Korinek, V. (2006). HIC1 attenuates Wnt signaling by recruitment of TCF-4 and beta-catenin to the nuclear bodies. *The EMBO Journal* **25**, 2326–2337.

Valvezan, A. J., Zhang, F., Diehl, J. A. and Klein, P. S. (2012). Adenomatous Polyposis Coli (APC) Regulates Multiple Signaling Pathways by Enhancing Glycogen Synthase Kinase-3 (GSK-3) Activity. *Journal of Biological Chemistry*.

van Amerongen, R. (2012). Alternative Wnt Pathways and Receptors. *Cold Spring Harbor Perspectives in Biology* **4**, a007914–a007914.

van de Wetering, M., Barker, N., Harkes, I. C., van der Heyden, M., Dijk, N. J., Hollestelle, A., Klijn, J. G. M., Clevers, H. and Schutte, M. (2001). Mutant E-cadherin Breast Cancer Cells Do Not Display Constitutive Wnt Signaling. *Cancer Research*.

van de Wetering, M., Castrop, J., Korinek, V. and Clevers, H. (1996). Extensive alternative splicing and dual promoter usage generate Tcf-1 protein isoforms with differential transcription control properties. *Molecular and Cellular Biology* **16**, 745–752.

Van Rechem, C., Boulay, G. and Leprince, D. (2009). HIC1 interacts with a specific subunit of SWI/SNF complexes, ARID1A/BAF250A. *Biochemical and Biophysical Research Communications* **385**, 586–590.

van Vugt, J. J. F. A., Ranes, M., Campsteijn, C. and Logie, C. (2007). The ins and outs of ATP-dependent chromatin remodeling in budding yeast: Biophysical and proteomic perspectives. *Biochimica et Biophysica Acta (BBA) - Gene Structure and Expression* **1769**, 153–171.

Veeman, M. T., Slusarski, D. C., Kaykas, A., Louie, S. H. and Moon, R. T. (2003). Zebrafish Prickle, a Modulator of Noncanonical Wnt/Fz Signaling, Regulates Gastrulation Movements. **13**, 680–685.

Versteege, I., Sévenet, N., Lange, J., Rousseau-Merck, M. F., Ambros, P., Handgretinger, R., Aurias, A. and Delattre, O. (1998). Truncating mutations of hSNF5/INI1 in aggressive paediatric cancer. *Nature* **394**, 203–206.

Vietor, I., Kurzbauer, R., Brosch, G. and Huber, L. A. (2005). TIS7 regulation of the beta-catenin/Tcf-4 target gene osteopontin (OPN) is histone deacetylase-dependent. *J. Biol. Chem.* **280**, 39795–39801.

Vincan, E. (2008). *Wnt Signaling*. Humana Press.

Vinson, C. R., Conover, S. and Adler, P. N. (1989). A Drosophila tissue polarity locus encodes a protein containing seven potential transmembrane domains. *Nature* **338**, 263–264.

Vonica, A. and Gumbiner, B. M. (2007). The Xenopus Nieuwkoop center and Spemann-Mangold organizer share molecular components and a requirement for maternal Wnt activity. *Developmental Biology* **312**, 90–102.

Vorobyeva, N. E., Nikolenko, J. V., Nabirochkina, E. N., Krasnov, A. N., Shidlovskii, Y. V. and Georgieva, S. G. (2012). SAYP and Brahma are important for 'repressive' and "transient" Pol II pausing. *Nucleic Acids Research* **40**, 7319–7331.

Vorobyeva, N. E., Soshnikova, N. V., Nikolenko, J. V., Kuzmina, J. L., Nabirochkina, E. N., Georgieva, S. G. and Shidlovskii, Y. V. (2009). Transcription coactivator SAYP combines chromatin remodeler Brahma and transcription initiation factor TFIID into a single supercomplex. *Proc. Natl. Acad. Sci. U.S.A.* **106**, 11049–11054.

Wallingford, J. B. (2012). Planar cell polarity and the developmental control of cell behavior in vertebrate embryos. *Annu. Rev. Cell Dev. Biol.* **28**, 627–653.

Waltzer, L. and Bienz, M. (1998). Drosophila CBP represses the transcription factor TCF to antagonize Wingless signalling. *Nature* **395**, 521–525.

Wang, K., Kan, J., Yuen, S. T., Shi, S. T., Chu, K. M., Law, S., Chan, T. L., Kan, Z., Chan, A. S. Y., Tsui, W. Y., et al. (2011). Exome sequencing identifies frequent mutation of ARID1A in molecular subtypes of gastric cancer. *Nature Genetics* **43**, 1219–1223.

Wang, W., Côté, J., Xue, Y., Zhou, S., Khavari, P. A., Biggar, S. R., Muchardt, C., Kalpana, G. V., Goff, S. P., Yaniv, M., et al. (1996). Purification and biochemical heterogeneity of the mammalian SWI-SNF complex. *The EMBO Journal* **15**, 5370–5382.

Wang, X., Nagl, N. G., Flowers, S., Zweitzig, D., Dallas, P. B. and Moran, E. (2004a). Expression of p270(ARID1A), a component of human SWI/SNF complexes, in human tumors. *Int. J. Cancer* **112**, 636–642.

Wang, X., Nagl, N. G., Wilsker, D., Van Scoy, M., Pacchione, S., Yaciuk, P., Dallas, P. B. and Moran, E. (2004b). Two related ARID family proteins are alternative subunits of human SWI/SNF complexes. *Biochem. J.* **383**, 319–325.

Watanabe, K., Biesinger, J., Salmans, M. L., Roberts, B. S., Arthur, W. T., Cleary, M., Andersen, B., Xie, X. and Dai, X. (2014). Integrative ChIP-seq/Microarray Analysis Identifies a CTNNB1 Target Signature Enriched in Intestinal Stem Cells and Colon Cancer. *PLoS ONE* **9**, e92317.

Watanabe, M., Yanagisawa, J., Kitagawa, H., Takeyama, K., Ogawa, S., Arao, Y., Suzawa, M., Kobayashi, Y., Yano, T., Yoshikawa, H., et al. (2001). A

subfamily of RNA-binding DEAD-box proteins acts as an estrogen receptor alpha coactivator through the N-terminal activation domain (AF-1) with an RNA coactivator, SRA. *The EMBO Journal* **20**, 1341–1352.

Wehrli, M., Dougan, S. T., Caldwell, K., O'Keefe, L., Schwartz, S., Vaizel-Ohayon, D., Schejter, E., Tomlinson, A. and DiNardo, S. (2000). arrow encodes an LDL-receptor-related protein essential for Wingless signalling. *Nature* **407**, 527–530.

Weinberg, P., Flames, N., Sawa, H., Garriga, G. and Hobert, O. (2013). The SWI/SNF chromatin remodeling complex selectively affects multiple aspects of serotonergic neuron differentiation. *Genetics* **194**, 189–198.

Whitehouse, I., Flaus, A., Cairns, B. R., White, M. F., Workman, J. L. and Owen-Hughes, T. (1999). Nucleosome mobilization catalysed by the yeast SWI/SNF complex. *Nature* **400**, 784–787.

Whitehouse, I., Flaus, A., Havas, K. and Owen-Hughes, T. (2000). Mechanisms for ATP-dependent chromatin remodelling. *Biochem. Soc. Trans.* **28**, 376–379.

Wiegand, K. C., Shah, S. P., Al-Agha, O. M., Zhao, Y., Tse, K., Zeng, T., Senz, J., McConechy, M. K., Anglesio, M. S., Kalloger, S. E., et al. (2010). ARID1AMutations in Endometriosis-Associated Ovarian Carcinomas. *N Engl J Med* **363**, 1532–1543.

Willert, K., Brown, J. D., Danenberg, E., Duncan, A. W., Weissman, I. L., Reya, T., Yates, J. R. and Nusse, R. (2003). Wnt proteins are lipid-modified and can act as stem cell growth factors. *Nature* **423**, 448–452.

Willert, K., Shibamoto, S. and Nusse, R. (1999). Wnt-induced dephosphorylation of axin releases beta-catenin from the axin complex. *Genes & Development* **13**, 1768–1773.

Wilsker, D., Patsialou, A., Zumbrun, S. D., Kim, S., Chen, Y., Dallas, P. B. and Moran, E. (2004). The DNA-binding properties of the ARID-containing subunits of yeast and mammalian SWI/SNF complexes. *Nucleic Acids Research* **32**, 1345–1353.

Wu, C.-H. and Nusse, R. (2002). Ligand receptor interactions in the Wnt signaling pathway in Drosophila. *J. Biol. Chem.* **277**, 41762–41769.

Wühr, M., Freeman, R. M., Jr, Presler, M., Horb, M. E., Peshkin, L., Gygi, S. P. and Kirschner, M. W. (2014). Deep Proteomics of the Xenopus laevis Egg using an mRNA-DerivedReference Database. *Curr. Biol.* **24**, 1467–1475.

Xi, Q., He, W., Zhang, X. H. F., Le, H. V. and Massague, J. (2008). Genome-wide Impact of the BRG1 SWI/SNF Chromatin Remodeler on the Transforming Growth Factor Transcriptional Program. *Journal of Biological Chemistry* **283**, 1146–1155.

Xue, Y., Canman, J. C., Lee, C. S., Nie, Z., Yang, D., Moreno, G. T., Young, M. K., Salmon, E. D. and Wang, W. (2000). The human SWI/SNF-B chromatin-remodeling complex is related to yeast rsc and localizes at kinetochores of mitotic chromosomes. *Proc. Natl. Acad. Sci. U.S.A.* **97**, 13015–13020.

Yamamoto, H., Kishida, S., Kishida, M., Ikeda, S., Takada, S. and Kikuchi, A. (1999). Phosphorylation of axin, a Wnt signal negative regulator, by glycogen synthase kinase-3beta regulates its stability. *J. Biol. Chem.* **274**, 10681–10684.

Yamamoto, H., Komekado, H. and Kikuchi, A. (2006). Caveolin is necessary for Wnt-3a-dependent internalization of LRP6 and accumulation of beta-catenin. *Developmental Cell* **11**, 213–223.

Yamamoto, S., Tsuda, H., Takano, M., Tamai, S. and Matsubara, O. (2011). Loss of ARID1A protein expression occurs as an early event in ovarian clear-cell carcinoma development and frequently coexists with PIK3CA mutations. *Modern Pathology* **25**, 615–624.

Yan, Z., Wang, Z., Sharova, L., Sharov, A. A., Ling, C., Piao, Y., Aiba, K., Matoba, R., Wang, W. and Ko, M. S. H. (2008). BAF250B-associated SWI/SNF chromatin-remodeling complex is required to maintain undifferentiated mouse embryonic stem cells. *Stem Cells* **26**, 1155–1165.

Yang, J., Zhang, W., Evans, P. M., Chen, X., He, X. and Liu, C. (2006a). Adenomatous Polyposis Coli (APC) Differentially Regulates beta-Catenin Phosphorylation and Ubiquitination in Colon Cancer Cells. *Journal of Biological Chemistry* **281**, 17751–17757.

Yang, L., Lin, C. and Liu, Z.-R. (2006b). P68 RNA Helicase Mediates PDGF-Induced Epithelial Mesenchymal Transition by Displacing Axin from β-Catenin. *Cell* **127**, 139–155.

Yang-Snyder, J., Miller, J. R., Brown, J. D., Lai, C. J. and Moon, R. T. (1996). A frizzled homolog functions in a vertebrate Wnt signaling pathway. *Curr. Biol.* **6**, 1302–1306.

Yaniv, M. (2014). Chromatin remodeling: from transcription to cancer. *Cancer Genetics* 1–6.

Yokota, C. (2003). A novel role for a nodal-related protein; Xnr3 regulates convergent extension movements via the FGF receptor. *Development* **130**, 2199–2212.

Yoo, Y., Wu, X. and Guan, J. L. (2006). A Novel Role of the Actin-nucleating Arp2/3 Complex in the Regulation of RNA Polymerase II-dependent Transcription. *Journal of Biological Chemistry* **282**, 7616–7623.

Yoshikawa, S., Bonkowsky, J. L., Kokel, M., Shyn, S. and Thomas, J. B. (2001). The derailed guidance receptor does not require kinase activity in vivo. *The Journal of neuroscience: the official journal of the Society for Neuroscience* **21**,

RC119–RC119.

Yoshikawa, S., McKinnon, R. D., Kokel, M. and Thomas, J. B. (2003). Wnt-mediated axon guidance via the Drosophila Derailed receptor. *Nature* **422**, 583–588.

Yost, C., Torres, M., Miller, J. R., Huang, E., Kimelman, D. and Moon, R. T. (1996). The axis-inducing activity, stability, and subcellular distribution of beta-catenin is regulated in Xenopus embryos by glycogen synthase kinase 3. *Genes & ….*

Zani, V. J., Asou, N., Jadayel, D., Heward, J. M., Shipley, J., Nacheva, E., Takasuki, K., Catovsky, D. and Dyer, M. J. (1996). Molecular cloning of complex chromosomal translocation t (8; 14; 12)(q24. 1; q32. 3; q24. 1) in a Burkitt lymphoma cell line defines a new gene (BCL7A) with homology to caldesmon. *Blood* **87**, 3124–3134.

Zeng, L., Fagotto, F., Zhang, T., Hsu, W., Vasicek, T. J., Perry Iii, W. L., Lee, J. J., Tilghman, S. M., Gumbiner, B. M. and Costantini, F. (1997). The Mouse Fused Locus Encodes Axin, an Inhibitor of the Wnt Signaling Pathway That Regulates Embryonic Axis Formation. *Cell* **90**, 181–192.

Zeng, X., Huang, H., Tamai, K., Zhang, X., Harada, Y., Yokota, C., Almeida, K., Wang, J., Doble, B., Woodgett, J., et al. (2008). Initiation of Wnt signaling: control of Wnt coreceptor Lrp6 phosphorylation/activation via frizzled, dishevelled and axin functions. *Development* **135**, 367–375.

Zeng, X., Lin, X. and Hou, S. X. (2013). The Osa-containing SWI/SNF chromatin-remodeling complex regulates stem cell commitment in the adult Drosophila intestine. *Development* **140**, 3532–3540.

Zeng, X., Tamai, K., Doble, B., Li, S., Huang, H., Habas, R., Okamura, H., Woodgett, J. and He, X. (2005). A dual-kinase mechanism for Wnt co-receptor phosphorylation and activation. *Nature* **438**, 873–877.

Zhang, C., Cho, K., Huang, Y., Lyons, J. P., Zhou, X., Sinha, K., McCrea, P. D. and de Crombrugghe, B. (2008). Inhibition of Wnt signaling by the osteoblast-specific transcription factor Osterix. *Proceedings of the ….*

Zhang, Y., Cheng, M.-B., Zhang, Y.-J., Zhong, X., Dai, H., Yan, L., Wu, N.-H., Zhang, Y. and Shen, Y.-F. (2010). A switch from hBrm to Brg1 at IFNγ-activated sequences mediates the activation of human genes. *Nature Publishing Group* **20**, 1345–1360.

Zhang, Y., Smith, C. L., Saha, A., Grill, S. W., Mihardja, S., Smith, S. B., Cairns, B. R., Peterson, C. L. and Bustamante, C. (2006). DNA Translocation and Loop Formation Mechanism of Chromatin Remodeling by SWI/SNF and RSC. *Molecular Cell* **24**, 559–568.

Zhao, K., Wang, W., Rando, O. J., Xue, Y., Swiderek, K., Kuo, A. and Crabtree, G. R. (1998). Rapid and phosphoinositol-dependent binding of the SWI/SNF-

like BAF complex to chromatin after T lymphocyte receptor signaling. *Cell* **95**, 625–636.

Zhou, J., Zhang, M., Fang, H., El-Mounayri, O., Rodenberg, J. M., Imbalzano, A. N. and Herring, B. P. (2009). The SWI/SNF chromatin remodeling complex regulates myocardin-induced smooth muscle-specific gene expression. *Arterioscler. Thromb. Vasc. Biol.* **29**, 921–928.

Zimmerman, L. B., De Jesús-Escobar, J. M. and Harland, R. M. (1996). The Spemann Organizer Signal noggin Binds and Inactivates Bone Morphogenetic Protein 4. *Cell* **86**, 599–606.